NOVEMBER 1970

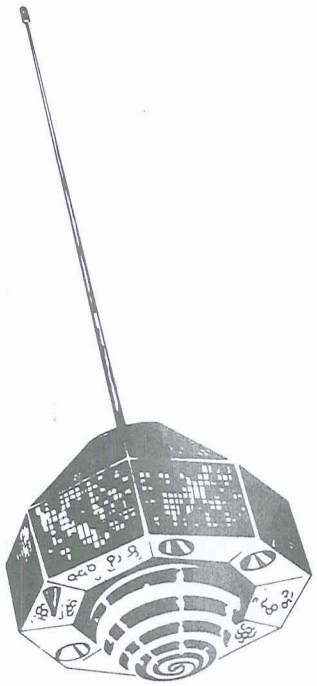

PROCEEDINGS OF THE GEOS-2 PROGRAM REVIEW MEETING 22-24 JUNE 1970

VOLUME I

GRAVIMETRIC AND GEOMETRIC INVESTIGATIONS WITH GEOS-I AND GEOS-2

EDITED BY:
CSC
COMPUTER SCIENCES CORPORATION
(703) 533-8877
6565 ARLINGTON BOULEVARD POST OFFICE BOX 530 FALLS CHURCH VA 22046

NATIONAL AERONAUTICS AND SPACE ADMINISTRATION
NASA

PROCEEDINGS OF THE GEOS-2 PROGRAM REVIEW MEETING

22-24 June 1970
NASA Goddard Space Flight Center
Greenbelt, Maryland

Volume I

Gravimetric and Geometric Investigations With GEOS-1 and GEOS-2

Edited by Computer Sciences Corporation
6565 Arlington Boulevard, Falls Church, Virginia

November 1970

TABLE OF CONTENTS

SECTION II

(Cont.)

FOREWORD

On 22-24 June 1970, a GEOS Program Review Meeting was held at the NASA Goddard Space Flight Center in Greenbelt, Maryland. The purpose of the meeting was to review the results obtained from the GEOS-1 and GEOS-2 spacecraft. GEOS-1 was launched on 6 November 1965 and GEOS-2 was launched on January 11, 1968.

At a previous GEOS Program Review Meeting held at NASA Headquarters on 12-14 December 1967, the results obtained from GEOS-1 as of that date were presented and published in the proceedings dated March 1968. The results presented herein are those obtained subsequent to that meeting and include those obtained from GEOS-2.

The proceedings of this latter meeting are published in four volumes. The volumes are entitled:

Volume I - Gravimetric and Geometric Investigations with GEOS-1 and GEOS-2.

Volume II - Tracking System Intercomparisons with GEOS-2

Volume III - LASER and RADAR Investigations

Volume IV - General

This volume (Volume I) is divided into two sections. The first section contains the gravimetric investigations and section two contains geometric investigations.

LIST OF ATTENDEES

Abby, Darwin G., CAPT
MAC/MAXPDG
Scott AFB, Illinois 6225

Agreen, Russel
GSFC
Greenbelt, Md
Code 552

Allen, John L.
DRC
60 Concord Street
Wilmington, Mass 01887

Allen, William A
Research Institute, USAETL
701 Prince Street
Alexandria, Virginia 22314

Anderle, Richard J.
Naval Weapons Laboratory
Dahlgren, Virginia 22448

Baker, Robert M. L., Jr
117 Catamaran Apt. 7
Marina del Rey, California 90291

Berbert, John H.
GSFC
Greenbelt, Md
Code 514

Bernard, J.A.
USATOPOCOM
Code 14000
6500 Brooks Lane
Washington, D.C. 20315

Beuglass, Larry K.
U.S. Naval Weapons Laboratory
Dahlgren, Virginia 22448
Code: KAG

Black, H. D.
Johns Hopkins University
Applied Physics Laboratory
8621 Georgia Avenue
Silver Spring, Md

Brooks, Ronald L.
Wolf Research & Development
P.O. Box 91
Pocomoke, Md

Brown, A.C., Jr.
RCA
8855 Annapolis Rd
Lanham, Md

Brown, Duane
DBA Systems, Inc.
Post Office Drawer 550
Melbourne, Florida 32901

Bryan, John W.
GSFC
Greenbelt, Md
Code 551

Bush, Norman
Pan American World Airways
MU 844, Bldg 989-1
Patrick AFB, Florida 32925

Chovitz, Bernard
C111
ESSA
Rockville, Md 20852

Dailey, L.R.
Aerospace Corporation
2350 E. El Segundo Blvd
El Segundo, California

Dempsey, Donald J.
RCA
Mail Stop 108-238
Moorestown, New Jersey

Douglas, Bruce G.
Wolf Research & Development
6801 Kenilworth Avenue
Riverdale, Md

Dubinsky, R.
Computer Sciences Corporation
803 W. Broad Street
Falls Church, Virginia 22046

Dudley, George H.
USATOPOCOM
6500 Brooks Lane
Washington, D.C. 20315
Code 14200

Fischel, J. R.
Computer Sciences Corporation
6565 Arlington Boulevard
Falls Church, Virginia 22046

Forsythe, Ronald G.
NASA Wallops Station
Wallops Island, Virginia 23337

Frederick, D. G.
Room BF 866
Pentagon
Washington, D.C. 20301

Fubara, D.M., Dr.
Battelle Memorial Institute
Columbus Laboratories
505 King Avenue
Columbus, Ohio 43201

Gaignebet, Jean, C.
CNRS. BPN 10
97 Verrieres/e Buisson France

Gambino, Lawrence A.
U.S.A. Engineer Topographic
Laboratories
Ft. Belvoir, Virginia

Gaposchkin, E.M., Dr.
Smithsonian Astrophysical
Observatory
60 Garden Street
Cambridge, Mass 02138

Gilchrist, C.F.
BF 866C,
Pentagon
Washington, D.C. 20301

Godbey, T.
General Electric Company
FR.RD. Utica 13502
Md 233

Doebbels, Alain CB/ES
Dentre National
O'ET UOES SPATIALES
97 Bretigny, B.P. 4
France

Goff, Nollie R.
1st Geodetic Survey Squadron
F.E. Warren AFB Wyoming 82001
Attn: UCX

Hadgigeorge, George
487 River Rd
Tewksbury, Mass

Hallmark, Nelson T.
U.S. Army Engineer
Topographic Laboratory
4513 Mayfield Drive
Annandale, Virginia 22003

Hardy, Marian
USATOPOCOM
6500 Brooks Lane
Washington D.C. 20315

Harris, David W.
GSFC
Greenbelt, Md
Code 514

Heckel, R.D.
OTDA/TN
NASA Hdqts, Washington, D.C.

Henriksen, S. W.
4217 Wheeler Street
Alexandria, Virginia

Herring, John C., Maj
52 Grassland Street
Lexington, Mass 02173

Heuring, F. T.
Computer Sciences Corporation
803 W. Broad Street
Falls Church, Virginia 22046

Hillhouse, Milton
AFETR
Patrick Air Force Base, Florida

Hlavin, Joseph M.
8858 Annapolis Rd
Lanham, Md

Huck, William J.
Computer Sciences Corporation
6565 Arlington Boulevard
Falls Church, Virginia 22046

Hudson, Edward F.
Raytheon Company
Mail Station IR-2
Sudbury, Mass 01776

Huber, Donovan N.
ACIC (ACDEG-3)
2nd & Arsenal
St. Louis, Mo

Iliff, Robert L.
Air Force Camb Ros Fld
Bedford, Mass 01730

Jackson, Frederick C.
New York University
Department of Met. and Ocean
University Heights
Bronx, N.Y. 10453

Johns, Joseph R.
NSSDC
GSFC
Greenbelt, Md
Code 601

Johnson, Thomas S.
GSFC
Greenbelt, Md
Code 524

Kay, Joseph
Naval Air Systems Command
Washington, D.C.

Ketterer, Donald
GSFC
Greenbelt, Md
Code 832

King. Clifford W.
ACIC Det-1 (ACWS)
1221 S. Fern Street
Arlington, Virginia 22202

Klosko, Steve
Wolf Research & Development
6801 Kenilworth Avenue
Riverdale, Md

Kolker, M.
Raytheon Company
528 Boston Post Rd
Sudbury, Mass 01776

Kowal, Stanley J.
Johns Hopkins University
Applied Physics Laboratory
8621 Georgia Avenue
Silver Spring, Md

Kuydendall, H.L.
ACIC (ACDEG)
2nd & Arsenal
St. Louis, Mo. 63118

Latimer, James H.
Smithsonian Astrophysical
Observatory
60 Garden Street
Cambridge, Mass 02138

Lehr, Carlton G.
Smithsonian Astrophysical
Observatory
60 Garden Street
Cambridge, Mass 02138

Leitao, Clifford D.
Wallops Station
Wallops Island, Virginia

LeRiche, Donna M.
GSFC
Greenbelt, Md
Code 832

Light, Donald L.
(96200)
Engr Appl Dio.
U.S. Army Topographic Command
Washington, D.C. 20315

Lochry, Robert R., Col
Dept of Defense
Research and Engineering
(Space Technology)
Pentagon, Room 3E-153

Loveless, Fred M.
DBA Systems
9301 Annapolis Rd
Lanham, Md

Lucas, James R.
6013 Jennings Lane
Springfield, Va 22150

Lundquist, Charles A., Dr.
Smithsonian Astrophysical
Observatory
60 Garden Street
Cambridge, Mass

Mann, H. Lindy
USAF Det #1 ACIC/ACWO
1221 S. Fern Street
Arlington, Virginia 22202

Markowitz, William
Dept of Physics
Marquette University
Milwaukee, Wisconsin 53233

Marsh, James G.
GSFC
Greenbelt, Md
Code 532

Maskasky, John A.
GSFC
Greenbelt, Md
Code 482

McCall, John S.
Geodesy & Geophysics Desk
Code 92140
Army Topographic Command
Washington, D.C. 20315

McGoogan, Joe T.
NASA
Wallops Station
Wallops Island, Virginia

Mennemeyer, Paul
Mechanical Engr Dept
Colo State University
Ft. Collins, Co. 80521

Menpes, Geraldine
Smithsonian Astrophysical
Observatory
60 Garden Street
Cambridge, Mass

Murphy, James P.
GSFC
Greenbelt, Md
Code 552

Murray, Charles W., Jr
Mission and Trajectory Anov Dir
GSFC
Greenbelt, Md
Code 551

Oosterhout, John D.
GSFC
Greenbelt, Md
Code 514

Oseroff, Harold
GSFC
Greenbelt, Md
Code 482

Parker, H.C.
8855 Annapolis Rd
Lanham, Md 20801

Pearlman, Michael R., Dr
Smithsonian Astrophysical
Observatory
60 Garden Street
Cambridge, Mass 02138

Pfingsten, D.
RCA
Tech Lab (bldg. 9 89) Mu 645
Patrick AFB, Florida 32925

Pisacane, Vincent L., Dr.
Johns Hopkins University
Applied Physics Laboratory
8621 Georgia Avenue
Silver Spring, Md

Plotkin, H. H.
GSFC
Greenbelt, Md
Code 520

Premo, D. A.
GSFC
Greenbelt, Md
Code 524

Rados, Robert
GSFC
Greenbelt, Md
Code 482

Ramasastry, Jayaram, Dr.
GSFC
Greenbelt, Md
Code 551

Rangaswamy, S., Dr.
Mission and Trajectory
Analysis Division
GSFC
Greenbelt, Md
Code 551

Rawlinson, Frank G.
GSFC
Greenbelt, Md
Code 514

Reece, Jim
Computer Sciences Corporation
803 W. Broad Street
Falls Church, Virginia

Rosenbaum, Marcus A.
Hq USAF (AFNIATB)
Washington, D.C.

Rosenberg, Jerome D.
NASA-Headquarters
Code SCD
Washington, D.C. 20546

Ruck, George T.
Battelle Memorial Institute
505 King Avenue
Columbus, Ohio

Rutscheidt, Erich H.
U.S. Army Topographic Command
Code 14200
Dept Geodesy & Geophysics
Washington, D.C.

Ruttkay, Paul
Wolf Research & Development
6801 Kenilworth Avenue
Riverdale, Md

Salzberg, I.
GSFC
Greenbelt, Md
Code 832

Sayer, Robert E.
7118 Sea Cliff Rd
McLean, Va

Schwarz, Charles R.
Ohio State University
230 Lord Hall
124 W. 17th Avenue
Columbus, Ohio 43212

Sharp, C. B.
USATOPOCOM
6500 Brooks Lane
Washington, D.C. 20315

Siry, J. W.
GSFC
Greenbelt, Md
Code 550

Smith, David E.
GSFC
Greenbelt, Md
Code 550

Smithe, Roy A
USATOPOCOM
Code 14410
6500 Brocks Lane
Washington, D.C. 20315

Smith, Steve J.
Naval Weapons Laboratory
Dahlgren, Virginia 22448
Code KAG

Sodano, Emanual M.
8105 Riverside Avenue
Bethesda, Md 20034

Stieg, Forrest
Computer Sciences Corporation
6565 Arlington Boulevard
Falls Church, Virginia

Strange, William E.
6520 Columbia Pike
Falls Church, Virginia

Talwani, Manik
La Mont - Doherty Geological
Observatory
Columbia University
Palisades, N.Y.

Taylor, Alfred W.
Det 1 ACIC
1221 S. Fern Street
Arlington, Virginia 22202

Trask, Don
Bldg 156 Rm 251
Jet Propulsion Laboratory
4800 Oak Drive
Pasadena, California

Tucker, Arnold J.
ARL/UT
P.O. Box 8029
Austin, Texas

Valente, William E.
NSSDC
Code 601

Vincent, Samir
Computer Sciences Corporation
803 W. Broad Street
Falls Church, Virginia

Vitek, Richard L.
USATOPOCOM
6500 Brooks Lane
Washington, D.C.

Wagner, Robert J.
Bldg 108-127
RCA DEP
Moorestown, New Jersey

Walker, James W.
3111 Walnut Street, N.E.
Washington, D.C.

Warden, Marvel A.
USATOPOCOM
6500 Brooks Lane
Washington, D.C.

Weiffenback, G.C.
Smithsonian Astrophysical
Observatory
60 Garden Street
Cambridge, Mass 02138

Weiffenback, G.C.
Smithsonian Astrophysical
Observatory
60 Garden Street
Cambridge, Mass 02138

Wells, W. T.
Wolf Research & Development
6801 Kenilworth Avenue
Riverdale, Md

White, Haschal L. (ACDEG-2)
Aeronautical Chart & Information
2nd & Arsenal Streets
St. Louis, Mo

Williams, W.E.
Code TN
NASA Headquarters

Willison, Ralph
Johns Hopkins University
Applied Physics Laboratory
8621 Georgia Avenue
Silver Spring, Md.

Witte, Bertold U., Dr.
Code, C 111
ESSA U.S.C. & GS
Rockville, Md

Wong, Lem
Aerospace Corporation
2350 E. El Segundo
El Segundo, Ca

Yionoulis, Steve M.
Johns Hopkins University
Applied Physics Laboratory
8621 Georgia Avenue
Silver Spring, Md

INTRODUCTION

Geodetic Satellite Data Service
Reduced Data Received and Processed
as of

June 15, 1970

J. Johns
Goddard Space Flight Center

GEODETIC SATELLITE DATA SERVICE

SATELLITE NAME	INTERNATIONAL DESIGNATION	LAUNCH DATE
ECHO-1	60-009A	August 12, 1960
ECHO-2	64-004A	January 25, 1964
BE-B or Explorer-22	64-064A	October 9, 1964
BE-C or Explorer-27	65-032A	April 29, 1965
GEOS-1 or Explorer-29	65-089A	November 6, 1965
PAGEOS-1	66-056A	June 23, 1966
D1-C or DIADEME-1	67-011A	February 8, 1967
D1-D or DIADEME-2	67-014A	February 15, 1967
GEOS-2 or Explorer-36	68-002A	January 11, 1968

GEODETIC SATELLITE DATA SERVICE
REDUCED DATA RECEIVED AND PROCESSED
AS OF
June 15, 1970

NETWORK	OBSERVATIONS	PASSES	PERIOD COVERED
ECHO-1			
US Coast & Geodetic Survey (Optical)	865	2	Feb. 1, 1967 - Feb. 1, 1967
ECHO-2			
US Coast & Geodetic Survey (Optical)	824	4	Dec. 15, 1966 - Jan. 17, 1967
BE-B			
SAO (Laser)	98	31	Mar. 10, 1966 - June 26, 1967
NASA (Laser)	342	2	May 12, 1967 - May 13, 1967
US Navy (Doppler)	26,957	1,635	Nov. 11, 1964 - Mar. 30, 1965
BE-C			
SAO (Laser)	661	161	Jan. 25, 1966 - June 24, 1967
NASA (Laser)	1,900	7	Apr. 3, 1967 - Apr. 26, 1967
US Navy (Doppler)	73,108	4,102	May 2, 1965 - Feb. 24, 1966

GEODETIC SATELLITE DATA SERVICE

GEOS-1

NETWORK	OBSERVATIONS	PASSES	PERIOD COVERED
SAO (Optical)	11,371	1,701	Nov. 8, 1965 - Nov. 29, 1966
NASA (Minitrack Optical Tracking System)	22,746	2,180	Nov. 18, 1965 - Nov. 24, 1966
US Air Force (Optical)	1,101	164	Dec. 20, 1965 - Nov. 20, 1966
US Air Force (Optical) (Special Pre-Processing)	1,382	213	Nov. 25, 1966 - Nov. 30, 1966
Us Coast & Geodetic Survey (Optical)	130	19	Nov. 28, 1965 - July 27, 1966
International (Optical)	1,803	201	Dec. 8, 1965 - Nov. 21, 1966
AMS (Secor)	78,357	756	Mar. 24, 1966 - Feb. 8, 1967
US Navy (Doppler)	664,204	19,087	Nov. 14, 1965 - Dec. 17, 1967
NASA (Range & Range Rate)	42,417	1,308	Nov. 17, 1965 - Nov. 28, 1966
NASA (Minitrack)	14,291	9,525	Nov. 6, 1965 - Jan. 14, 1967
SAO (Laser)	796	140	Jan. 27, 1966 - June 24, 1967
NASA (Laser)	4,849	19	Apr. 11, 1966 - Nov. 21, 1966
	5,602	8	Apr. 23, 1969 - May 30, 1969

GEODETIC SATELLITE DATA SERVICE

PAGEOS-1

NETWORK	OBSERVATIONS	PASSES	PERIOD COVERED
US Coast & Geodetic Survey (Optical)	70,743	244	July 20, 1966 - Mar. 31, 1967
US Air Force (Optical) (Special Pre-Processing)	212	30	Sept. 20, 1967 - Jan. 8, 1969

D1-C

SAO (Laser)	207	44	Feb. 17, 1967 - June 29, 1967
NASA (Laser)	1,921	7	Apr. 23, 1967 - May 10, 1967

D1-D

SAO (Laser)	238	38	Mar. 9, 1967 - June 2, 1967
NASA (Laser)	2,381	9	May 10, 1967 - May 27, 1967

GEODETIC SATELLITE DATA SERVICE

GEOS-2

NETWORK	OBSERVATIONS	PASSES	PERIOD COVERED
SAO (Optical)	8,901	930	Feb. 20, 1968 - Mar. 20, 1969
NASA (Minitrack Optical Tracking System)	8,314	973	Feb. 21, 1968 - Dec. 3, 1968
US Air Force (Optical)	21	3	Oct. 7, 1968 - Dec. 7, 1968
US Air Force (Optical) (Special Pre-Processing)	54	8	Mar. 28, 1968 - Jan. 8, 1969
International (Optical)	6,699	752	Feb. 20, 1968 - Jan. 7, 1970
AMS (Secor)	11,359	88	Apr. 1, 1968 - June 29, 1968
US Navy (Doppler)	86,296	3,110	Jan. 11, 1968 - Dec. 30, 1968
SAO (Laser)	236	66	Oct. 1, 1969 - Jan. 5, 1970
NASA (Laser)	144,547	322	Feb. 7, 1968 - May 14, 1970
PROCESSING			
SAO (Optical)	363	355	Oct. 6, 1969 - Jan. 31, 1970
NASA (Minitrack Optical Tracking System)	9,160	994	Feb. 21, 1968 - June 28, 1969
NASA (Range & Range Rate)	278,462	454	Feb. 21, 1968 - Sept. 30, 1968
SAO (Laser)	388	97	Sept. 2, 1969 - Jan. 31, 1970

SECTION I

GRAVIMETRIC INVESTIGATIONS

1969 SMITHSONIAN STANDARD EARTH AND GLOBAL TECTONICS

E. M. Gaposchkin, W. M. Kaula, and K. Lambeck

September 1970

Smithsonian Institution
Astrophysical Observatory
Cambridge, Massachusetts 02138

009-49

1969 SMITHSONIAN STANDARD EARTH AND GLOBAL TECTONICS

E. M. Gaposchkin, W. M. Kaula, and K. Lambeck

ABSTRACT

Geodetic parameters describing the earth's gravity field and the positions of satellite-tracking stations in a geocentric reference frame have been computed. These parameters were estimated from a combination of four different types of data — routine and simultaneous satellite observations, observations of deep-space probes, and surface gravimetry.

The global gravity field is represented by spherical harmonics complete to degree and order 16, plus a number of coefficients to which satellites are sensitive, a resolution of about 11° or 1200 km.

The accuracy is established primarily by intercomparison. The coordinates of 12 fundamental stations are known to ±10 m or better, and those of 39 stations (or groups of collocated stations) are known to ±20 m or better. The accuracy of the global field is ±3 m in geoid height, or ±9 mgal.

This solution leads to a new understanding of global tectonics and geodynamics. It shows ocean rises, as well as trench and island arcs, as mass excesses. Ocean basins, areas of recent glaciation, and the Asian portion of the Alpide belt are mass deficiencies. Most features appear to be the result of varying behavior of the lithosphere in response to asthenospheric flow.

INTRODUCTION

An original objective of space science was the improvement of geodetic parameters "to tie together the observing stations and the center of the geoid to a precision of the order of 10 m, ... to add appreciably to knowledge of the density distribution in the earth, particularly in the crustal volumes"

This work was supported in part by grants NGR 09-015-002 from the National Aeronautics and Space Administration and GA-10963 from the National Science Foundation.

(Whipple and Hynek, 1958). This objective has been achieved and surpassed, as demonstrated in 1966 with the publication by the Smithsonian Astrophysical Observatory (SAO) of numerical parameters for the earth's gravity field and the coordinates of satellite-tracking stations (Gaposchkin, 1967; Köhnlein, 1967a; Veis, 1967a, b; Whipple, 1967; Lundquist and Veis, 1966).

Four things were apparent in light of the 1966 results: 1) further work would be valuable, 2) both additional and other kinds of data could be profitably incorporated, 3) new observing techniques such as laser tracking would be important, and 4) other disciplines such as solid-earth geophysics and oceanography could be well served by what had previously been a wholly geodetic program.

These last two points were the focus of a series of seminars conducted at SAO (Lundquist and Friedman, 1966). A later and more comprehensive study along similar lines was conducted at Williamstown (Kaula, 1970). The latter part of this paper addresses itself to several aspects of earth physics in light of results from satellite geodesy.

The geodetic results in 1966 benefited from the use of two types of data — simultaneous observations and individual observations. The solution was strengthened by combining the data, and the accuracy was established by intercomparison rather than by reliance on formal statistics or internal consistency. Subsequently, other types of data were used; Köhnlein (1967b) made a combination of satellite and surface gravimetry, and Veis (1966) made a further comparison of station coordinates using Deep Space Net (DSN) data to determine the relative positions of the DSN antennas. The results in 1969 included these additional types of data as integral parts of the solution.

The geometry of Baker-Nunn stations in 1966 was poor in some regions. A series of station moves and subsequent observing programs produced a considerably improved geometrical determination, especially in South America. The data used in the dynamical solution were improved by a series of observations made specifically for this purpose, by an improvement in the reduction procedures, and by use of more accurate clocks at the stations.

A complete revision of the computer programs was initiated, with many of the theoretical aspects rediscussed.

Finally, the process of statistical inference was improved. Each type of data was treated consistently by establishing weights and covariances. Different sets of data were combined and relative weights were adopted, which improved the residuals for each set of data. For example, the terrestrial gravimetry was weighted so that the combined solution improved the orbits as well as reduced the RMS gravity-anomaly residuals. Once each type of data was internally consistent, reliability estimates could be established; and when each quantity had been determined by independent methods, a direct comparison of the estimates was possible. In this way, a realistic evaluation of the accuracy was possible.

In summary, a combination of four types of data gave the best estimate of geodetic parameters, and reliable estimates of the accuracy were provided by intercomparison. Further comparisons with data not used in the solution — orbital data, terrestrial gravimetry, astrogeodetic leveling, and triangulation — completely confirmed the accuracy obtained by intercomparison.

STRUCTURE OF THE PROCESS

The combination of four types of data is essentially an iterative process. The initial values for the gravity field and station coordinates were taken from the 1966 M1 solution, as modified by some resonant harmonics, and the C6 coordinates. The values of the zonal harmonics were revised by Kozai (1969) as a precursor to this analysis. In addition, three constants, defining the length and time scales — GM, a_e, and c — need to be chosen. Table 1 lists the coefficients and constants used throughout this analysis.

Figure 1 describes the information flow. Each component in Figure 1 is described in Gaposchkin and Lambeck (1970). The first two rows indicate very briefly the process before analysis. There are two major loops in the scheme. The large loop is a complete recalculation of the observation

TABLE 1. Adopted zonal harmonics to J(21) (Kozai, 1969).

J(2) = 1.08262800E-03	J(3) = -2.5380E-06
J(4) = -1.5930E-06	J(5) = -2.3000E-07
J(6) = 5.0200E-07	J(7) = -3.6200E-07
J(8) = -1.1800E-07	J(9) = -1.0000E-07
J(10) = -3.5400E-07	J(11) = 2.0200E-07
J(12) = -4.2000E-08	J(13) = -1.2300E-07
J(14) = -7.3000E-08	J(15) = -1.7400E-07
J(16) = 1.8700E-07	J(17) = 8.5000E-08
J(18) = -2.3100E-07	J(19) = -2.1600E-07
J(20) = -5.0000E-09	J(21) = 1.4400E-07

$GM = 3.986013 \times 10^{20}$ cm^3/sec^2

$a_e = 6.378155 \times 10^{6}$ m

$c = 2.997925 \times 10^{10}$ cm/sec

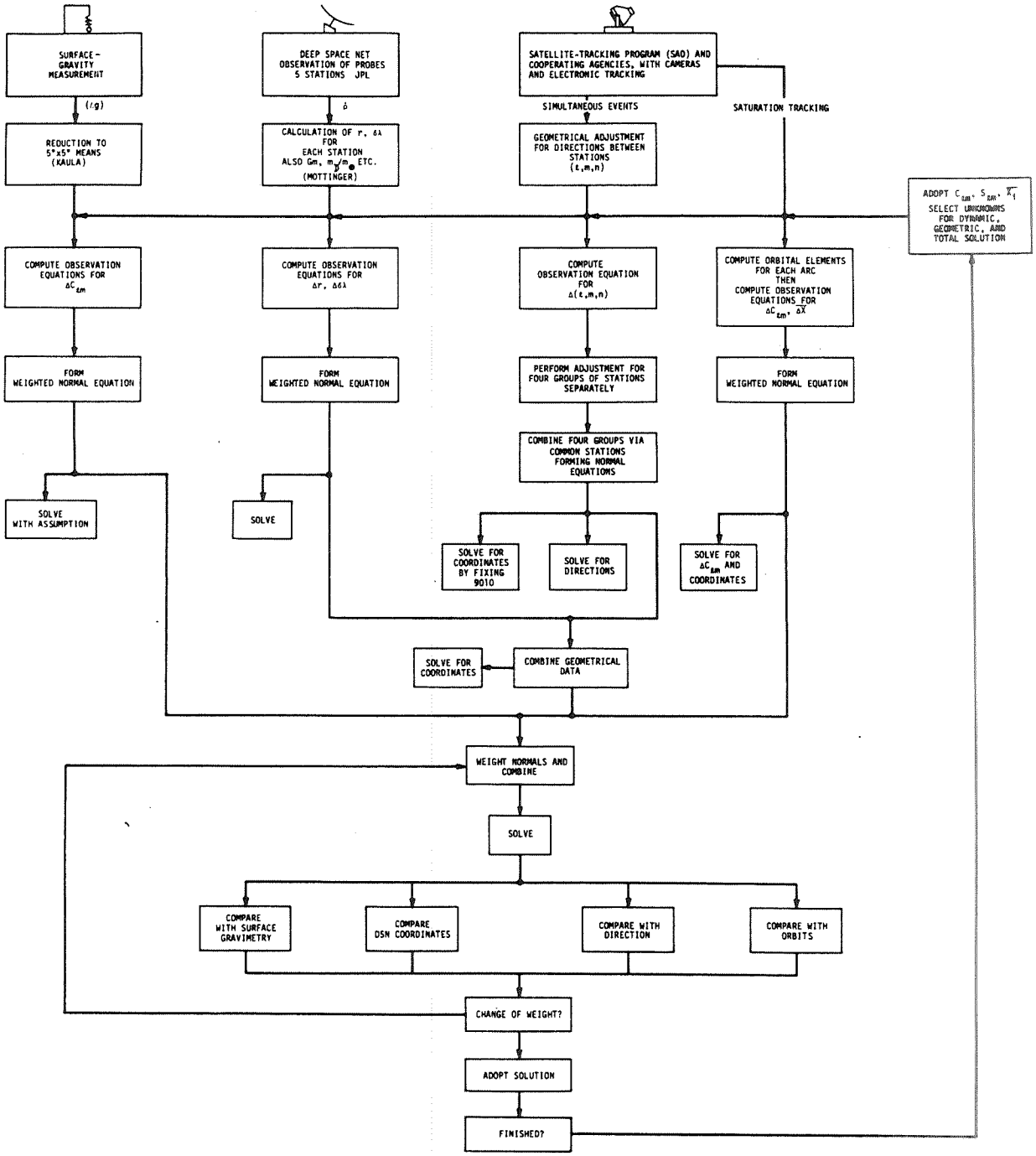

Fig. 1. Structure of the process.

equations and residuals and could be called an iteration. Each separate set of data is solved independently, with some assumptions when necessary. These solutions and residuals are compared.

The second, smaller loop is used to determine the appropriate relative weights of the four components. The weights are chosen, a solution is calculated, and the residuals are investigated. If revision is necessary, the weights are changed and another solution is made. At this point, certain orbital information and geometric data may be either added or deleted if appropriate.

Each solution is compared with some independent orbits, as well as with the observations used in the solution and with the separate solutions themselves. In practice, five or six such solutions are calculated, and one is adopted for the subsequent analysis.

DATA USED

The position of the earth in the inertial reference frame is monitored, tabulated, and published in terms of pole position (x, y) and sidereal time (UT1) by the Bureau International de l'Heure (BIH), the United States Naval Observatory (USNO), and, for pole position only, the International Polar Motion Service (IPMS). The largest difference of the published values is 5 m in UT1, although it is impossible to tell what the correct values are and to establish further the real accuracy of these data. The position of the earth seems to be known to no better than several meters. The uncertainty in these data sets the limit of accuracy in station positions. For the analysis described here, we have adopted the UT1 data published by the BIH and the pole position published by the IPMS.

The locations of stations contributing satellite observations are indicated in Figure 2. There is a clustering of stations in North America and western Europe. Most of these stations contributed many simultaneous observations but of only a few satellites. These data were extremely valuable for a

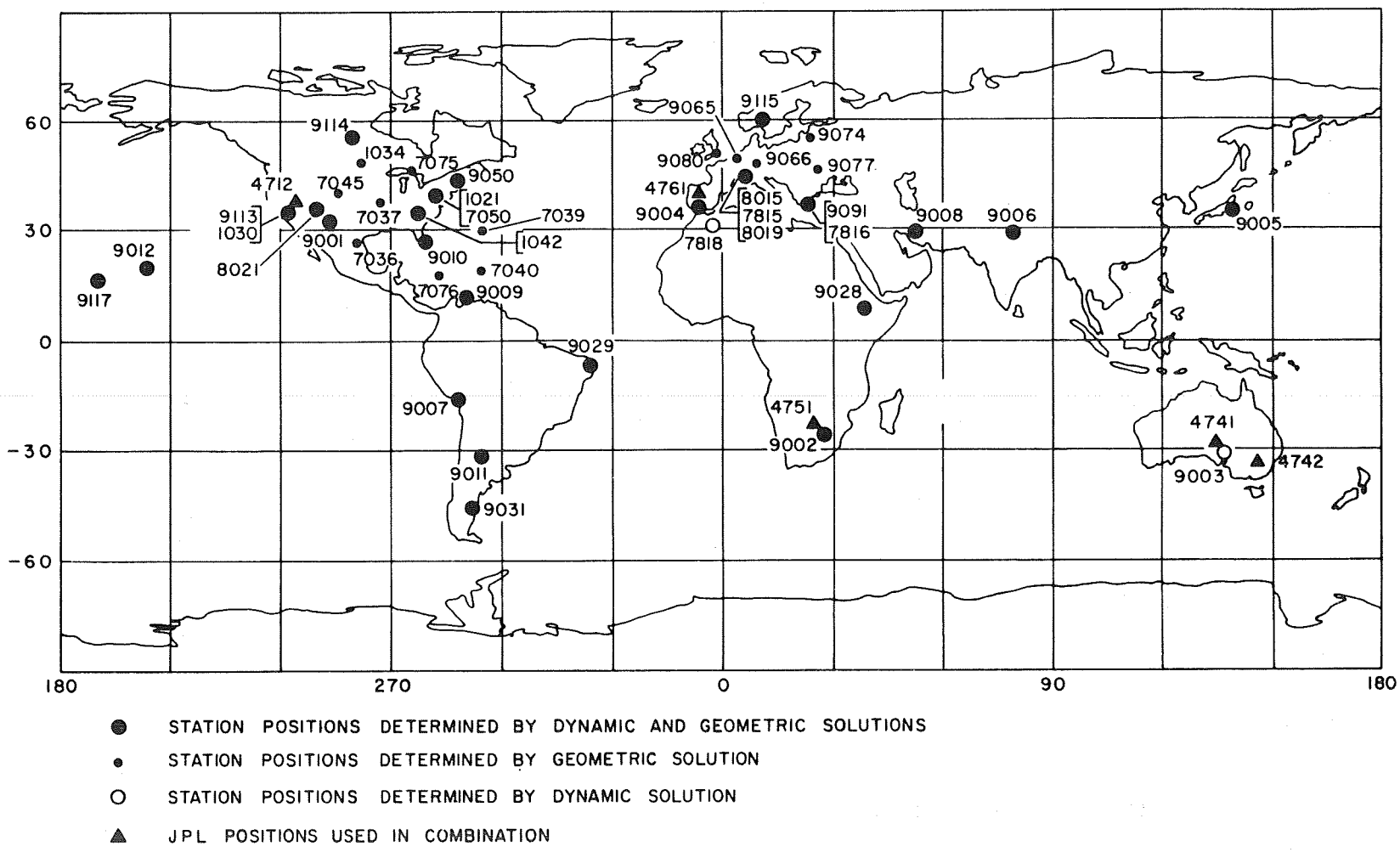

Fig. 2. Location of stations used in the combination solutions. Collocated stations are bracketed together.

geometrical net adjustment but were not appropriate for a dynamical determination of station coordinates. More than 50,000 observations were combined in the geometrical solution.

The final dynamical solution used more than 60,000 observed quantities on the 21 satellites listed in Table 2. The distribution of orbital characteristics is illustrated in Figure 3.

The DSN data from five stations were compiled by Mottinger (1969). Each DSN station can be related to a Baker-Nunn camera by the use of classical survey data. We then have for these stations additional observational constraints on the relative longitudes and the distance from the spin axis of the earth.

The terrestrial gravimetry data used in the solution were compiled by Kaula (1966) and consisted of 300-nautical-mile (n mi) free-air anomalies. His basic data consisted of $1° \times 1°$ mean free-air anomalies. The results were 935 mean anomalies for 300-n mi squares covering 56.5% of the globe.

Since the details of the analysis are given elsewhere, the following discussion is limited to the accuracy of the final results.

The final results for the geocentric cartesian station coordinates are given in Tables 3 and 4, and for the tesseral harmonics, in Table 5. Table 1 contains the precision estimates of the station coordinates, and Figure 4 gives the precision of the geoid height as a function of latitude. These estimates have been taken from the statistics of the final iteration, using the weighting factors from the combination, and are corroborated by all the intercomparisons. The geoid-height estimates, of course, refer to the generalized geoid only and do not imply that the geoid is known everywhere with this accuracy.

TABLE 2. Summary of dynamical data.

Satellite	Name or Other Designation	Inclination (deg.)	Eccentricity	Semimajor Axis (km)	Perigee Height (km)	Number of Arcs	Days/Arc	New Satellite	Select Files	Laser Data
6001301	Courier 1B 60 ν1	28	0.016	7465	965	6	30	X	X	
5900101	Vanguard 2 59 α1	33	0.165	8300	557	7	30		X	
6100401	61 δ1	39	0.119	7960	700	3	14			
6701401	D1D	39	0.053	7337	569	6	14	X	X	X
6701101	D1C	40	0.052	7336	579	4	14	X	X	X
6503201	Explorer 27 BE-C	41	0.026	7311	941	4	30	X	X	X
6000902	60 ι2	47	0.011	7971	1512	7	30			
6206001	Anna 1B 62 $\beta\mu$1	50	0.007	7508	1077	12	30		X	
6302601	Geophysical Research	50	0.062	7237	424	6	14			
6508901	Explorer 29 Geos 1	59	0.073	8074	1121	21	30	X	X	X
6101501	Transit 4A 61 o1	67	0.008	7318	885	8	30			
6101502	Injun 1 61 o2	67	0.008	7316	896	4	30			
6506301	Secor 5	69	0.079	8159	1137	2	30	X	X	
6400101		70	0.002	7301	921	3	30	X		
6406401	Explorer 22 BE-B	80	0.012	7362	912	2	30	X		X
6508101	OGO 2	87	0.075	7344	420	2	14	X		
6600501	Oscar 07	89	0.023	7417	868	1	30	X	X	
6304902	5BN-2	90	0.005	7473	1070	5	30	X		
6102801	Midas 4 61 $\alpha\delta$1	96	0.013	10005	3503	3	50			
6800201	Explorer 36 Geos 2	106	0.031	7709	1101	6	14	X		X
6507801	OV1 2	144	0.182	8306	416	2	14	X		
						114				

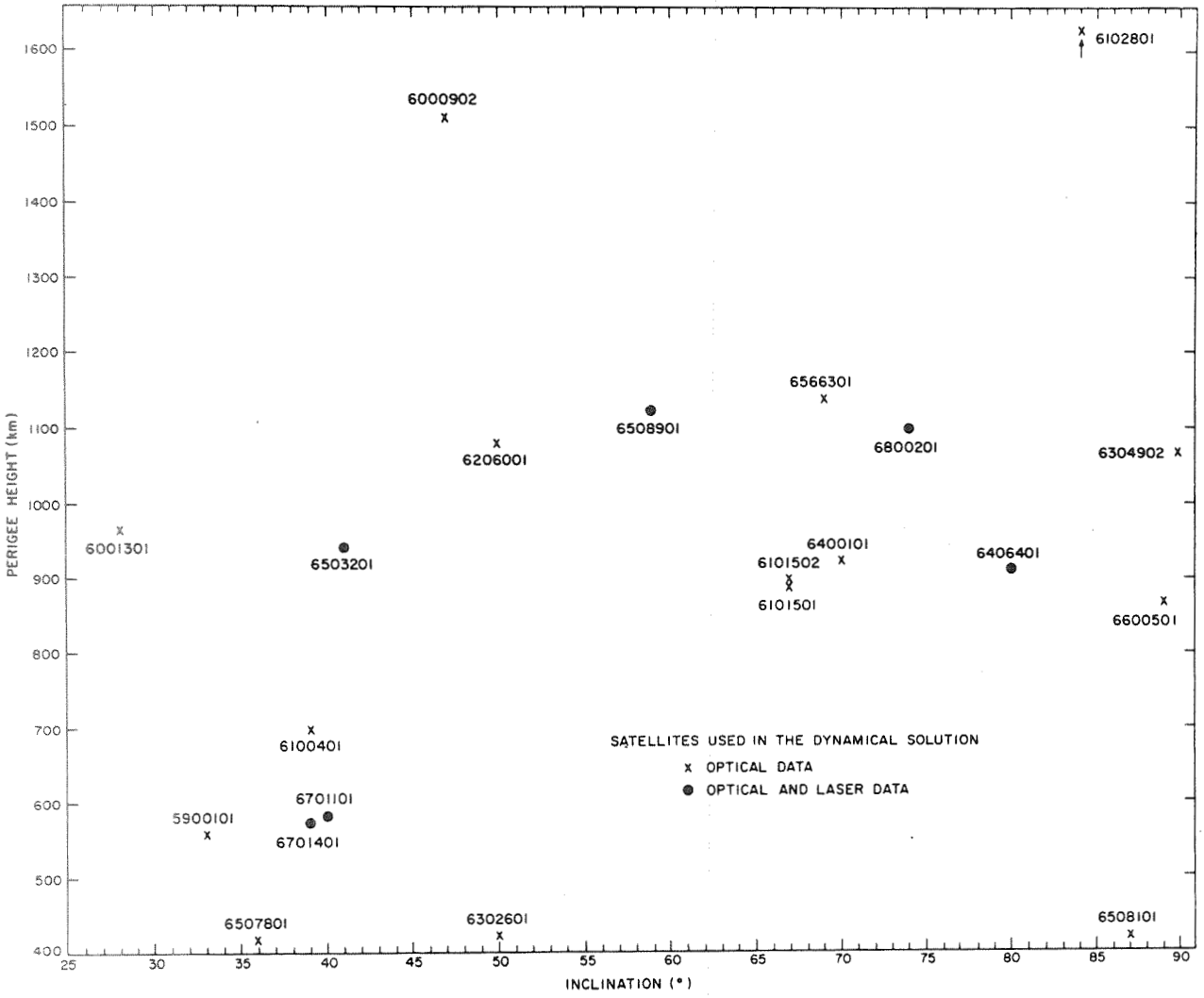

Fig. 3. Distribution of satellites used in the 1969 Smithsonian Standard Earth (II) (Gaposchkin and Lambeck, 1970).

TABLE 3. Geocentric coordinates (in Mm) of the stations determined in the final combination solution. The fifth column gives the formal precision estimates of the coordinates in meters.

Station	X	Y	Z	σ	Station Name
1021	1.118029	-4.876316	3.942984	7	BLOSSOM POINT, MD.
1034	-.521702	-4.242049	4.718731	7	GRAND FORKS, MINN.
1042	.647515	-5.177924	3.656707	7	ROSMAN, N. C.
7036	-.828496	-5.657458	2.816812	7	EDINBURG, TEX.
7037	-.191286	-4.967280	3.983262	7	COLUMBIA, MO.
7039	2.308239	-4.873597	3.394580	10	BERMUDA
7040	2.465067	-5.534924	1.985510	10	PUERTO RICO
7045	-1.240479	-4.760229	4.048995	9	DENVER, COL.
7050	1.130674	-4.831368	3.994111	7	Goddard Space Flight Center
7075	.692628	-4.347059	4.600483	9	SUDBURY, ONT.
7076	1.384174	-5.905685	1.966533	10	JAMAICA
7815	4.578370	.457951	4.403134	5	HAUTE PROVENCE, FRANCE
7816	4.654337	1.959134	3.884366	5	STEPHANION, GREECE
7818	5.426329	-.229330	3.334608	15	COLOMB-BECHAR, ALGERIA
7901	-1.535757	-5.166996	3.401042	5	ORGAN PASS, N.M.
8015	4.578328	.457966	4.403179	5	HAUTE PROVENCE, FRANCE
8019	4.579466	.586599	4.386408	5	NICE, FRANCE
9001	-1.535757	-5.166996	3.401042	5	ORGAN PASS, N.M.
9002	5.056125	2.716511	-2.775784	7	PRETORIA, S.AFRICA
9003	-3.983776	3.743087	-3.275566	6	WOOMERA, AUSTRALIA
9004	5.105588	-.555228	3.769667	5	SAN FERNANDO, SPAIN
9005	-3.946693	3.366299	3.698832	10	TOKYO, JAPAN
9006	1.018203	5.471103	3.109623	9	NAINI TAL, INDIA
9007	1.942775	-5.804081	-1.796933	7	AREQUIPA, PERU
9008	3.376893	4.403976	3.136250	9	SHIRAZ, IRAN
9009	2.251829	-5.816919	1.327160	7	CURACAO, ANTILLES
9010	.976291	-5.601398	2.880240	5	JUPITER, FLA.
9011	2.280589	-4.914573	-3.355426	9	VILLA DOLORES, ARGENTINA
9012	-5.466053	-2.404282	2.242171	7	MAUI, HAWAII
9021	-1.936782	-5.077704	3.331916	15	MT. HOPKINS, ARIZ.
9023	-3.977766	3.725102	-3.303035	6	ISLAND LAGOON, AUSTRALIA
9025	-3.910437	3.376361	3.729217	10	DODAIRA, JAPAN
9028	4.903750	3.965201	.963872	12	ADDIS ABABA, ETHIOPIA
9029	5.186461	-3.653856	-.654325	12	NATAL, BRAZIL
9031	1.693803	-4.112328	-4.556649	15	COMODORO RIVADAVIA, ARGENTINA
9050	1.489753	-4.467478	4.287304	14	HARVARD, MASS.
9065	3.923411	.299882	5.002945	12	DELFT, HOLLAND
9066	4.331310	.567511	4.633093	7	ZIMMERWALD, SWITZERLAND
9074	3.183901	1.421448	5.322772	10	RIGA, LATVIA
9077	3.907421	1.602397	4.763890	10	UZGHOROD, U.S.S.R.
9080	3.920178	-.134738	5.012708	9	MALVERN, ENGLAND
9091	4.595157	2.039425	3.912650	5	DIOYSOS, GREECE
9113	-2.450011	-4.624421	3.635035	7	ROSAMUND, CAL.
9114	-1.264838	-3.466884	5.185467	12	COLD LAKE, CANADA
9115	3.121280	.592643	5.512701	17	Harestua, Norway
9117	-6.007402	-1.111859	1.825730	15	JOHNSTON ISL., PACIFIC

TABLE 4. Coordinates of the JPL stations referred to the SAO reference system.

Station	X (Mm)	Y (Mm)	Z (Mm)
4751	5.085451	2.668252	-2.768728
4741	-3.978706	3.724858	-3.302213
4742	-4.460972	2.682424	-3.674618
4761	4.849242	-0.360290	4.114869
4712	-2.350454	-4.651975	3.665631

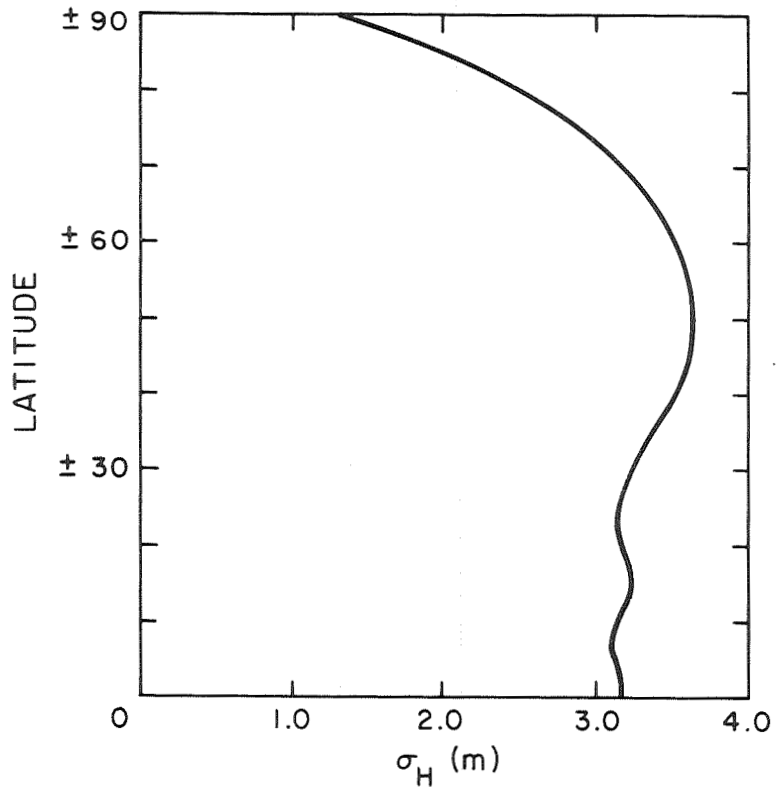

Fig. 4. Precision estimates of geoid heights determined from the harmonic coefficient precision estimates.

TABLE 5. Fully normalized coefficients of the spherical harmonic expansion of the geopotential obtained in the final iteration of the combination solution. $C_{\ell m}$ are the cosine terms of degree ℓ and order m and $S_{\ell m}$ are the sine terms.

ℓ	m	$C_{\ell m}$	$S_{\ell m}$	ℓ	m	$C_{\ell m}$	$S_{\ell m}$
2	2	2.4129E-06	-1.3641E-06	3	1	1.9698E-06	2.6015E-07
3	2	8.9204E-07	-6.3468E-07	3	3	6.8630E-07	1.4304E-06
4	1	-5.2989E-07	-4.8765E-07	4	2	3.3024E-07	7.0633E-07
4	3	9.8943E-07	-1.5467E-07	4	4	-7.9692E-08	3.3928E-07
5	1	-5.3816E-08	-9.7905E-08	5	2	6.1286E-07	-3.5087E-07
5	3	-4.3083E-07	-8.6663E-08	5	4	-2.6693E-07	8.3010E-08
5	5	1.2593E-07	-5.9910E-07	6	1	-9.8984E-08	3.7652E-08
6	2	5.4825E-08	-3.5175E-07	6	3	2.7873E-08	4.4626E-08
6	4	-4.0342E-10	-4.0388E-07	6	5	-2.1143E-07	-5.2264E-07
6	6	8.8693E-08	-7.4756E-08	7	1	2.4142E-07	1.1567E-07
7	2	2.8306E-07	1.5645E-07	7	3	2.0285E-07	-2.3448E-07
7	4	-1.9727E-07	-1.1390E-07	7	5	-8.7024E-10	9.8461E-08
7	6	-2.5847E-07	1.0209E-07	7	7	1.5916E-07	-6.7710E-08
8	1	3.1254E-08	2.5696E-08	8	2	4.8161E-08	8.4140E-08
8	3	-5.7444E-08	1.8086E-08	8	4	-1.5378E-07	7.5264E-08
8	5	-5.6733E-08	6.1636E-08	8	6	-5.3903E-08	2.5930E-07
8	7	3.4390E-08	8.9168E-08	8	8	-7.7364E-08	6.7607E-08
9	1	1.3823E-07	-1.6100E-08	9	2	6.6741E-09	-8.1733E-08
9	3	-9.6463E-08	-1.1817E-07	9	4	5.7125E-08	1.1183E-07
9	5	-6.1435E-09	3.3551E-09	9	6	2.4186E-08	2.2028E-07
9	7	-5.0450E-08	-1.2700E-07	9	8	2.3359E-07	5.7239E-08
9	9	-8.2490E-08	9.2326E-08	10	1	1.1251E-07	-1.0167E-07
10	2	-3.1225E-08	-1.0450E-07	10	3	-2.3346E-08	-1.4137E-07
10	4	-4.8185E-08	-4.3248E-08	10	5	-8.0004E-08	-1.4279E-07
10	6	-3.2486E-08	-2.0153E-07	10	7	5.4961E-08	3.2003E-08
10	8	7.3957E-08	-7.9706E-08	10	9	-6.8563E-09	6.2498E-09
10	10	1.2377E-07	-2.9885E-08	11	1	4.3900E-09	2.9751E-08
11	2	4.8900E-08	-9.1994E-08	11	3	-6.3247E-08	-1.3109E-07
11	4	-3.0193E-08	5.4317E-08	11	5	3.2523E-08	1.3215E-07
11	6	3.7517E-08	6.9005E-09	11	7	4.5726E-08	-1.3862E-07
11	8	6.4546E-08	-1.6993E-08	11	9	1.1750E-07	-9.9451E-09
11	10	-1.1736E-07	-1.8900E-08	11	11	1.1785E-07	-4.0688E-08
12	1	-4.5955E-08	-3.1000E-08	12	2	2.7481E-08	7.5986E-08
12	3	5.8386E-08	5.4784E-08	12	4	-4.3649E-08	-2.2262E-08
12	5	2.3375E-08	4.2637E-08	12	6	-2.3868E-08	-6.6770E-10
12	7	1.4507E-08	9.9784E-08	12	8	-5.7854E-09	3.3752E-08
12	9	-3.2232E-08	4.2858E-08	12	10	-1.8590E-08	4.8382E-09
12	11	-4.4921E-08	-4.8206E-08	12	12	-1.9407E-08	-5.7771E-08
13	1	-5.6042E-08	2.6288E-08	13	2	-4.7456E-08	1.7367E-08
13	3	2.3833E-08	-2.8930E-08	13	4	-1.9980E-08	5.7030E-08
13	5	9.6637E-08	-4.7760E-08	13	6	-8.3417E-08	5.9782E-08
13	7	-5.2217E-08	-3.2562E-09	13	8	-4.1759E-08	-2.0231E-08
13	9	-2.5623E-08	1.0767E-07	13	10	8.6589E-08	-1.0528E-08
13	11	-3.3749E-08	5.8541E-08	13	12	-1.3229E-09	8.2192E-08
13	13	-7.0288E-08	7.4643E-08	14	1	-2.3090E-08	4.9664E-08
14	2	3.2120E-08	-4.5289E-08	14	3	1.9042E-08	1.1919E-09
14	4	7.8017E-09	-3.7527E-08	14	5	-2.5958E-08	-2.3344E-08
14	6	1.9140E-08	-5.8721E-08	14	7	1.1061E-08	8.4132E-09
14	8	-3.0273E-08	-6.0838E-08	14	9	4.9539E-08	9.2345E-08
14	10	5.3732E-08	-4.3168E-08	14	11	2.7833E-08	-8.1637E-08
14	12	1.2481E-08	-5.7314E-08	14	13	5.1554E-08	4.5453E-08
14	14	-5.2082E-08	-1.2840E-08	15	1	-3.5971E-09	4.0142E-08
15	2	-4.4833E-08	-1.6056E-08	15	3	8.3016E-09	-5.7218E-09
15	4	1.3916E-08	6.6644E-08	15	5	3.1684E-08	1.8250E-09
15	6	7.0020E-08	-1.1872E-07	15	7	1.1856E-07	4.2690E-08
15	8	-9.7657E-08	-3.5710E-08	15	9	2.2064E-08	2.6632E-08
15	10	-2.0648E-08	5.3724E-10	15	11	-3.2585E-08	9.4052E-08
15	12	1.0524E-08	6.8726E-09	15	13	-3.7348E-08	4.0249E-09
15	14	1.2193E-08	-2.6786E-08	15	15	1.4515E-09	-1.4802E-08
16	1	-2.3789E-08	7.6413E-08	16	2	2.1327E-08	3.0669E-08
16	3	-4.7358E-08	3.2610E-08	16	4	-1.1591E-08	4.3001E-08
16	5	-4.4201E-08	3.2230E-08	16	6	-5.8439E-08	-4.2809E-08
16	7	1.0591E-07	8.1008E-09	16	8	-8.4738E-08	-2.4677E-09
16	9	9.0001E-09	-1.0628E-07	16	10	-2.9849E-08	-5.2467E-10
16	11	6.8502E-09	-7.0765E-08	16	12	2.2834E-08	-3.4087E-08
16	13	3.5475E-08	2.0683E-08	16	14	-7.3590E-09	-2.2626E-08
16	15	-3.5485E-08	8.4126E-10	16	16	-2.9522E-08	8.6217E-09
17	12	8.3097E-08	3.5424E-09	17	13	3.2749E-08	4.2920E-10
17	14	-1.6058E-08	2.7286E-08	18	12	1.1662E-08	8.4724E-09
18	13	4.6903E-09	-3.5547E-08	18	14	-2.7446E-08	-4.8376E-08
19	12	6.7115E-08	-8.2623E-09	19	13	3.3201E-08	-6.3128E-08
19	14	-3.9779E-09	-2.3817E-08	20	13	5.8374E-08	3.3320E-08
20	14	1.1130E-08	-1.6183E-08	21	13	3.6928E-09	-1.6288E-08
21	14	5.2067E-08	3.0801E-10	22	14	-8.0549E-09	2.6440E-08

COMPARISON WITH SATELLITE ORBITS

Each iteration resulted in improved orbital residuals using the combination solution. For the final solution, the orbital residuals for satellites such as Geos 1 and Geos 2 are less than 10 m. These 30-day orbits are computed from a combination of laser and Baker-Nunn data. The optical-data residuals have an RMS less than 3 arcsec, and the laser data residuals have an RMS value of 7 m. These residuals are, of course, made up of observation errors, model errors, errors in station coordinates, and errors in the gravity field.

COMPARISON OF GEOMETRIC AND DYNAMIC SATELLITE SOLUTIONS

Figure 5 compares directions between stations resulting from the geometric solution (△), the dynamic solution (□), and the combination solution (◇). The difference in the positions derived from the individual solutions is a good indication of their relative accuracies and of the accuracy of the combination solution. These differences result from uncertainties in the coordinates at both stations, and at each station a number of such comparisons can usually be made. The comparisons shown here are the most unfavorable in that the errors of both stations are reflected in the comparison. Thus, the accuracy of the station positions of the combination solution, relative to the earth's center of mass, should be somewhat better than these figures indicate.

These comparisons indicate that for the fundamental Baker-Nunn stations (those numbered 9001 to 9012 and 9023) the combination-solution coordinates should be reliable to better than 10 m. For the new Baker-Nunn stations (9021, 9028, 9029, 9031, and 9091), from which there are fewer observations, the combination-solution coordinates should be accurate to better than 15 m. These estimates are in agreement with the formal statistics given in Table 3. The longitude difference between the two satellite solutions obtained from the combination solution is -0.2 ± 0.5 μrad and is not significant.

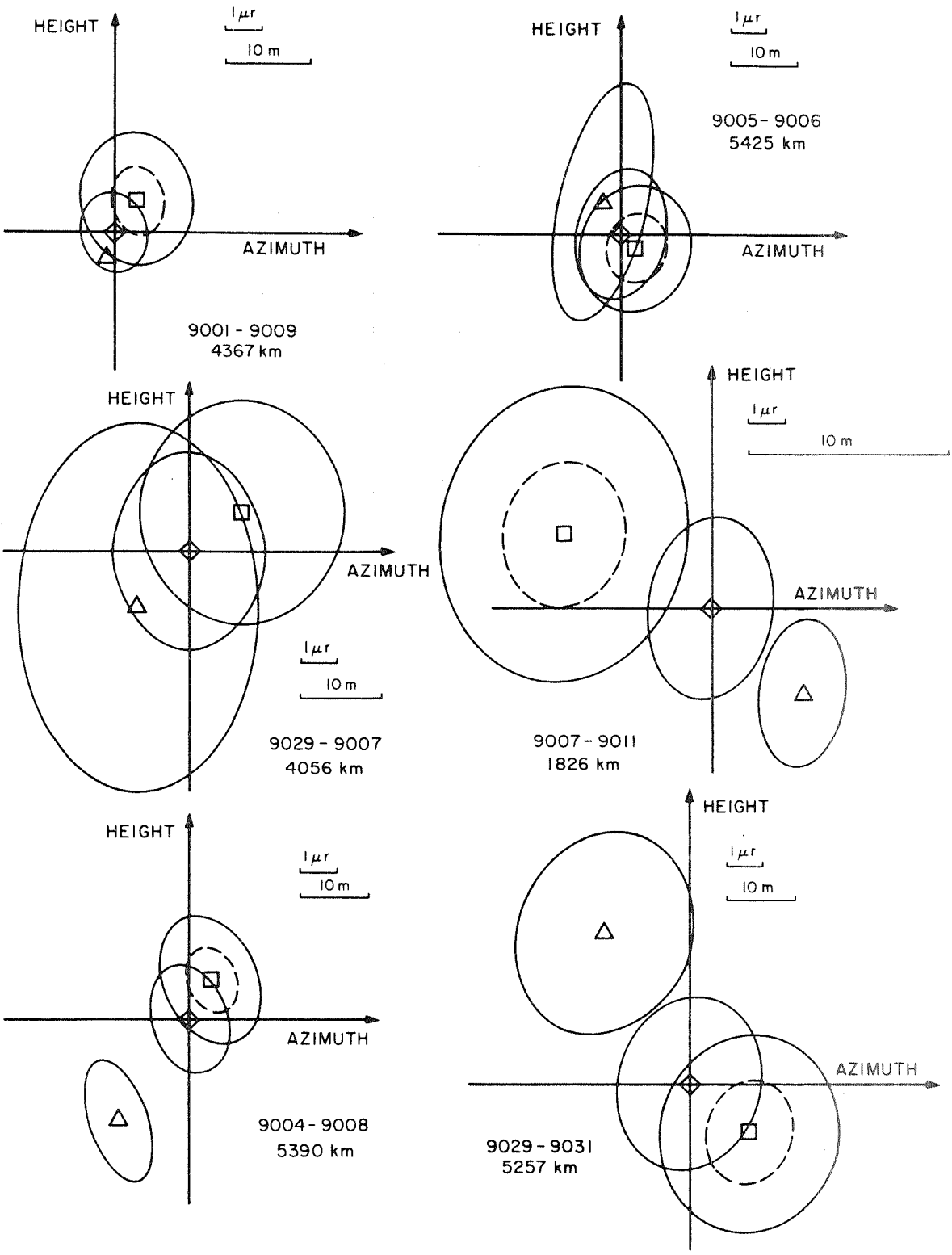

Fig. 5. Comparisons for station-station vectors computed from the geometric solution △, the dynamic solution □, and the combination solution ◇. The two error ellipses centered at □ refer to the formal statistics of the dynamic solution (the inner ellipse) and after the covariance matrix has been multiplied by the factor k_1^2 (outer ellipse).

COMPARISON OF SATELLITE AND DSN SOLUTIONS

The DSN sites can be related to Baker-Nunn station positions by ground survey. For three station groups (9002-4751), (9003-4741), and (9113-4712), the distance between the two instrumentation types does not exceed 200 km. For the other two groups (9003-4742) and (9004-4761), the distances are larger, about 500 and 1000 km, respectively, and uncertainties in the ground-survey information may influence the comparison results. Table 6 gives the results in the form of differences in longitude $\Delta\lambda_i$ and in distance to the earth's instantaneous rotation axis Δr_i. The table also gives the accuracy estimates deduced from the statistics of the two solutions and the ground-survey data. The comparisons reflect a systematic longitude difference, $\overline{\Delta\lambda} = -3.2$ μrad (the DSN longitudes are east of the SAO longitudes). When this systematic part is removed, the residuals are all less than about 10 m and support the accuracy estimates given in Table 3 for the Baker-Nunn stations 9002, 9003, 9004, and 9113.

COMPARISON WITH TERRESTRIAL GRAVIMETRY

Table 7 summarizes the comparison of the geopotential derived from (1) the new combination solution presented here, (2) the new satellite solution, and (3) the 1966 Standard Earth solution (also known as the M1 solution), using 300-n mi squares, for which at least 20 surveyed 60-n mi squares were available for the compilation. The comparisons are made for the three fields truncated at different degrees as well as for the total fields.

The quantities in Table 7 have been defined by Kaula (1966) and Gaposchkin and Lambeck (1970). Briefly, g_T is the terrestrial gravity anomaly and g_S is the satellite or combination solution anomaly; ϵ_T and ϵ_S are the expected errors in the estimates g_T and g_S, and δg is the expected truncation error. The estimate D of the gravity field contained by the spherical-harmonic expansion is obtained from the surface gravity. If both the satellite solution and the surface gravity give "perfect" results for all terms up to a certain degree, then

TABLE 6. Results of SAO-JPL stations comparison. $\Delta\lambda_i$ is the longitude difference and Δr_i the difference in distance to the earth's axis of rotation for the two solutions. $\overline{\Delta\lambda}$ is the weight mean longitude difference.

Stations	$\lambda_{SAO}-\lambda_{JPL}=\Delta\lambda_i$ (μrad)	$\overline{\Delta\lambda}-\Delta\lambda_i$ (μrad)	(μrad) (m)	$\sigma_{\Delta\lambda_i}$ (m)	$r_{SAO}-r_{JPL}=\Delta r_i$ (m)	$\sigma_{\Delta r_i}$ (m)
4751-9002	-3.5	+0.3	+1.9	7.7	+5.9	4.9
4741-9003	-2.2	-0.9	-5.2	6.8	-7.3	4.5
4742-9003	-1.2	-2.0	-10.4	9.0	-6.5	4.5
4761-9004	-4.5	+1.4	+6.9	6.6	-1.2	4.5
4712-9113	-4.9	+1.7	+9.2	12.4	+7.6	5.5

TABLE 7. Comparison of satellite and combination solutions with surface-gravity measurements ($mgal^2$).

Solution	$\langle (g_T - g_S)^2 \rangle$	$\langle g_T g_S \rangle$	$\langle g_S^2 \rangle$	D	$\langle g_T^2 \rangle$	$E\{\epsilon_S^2\}$	$E\{\epsilon_T^2\}$	$E\{\delta g^2\}$
		$n \geq 20$, N = 136, 300-n mi squares						
Combination Solution								
$\ell \leq 8$ $m \leq 8$	165	90	92	102	253	2	11	152
$\ell \leq 10$ $m \leq 10$	132	119	116	120	253	-3	11	123
$\ell \leq 11$ $m \leq 11$	135	126	134	126	253	8	11	116
$\ell \leq 12$ $m \leq 12$	134	129	138	129	253	9	11	113
$\ell \leq 14$ $m \leq 14$	109	156	166	146	253	10	11	87
$\ell \leq 16$ $m \leq 16$	75	184	186	163	253	2	11	58
		$n \geq 20$, N = 136, 300-n mi squares						
Satellite Solution								
$\ell \leq 8$ $m \leq 8$	179	86	98	102	253	12	11	156
$\ell \leq 10$ $m \leq 10$	145	109	110	120	253	1	11	133
$\ell \leq 11$ $m \leq 11$	151	115	126	126	253	11	11	127
$\ell \leq 12$ $m \leq 12$	163	111	128	129	253	17	11	131
$\ell \leq 14$ $m \leq 14$	173	117	150	146	253	33	11	125
Total Field	177	118	161	143	253	43	11	124
		$n \geq 20$, N = 136, 300-n mi squares						
M1 Solution								
$\ell \leq 8$ $m \leq 8$	168	85	85	102	253	0	11	157
Total Field	168	93	101	108	253	7	11	148

$$\langle g_S^2 \rangle = \langle g_T g_S \rangle = D$$

and

$$E\{\epsilon_S^2\} = E\{\epsilon_T^2\} = 0 \quad .$$

The combination solution gives the best results, in that there is good agreement between the three estimates $\langle g_S^2 \rangle$, $\langle g_T g_S \rangle$, and D of the true value of the contribution to the gravity anomaly from the geopotential coefficients. Also, the $E\{\epsilon_T^2\}$ and $E\{\epsilon_S^2\}$ are small. This might have been expected, since the combination solution contains the data against which the tests were made.

The estimates of the errors of omission $E\{\delta g^2\}$ are still quite large compared to the estimates of ϵ_S^2 and ϵ_T^2, a fact that indicates that the surface-gravity data contain some additional information that has not been extracted in this solution.

There is no significant difference between the satellite solution, the combination solution, and the M1 solution truncated to 8,8. Beyond degree 10, the combination is superior and the high-degree terms are determined primarily by the surface-gravity data.

Further comparisons with surface gravimetry are possible. There are compilations by Talwani and Le Pichon (1969) for the Atlantic Ocean and by Le Pichon and Talwani (1969) for the Indian Ocean. Figure 6 shows free-air gravity-anomaly profiles computed from 5° × 5° area means obtained from these compilations and from the combination solution. All profiles are referenced to the international gravity formula. The accuracy of the 5° × 5° area means is assumed to be 5 mgals. Table 8 gives $\langle (g_S - g_T)^2 \rangle$ for each of these profiles, and from these numbers the accuracy of the gravity anomalies computed from the combination solution can be determined. The average value is 10 mgal, or about 3.5 m in geoid height, in very good agreement with the value $\sqrt{75}$ mgal taken from Table 7.

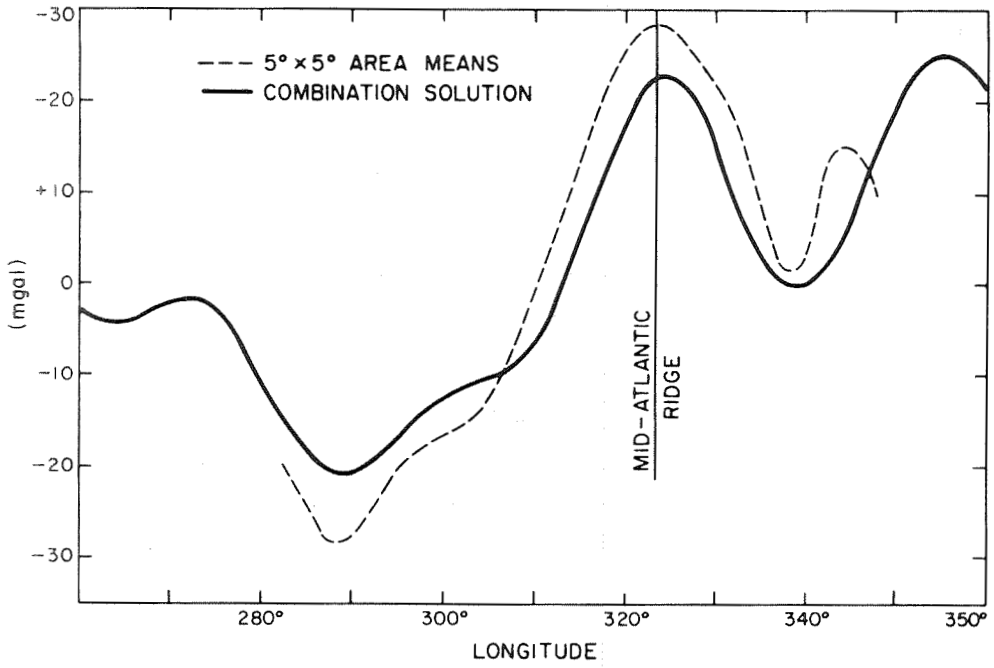

North Atlantic
$\Phi = +32.5$

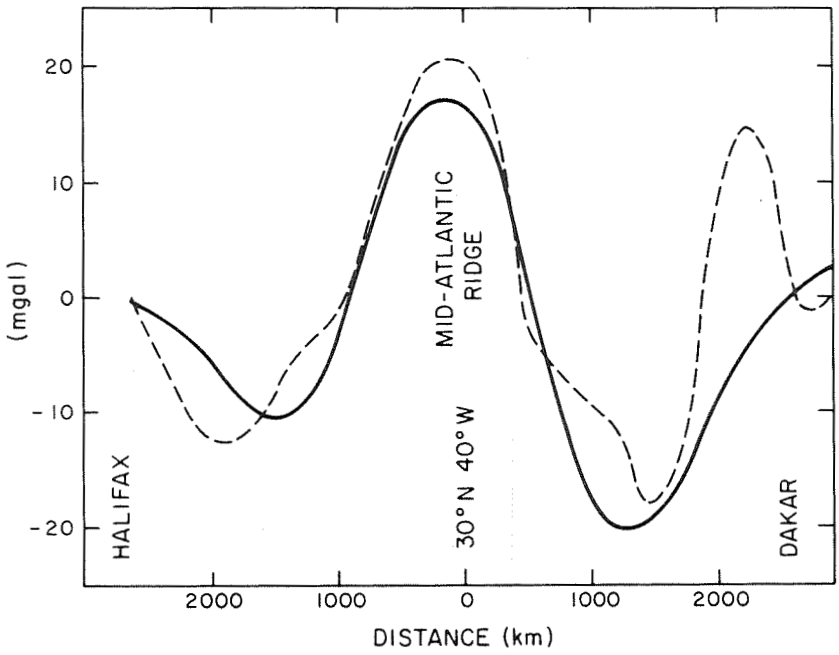

North Atlantic
Northwest–Southeast
Profile from Halifax to Dakar

Fig. 6. Comparisons of continuous gravity profiles from shipboard measurements compiled by Talwani and Le Pichon (broken lines) with profiles computed from the combination solution (solid lines).

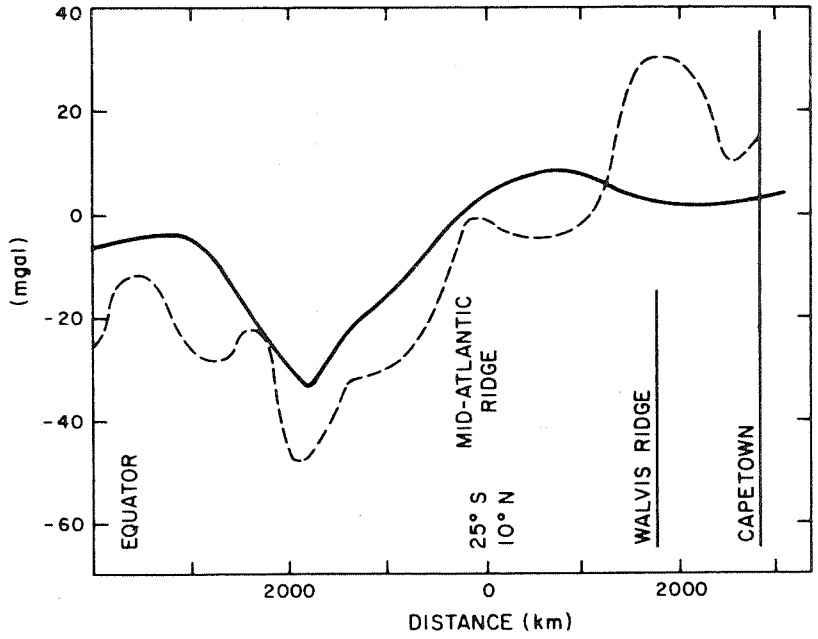

South Atlantic
Northwest–Southeast
Profile from Equator to Capetown

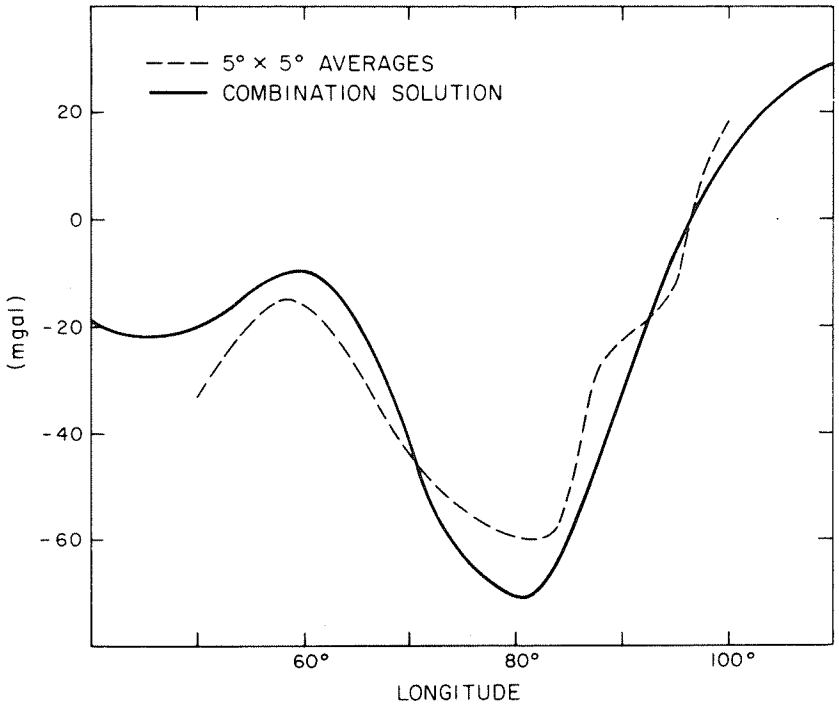

Indian Ocean
$\Phi = 0°$

Fig. 6 (Cont.)

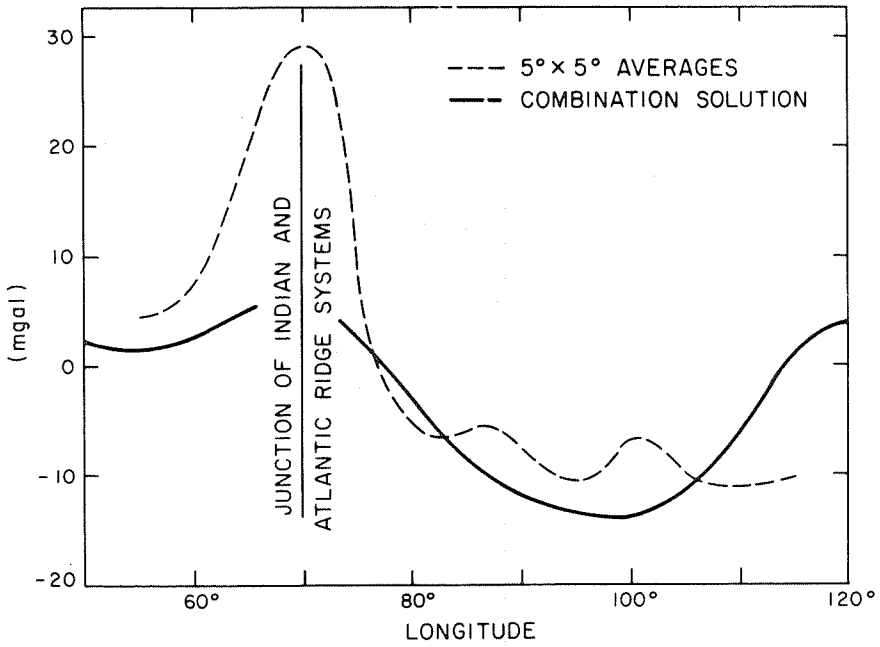

Indian Ocean
$\Phi = -25°$

Fig. 6 (Cont.)

TABLE 8. Summary of comparisons between surface-gravity measurements g_T by Talwani and Le Pichon and gravity anomalies g_S computed from the combination solution for selected profiles.

Profile	$\langle (g_S - g_T)^2 \rangle$ (mgal^2)	$\sigma^2_{g_T}$ (mgal^2)	$\sigma^2_{g_S} = \langle (g_S - g_T)^2 \rangle - \sigma^2_{g_T}$ (mgal^2)
$\phi = 32.5$ North Atlantic	84	25	59
NW-SE North Atlantic	68	25	43
NW-SE South Atlantic	222	25	197
$\phi = 0°$ Indian Ocean	80	25	55
$\phi = -25°$ Indian Ocean	166	25	144
			$(\sigma^2_{g_S})_{AV} = 99$ mgal$^2 \approx 10$ m^2

COMPARISON WITH ASTROGEODETIC DATA

Geoid heights obtained from astrogeodetic leveling are available for several major datums. These data, like the surface-gravity data, could be used as further input to the combination solution. However, the coverage extends only to areas where reliable surface-gravity data are also available, and the contribution to the global solution would be limited. Instead, the astrogeodetic data have been used for comparison purposes, thus providing an independent estimate of the accuracy of the global solution.

For comparison, these geoids must be transformed to a geocentric reference system. Such a transformation can be established through a comparison of geodetic datum coordinates with coordinates derived from satellite analyses (Lambeck, 1970).

Figure 7 gives the geoids and the difference once the adjustment has been made. Table 9 gives the numerical differences; the $\sqrt{10.5}$ m is in excellent agreement with other accuracy estimates.

POWER SPECTRA

Table 10 gives the degree variances of the solution. As usual, the gravimetric solution gives underestimates of the degree variances. Figure 8 plots the same information, in addition to the $10^{-5}/\ell^2$ law, which fits the data very well. The standard deviation for each degree is also plotted. It is apparent that between degrees 18 and 20 the amplitude of the harmonic coefficients will be smaller than their uncertainties. The same limit is seen by an examination of $E\{\delta g^2\}$ from Table 7. We can estimate that the remaining 58 $mgal^2$ of information is completely contained in degrees 17 through 20. This is to some extent surprising, since we would expect that as 20th-degree terms have a half-wavelength of 9°, 5° × 5° anomalies would contain information of greater detail. Surface gravimetry certainly has a great deal of high-frequency detail. The methods for reducing the data to 1° × 1° squares and then to 5° × 5° squares may smooth the higher frequency data, or it

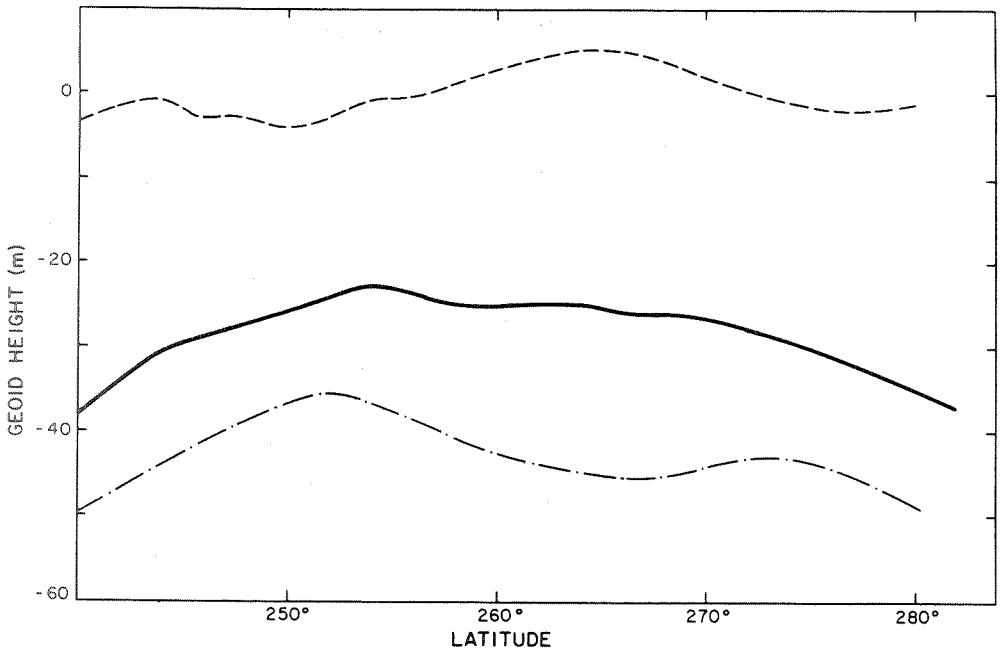

$\phi = 35°$

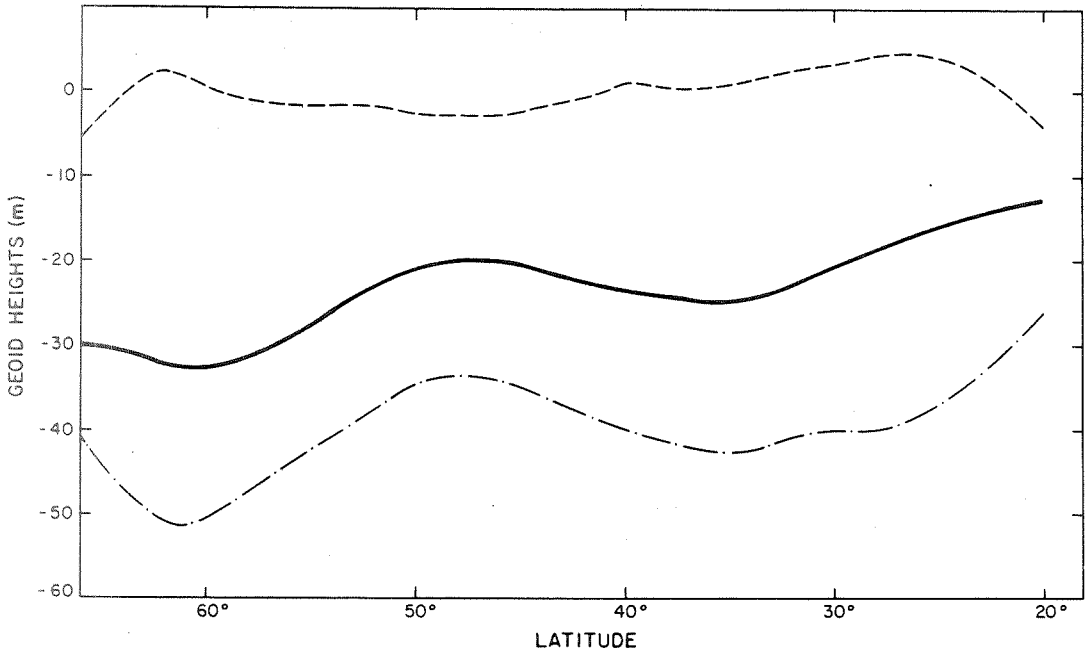

$\lambda = 260°$

North American Datum

Fig. 7. Comparisons between geoid profiles obtained from the combination solution (solid lines) with profiles obtained from astrogeodetic measurements transformed into the global reference system (dashed lines). The difference between the two profiles, after the systematic part has been subtracted, is indicated by the dotted line.

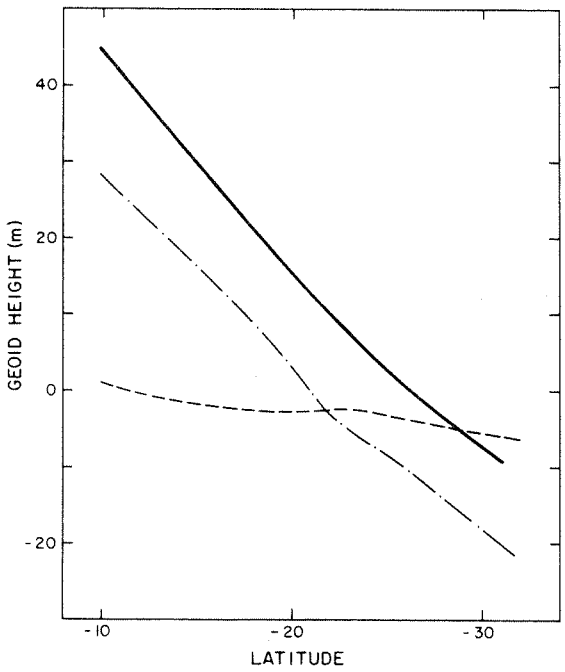

$\lambda = 136.^{\circ}25$

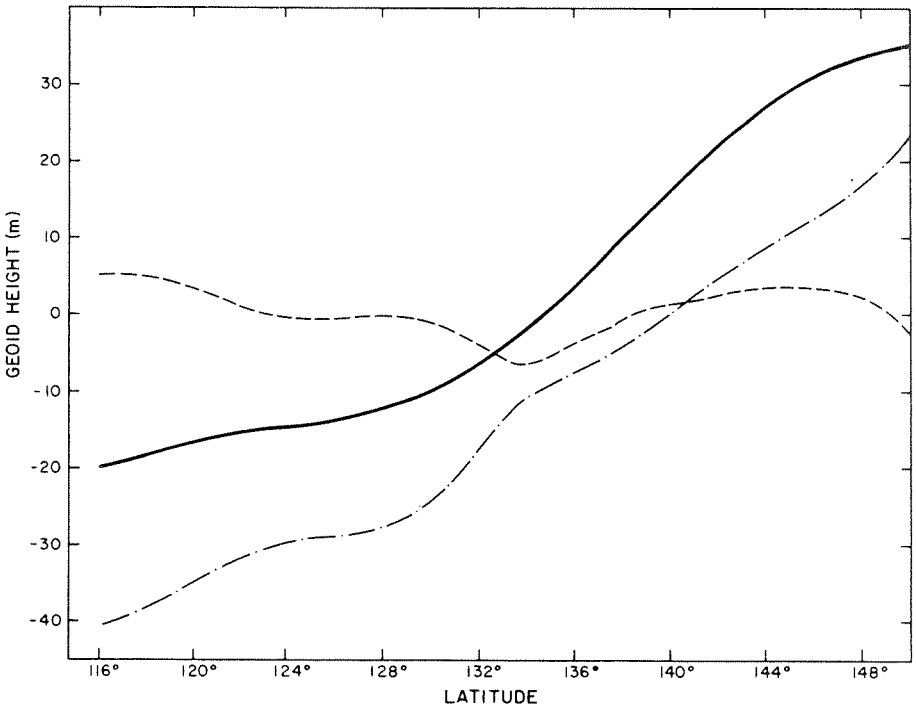

$\phi = -28.^{\circ}75$

Australian Geodetic Datum

Fig. 7 (Cont.)

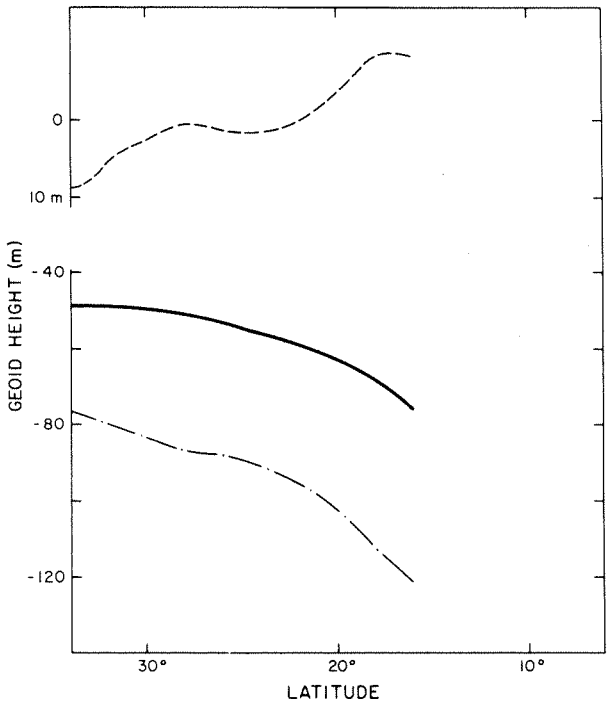

$\lambda = 75°$

Indian Datum

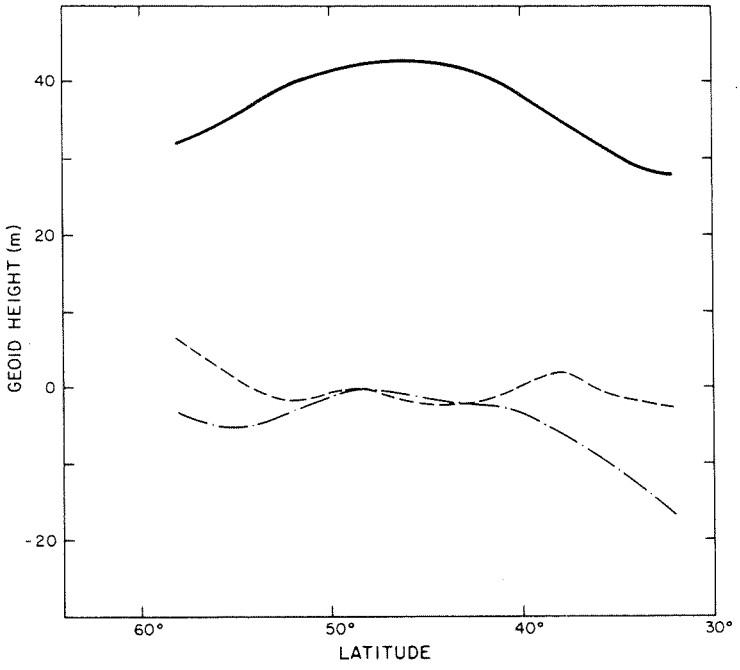

$\lambda = 16°$

European Datum

Fig. 7 (Cont.)

TABLE 9. Summary of the comparisons between the geoid profiles obtained from the combination solution and the astrogeoids referred to the geocentric system. $\overline{\Delta h}$ is the systematic height difference between the profiles, $\sigma^2_{\delta h}$ the variance of the difference between the two profiles, σ^2_a the variance of the astrogeoid heights, and σ^2_S the contribution of the combination solution to $\sigma^2_{\delta h}$.

Datum	Profile	$\overline{\Delta h}$	$\sigma^2_{\delta h}$	σ^2_a	$\sigma^2_S = \sigma^2_{\delta h} - \sigma^2_a$
NAD	$\phi = 35°$	-15	8	1.5	6.5
NAD	$\lambda = 260°$	-16	6	1.5	4.5
AGD	$\phi = -28.^\circ75$	-12	10	1.5	8.5
AGD	$\lambda = 136.^\circ25$	-12	12	1.5	10.5
IND	$\lambda = 75°$	-36	30	1.5	28.5
EUR	$\lambda = 16°$	-42	6	1.5	4.5
					$(\sigma^2_S)_{AV} = 10.5\ m^2$

TABLE 10. Power spectra of free-air gravity anomalies.

Degree	Degree Variance ($mgal^2$)		
	Gravimetric Solution	Satellite Solution	Combination Solution
0	2.9		
1	-0.2		
2	5.9	7.4	7.4
3	31.0	33.3	33.0
4	18.2	19.7	20.0
5	7.3	17.5	17.8
6	20.7	14.4	15.7
7	9.2	16.4	15.5
8	7.0	8.5	6.7
9	8.7	15.1	12.7
10	9.4	17.7	12.9
11	5.7	13.7	12.2
12	3.5	8.4	5.1
13	7.0		11.1
14	9.4		8.4
15	9.9		13.2
16	5.5		13.8

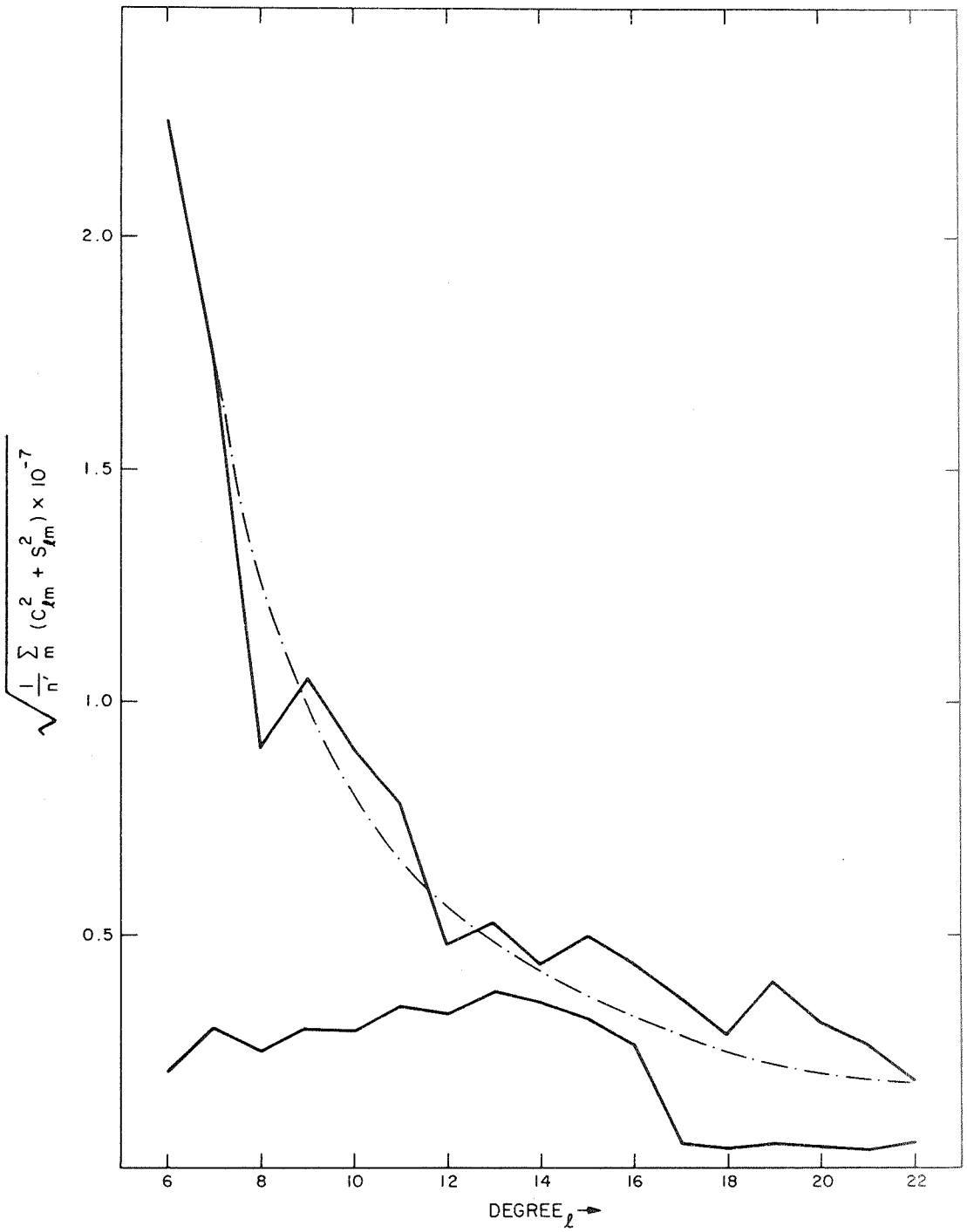

Fig. 8. Degree variances for $6 < \ell < 22$ for the combination solution. Kaula's rule of thumb is indicated by the dashed line. For $2 < \ell < 6$ the degree variances are in complete agreement with this rule. The lower curve gives the degree variances corresponding to the precision estimates of the harmonics, i.e., $1/n' \sum_m \left(\sigma^2_{C_{\ell m}} + \sigma^2_{S_{\ell m}}\right)$.

may be that the real earth actually has an attenuated power spectrum between $\ell = 20$ and the point where anomalies of 150 to 50 km become important ($\ell = 100$ to 300).

COMPARISON WITH GLOBAL TECTONICS

In one sense, a determination of the geophysical significance of the gravity field is a confirmation of the field, and in another, it is the raison d'être for the analysis. Although the following discussion is oriented toward the latter, it should be remembered that by having sorted out the geophysical implications of the gravity field, both results have been verified.

Figure 9 is a plot of free-air anomalies, referred to the figure of hydrostatic equilibrium (an ellipsoid of flattening 1/299.8), in accord with the explanation of Goldreich and Toomre (1969) for the excess oblateness.

There are two major effects of the new data:

A. The improved resolution results in the breakup of the two largest features in the southern oceans. The large area of mild anomaly in the South Pacific is now resolved into two negative areas with a positive area between, the former over basins and the latter along the East Pacific Rise. In the area between Africa and Antarctica, a single large positive feature centered in the "vee" between the two rises is now divided into two positive features over the rises and an area of mild anomaly between. In general, most of the vigorous ocean rises are now positives, rather than "mild" features.

B. The use of the hydrostatic flattening results in the intensification of the negative anomalies in the glaciated areas near the poles: to an extent at the South Pole, which is much greater than can be imputed to glacial loading.

Lesser effects are the appearance of the highest Himalayas as a small positive belt; the removal of the overlap of the ocean rise by the South Australian basin negative; the emphasis of the positive belt from the

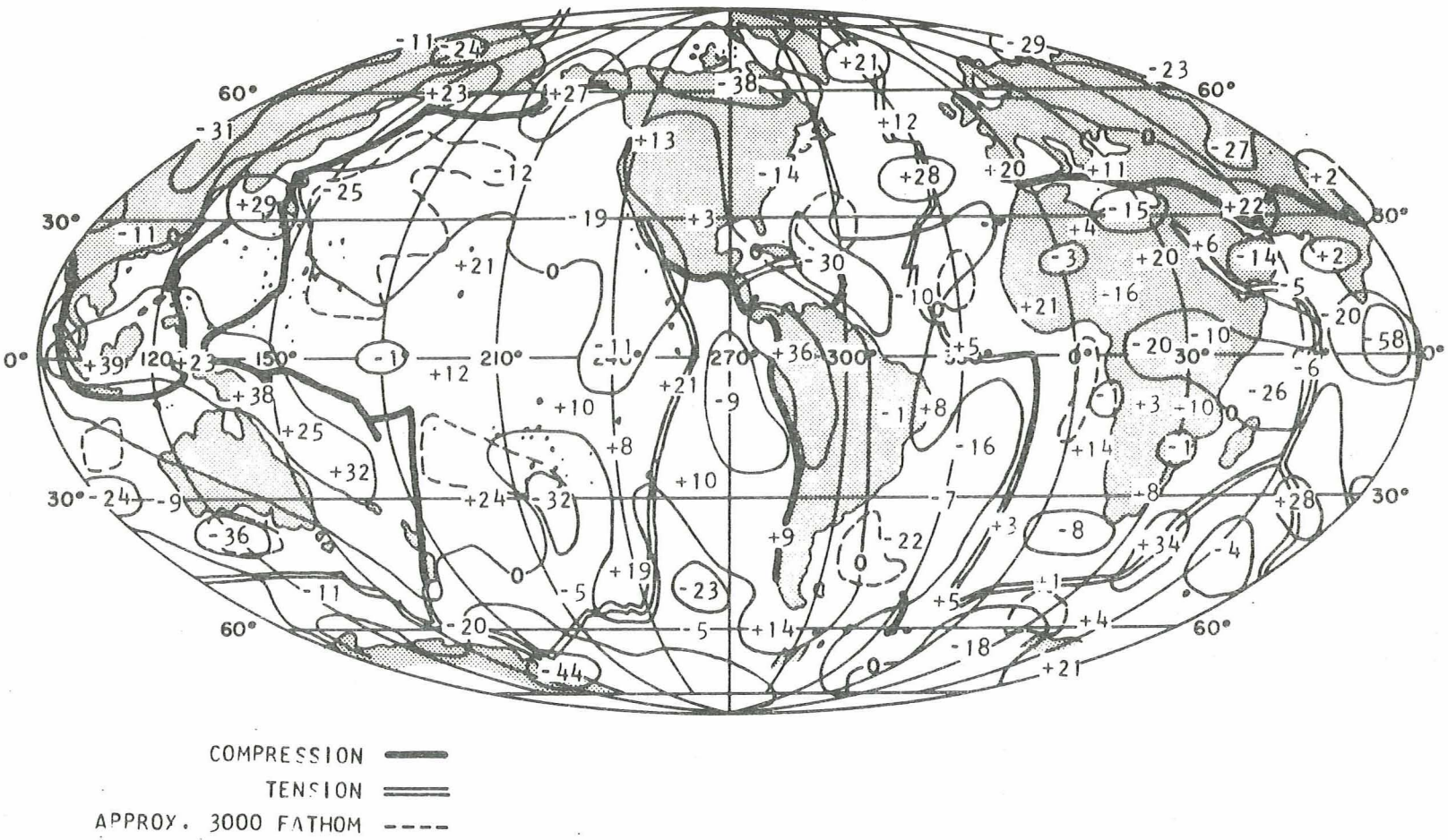

Fig. 9. Free-air anomalies in milligals referred to an ellipsoid of flattening 1/299.8. Calculated from the spherical-harmonic coefficients of the gravitational field of degrees 2 through 16 of Gaposchkin and Lambeck (1970). (Nonzero contours enclosing only one value have been omitted on all figures.) Global tectonic lines of compression and tension from Isacks, Oliver, and Sykes (1968), and major basins indicated by approximate 3000-fathom line on all figures.

Carpathians to Iran; the reduction of the East Mediterranean negative; and the reduction or removal of positive features in areas of slight recent tectonic activity in northeast USSR, the Central Pacific, and Australia.

Figure 10 is the corresponding isostatic anomaly map, using the spherical harmonic expansion of the Airy-Heiskanen 30-km crust isostatic correction calculated by Uotila (1962). As anticipated, oceanic maxima and continental minima are enhanced in the isostatic map.

As previously pointed out (Kaula, 1967), the correlation of gravity with topography is poor for the fifth and lower degrees. On the other hand, Hide and Malin (1970) have recently shown that the low-degree harmonics of the gravity field have a high correlation with the corresponding harmonics of the magnetic field, provided the latter is rotated 160° eastward. The obvious application for the purpose of interpreting upper mantle and crustal phenomena is to use a residual field. Figure 11 is the free-air anomaly field calculated from spherical harmonic coefficients of degrees 6 through 16, and Figure 12 is the corresponding isostatic anomaly field. In the four successive representations of Figures 9 through 12, the correlation of ocean rises with positive anomalies appears more and more emphasized.

As discussed in Kaula (1969), it seems appropriate to analyze the gravity field in terms of reasonably contiguous blocks of anomaly × area, since, by the half-space application of Gauss's theorem, this quantity is directly proportional to excess mass, which in turn is a primary measure of the stresses required. Table 11 gives the 30 largest blocks in terms of free-air anomalies referred to the hydrostatic figure, while Table 12 gives the 25 largest blocks in terms of isostatic anomalies referred to the fifth-degree figure. Of the 12 question marks in Table 4 of Kaula (1969), about 10 seem to be resolved. The greatest question remaining is the great negative over Antarctica; it is too large by more than a factor of 3 to be attributable to the loss of ice in recent geologic time (O'Connell, 1970).

The types given in Tables 11 and 12 are those used in Kaula (1969), with some obvious modifications.

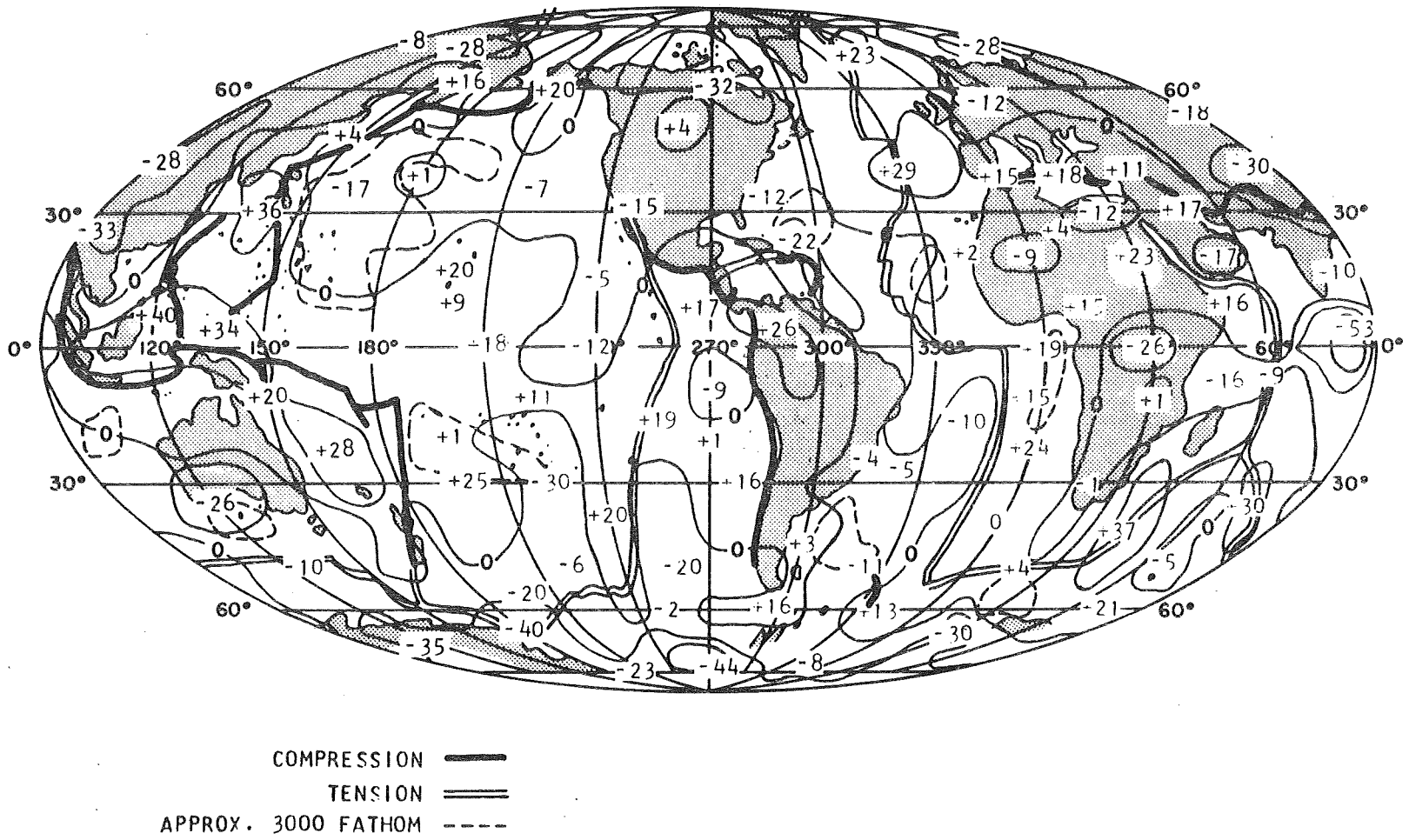

Fig. 10. Isostatic anomalies in milligals referred to an ellipsoid of flattening 1/299.8. Airy–Heiskanen compensation with nominal crustal thickness of 30 km. Calculated from Figure 9, less the spherical-harmonic coefficients for the isostatic correction of degrees 2 through 16 of Uotila (1962).

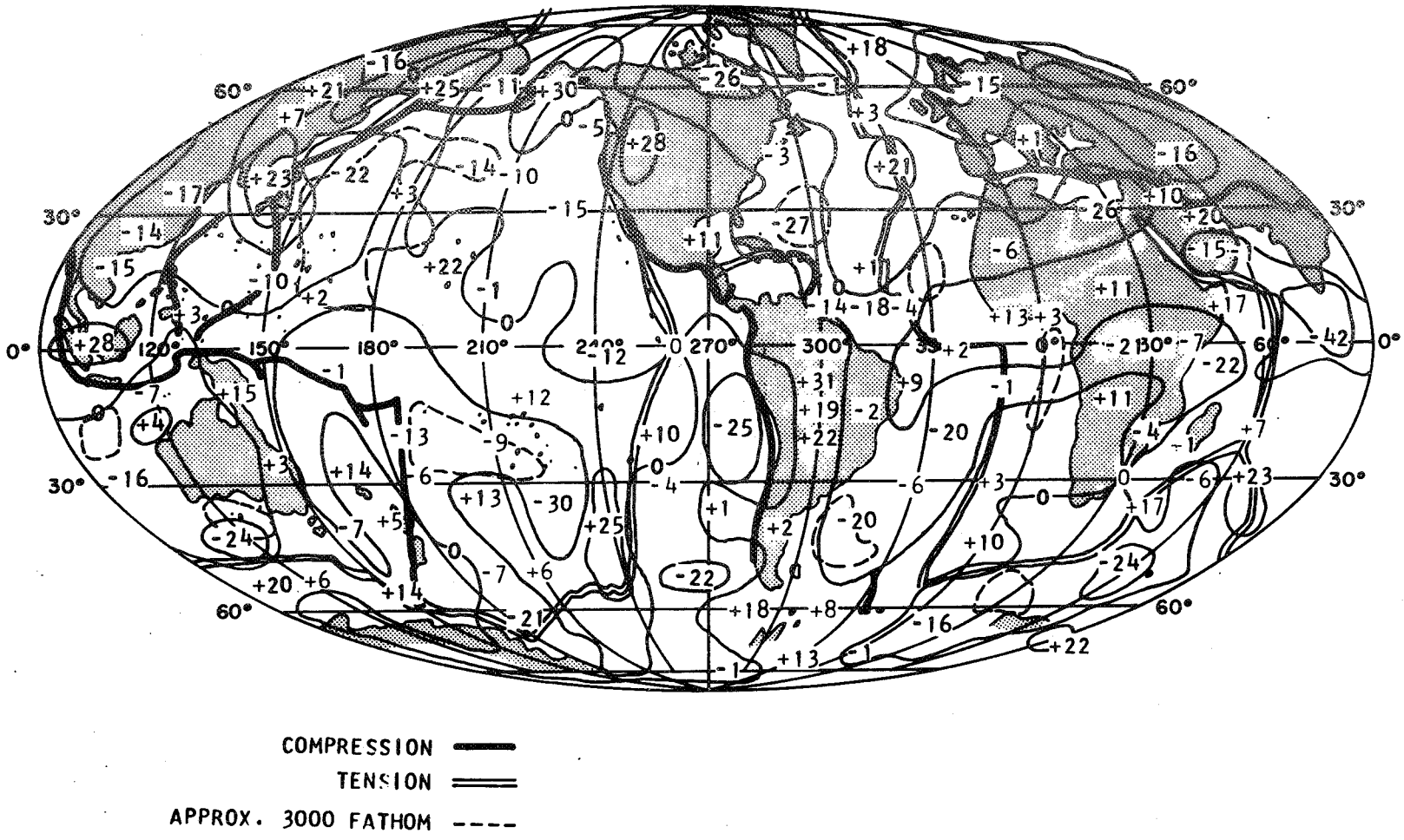

Fig. 11. Free-air anomalies in milligals referred to a fifth-degree figure. Calculated from the spherical-harmonic coefficients of the gravitational field of degrees 6 through 16 of Gaposchkin and Lambeck (1970).

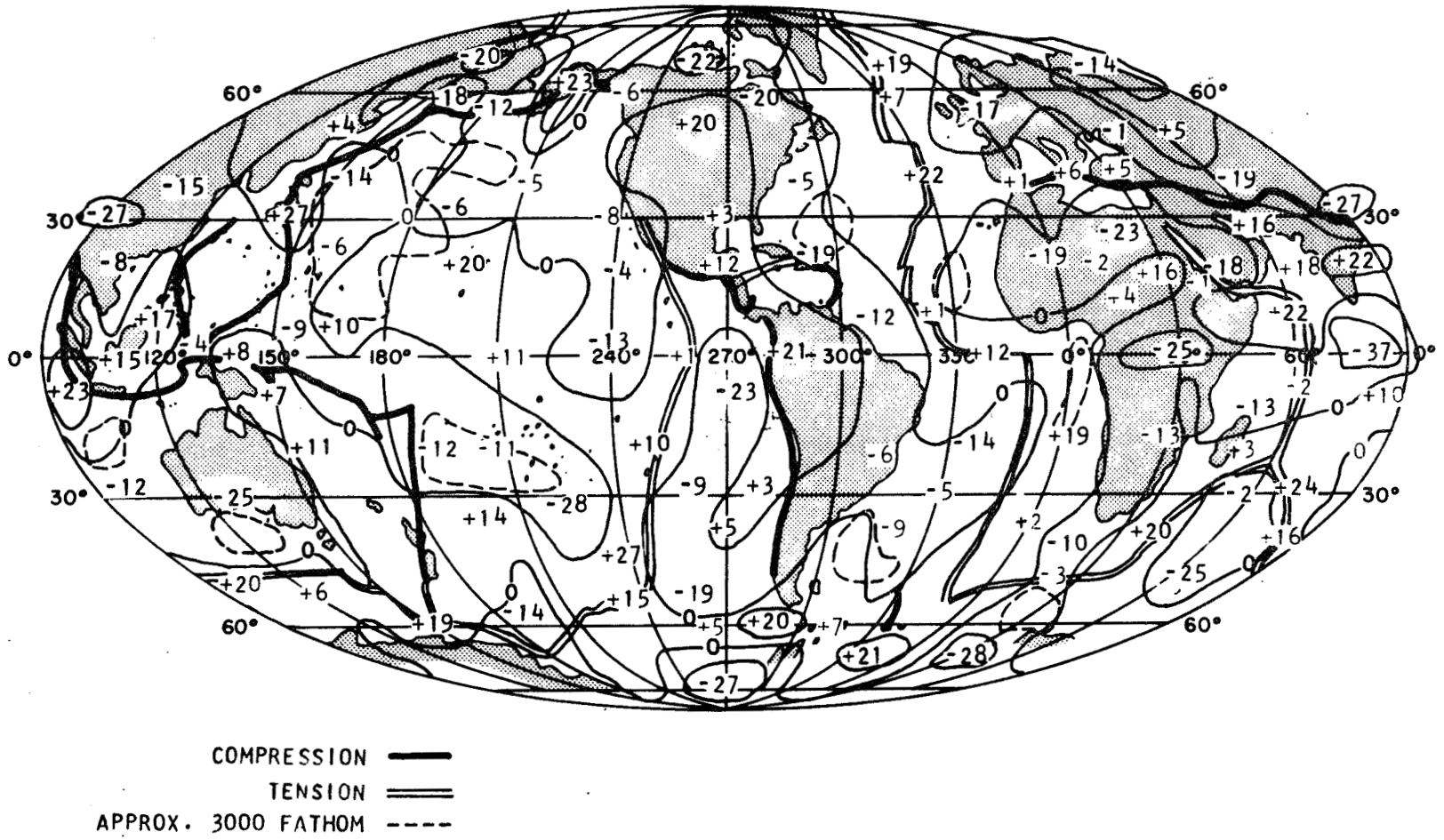

Fig. 12. Isostatic anomalies in milligals referred to a fifth-degree figure. From Figure 11, less the spherical-harmonic coefficients for the isostatic correction of degrees 6 through 16 of Uotila (1962).

TABLE 11. Areas of exceptional gravity anomaly, defined as having an area × free-air anomaly referred to the hydrostatic figure of more than 50 mgal × 10^6 km^2 (1.17 × 10^{21} g) in absolute magnitude and an absolute anomaly of more than 10 mgal throughout the area.

General Location	Area (10^6 km^2)	Free-Air Anomaly × Area (mgal × 10^6 km^2)	Mean Free-Air Anomaly (mgal)	Type
A. Positive Features				
1. Sumatra–Philippines–Solomons	18.9	461	27	Arc
2. Andes–West Amazon Basin	9.4	206	22	Arc-Orogenic
3. Solomons–Tonga–Kermandec	10.4	178	17	Arc
4. Mid-Indian Rise–Indian–Antarctic Rise	9.4	175	19	Rise
5. Crozet Plateau–South Madagascar Rise	6.3	117	19	Rise
6. Mexico–Northwest Colombia	7.3	107	15	Arc
7. Carpathians–Turkey–Iran	7.2	103	14	Orogenic
8. Hawaii	6.1	96	16	Shield
9. Azores Plateau	5.8	95	16	Rise
10. Japan–Bonins	4.6	92	20	Arc
11. Atlas–Iberia–West Mediterranean	5.5	86	16	Arc-Orogenic
12. West Africa–Guinea Basin	6.2	85	14	Orogenic
13. Ahaggar–Tibesti–Nigeria	4.7	77	16	Orogenic
14. Greenland–Iceland–Norwegian Sea	4.6	76	16	Rise
15. East Pacific Rise, North of Easter Island	4.2	64	15	Rise
16. Walvis Rise–Southwest Africa	4.5	58	13	Rise
B. Negative Features				
1. Antarctica	22.4	-511	-23	Glac.-Basin?
2. Siberian Plateau–Turkestan–Himalayas	15.1	-289	-19	Glac.-Orogenic
3. North Canada	10.1	-218	-22	Glaciated
4. North American–Guiana Basins	11.7	-212	-18	Basin
5. Somali Basin–Central Indian Ocean	6.2	-193	-31	Basin
6. North Pacific Basin–Northeast Pacific Slope	12.3	-175	-14	Basin
7. West Australian Shield–South Australian Basin	4.6	-121	-26	Basin
8. Northwest Pacific Basin	5.3	-116	-22	Basin
9. Wharton Basin	5.6	- 98	-17	Basin
10. Northwest Siberia–Aleutian Basin	5.6	- 87	-16	Glac.-Basin
11. Society Island–Southwest Pacific Basin	3.2	- 69	-22	Basin
12. Congo–Kenya	5.0	- 60	-12	Basin-Rift
13. Argentine Basin	3.6	- 54	-15	Basin
14. Chile Rise–Pacific Antarctic Basin	2.8	- 50	-18	Basin

TABLE 12. Areas of exceptional gravity anomaly, defined as having an area × isostatic anomaly referred to a fifth-degree figure of more than 50 mgal × 10^6 km^2 (1.17×10^{21} g) in absolute magnitude and an absolute anomaly of more than 10 mgal throughout the area.

General Location	Area (10^6 km^2)	Isostatic Anomaly × Area (mgal × 10^6 km^2)	Mean Isostatic Anomaly (mgal)	Type
A. Positive Features				
1. Southeast Pacific Rise	6.6	135	20	Rise
2. Mid-Indian–Amsterdam–Naturaliste Ridge	6.1	100	16	Rise
3. Borneo–Sumatra–Cocos	5.3	98	18	Arc
4. Indian Peninsula–Bay of Bengal	4.7	82	17	Sediment?
5. Southeast Indian, MacQuarrie Rises	5.1	76	15	Rise
6. North Atlantic–Arctic Ocean	7.1	73	10	Glaciated(?) Rise
7. Azores Plateau	4.7	73	16	Rise
8. Indian–Antarctic, Gaussberg Ridges	4.5	72	16	Rise
9. North Andes–West Amazon Basin	5.0	72	14	Arc-Orogenic
10. Northeast Georgia–South Sandwiches–Mid-Atlantic	4.3	68	16	Rise-Arc
11. Japan–Bonins	4.0	66	16	Arc
12. Carlsberg Ridge–Gulf of Aden	3.7	65	18	Rise
13. South Alaska	3.6	65	18	Arc-Orogenic
14. Walvis Rise	4.5	61	14	Rise
B. Negative Features				
1. Himalayas–China	8.0	-141	-18	Orogenic
2. Antarctica	8.1	-140	-17	Glaciated Basin?
3. Laccadives–Ceylon–Mid-Indian Ocean	5.0	-130	-26	Basin?
4. North Canada–Greenland	7.5	-123	-16	Glaciated
5. Australian Shield–South Australian Basin	7.7	-113	-15	Basin
6. North American–Guiana–Parnaiba Basins	7.3	- 96	-13	Basin
7. Galapagos–Peru Basin	6.1	- 96	-16	Basin
8. Society–Tuamotu–Australian Sea Mt.	6.8	- 96	-14	Basin?
9. Congo–Kenya	3.7	- 74	-20	Basin-Rift
10. East Crozet Basin–Kerguelen	2.6	- 53	-20	Basin
11. Northwest Europe	3.5	- 51	-15	Glaciated

INTERPRETATION

The principal inference from the large areas of postglacial uplift is, of course, the asthenosphere — a relatively plastic layer in the upper mantle, 80 to 400 km or more deep. Of the seven or eight major feature types, the glaciated areas are alone in being transient, with a decay time on the order of a few thousand years (O'Connell, 1970).

Since the lithosphere is not capable of supporting elastically the necessary stresses for features thousands of kilometers in extent (McKenzie, 1967), the other broad departures in the earth from equilibrium must entail flow in the asthenosphere. However, the asthenosphere is stiff enough, and the thermal conductivity of the earth poor enough (i. e., the Prandtl number is large), that it is generally agreed that the flow is essentially steady state (Turcotte and Oxburgh, 1967, 1969). As indicated by magnetic reversal patterns, the present pattern of tectonic motion has persisted for about 10 million years (Heirtzler, Dickson, Herron, Pitman, and Le Pichon, 1968).

In a steady-state flow system, for a mass excess in a particular region to be maintained, there must be effectively a deceleration in the Lagrangian sense of matter entering the region and an acceleration of matter leaving it; the converse must apply to a region of mass deficiency. Since the compressibility of upper mantle material is slight, these "decelerations" must be accomplished by 1) the piling up of material at the surface, 2) the replacement of less dense by more dense material at an interior interface, 3) thermal contraction, 4) transition to a denser phase, or 5) petrological fractionation in which a less dense component is left behind. The reverse of one or more of these processes is needed to accomplish an "acceleration."

If the asthenosphere is a relatively thin layer, then the obvious direction to transfer matter so as to affect the external gravitational field is lateral. However, vertical transfers are not to be ruled out: an upward displacement of material making the density higher than the average at a shallow level, balanced by a mass deficiency at considerable depth (say below 200 km), could

account for a gravity excess. From the formula for the potential arising from a spherical-harmonic surface distribution of mass (Kaula, 1968, p. 67) we have, for a mass excess of $\Delta\rho h$ of width L compensated at depth d,

$$\Delta g \approx 2\pi^2 G \frac{d}{L} \Delta\rho h \quad .$$

But then to say the data are satisfied by isostatic compensation at great depth is to beg the question as to the response of the asthenosphere to the stresses that must necessarily exist at the intervening levels.

The relationship of gravity anomalies to the flow system depends drastically on the boundary conditions. In a system of thermal convection, if the boundary is fixed, an upcurrent is associated with a negative anomaly, because of its lower density (Runcorn, 1965). But if the boundary is free, an upcurrent is associated with a positive anomaly because the effect of the mass pushed up at the surface outweighs the density effect (Pekeris, 1935; McKenzie, 1968).

In the case of the real earth, the question becomes to what extent the lithosphere (the layer of relative strength) and the crust (the lower density, uppermost layer of the lithosphere) act as part of the convective flow and to what extent they act as a restraining boundary to the flow. Manifestly, they act both roles to differing degrees in different parts of the earth. The lithosphere can even be simultaneously a fixed boundary for horizontal forces, in being able to act as a rigid plate in tectonic motions, and a free boundary for vertical forces, in not resisting convective upthrusts. The extent to which a particular portion of the lithosphere acts as a free or fixed boundary depends on its temperature, size of feature, rate of motion of material into and out of a feature, and composition (in particular, its water content). The situation may be further complicated by steady surface transfers of matter — i. e., erosion and sedimentation.

How a boundary acts in the range between perfectly free and perfectly fixed depends on both 1) its elastic properties – its rigidity and thickness, and 2) its plastic properties – most simply expressed as a decay time in response to a transient loading, dependent on the dimensions of the loading and stress as well as on the creep properties of the material. Under small stresses, the decay time of the lithosphere is very long: it is effectively acting as an elastic layer in areas of postglacial uplift. But under greater stresses, such as in the major areas of mass excess, the notion of decay time is complicated by the nonlinear dependence of strain rate on stress (Weertman, 1970), as manifested by the seismicity of these regions. Qualitatively, for both elastic and plastic behavior, we should expect that the thicker, the colder, the less hydrous the lithosphere is in a particular region, the more it will behave like a fixed boundary. But quantitatively, we should expect that in some cases it may be difficult even to infer the correct sign of the gravity anomaly.

The flow system for a body with boundaries that are partly fixed and partly free would be a difficult problem to treat rigorously. However, we might expect that usually the nature of the local boundary conditions would predominate in determining the characteristics of a particular region. We shall apply this assumption in the analysis of feature types below.

In Kaula (1969), 11 gravity-anomaly area types were proposed, 6 of which appeared to be associated with current internal activity in the earth. We shall discuss these six (somewhat modified) in an order suggested by their apparent relationship to the global-tectonic pattern: 1) active ocean rises, 2) oceanic shield basalts still active in Quaternary, 3) basins, 4) trench and island arcs currently active, 5) current orogeny without extrusives, and 6) Cenozoic orogeny with extrusives in Quaternary.

Active Ocean Rises. The indication from the new data that these areas are generally of positive gravity anomaly is consistent with their being free boundaries over upcurrents in a convective system. Their well-known characteristics of high heat flow, shallow depth in the ocean, thin sediments,

large-scale volcanism, frequent moderate earthquakes, lack of a distinct Moho, and prevalence of intermediate seismic primary velocities in the range 7.2 to 7.7 km/sec are generally taken to indicate that the rises are the sites of upwelling and spreading out in a convective cycle. The intensity and uniformity of heating is apparently sufficient to prevent this mass imbalance from being large. Such small temperature gradients are the expected consequence of a strong temperature dependence of viscosity (Tozer, 1967; Turcotte and Oxburgh, 1969).

Oceanic Shield Basalts. With the improved data, all major oceanic positive areas appear to be associated with spreading centers except one — Hawaii. Hawaii appears to be the buildup of an appreciable mass excess by extrusive activity off the rise. This buildup is in spite of a sinking of the crust, as pointed out by Menard (1969). An approach to isostatic adjustment is also suggested by depths to the Moho somewhat greater than the oceanic average (Drake and Nafe, 1968). But apparently the lithosphere has cooled sufficiently to cause a lag in the attainment of equilibrium. This notion is corroborated by the relatively low heat flow. The existence of such a feature indicates that the asthenospheric flows that generate the required pressure do not necessarily have a simple and direct relationship to the lithospheric plate motions (McKenzie, 1969).

Basins. This commonest of the major features always occurs somewhere to the flanks of ocean rises. However, landward of the basin may be a trench and island arc, an orogenic belt, or a relatively quiescent continent on the same tectonic plate. This suggests that the nature of the flows associated with basins depends more on where the material came from than where it is going.

The direct cause of the negative isostatic anomaly is most likely that the crust carried along in the sea-floor spreading is thicker than compatible with the depth of the basin; a Moho deeper by less than a kilometer is adequate to account for the average isostatic anomaly of -14 mgal.

The real problem, of course, is what is the nature of the asthenospheric withdrawal that causes the 3-km drop from the rise to the basin. Such a drop could be caused by a downcurrent component in the convective system resulting from the settling out of denser components. Such settling out would be expected in a laterally moving flow that was cooling. But a 3-km drop requires much more than thermal contraction; furthermore, if there is an appreciable negative anomaly as well, the settling out cannot just be immediately below the basin lithosphere but must be either 1) at a depth of several hundred kilometers below the basin, or 2) between the ocean rise and the basin. Process 1) could be effected by the phase transitions of olivine and pyroxene, which occur at depths of 300 to 600 km, while process 2) might be facilitated by gabbro-to-eclogite transitions at shallower depths.

The sharpness of the crust-mantle boundary, with the 7.2- to 7.7-km/sec gap in velocities (Drake and Nafe, 1968), makes it impossible for the crust to be directly involved in causing the negative anomaly. But if the crust is being carried passively along — as suggested by the lack of seismicity, volcanism, or disturbance of the sea floor — then it is hard to understand why it is thicker under the basins than it is on the flanks of the rises, as emphasized by Le Pichon (1969). Could it be that consolidated sediments are mistaken for basement rock? Sedimentation itself is a secondary process in explaining the gravity-anomaly pattern, more a result than a cause: if the thick sediments are the driving force, then the isostatic anomalies in ocean basins would be positive, rather than negative.

Possibly to be included in the category of basins caused by the behavior of the lithosphere as a free-boundary overflow with settling out of denser components are two land features, Antarctica and the Congo Basin. Antarctica is an extremely large feature — large enough to require a unique explanation.

Trench and Island Arcs. The now generally accepted model of McKenzie (1969) and others of a colder, denser oceanic lithospheric slab being thrust down under a less dense but stiffer continental margin fits a simple notion

of the gravity pattern: the dominant feature is the broad positive anomaly associated with the denser downthrust slab, while the secondary feature is the narrow negative belt associated with the trench caused by tensile cracking and the downward-breaking line. But this simple picture is based on the assumption that the applicable boundary condition of the convective flow is more "fixed" than "free": in other words, the time scale of the process is short enough that the strength of the continental lithosphere (and perhaps the oceanic lithosphere as well) significantly resists being pulled down by the downcurrent. This general idea that resistance to flow is necessary to make positive gravity anomalies of densifications applies not only to the boundary layer but also to deeper strata: the downthrust slab could in part be supported by stiffer matter below the asthenosphere, as suggested by Isacks and Molnar (1969) and others from seismic data.

The association of the downthrust slab with positive anomalies also suggests that the driving force is a push from above rather than withdrawal from below. Whether this "push" is the gravitationally caused sinking of the denser oceanic lithosphere, the pressure of the spreading sea floor behind it, or the viscous drag by the sublithospheric flow does not seem resolvable from the gravity data.

Current Orogeny without Extrusives. The hypothesis of McKenzie (1969) that purely continent vs. continent compression results in folding rather than in downthrust because of the excessive buoyancy of the thicker crust is appealing as an explanation for the strongly negative gravity anomalies associated with the Asian part of the Alpide belt. The resulting pileup of lower density material results in a mass deficiency in the short run, because the stiffness of the lithosphere containing low-density crust enables it to push out of the way higher density asthenospheric material. But in the longer run, the trend from "fixed" to "free" boundaries is expressed by the forcing upward of the lithosphere; geologic and geodetic indications are that the Himalayas–Turkestan complex is currently rising (Gansser, 1964; Artyushkov and Mescherikov, 1969).

The thick layers of sedimentary and metamorphic rocks constituting the upper part of the Himalayas have existed since pre-Cambrian times, and hence the excess heat generation and thermal blanketing may influence the situation. Furthermore, there may be a contribution from erosion, as corroborated by the positive features over the Bay of Bengal and the Arabian Sea, which appear most strongly in Figure 12.

Cenozoic Orogeny with Extrusives. These mountain-building areas, listed as orogenic among the positive features in Table 11, seem to require less explanation in that they are of more limited extent and are closer to isostatic equilibrium. Most are associated with compressive belts of the global tectonic system, but this is not entirely so. Why they differ from the Himalayas–Turkestan complex in being positive may be the lack of the preexisting great thicknesses of sedimentary and metamorphic rocks, or it may be the presence of oceanic crust to be consumed (McKenzie, 1970). They may also be the continental equivalents of Hawaii to some extent: the coincidence of weak features in the lithsophere with regions of excess pressure and heat in a convective system that is not directly related to surface features. Most of these areas have positive seismic-delay residuals, suggesting high temperatures to considerable depth.

DISCUSSION AND CONCLUSIONS

The gravity data now appear to confirm rather well the dependence of plate tectonics on mantle convection inferred from other phenomena associated with the midocean rises and the compressive belts (Isacks, Oliver, and Sykes, 1968). The principal respect in which this picture is enhanced is the inference that ocean basins are associated with significant downcurrents entailing settling out of denser components and, probably, phase transitions. That this process results in negative gravity anomalies depends on the time scale of the effect being long enough that the lithosphere is of negligible strength and hence acts like a free boundary.

The greatest feature not readily related to the global tectonic system is the Antarctic negative, much too large to be explained by glacial melting. Antarctica is almost surrounded by ocean rises. Hence, either these rises are migrating away from Antarctica, or Antarctica is a sink. The latter seems implausible, since there is none of the seismicity expected with the destruction or folding of the lithosphere: it is difficult for Antarctica to pass on the lithosphere to some other area, as do the ocean basins.

Other features not well explained by the global tectonic pattern are the gravity excesses associated with extrusive flows away from the ocean rises and trench and island arcs, in both oceanic and continental areas. Both these features appear to require higher temperatures in the asthenosphere generating excess pressures, together with weaknesses in the lithosphere allowing the extrusions. It is, however, difficult to choose whether the resulting net mass excess is a consequence of sufficient overall strength in the lithosphere to support the extruded load or of behavior as a free boundary over an upcurrent: perhaps a partial current that is the upward motion of a less dense component, the reverse of the process that appears necessary to account for the ocean basins.

Anticipated properties of the mantle-convective system that need to be better related to the gravity field are the stress dependence and temperature dependence of the effective viscosity, the horizontal temperature gradients arising from variations in radiogenic heating, and the contributions to driving the system by fractionations and phase transitions. All these properties are important, of course, to the solution of the entire global tectonic problem.

ACKNOWLEDGMENTS

The authors wish to acknowledge the large contribution of other members of the Observatory staff.

We thank the following agencies for providing many of the data:

NASA Goddard Space Flight Center MOTS System and NASA National Geodetic Satellite Program Data Bank, Maryland.

French Centre National d'Etudes Spatiales, Paris.

14th Aerospace Force, USAF.

Observatoire de Paris, Section d'Astrophysique, Meudon.

Universität Bern Astronomisches Institut, Switzerland.

British Ministry of Technology, Royal Radar Establishment, Ordnance Survey, Malvern.

USSR Academy of Sciences, Astronomical Council, Moscow.

Technische Hogeschool, Laboratorium voor Geodesie, Delft, The Netherlands.

California Institute of Technology, Jet Propulsion Laboratory, California.

National Technical University, Athens, Greece.

Uttar Pradesh State Observatory, Naini Tal, India.

Tokyo Astronomical Observatory, Japan.

Australian Department of Supply, American Projects Division.

We also express our gratitude to the following agencies, who cooperated in the operation of the SAO satellite-tracking network.

Argentina

Comisión Nacional de Investigaciones Espaciales

Observatorio Astronomico
Universidad Nacional de Cordoba

Brazil

Comissão Nacional de Atividades Espaciais

Ethiopia

Haile Selassie I University

Hawaii

University of Hawaii

Institute for Astronomy

Institute of Geophysics

Iran

Université de Teheran
Institute Géophysique

Netherlands Antilles

Curaçao Welfare Bureau

Peru

Instituto Geofisico del Peru

Universidad Nacional de San Agustin

South Africa

Council for Scientific and Industrial Research

Spain

Instituto y Observatorio de Marina

REFERENCES

Artyushkov, E. V., and Mescherikov, Yu. A., Recent movements of the earth's crust and isostatic compensation, in The Earth's Crust and Upper Mantle, AGU Monog. 13, edited by P. J. Hart, 379-390, 1969.

Drake, C. L., and Nafe, J. E., The transition from ocean to continent from seismic refraction data, in The Crust and Upper Mantle of the Pacific Area, AGU Monog. 15, edited by L. Knopoff, C. L. Drake, and P. J. Hart, 174-186, 1968.

Gansser, A., Geology of the Himalayas, John Wiley & Sons, Inc., Interscience Publ., London, 289 pp., 1964.

Gaposchkin, E. M., A dynamical solution for the tesseral harmonics of the geopotential and station coordinates using Baker-Nunn data, in Space Research VII, edited by R. L. Smith-Rose, S. A. Bowhill, and J. W. King, North-Holland Publ. Co., Amsterdam, 683-693, 1967.

Gaposchkin, E. M., and Lambeck, K., 1969 Smithsonian Standard Earth (II), Smithsonian Astrophys. Obs. Spec. Rep. No. 315, 93 pp., 1970.

Goldreich, P., and Toomre, A., Some remarks on polar wandering, J. Geophys. Res., 74, 2555-2567, 1969.

Heirtzler, J. R., Dickson, G. O., Herron, E. M., Pitman, W. C., III, and Le Pichon, X., Marine magnetic anomalies, geomagnetic field reversals, and motions of the ocean floor and continents, J. Geophys. Res., 73, 2119-2136, 1968.

Hide, R., and Malin, S. R. C., Novel correlations between global features of the earth's gravitational and magnetic fields, Nature, 225, 605-609, 1970.

Isacks, B., Oliver, J., and Sykes, L. R., Seismology and the new global tectonics, J. Geophys. Res., 73, 5855-5899, 1968.

Isacks, B., and Molnar, P., Mantle earthquake mechanisms and the sinking of the lithosphere, Nature, 223, 1121-1124, 1969.

Kaula, W. M., Test and combination of satellite determinations of the gravity field with gravimetry, J. Geophys. Res., 71, 5303-5314, 1966.

Kaula, W. M., Geophysical implications of satellite determinations of the earth's gravitational field, Space Sci. Rev., 7, 769-794, 1967.

Kaula, W. M., An Introduction to Planetary Physics: the Terrestrial Planets, John Wiley & Sons, Inc., New York, 490 pp., 1968.

Kaula, W. M., A tectonic classification of the main features of the earth's gravitational field, J. Geophys. Res., 74, 4807-4826, 1969.

Kaula, W. M., Chairman, The Terrestrial Environment: Solid-Earth and Ocean Physics, NASA Contractor Report CR-1579, 1970.

Köhnlein, W. J., Corrections to station coordinates and to nonzonal harmonics from Baker-Nunn observations, in Space Research VII, edited by R. L. Smith-Rose, S. A. Bowhill, and J. W. King, North-Holland Publ. Co., Amsterdam, 694-701, 1967a.

Köhnlein, W. J., The earth's gravitational field as derived from a combination of satellite data with gravity anomalies, Smithsonian Astrophys. Obs. Spec. Rep. No. 264, 57-72, 1967b.

Kozai, Y., Revised values for coefficients of zonal spherical harmonics in the geopotential, Smithsonian Astrophys. Obs. Spec. Rep. No. 295, 17 pp., 1969.

Lambeck, K., The relation of some geodetic datums to a global geocentric reference system, Bull. Géod., in press, 1970.

Le Pichon, X., Models and structure of the oceanic crust, Tectonophys., 7, 385-401, 1969.

Le Pichon, X., and Talwani, M., Regional gravity anomalies in the Indian Ocean, Deep Sea Res., 16, 263-274, 1969.

Lundquist, C. A., and Friedman, H. D., Eds., Scientific horizons from satellite tracking, Smithsonian Astrophys. Obs. Spec. Rep. No. 236, 250 pp., 1966.

Lundquist, C. A., and Veis, G., Eds., Geodetic parameters for a 1966 Smithsonian Institution Standard Earth, Smithsonian Astrophys. Obs. Spec. Rep. No. 200, 3 vol., 1966.

McKenzie, D. P., Some remarks on heat flow and gravity anomalies, J. Geophys. Res., 72, 6261-6273, 1967.

McKenzie, D. P., The influence of the boundary conditions and rotation on convection in the earth's mantle, Geophys. J. Roy. Astron. Soc., 15, 457-500, 1968.

McKenzie, D. P., Speculations on the consequences and causes of plate motions, Geophys. J. Roy. Astron. Soc., 18, 1-32, 1969.

McKenzie, D. P., Plate tectonics of the Mediterranean region, Nature, 226, 239-243, 1970.

Menard, H. W., Growth of drifting volcanoes, J. Geophys. Res., 74, 4827-4837, 1969.

Mottinger, N., Status of D.S.F. locations solution for deep space probe missions, Space Programs Summary No. 37-60, Jet Propulsion Laboratory, Pasadena, California, vol. II, 77-89, 1969.

O'Connell, R. J., Pleistocene glaciation and the viscosity of the lower mantle, J. Geophys. Res., 75, in press, 1970.

Pekeris, C. L., Thermal convection in the interior of the earth, Mon. Not. Roy. Astron. Soc. Geophys. Suppl., 3, 343-367, 1935.

Runcorn, S. K., Changes in the convective pattern in the earth's mantle and continental drift: evidence for a cold origin of the earth, Phil. Trans. Roy. Soc. London A, 258, 228-251, 1965.

Talwani, M., and Le Pichon, X., Gravity field over the Atlantic Ocean, in The Earth's Crust and Upper Mantle, AGU Monog. 13, edited by P. J. Hart, 341-351, 1969.

Tozer, D. C., Towards a theory of thermal convection in the earth's mantle, in The Earth's Mantle, edited by T. F. Gaskell, Academic Press, New York, 325-353, 1967.

Turcotte, D. L., and Oxburgh, E. R., Finite amplitude convection cells and continental drift, J. Fluid Mech., 28, 29-42, 1967.

Turcotte, D. L., and Oxburgh, E. R., Convection in a mantle with variable physical properties, J. Geophys. Res., 74, 1458-1474, 1969.

Uotila, U. A., Gravity anomalies for a model earth, Ohio State Univ. Dept. Geodetic Sci. Tech. Rep., 37, 15 pp., 1962.

Veis, G., Relation with DSIF stations, Smithsonian Astrophys. Obs. Spec. Rep. No. 200, vol. 3, 115-125, 1966.

Veis, G., Results from geometric methods, in Space Research VII, edited by R. L. Smith-Rose, S. A. Bowhill, and J. W. King, North-Holland Publ. Co., Amsterdam, 778-782, 1967a.

Veis, G., Geodetic interpretation of the results, in Space Research VII, edited by R. L. Smith-Rose, S. A. Bowhill, and J. W. King, North-Holland Publ. Co., Amsterdam, 776-777, 1967b.

Weertman, J., The creep strength of the earth's mantle, Rev. Geophys. Space Phys., 8, 145-168, 1970.

Whipple, F. L., On the satellite geodesy program at the Smithsonian Astrophysical Observatory, in Space Research VII, edited by R. L. Smith-Rose, S. A. Bowhill, and J. W. King, North-Holland Publ. Co., Amsterdam, 675-683, 1967.

Whipple, F. L., and Hynek, J. A., Optical and visual tracking of artificial satellites, in Proceedings VIIIth International Astronautical Congress, Springer-Verlag, Vienna, 429-435, 1958.

TESTS AND COMPARISONS OF GRAVITY MODELS USING CAMERA OBSERVATIONS OF GEOS-I AND GEOS-II

by

J. G. Marsh
B. C. Douglas
M. L. Dutcher

ABSTRACT

Optical observations of the GEOS satellites are used to obtain orbital solutions with different sets of geopotential coefficients. The solutions are compared before and after modification to high order terms (necessary because of resonance) and then are analyzed by comparing subsequent observations with predicted trajectories. The most important source of error in orbit determination and prediction for the GEOS satellites is the poorly modeled effect of resonance found in most published sets of geopotential coefficients. Modifications to the sets yield greatly improved orbits in most cases.

The sets of coefficients analyzed are APL 3.5, NWL5E-6, Köhnlein (1967), Rapp (1967), Kaula (1967), Smithsonian Astrophysical Observatory (SAO)M-1 (1966), SAO COSPAR (1969) and SAO 1969. The SAO 1969 model generally gives better orbital fits and prediction results. However even this model can be improved by corrections to resonant coefficients.

The results of these comparisons suggest that with the best optical tracking systems and gravity models, satellite position uncertainty can reach 50-100 meters during a heavily observed 5-6 day orbital arc.

CONTENTS

TESTS AND COMPARISONS OF GRAVITY MODELS USING CAMERA OBSERVATIONS OF GEOS-I AND GEOS-II

INTRODUCTION

For GEOS-I and II data to be utilized for tracking system intercomparison, calibration, and station location determination, satellite positions must be accurately determined. Thus, an accurate model of the forces on the satellite is essential. For the GEOS satellites, the small effects of drag and radiation pressure are easily modeled. The much larger effects of the geopotential present a more serious problem. This study consists of analysis, comparison, and modification of existing geopotential models.

The sets of geopotential coefficients (gravity models) were used in the NONAME Cowell-type orbit determination program (Reference 1) to obtain orbital solutions. These were then compared by examining rms of fit, differencing the fitted orbits, and predicting the orbits through later GEOS data.

All except the SAO 1969 solutions were obtained using the SAO C-7 Standard Earth (Reference 2). The gravity models studied were SAO M-1, SAO COSPAR (1969), SAO 1969, APL 3.5, NWL5E-6, Kaula 1966, Köhnlein 1967, and Rapp (1967) (References 3-10).

The most significant defect of most published gravity models, particularly the older ones, for precision orbit determination is their lack of high-order terms to model the shallow resonances which exist for all satellites. For GEOS-I and II, resonant effects amount to approximately 500 meters alongtrack. In every case, improvements could be obtained by modifying the resonant coefficients of a model.

It is a common practice in orbit determination to represent an orbit by more than 6 parameters in order to absorb model errors. Since we were trying to discover model errors we solved only for the minimum set of 6 elements.

SECTION 1
ORBITAL CHARACTERISTICS OF GEOS-I AND II

GEOS-I and II are nearly ideal for gravity model testing because of the extent of coverage by accurate tracking instruments and low drag and radiation pressure effects. The orbital inclinations of GEOS-I and II differ markedly, thus ensuring that conclusions from tracking results of both satellites have some generality.

1.1 ORBITAL SPECIFICATIONS

Table 1 presents the orbital specifications for GEOS-I and II. GEOS-I has a period of approximately two hours and an orbital inclination of 59°.4; GEOS-II has a somewhat shorter period and a much higher inclination of 105°.8. Both orbits are nearly circular with perigees above 1000 km and small area-to-mass ratios. Consequently, drag can be ignored and radiation pressure is small and easily modeled.

Table 1
Orbital Elements of GEOS I and II

	GEOS I	GEOS II
Epoch	January 2, 1966	April 28, 1968
Apogee Height	2273 Kilometers	1569 Kilometers
Perigee Height	1116 Kilometers	1077 Kilometers
Eccentricity	0.07	0.03
Inclination	59.4 Degrees	105.8 Degrees
Anomalistic Period	120.3 Minutes	112.1 Minutes

Table 2 presents the along-track effects of the SAO M1 geopotential up to (6,6) for GEOS-I and II. A few terms of higher degree such as (8,1) also have effects of about 20 m. Notice that GEOS-II is more perturbed by the geopotential than is GEOS-I due to the smaller orbital semimajor axis and higher inclination.

1.2 RESONANCE

GEOS-I is resonant with 12 th order (m) terms of the geopotential and GEOS-II is resonant with terms of the 13th order. The result is a perturbation along-track of about 1/2 Km in each case.

Table 3 shows the expected along track effects assuming the normalized coefficients follow the rule ($\overline{C}_{n,m}, \overline{S}_{n,m}$ $10^{-5}/_{n}{}^{2}$). Although both satellites have nearly circular orbits, the even degree (n) terms have important effects. These terms contain a factor proportional to the eccentricity and are called eccentric resonant terms. Table 3 indicates the necessity of modeling these terms.

Table 2

Along Track Effects of Low Degree and Order Terms

Based on the SAO M-1 Coefficients

n,m	METERS	
	GEOS I	GEOS II
2,2	350	500
3,1	80	150
3,2	50	30
3,3	25	50
4,1	130	200
4,2	50	50
4,3	85	75
4,4	10	20
5,1	< 10	15
5,2	35	10
5,3	15	15
5,4	10	< 10
5,5	< 10	10
6,1	< 10	10
6,2	35	< 10
6,3	< 10	< 10
6,4	25	< 10
6,5	25	30
6,6	< 10	< 10

Table 3

Along Track Effects of Resonant Terms

Assuming $\bar{C}_{n,m}$, $\bar{S}_{n,m}$ $10^{-5}/n^2$

GEOS I Beat Period = -7.1 Days		GEOS II Beat Period = -6.5 Days	
n,m	Meters	n,m	Meters
12,12	< 170	13,13	< 400
13,12	400	14,13	150
14,12	280	15,13	280
15,12	225	16,13	50
16,12	80	17,13	100
17,12	50	18,13	40
18,12	50	19,13	10
19,12	40	20,13	20
20,12	30	21,13	25
21,12	25	22,13	10
22,12	15	23,13	20
n > 23	< 10	n > 24	< 10

Both orbits contain a large number of resonant terms significantly affecting the satellite position. However, an extensive set of resonant coefficients may not be absolutely necessary for accurate orbit determination and prediction. Resonant terms of either even or odd degree perturb the orbit with about the same frequency (Kaula Reference 11). Thus most or all of the effects of all the resonant terms can be absorbed by solving for one or two pairs of them. The good results obtained in this study would not have been possible otherwise, since the number of resonant terms in most models is relatively small. A detailed analysis of GEOS-II orbital resonance is given in Reference 13.

SECTION 2
DESCRIPTION OF DATA SETS

2.1 TYPE OF DATA

Three types of camera data were used for this study. These are Baker-Nunn (SAO), PC-1000 (United States Air Force), and MOTS 40" (NASA STADAN and SPEOPT). The same a priori standard deviations on the measurements were used:* two seconds of arc on all declination measurements and 2/cos (declination) seconds of arc on all right ascension measurements.

It should be noted that although the measurements are assumed to have the same accuracy, the locations of most of the Baker-Nunn stations are possibly better known.

2.2 DESCRIPTION OF ARCS

Four approximately 5-1/2 day arcs were chosen for this study; two GEOS-I and two GEOS-II arcs. Table 4 describes these arcs.

Table 4
Description of Orbital Arcs and Data Sets

Satellite	Period	Camera Type	No. OBS.
GEOS I	Dec. 31-Jan. 5, 1966	MOTS, PC-1000	1057
	July 11-16, 1966	Baker-Nunn (90%)	1766
GEOS II	Apr. 28-May 4, 1968	MOTS 40"	1098
	Sept. 16-22, 1968	Baker-Nunn (95%)	1388
		MOTS 40" (5%)	

The July 11-16, 1966, GEOS-I arc is predominantly Baker-Nunn (SAO) data from the original twelve best located SAO tracking stations, while the Dec. 31-Jan. 5, 1966, GEOS-I arc is mostly MOTS 40" data.

The Apr. 28-May 4, 1968 GEOS-II arc also consists mostly of MOTS data. The second GEOS-II arc, Sept. 16-22, 1968 is largely Baker-Nunn data from less accurately located SAO stations and, at six days, is the longest of the four arcs.

Solutions from the best of the GEOS-I arcs, the July arc, and best of the GEOS-II arcs, the April-May arc, were used in the prediction results and RV comparisons presented in Section 3. Thus it is important to note the following: the Baker-Nunn cameras in the GEOS-I arc are much more widely distributed about the Earth than are the MOTS cameras in the GEOS-II arc. The GEOS-I arc

*Used in making up the covariant weight matrix.

has a significant number of observations from stations in Spain, India, Australia and Hawaii, as well as North and South America. The tracking stations used in the GEOS-II arc are almost totally located in North-Central America, with one station in Chile and two in Africa. Such a difference between the two arcs is more likely to cause differences in prediction results than in orbit determination.

SECTION 3
COMPARISON OF GRAVITY MODELS

3.1 MODEL AND RESONANT TERM DESCRIPTIONS

Table 5 summarizes the geopotential models evaluated. Until the presentation of the SAO 1969 model at the COSPAR meeting in Prague by E. M. Gaposchkin in May, 1969, the 1966 SAO M-1 was the most extensive published model based on satellite data alone. Derived by the Smithsonian Astrophysical Observatory from Baker-Nunn optical observations of 16 satellites, the set is complete to (8,8) with 46 additional coefficients of higher degree totalling 122 coefficients. The two recent SAO models, the COSPAR and the 1969, are complete to (14,14) and (16,16) respectively with many additional coefficients of higher degree and were derived from a combination of optical, Goddard Range and Range Rate and laser data, from 24 satellites. The 1969 model also incorporates gravimetric data.

Table 5

Geopotential Models

SAO M-1 (1966)	Complete to (8,8)	122 Coefficients
SAO COSPAR (1969)	Complete to (14,14)	280 Coefficients
SAO 1969	Complete to (16,16)	314 Coefficients; Includes Gravimetric Data
APL 3.5 (1965)	Complete to (8,8)	84 Coefficients
NWL 5E-6 (1965)	Complete to (7,6)	64 Coefficients
KAULA (1966)	Complete to (7,5)	99 Coefficients
Köhnlein (1967)	Complete to (15,15)	250 Coefficients; Includes Gravimetric Data
Rapp (1967)	Complete to (14,14)	219 Coefficients; Includes Gravimetric Data

The APL 3.5 model was derived from Tranet Doppler satellite observations by the Applied Physics Laboratory. This set is complete to (8,8) with additional higher degree terms totalling 84 coefficients.

The Naval Weapons Laboratory derived the NWL 5E-6 model also using Tranet Doppler data. It is complete to (7,6) with a few additional higher degree coefficients.

The Kaula model, derived in 1966 from a combination of Tranet Doppler and optical observations of 12 satellites is complete to (7,5) with a few higher degree coefficients making a total of 99 coefficients.

The Köhnlein and Rapp models, complete to (15,15) and (14,14) respectively, were derived by combining gravimetric measurements with the SAO M-1 coefficients in 1967.

Table 6 describes the resonant terms used to modify the geopotential models. The Gaposchkin and Veis values for (13,12), (14,12) and (15,12) (Reference 14) are used with the 1966 M-1 values for (12,12) and replace all existing 12th order terms in the modified models in GEOS I arcs. The Yionoulis (Reference 12) values for (13,13), (15,13) and (17,13) replace all existing 13th order terms in the modified models in GEOS II arcs. The Douglas and Marsh values for (14,13) (Reference 12) are used with the Yionoulis 13th order terms and together replace all existing 13th order terms in the modified models in the April-May GEOS II arc.

Table 6

Sets of Resonant Coefficients Used

To Modify Geopotential Models

Source	Resonant coefficients	Comments
Gaposchkin and Veis (1967)	C13,12 -1.26×10^{-19} S13,12 1.16×10^{-19} C14,12 1.40×10^{-21} S14,12 $-1.32 \cdot 10^{-20}$ C15,12 $-1.38 \cdot 10^{-20}$ S15,12 $-1.9 \cdot 10^{-21}$	To be used with 1966 M-1 (12,12) where C12,12 $-2.78 \cdot 10^{-19}$ S12,12 $7.18 \cdot 10^{-21}$
Yionoulis (1968)	C13,13 -2.39×10^{-20} S13,13 2.12×10^{-21} C15,13 -7.7×10^{-22} S15,13 -3.74×10^{-22} C17,13 1.59×10^{-23} S17,13 2.8×10^{-23}	
Douglas and Marsh (1969)	C14,13 5.7×10^{-22} S14,13 6.5×10^{-21}	To be used with Yionoulis (1968) for the April-May arc.

For the SAO 1969, the appropriate C6 station positions were used. All other cases used the appropriate C7 positions.

3.2 ORBIT DETERMINATION

The quality of a determined orbit is measured by the root mean square (rms) of the data points about the orbital solution. Tables 7 and 8 present the rms's of fit in seconds of arc about the orbital solutions for each of the models studied, with and without modification of resonant terms.

With the exception of the 1969 SAO models, the unmodified gravity models gave relatively poor fits. Modifications for resonance greatly reduced the rms's of most of the models. The exception, the Kaula model, gave best results for GEOS-I before modification.

As mentioned in Section 1.2 and shown conclusively in Tables 7 and 8, resonance for GEOS-I and II is important. The Gaposchkin and Veis 12th order terms for GEOS I and the Yionoulis 13th order terms for GEOS-II produced significantly better fits in the models which contained an insufficient number of accurate resonant terms.

It is interesting to notice in Table 7 that the original SAO M-1 12th order coefficients produced a very poor fit for the July arc and a very good one for the December-January arc. The reason for this is not yet clear. The July arc residuals indicate that the high rms is due to resonance: a distinct six-day period can be seen on a plot of the residuals.

Table 7
Rms's about Fitted Orbits
GEOS I

ARC 1: July 11-16, 1966
(1766 observations)

Model	Rms (secs of arc)*	
	unmodified	modified**
SAO M-1	19.04	2.52
SAO COSPAR (No 11th)	2.42	- -
SAO 1969	1.93	- -
Köhnlein	14.65	2.89
Rapp	7.81	6.91
NWL 5E-6	11.82	3.33
APL 3.5	13.51	6.64
Kaula	5.80	5.95

ARC 2: December 31 - January 5, 1966
(1057 observations)

Model	Rms (secs of arc)	
	unmodified	modified*
SAO M-1	3.87	3.66
SAO COSPAR (No 11th)	3.17	- -
SAO 1969	2.80	- -
Köhnlein	11.18	4.01
Rapp	7.68	4.02
NWL 5E-6	12.75	3.50
APL 3.5	12.65	4.53
Kaula	5.43	5.86

*Addition of Gaposchkin & Veis (1967) 12th order terms.
**1 second of arc equals approximately 7 meters.

Table 8
Rms's About Fitted Orbits
GEOS II

ARC 1: April 28 - May 4, 1968
(1098 observations)

Model	Rms (secs of arc)	
	unmodified	modified*
SAO M-1	17.36	3.08
SAO M-1	- -	6.12**
SAO COSPAR	5.54	- -
SAO 1969	2.50	- -
Köhnlein	9.41	3.12
Rapp	11.30	5.48
NWL 5E-6	27.99	8.08
APL 3.5	59.71	5.79
Kaula	16.67	9.32

ARC 2: September 16 - 22, 1968
(1388 observations)

Model	Rms (secs of arc)	
	unmodified	modified*
SAO M-1	12.87	6.11
SAO M-1	- -	5.53**
SAO 1969	2.37	- -
Köhnlein	6.52	- -
Rapp	7.05	- -
NWL 5E-6	21.35	- -
APL 3.5	68.95	- -
Kaula	11.25	- -

*Addition of Yionoulis (1968) + Douglas & Marsh (1969).
**Addition of Yionoulis (1968) only.

For GEOS II, the Yionoulis odd-degree 13th order terms alone greatly reduced the rms of fit (the SAO M-1 result in Table 8 is similar to the results obtained when the other models were modified by Yionoulis values only), but an along track effect of about 150 meters remained. The approximate calculations of Table 3 show that the most important even-degree resonant term for GEOS-II is

(14,13). By analyzing the variation in the along track residuals obtained from the SAO M-1 with Yionoulis 13th order term solution, Douglas and Marsh (1969) produced values of (14,13) which eliminated the effect of the even-degree terms for GEOS-II on the April-May arc. On the September arc, models which contained an insufficient number of resonant terms also were modified by incorporating the Yionoulis and Douglas and Marsh 13th order terms. But when the Douglas and Marsh term plus the Yionoulis coefficients were added to the SAO M-1 model, the rms of fit increased for the September arc, in contrast to the substantial improvement obtained for the April - May arc. This suggests that multi-arc solutions for composite coefficients are required rather than the single arc used by Douglas and Marsh. The arcs should be chosen so that the values of the orientation elements ω, Ω are as varied as possible.

Preliminary analyses with the SAO COSPAR (1969) model indicated the 11th order coefficients were in error. When the complete COSPAR model was used in obtaining orbital solutions for GEOS-I, the rms's on both arcs were about 10 seconds of arc. Hence, all SAO COSPAR solutions used in this study were obtained without using any 11th order coefficients. The more recent SAO model, the 1969, did not contain any such errors, as shown by the excellent solutions produced by the unmodified version.

3.3 PREDICTION CAPABILITIES

An important application of an accurate geopotential model is its ability to predict the position of a satellite considerably ahead of the last fitted data point. This ability can be measured by computing the root mean squares of observations about a trajectory generated ahead of the fitted orbital arc. Table 9 presents the rms's about the predicted trajectories from the July GEOS-I solutions and the April-May GEOS-II solutions. Prediction results from the GEOS-I and GEOS-II arcs were consistent with the fits in Tables 7 and 8.

The large difference in prediction capability of the GEOS-I solutions and the GEOS-II solutions is immediately obvious. A possible cause of this difference is the fact that GEOS-II is relatively more perturbed by the geopotential than GEOS-I (see Section 1.1); thus a relatively more precise model is necessary for GEOS-II to achieve the same results as GEOS-I. Also the MOTS camera stations (which supplied most of the April - May data) are relatively poorly distributed geographically.

The SAO 1969 model consistently gave better results, both for GEOS-I and II, followed closely by the modified Köhnlein and SAO M-1 models. Prediction results were not obtained for the smaller, unmodified models because the rms's of the fits were so high that reasonable predictions would be unlikely.

3.4 SATELLITE POSITION COMPARISONS

Another method of comparing orbits determined with different gravity models consists of taking computed satellite positions determined with different models and differencing them. The

satellite position differences are resolved into radial, cross track and along track components. This method is very useful in spotting differences in orbits due to resonance.

In this study, all GEOS-I orbits were compared against the orbit determined by the SAO M-1 with Gaposchkin and Veis 12th order terms. The GEOS-II orbits were compared with the orbit determined by the SAO M-1 with the Yionoulis and Douglas and Marsh 13th order terms. This does not imply that these models are always "best" in every sense. We chose the M1 model as the basis for comparison because it is so widely used.

Table 9

Fits About Predicted Trajectories GEOS-I and GEOS-II

GEOS-I, ARC 1

Definitive Period: July 11-16, 1966 (1766 Obs.)

Prediction Period: July 17-22, 1966 (1858 Obs.)

Model	Rms (secs of arc)	
	unmodified	modified*
SAO M-1	- - -	5.88
SAO 1969	4.75	- - -
Köhnlein	- - -	5.25
Rapp	- - -	23.68
NWL 5E-6	- - -	7.08
APL 3.5	- - -	20.57
Kaula	6.58	7.43

GEOS-II, ARC 1

Definitive Period: April 28-May 4, 1968 (1098 Obs.)

Prediction Period: May 5-9, 1968 (622 Obs.)

Model	Rms (secs of arc)	
	unmodified	modified**
SAO M-1	- - -	12.17
SAO 1969	13.04	----
Köhnlein	28.16	11.20
Rapp	33.51	13.89
NWL 5E-6	- - -	31.87
APL 3.5	- - -	22.63
Kaula	78.09	17.09

*Addition of Gaposchkin & Veis (1967)

**Addition of Yionoulis (1968) and Douglas & Marsh (1969)

Table 10 summarizes the results of the gravity model comparisons over the fitted arcs. As expected, the along track differences were more outstanding than the radial and cross track differences (see Section 1.2), even though the radial and cross track differences were larger for GEOS-II orbits than for GEOS I. This is probably due to the less widely distributed tracking stations for the GEOS II arc and the fact that GEOS-II is slightly more perturbed by the geopotential than is GEOS-I. The one exception to this is the SAO M-1 modified versus the NWL 5E-6 modified orbits on the GEOS-II arc, where the cross track differences are frequently as great as 200 meters. The along track differences are only occasionally that large. Table 10 reveals something very important about orbit determination accuracy. We see, for example, that for GEOS-II, the orbit obtained with the modified SAO M1 model differs along-track from the orbit obtained with the SAO 1969 model by about 64 m (rms). Although the SAO 1969 model gives a better fit, the modified M1 model gives better predictions. Thus we cannot directly say which is "best". Figure 1 may shed some light. It shows the apparent timing errors obtained for passes of range data recorded from the Rosman, N. C., S-Band Radar tracking site based upon the April - May GEOS-II optical arc using the SAO 1969 and Modified M1 models. The range data were not used in the determination of the optical reference orbit. These "timing errors" are of course due to unmodeled orbit variations, and not to system or hardware errors and in the case of the SAO 1969 model are obviously due mainly to inadequately modeled resonance in the amount of about 40 m along-track.

The results in Table 10 are consistent with previous tables of fitted and predicted orbits. Considering results for both GEOS I and II, they suggest that for 5 - 6 day arcs, we cannot be certain of satellite position to perhaps 50-100 meters (with published gravity models) even during the period of observation. The need for improved gravity models is unquestionable.

Figures 2 (a - c) present the first, third and sixth day plots of along track differences presented in Table 10 for the three best GEOS-I orbits: the modified Köhnlein, the modified NWL 5E-6 and the SAO 1969. Figures 3 (a - c) present the along track differences for the same models for the GEOS-II April - May arc. Again note that the modified M-1 and SAO-1969 orbits differ by over 100 meters fairly regularly for both GEOS-I and GEOS-II comparisons.

Figures 4 (a-f) contain a plot comparing the GEOS-I unmodified Köhnlein and the modified Köhnlein along track differences for the period July 11 - 16, 1966. The six-day period of the differences of the unmodified model clearly indicate that they are due to inadequate 12th order coefficients. Addition of the Gaposchkin and Veis 12th order terms greatly reduced these differences. On the basis of the rms's of fits (Table 7) we can say that the Kohnlein orbit was significantly improved. Similar reductions in along track differences were seen in nearly every such comparison of modified and unmodified models. Of course those gravity models that contain no GEOS resonant terms give very poor results.

Table 10

Rms's of Position Differences

GEOS I (July 11 - 16, 1966) and GEOS II (April 28 - May 4, 1968)

SAO M-1 (modified*) vs.	Position (meters)							
	GEOS I				GEOS II			
	Radial	Cross Track	Along Track	Total	Radial	Cross Track	Along Track	Total
SAO M-1 (unmodified)	30.0	17.1	286.4	288.5	22.3	10.3	232.2	234.2
SAO COSPAR (no. 11th)	8.9	12.8	29.5	33.4	24.7	18.2	92.8	97.8
SAO 1969	8.3	13.5	26.9	31.2	16.6	19.3	59.2	64.4
Köhnlein	16.4	16.1	213.0	214.2	20.1	16.9	129.1	131.7
Köhnlein (modified)	9.2	10.9	28.0	31.4	11.8	15.1	41.3	46.1
Rapp	48.3	29.5	129.4	141.2	38.8	37.7	157.6	166.6
Rapp (modified)	46.4	33.2	99.9	115.0	36.2	39.1	84.8	100.1
APL 3.5	46.1	46.8	175.7	187.1	71.8	55.2	674.3	680.4
APL 3.5 (modified)	42.5	41.6	90.1	107.9	34.7	45.4	88.1	105.2
NWL 5E-6	16.3	16.6	204.0	205.3	46.4	80.9	374.6	386.1
NWL 5E-6 (modified)	16.7	12.9	49.1	53.4	26.3	80.0	82.9	118.2
Kaula	32.5	42.2	114.1	125.9	47.6	43.5	232.8	241.4
Kaula (modified)	32.1	42.5	110.2	122.4	48.7	42.0	140.5	154.6

*Gaposchkin & Veis (1967) 12th order terms for GEOS-I and Yionoulis (1968) and Douglas & Marsh (1968) 13th order terms for GEOS-II.

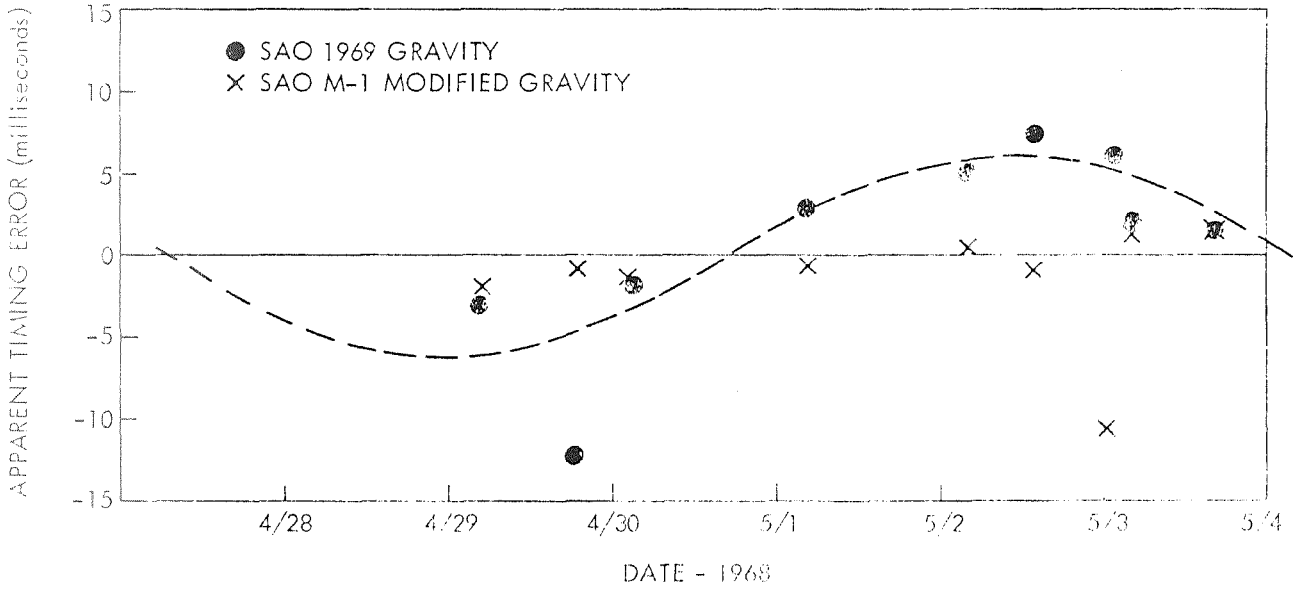

Figure 1. Apparent Timing Errors in Rosman Range Data Due to Unmodeled Orbit Variations Based Upon 6 Day GEOS-II Optical Reference Orbits

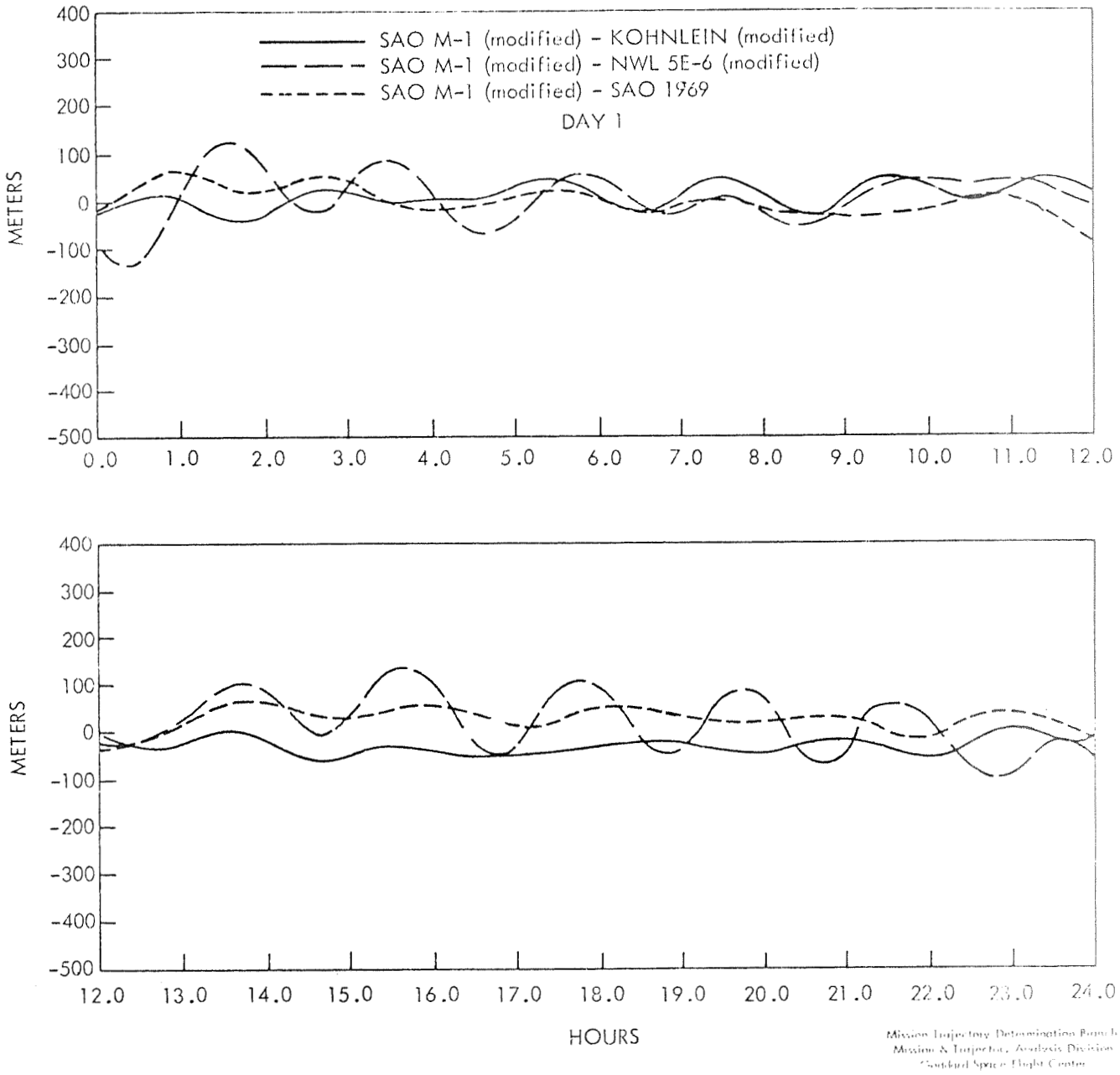

Figure 2(a). Along Track Position Differences – GEOS-I July 11-16, 1966

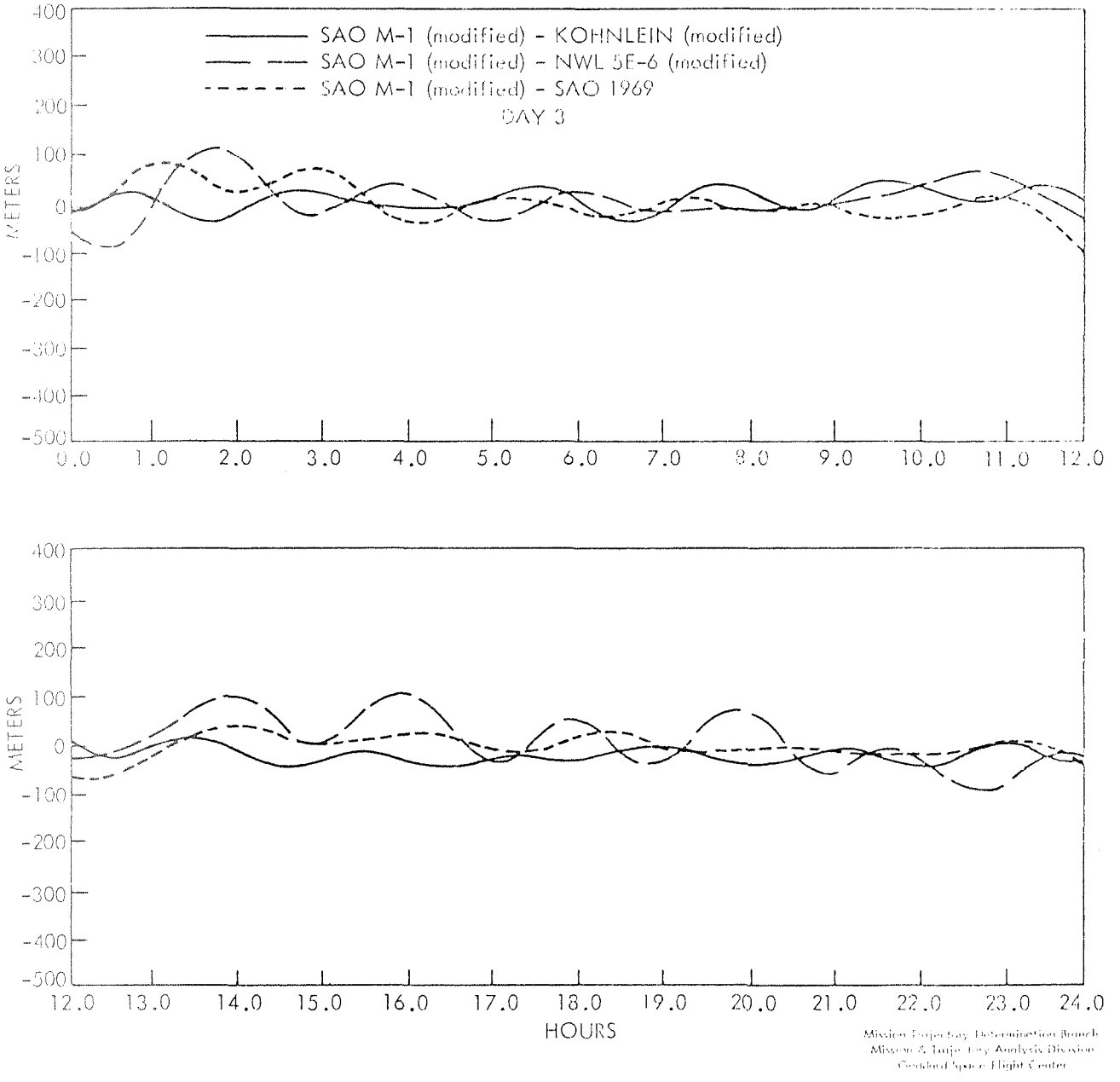

Figure 2(b). Along Track Position Differences – GEOS-I July 11-16, 1966

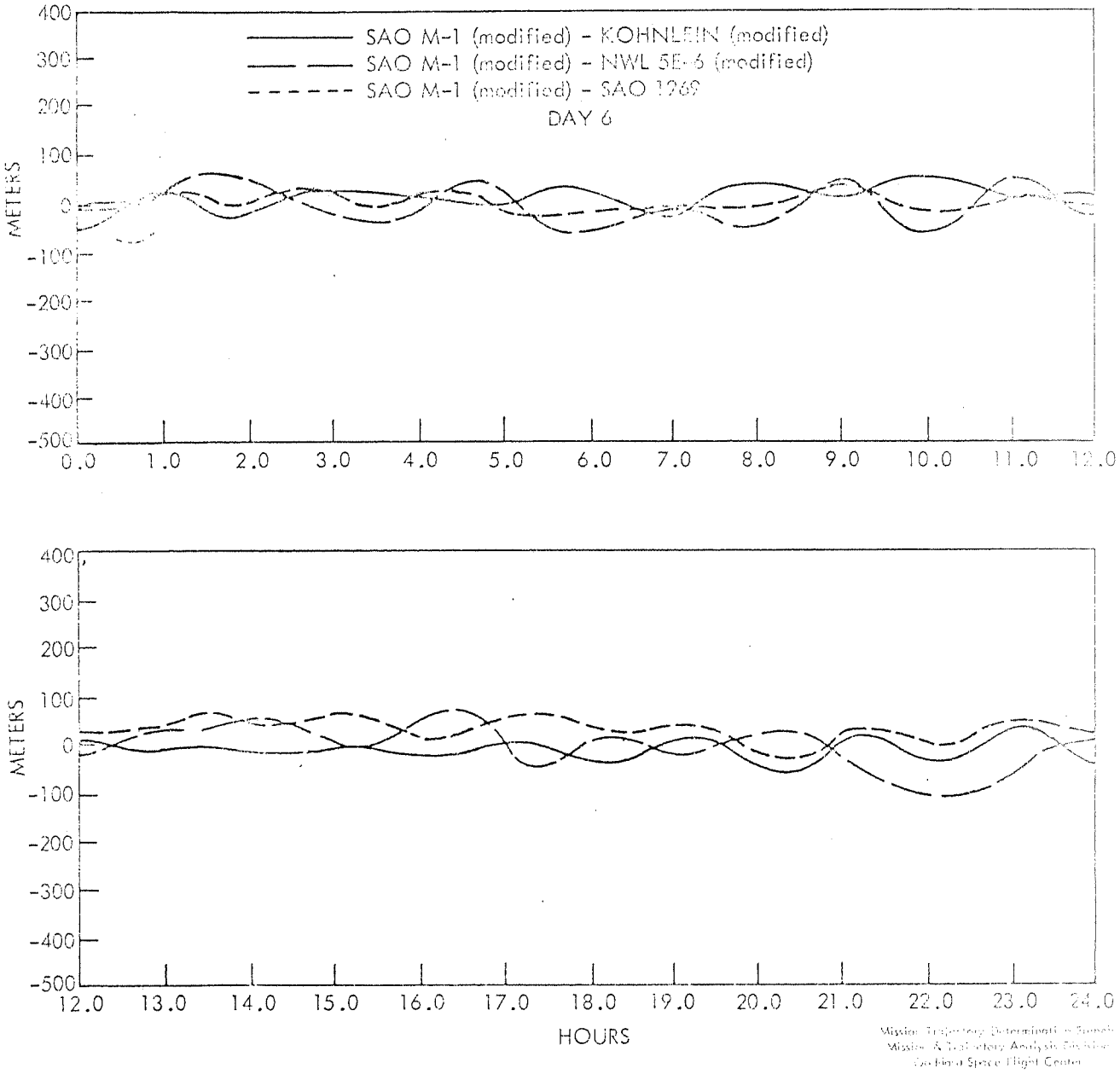

Figure 2(c). Along Track Position Differences – GEOS-I July 11-16, 1966

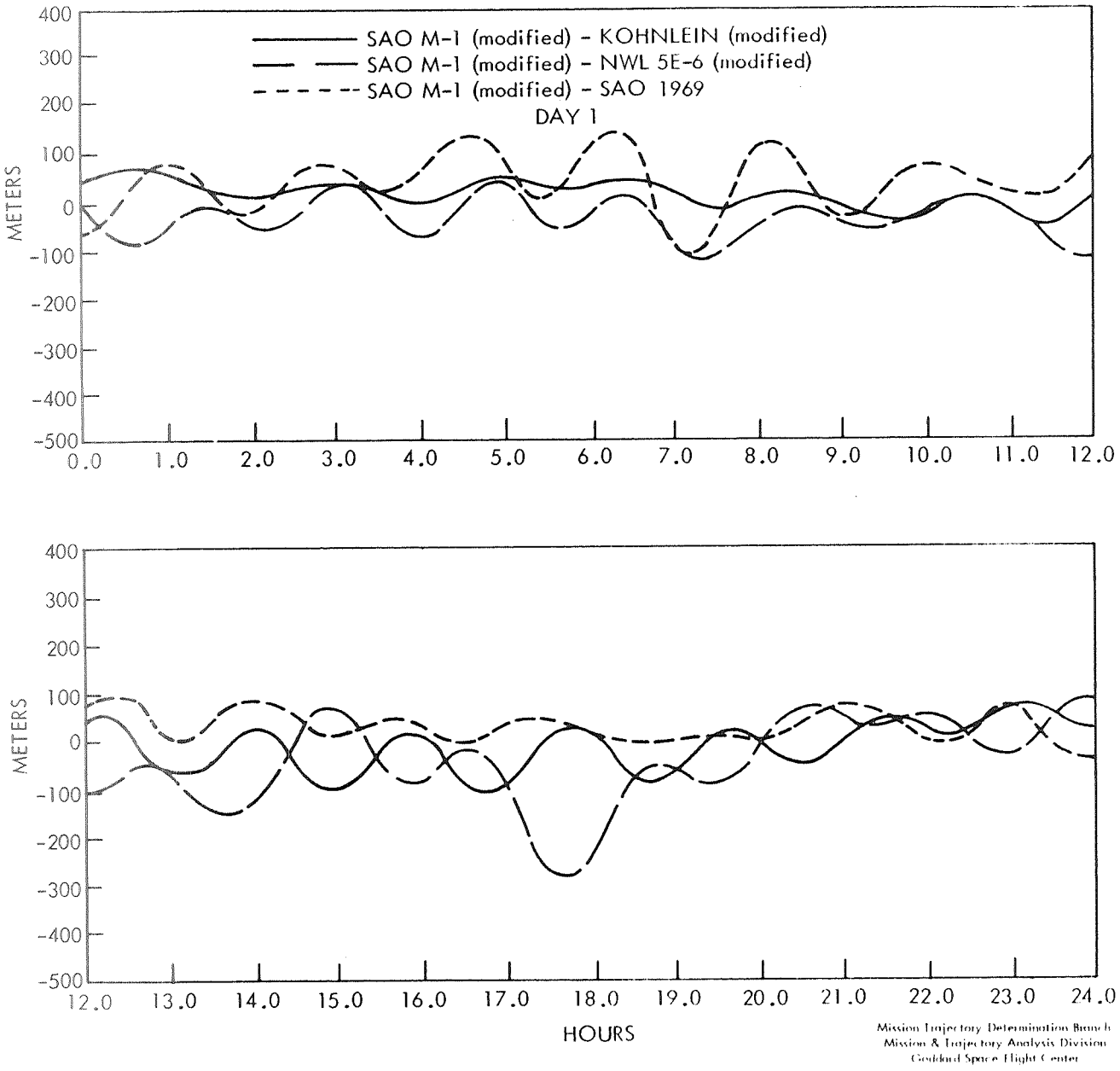

Figure 3(a). Along Track Position Differences – GEOS-II April 28-May 4, 1968

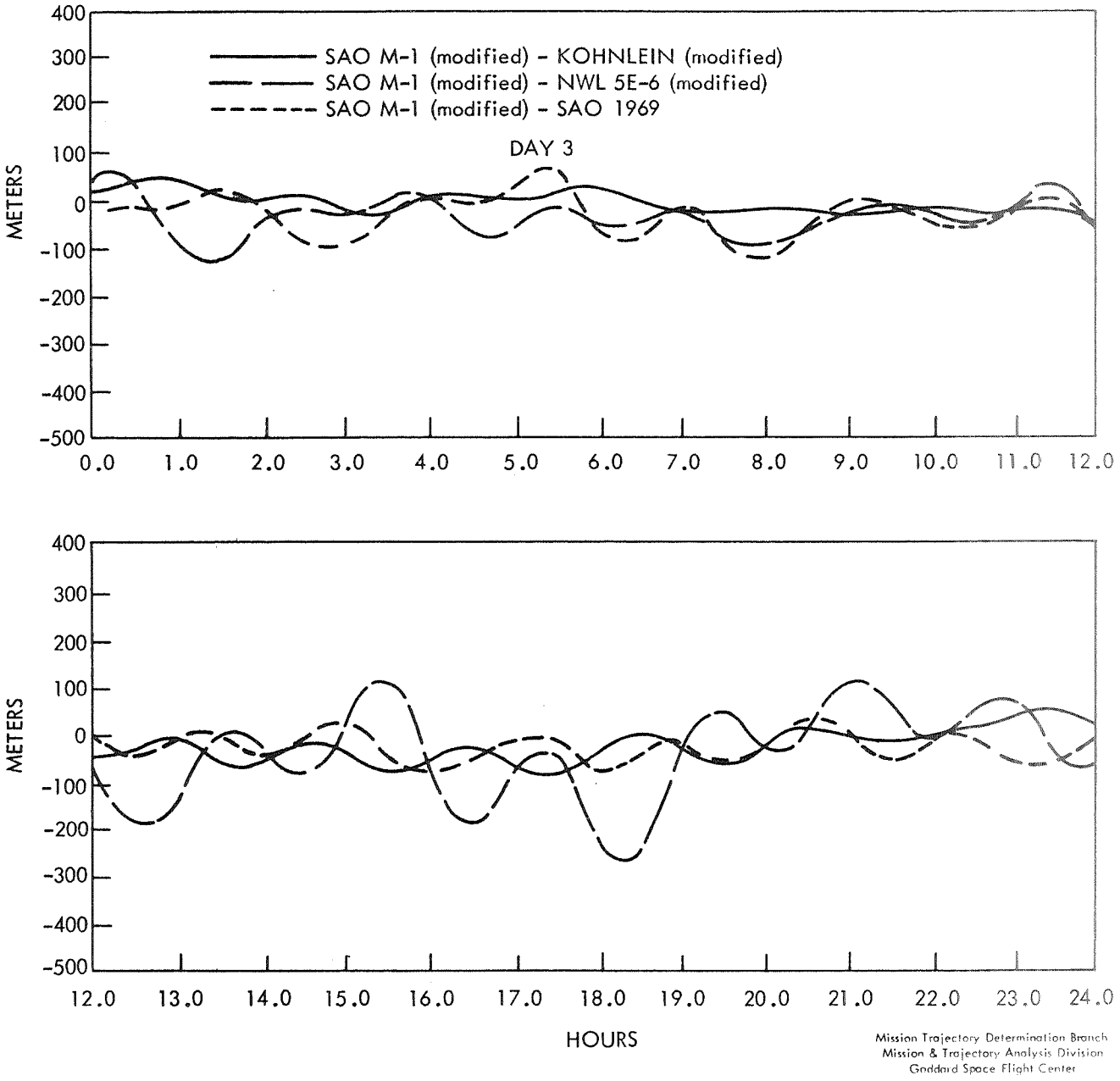

Figure 3(b). Along Track Position Differences – GEOS-II April 28-May 4, 1968

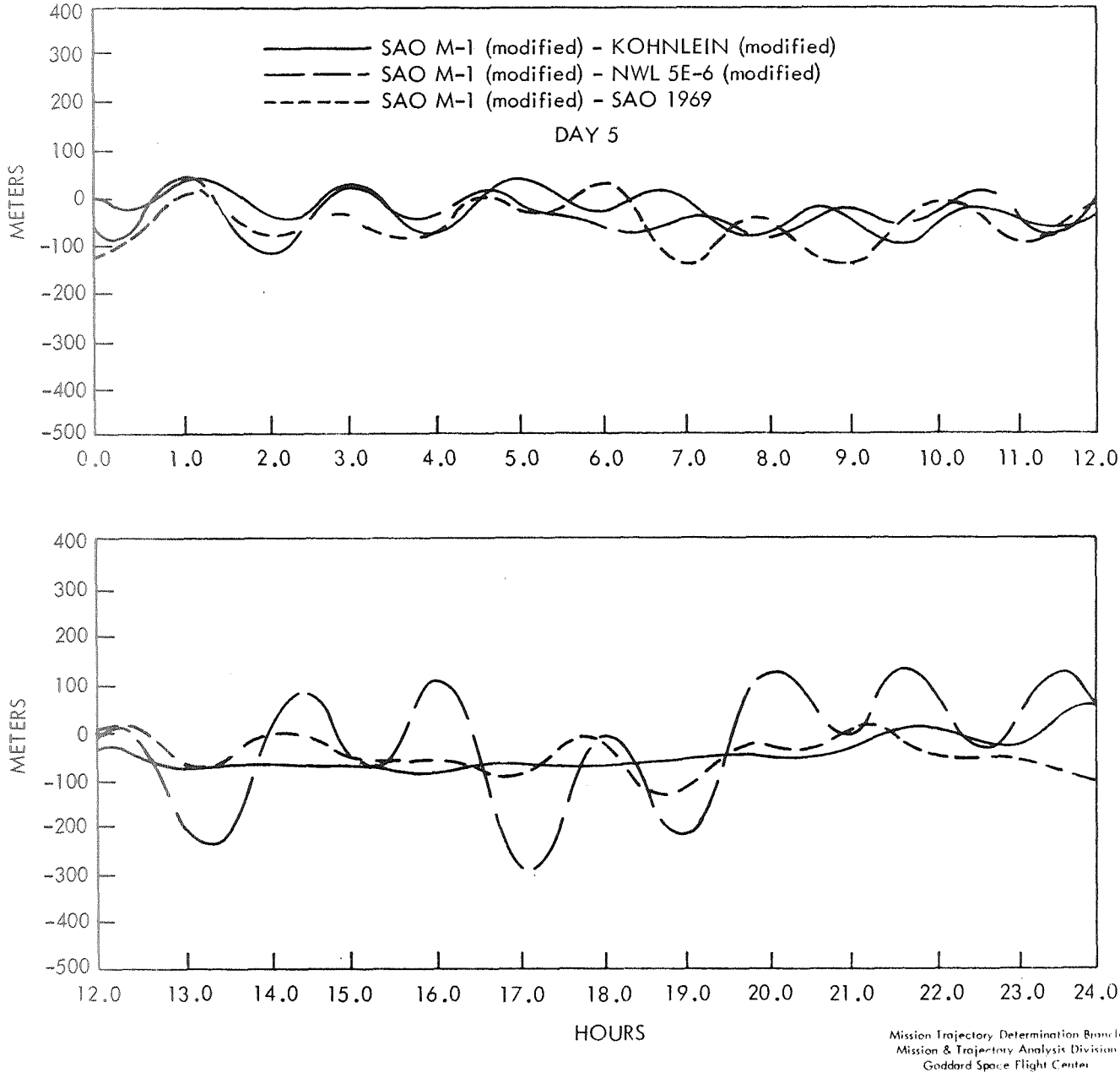

Figure 3(c). Along Track Position Differences – GEOS-II April 28-May 4, 1968

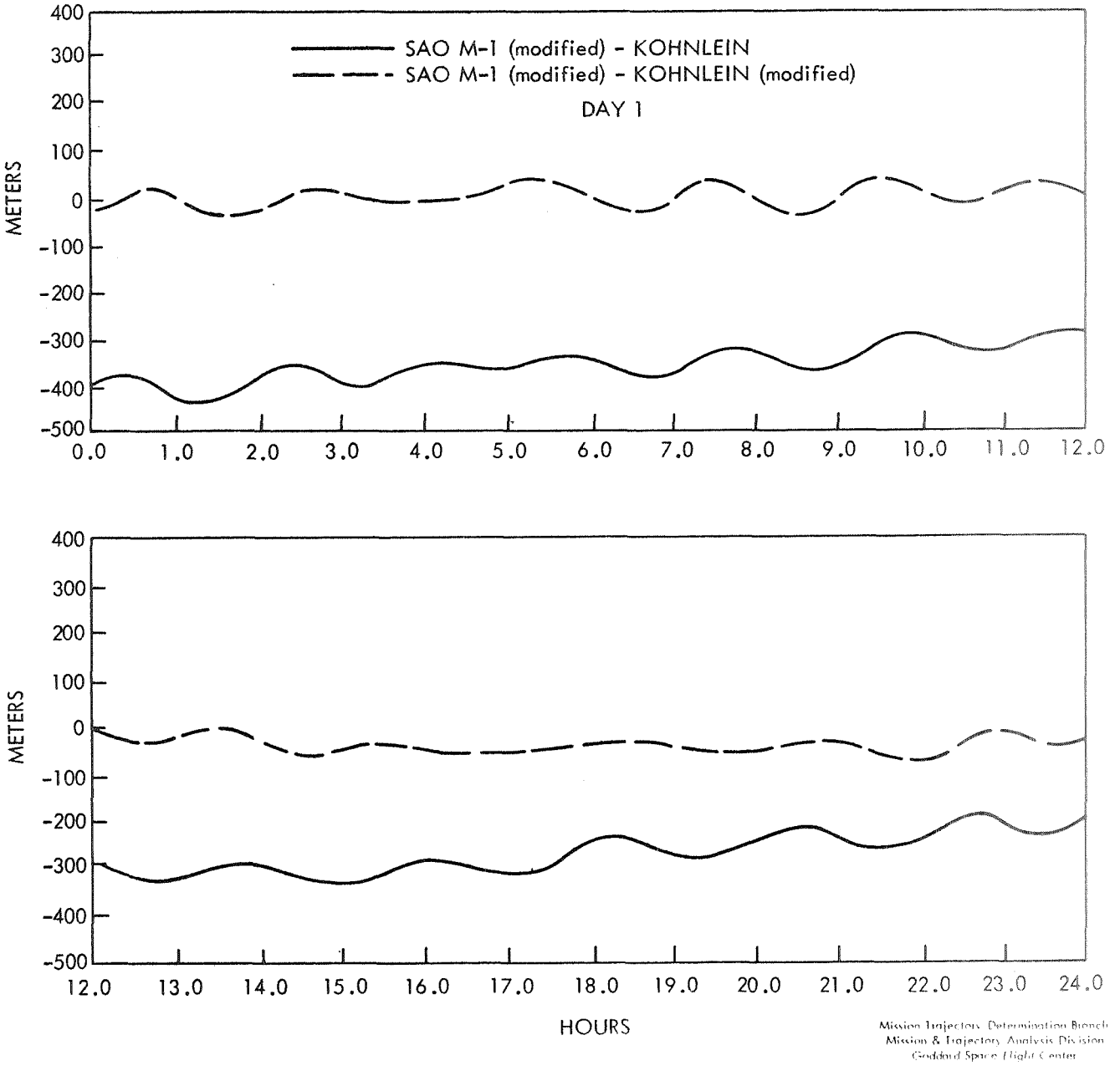

Figure 4(a). Along Track Position Differences – GEOS-I July 11-16, 1966

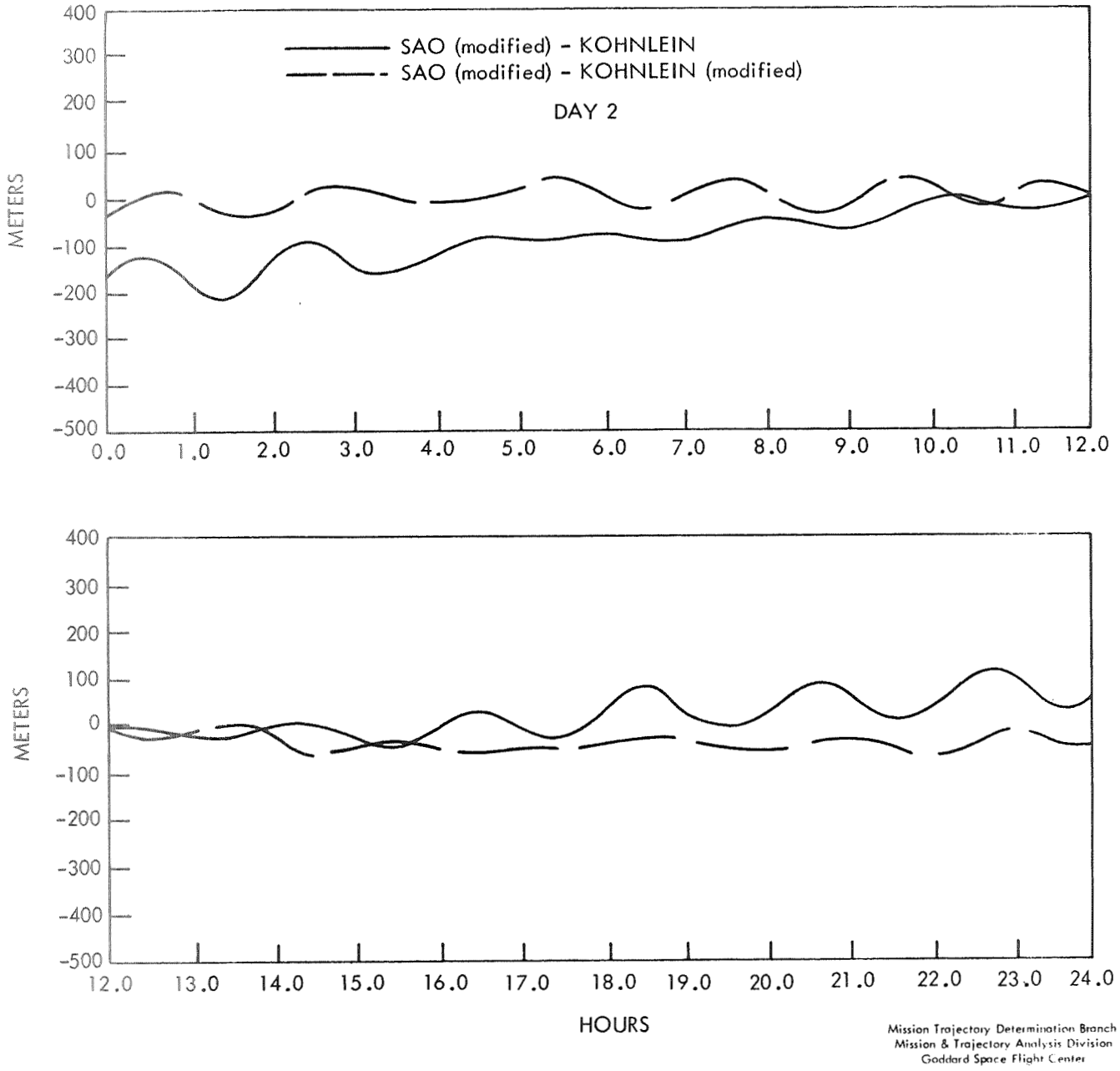

Figure 4(b). Along Track Position Differences – GEOS-I July 11-16, 1966

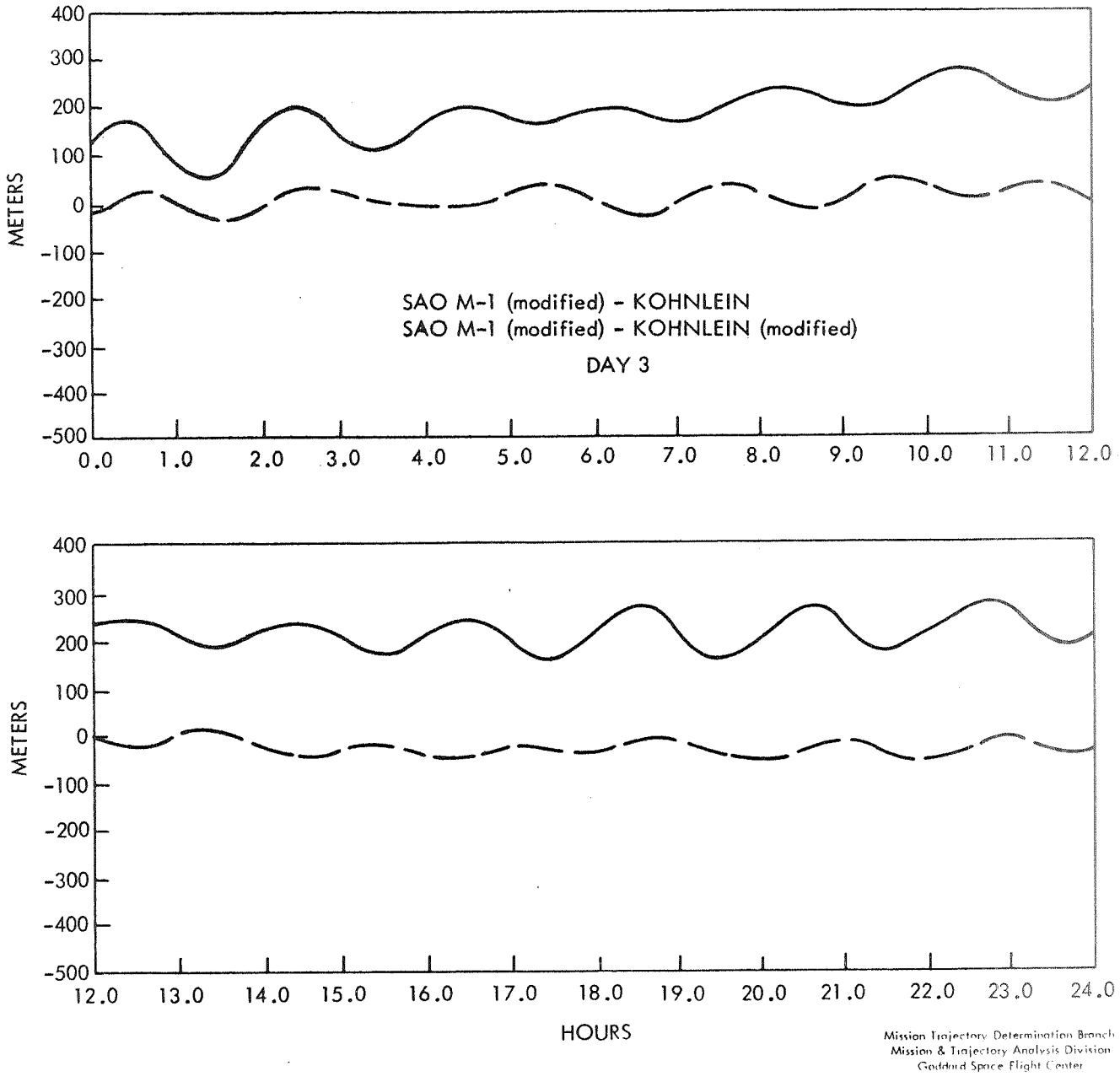

Figure 4(c). Along Track Position Differences – GEOS-I July 11-16, 1966

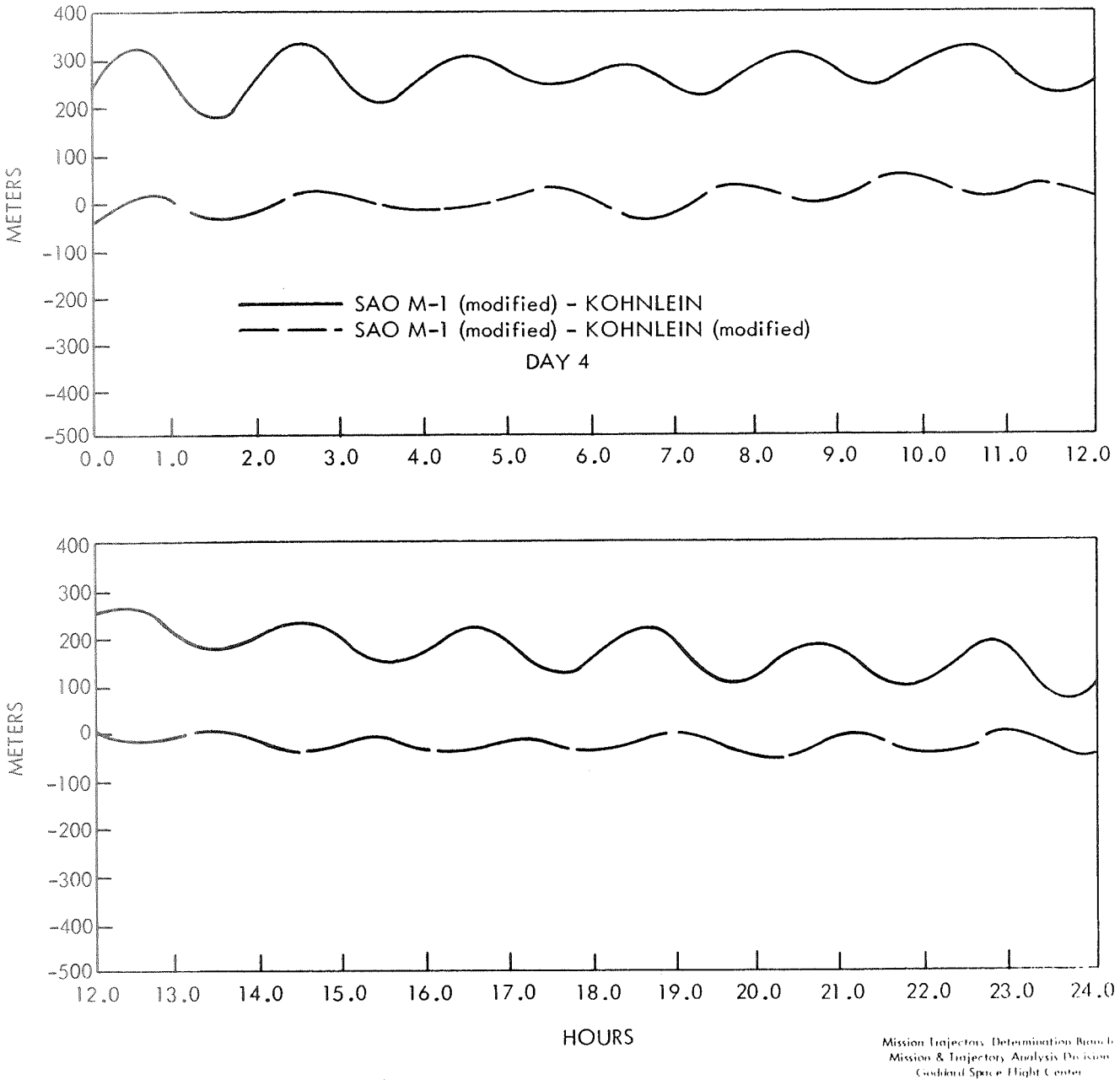

Figure 4(d). Along Track Position Differences – GEOS-I July 11-16, 1966

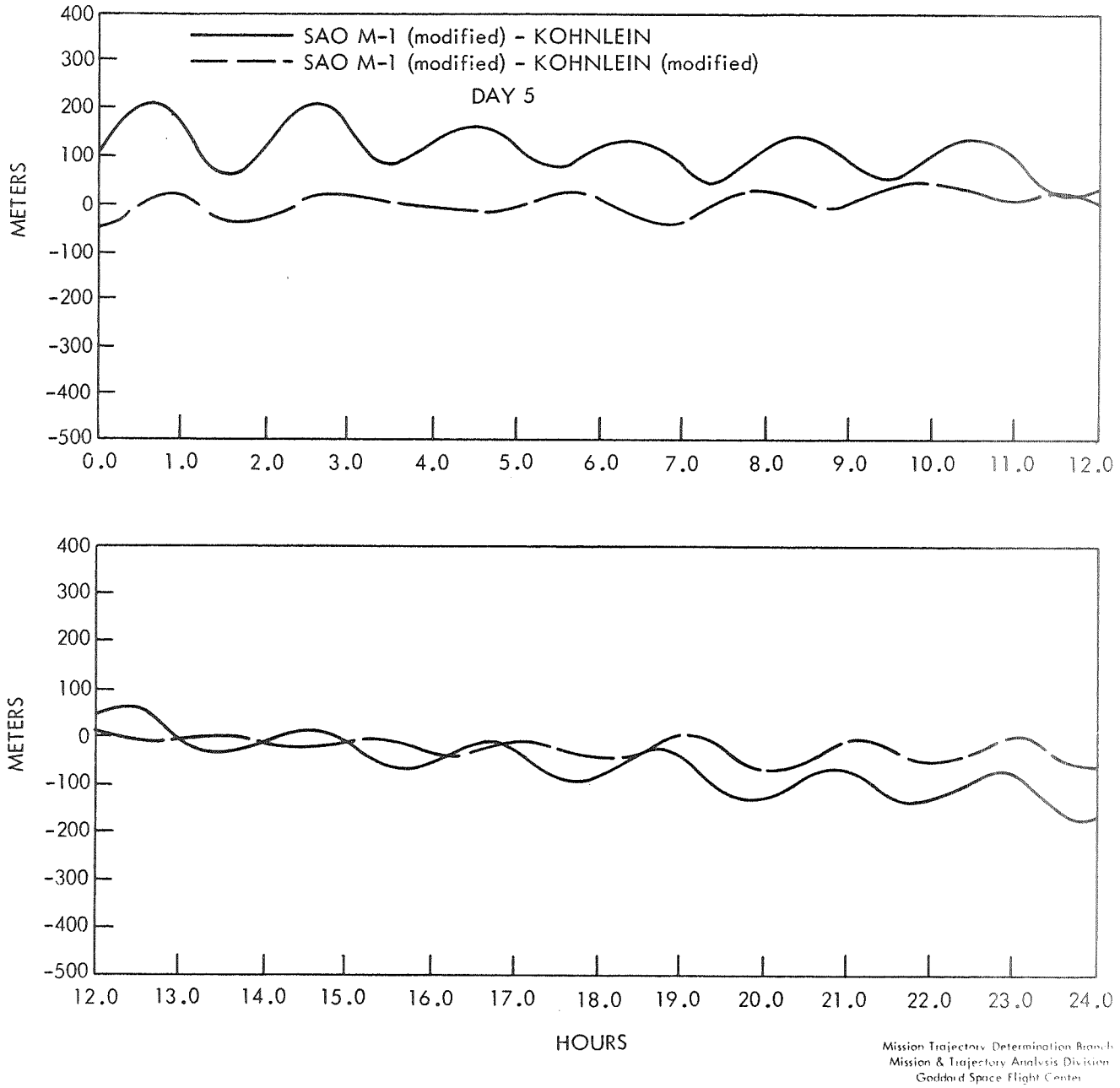

Figure 4(e). Along Track Position Differences – GEOS-I July 11-16, 1966

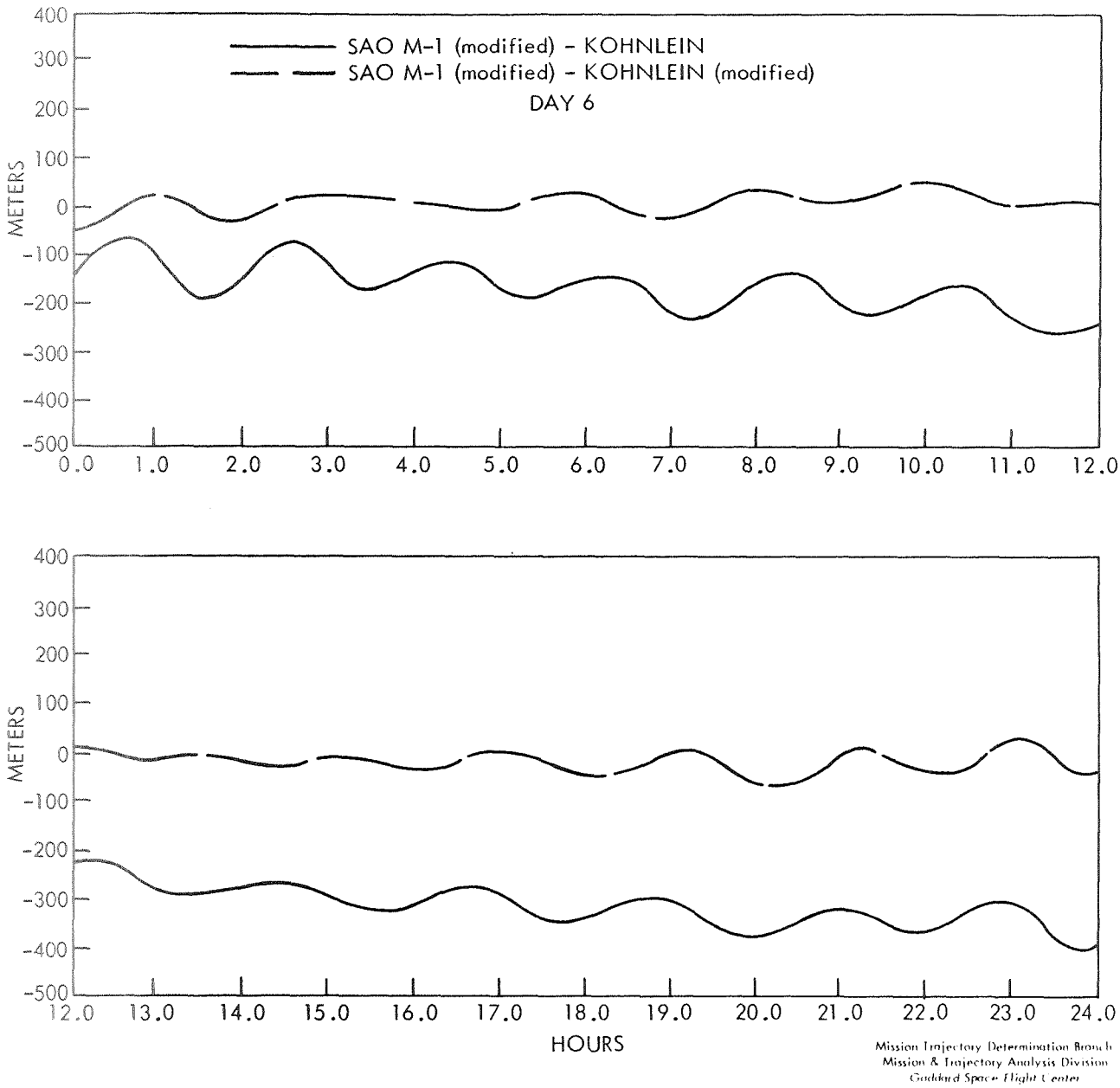

Figure 4(f). Along Track Position Differences – GEOS-I July 11-16, 1966

SECTION 4
CONCLUSIONS

The most obvious (and not so surprising) result of this study is that resonance must be accurately modeled for precision orbit determination. Both GEOS-I and GEOS-II orbits were greatly improved by using improved resonant coefficients. Also, the resonance effect can be modeled for a particular orbital arc by one or two "lumped" coefficients; however, the generality of such a solution is in question. The 1966 SAO M-1 12th order coefficients gave good results over the December-January arc but a high rms of fit in the July arc. The Douglas and Marsh values for (14,13) greatly improved the April-May, 1968, GEOS-II orbits but seemed to worsen the September, 1968, SAO M-1 and 1969 orbits. The very good results obtained when using the SAO 1969 model are almost certainly due to the richly varied resonant orbits used in the derivation of this model.

Based on the results presented in this study, the SAO 1969 geopotential model is a significant improvement over the 1966 SAO M-1 model, and is the most accurate model published to date. Yet improvement is still possible; note the unmodeled resonance effect in Figure 1 and the superior orbital prediction given by the modified M1 model for GEOS-II.

The good results obtained with the modified Köhnlein and Rapp and the SAO 1969 also indicate that gravimetric data may be used to good advantage in perfecting geopotential models for satellite orbit determination. As noted by Douglas and Marsh (Reference 12), the results for the Köhnlein and Rapp models demonstrate that gravimetric data has provided estimates of 12th and 13th order coefficients that remove much of the resonance effect for the GEOS satellites.

Finally, we are forced to conclude that even with the best available gravity models and observing equipment, satellite position along-track is uncertain at various points on the orbit by 50-100 meters for 5-6 day arcs. A degradation will be observed for longer arcs.

REFERENCES

1. O'Neill, B., "NONAME An Orbit and Geodetic Parameter Estimation System," Prepared under NASA Contract NAS-5-9756, August 1968.

2. Veis, G., "The Determination of the Radius of the Earth and Other Geodetic Parameters as Derived from Optical Satellite Data," Paper presented at the XIV General Assembly of the International Union of Geodesy and Geophysics, International Association of Geodesy, Sept. 1967.

3. Lundquist, C. A., and G. Veis, "Geodetic Parameters for a 1966 Smithsonian Institude Standard Earth," Smithsonian Astrophysical Observatory Special Report No. 200, Vol. 1, 1966.

4. Gaposchkin, E. M., "Improved Values for the Tesseral Harmonics of the Geopotential and Station Coordinates," presented at the XII COSPAR Meeting, Prague, May 1969, Smithsonian Institute Astrophysical Observatory.

5. Gaposchkin, E. M., Provisional Geodetic Parameters, U. S. Gov't Memorandum, Oct. 7, 1969.

6. Guier, W. H., and R. R. Newton, "The Earth's Gravitational Field as Deduced from the Doppler Tracking of Five Satellites," Journal of Geophysical Research, Vol. 70, No. 18, September 1965.

7. Anderle, R. J., "Geodetic Parameter Set NWL 5E-6 Based on Doppler Satellite Observations," NWL Report 1977, 1965.

8. Kaula, W. M., "Tests and Combination of Satellite Determinations of the Gravity Field with Gravimetry," Journal of Geophysical Research, Vol. 71, 1966.

9. Köhnlein, W., "The Earth's Gravitational Field as Derived from a Combination of Satellite Data with Gravity Anomalies," paper prepared for the XIV General Assembly, International Union of Geodesy and Geophysics, October, 1967.

10. Rapp, R. H., "The Geopotential to (14,14) from a Combination of Satellite and Gravimetric Data," paper prepared for the XIV General Assembly, International Union of Geodesy and Geophysics, October, 1967.

11. Kaula, W. M., Theory of Satellite Geodesy, Blaisdell, Waltham, Massachusetts, 1966.

12. Yionoulis, S. M., "Improved Coefficients of the Thirteenth-Order Harmonics of the Geopotential Derived from Satellite Doppler Data at Three Different Orbital Inclinations," Johns Hopkins/Applied Physics Laboratory Report TG-1003, May 1968.

13. Douglas, B. C. and J. G. Marsh, "GEOS-II and 13th Order Terms of the Geopotential," NASA X-Document No. X-552-69-291, July 1969.

14. Lundquist, C. A., "Geodetic Satellite Results During 1967," Smithsonian Astrophysical Observatory Special Report 264, December 1967.

Comparison of the SAO-1969 Gravity Field with Surface Gravity

by

William E. Strange

Computer Sciences Corporation
803 West Broad Street
Falls Church, Virginia

Introduction:

The gravity field representation produced by Smithsonian Astrophysical Observatory (SAO) in 1969-70 [1], [2] from a combination of surface and satellite data has been judged to be the most accurate representation of the long wavelength components of the earth's gravity field now available. This SAO 1969 gravity field consists of spherical harmonics through degree and order 16 with some higher degree resonant and zonal harmonics. The superiority of this field over previous determinations of the gravity fields has been attested to by the better orbits produced using it [1], [3] by some comparisons with surface gravity [1], [2] and by the increased correlation between known geologic parameters and the gravity field. [4] The objective of this paper is to carry out a more critical comparison of the SAO 1969 results and surface gravity than those previously reported in order to better establish the degree of accuracy of the SAO 1969 gravity field.

Basis of Comparison

In carrying out comparative analyses between surface gravity data and the SAO 1969 solution several factors must be kept in mind. These factors are:

(1) The surface gravity information must be smoothed in such a way that it is comparable to the satellite results before valid comparisons can be made.

(2) Surface gravity information varies as to its accuracy.

(3) Surface gravity information was used in deriving the SAO results.

Satellite derived gravimetric results in the form of coefficients of terms of low degree and order in a spherical harmonic expansion produce a smoothed

or "averaged" representation of the earth's gravity field. To a very close approximation a smoothed satellite field represented by harmonics through degree and order n is equivalent to averaging surface gravity over areas having dimensions of (180/n) degrees in latitude and longitude. The 1969 Smithsonian Standard Earth (II) gravity field, [2] having terms through degree and order 16 should, therefore, be compared with surface gravity averaged over $11.^{\circ}3$ by $11.^{\circ}3$ squares. Because of the nature of the available surface gravity data it was more convenient to obtain surface averages over 10° by 10° or 12° by 12° areas. This is believed to be sufficiently close to the correct area averaging so as to introduce no significant error.

It is well known that the accuracy of mean values of gravity computed from surface data vary greatly over the earth's surface. The mean gravity values in well surveyed land areas can be expected to be considerably more accurate than those in almost all ocean areas. This is true because (a) the density of coverage is greater in the land areas and, (b) individual observation accuracies are greater for land than for shipboard measurements. The uncertainties involved in using oceanic gravity data are well illustrated in Figure 1 where profiles of mean surface data as estimated by two different groups of investigators [5], [6] are compared for a profile across the North Atlantic, one of the best surveyed ocean areas. As may be seen, the two estimates of mean surface gravity anomalies differ from one another by as much as they differ from the SAO 1969 gravity result. To adequately test the SAO 1969 satellite gravity results it was, therefore, decided to use only non ship derived surface gravity data, primarily land data.

Surface gravity data was used by SAO in deriving the 1969 Standard Earth solution. Thus an adequate test of the overall accuracy of the SAO 1969 solution on a worldwide basis required that comparisons be made in areas other than those from which significant amounts of surface gravity data were used in deriving the SAO 1969 solution. The comparisons reported in this paper were made (a) along a profile in the continental United States, (b) along a profile in northern Canada, and (c) for individual points located in the Arctic Ocean, Australia, and India. The U. S. profile was chosen to represent an area from which a large amount of accurate surface data (although not the data used in

this comparison) was used in the SAO 1969 solution. The profile in northern Canada was chosen to represent an area just beyond the boundary of an area where large amounts of accurate surface data was available for the SAO solution. The Australian, Indian, and Arctic areas were chosen as areas where accurate surface data had recently become available but where no significant amounts of highly accurate surface data were used in the SAO 1969 solution.

Results

The results of the comparisons which were made are presented in Figures 2 and 3 and Table 1. Figure 2 presents, in the form of a profile along 40° north latitude, a comparison of the free air anomaly profile derived from the SAO 1969 results and a surface gravity profile obtained by computing 10° by 10° mean free air gravity anomaly values at 5° intervals using the surface gravity data from Strange and Woollard [7]. The degree of agreement is striking, with a mean difference of ±2 mgals and a maximum difference of 4.5 mgals. Since large amounts of surface data from the United States with reasonably high accuracy was used in the SAO 1969 solution rather good agreement was to be expected for this profile. Nevertheless, the degree of agreement exceeded what one might have reasonably hoped for and indicates that in carrying out the combined solution it was possible to model the available surface data extremely well.

Also presented in Figure 2 is a profile of 2° by 2° mean free air anomalies computed from the surface data. This profile is presented both to illustrate the need to average the surface data in a compatible manner before comparing with satellite results and to indicate the amount of information content available in the shorter wavelengths of the gravity field which are not obtained from present satellite solutions.

Figure 3 presents a comparison profile of surface gravity data and the SAO 1969 results along 59° north latitude in Canada. The surface gravity data is in the form of 12° by 12° mean free air anomalies which were computed at 6° intervals using the recent compilation of surface gravity data of Canada by the Canadian Dominion Observatory [8]. Although some Canadian surface gravity data was used in deriving the SAO 1969 results it could not, considering

the year of its origin, have been nearly as accurate as that used to derive the surface gravity profile in Figure 2. The remarkable agreement noted is, therefore, a mark of the overall accuracy of the SAO 1969 result. Again the RMS difference between the surface gravity data and the SAO 1969 results is ±2 mgals.

Table 1 presents a comparison of 10° by 10° mean values of free air gravity anomalies in India, Australia, and the Arctic Ocean with point values obtained from the SAO 1969 results. Point comparisons are made in these three areas because insufficient high quality surface data was available to compute a profile. All of the surface data used in Table 1 represents recent compilations of data [9], [10] which were not used in deriving the SAO 1969 results. It does not appear that sufficiently extensive or accurate surface data was available in these three areas when deriving the SAO 1969 solution to have exercised any strong control over the final results. As may be seen from Table 1, the maximum difference between the mean anomalies derived from surface data and from the SAO 1969 solution is ±6 mgals with the average difference being ±3 mgals. Again the agreement is exceptional. The agreement for the Arctic stations at latitudes up to 80° N is particularly significant since the zonal harmonics make the dominant contribution to the SAO results at high latitudes and the comparisons at these latitudes can be taken as indicative of the accuracy of the zonal harmonics.

Conclusions

Previous comparisons of surface gravity and the most recent SAO 1969 combination solution [2] have indicated that the RMS differences were of the order of ±8.5 to ±10 mgals. On the basis of these comparisons it has been generally felt that the accuracy with which the SAO 1969 solution represented average values of gravity over areas of dimensions of approximately 11° by 11° was about 8 to 10 mgals. However, the comparisons with carefully selected, high accuracy surface data presented here indicate that the accuracy with which the SAO 1969 solution represents 11° by 11° mean gravity anomalies is in all probability more nearly in the range of ±4 to ±6 mgals.

Bibliography

(1) Gaposchkin, E. M. and Lambeck, K., 1969, New Geodetic Parameters for a Standard Earth, preprint, Western National Meeting, AGU, San Francisco, 19 pp.

(2) Gaposchkin, E. M. and Lambeck, K., 1970, 1969 Smithsonian Standard Earth (II), Smithsonian Astrophysical Observatory, Special Report 315, 93 pp.

(3) Marsh, J. G., Douglas, B. C., and Dutcher, M., 1970, Tests and Comparisons of Gravity Models Using Camera Observations of GEOS I and II, NASA-GSFC Document No. X-552-70-48.

(4) Kaula, W. M., 1970, Earth's Gravity Field: Relation to Global Tectonics, submitted for publication in Science.

(5) Talwani, M. and LePichon, X., 1969, Gravity field in the Atlantic Ocean, in The Earth's Crust and Upper Mantle, P. J. Hart, ed., American Geophysical Union, Washington, D. C.

(6) Khan, M. A., and Woollard, G. P., 1968, Methods of Analysis and Comparison of Geophysical Data on a Plane, with Specific Application to the Soloman Islands Area, Report No. HIG-68-17, Hawaii Institute of Geophysics, University of Hawaii, 79 pp. and appendix.

(7) Strange, W. E. and Woollard, G. P., 1964, The Prediction of Gravity in the United States Utilizing Geologic and Geophysical Parameters; Report No. HIG-64-18, Hawaii Institute of Geophysics, University of Hawaii, 61 pp.

(8) Nagy, D., 1970, personal communication.

(9) Woollard, G. P., 1968, Collection, Processing and Geophysical Analysis Gravity and Magnetic Data, Final Report, Contract No. F23(601)-67-C-0168, Hawaii Institute of Geophysics, 114 pp and appendices.

(10) Wold, R., 1970, personal communication.

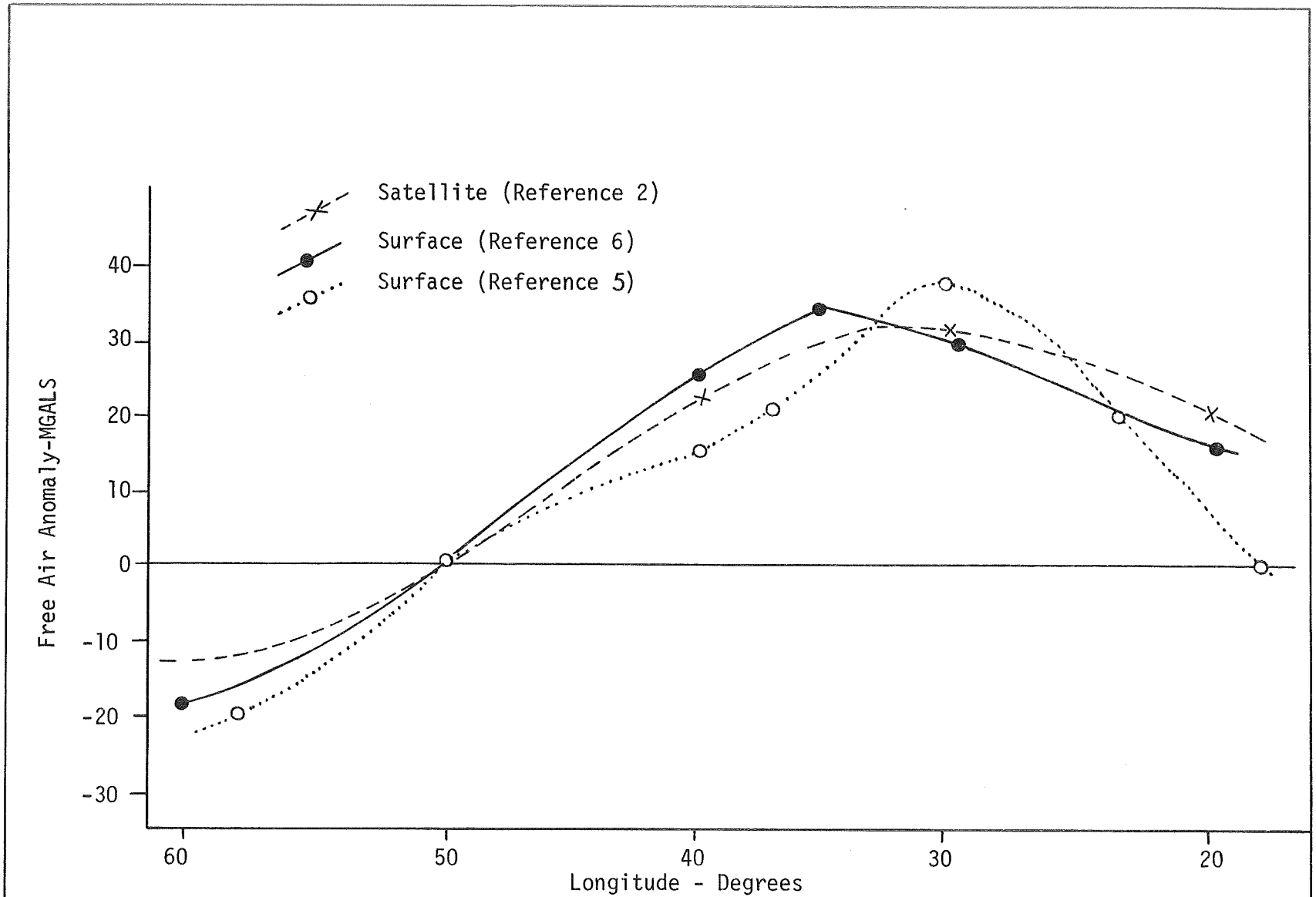

FIGURE 1

PROFILE ACROSS NORTH ATLANTIC
AT 40° N. LATITUDE

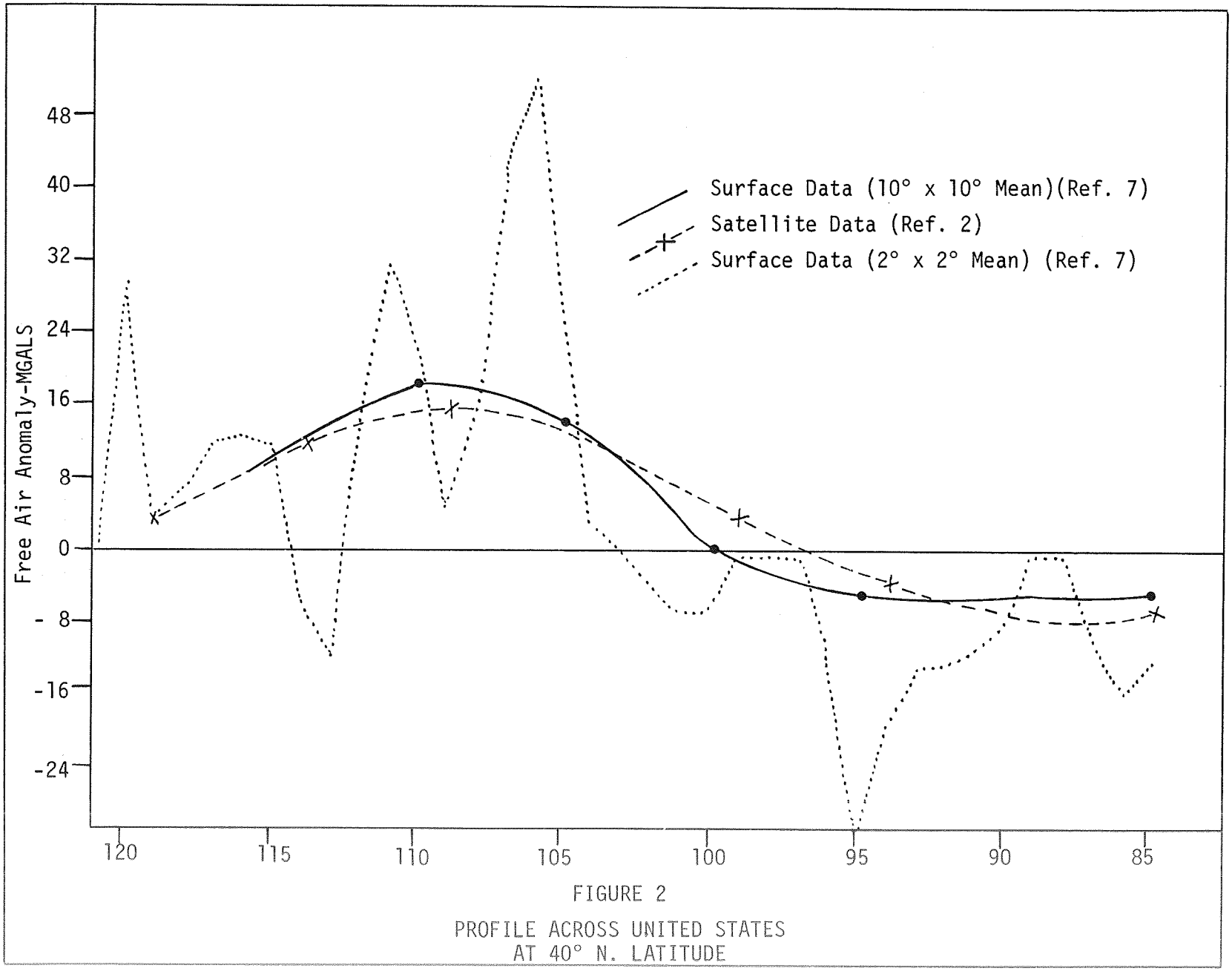

FIGURE 2

PROFILE ACROSS UNITED STATES
AT 40° N. LATITUDE

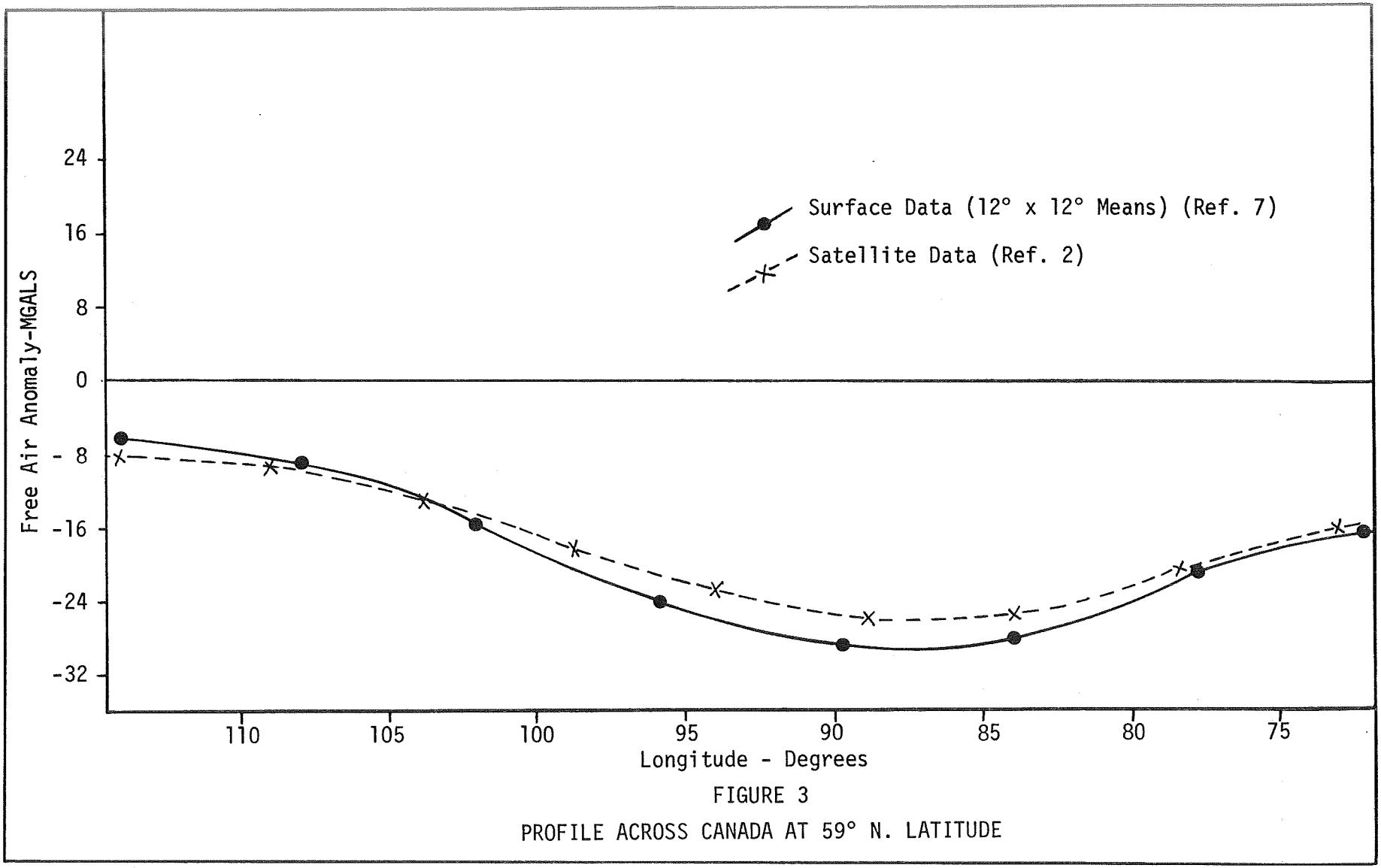

FIGURE 3

PROFILE ACROSS CANADA AT 59° N. LATITUDE

TABLE 1

WORLDWIDE POINT COMPARISONS

	FREE AIR ANOMALY	
	SURFACE (MGALS)	SATELLITE (MGALS)
INDIA		
LATITUDE 21° N LONGITUDE 79° E	-5	-6
AUSTRALIA		
LATITUDE 21° S LONGITUDE 139° E	+6	0
ARCTIC OCEAN		
LATITUDE 80° N LONGITUDE 155° W	+8	+8
LATITUDE 76° N LONGITUDE 135° W	+3	+4
LATITUDE 75° N LONGITUDE 165° W	+7	+10
LATITUDE 70° N LONGITUDE 170° W	+1	+ 7

X-522-70-104
PREPRINT

DERIVATION AND TESTS OF THE GODDARD COMBINED GEOPOTENTIAL FIELD (GSFC 1.70-C)

James P. Murphy
James G. Marsh

January 1970

Mission Trajectory Determination Branch
Mission and Trajectory Analysis Division
Goddard Space Flight Center
Greenbelt, Maryland

CONTENTS

DERIVATION AND TESTS OF THE GODDARD COMBINED GEOPOTENTIAL FIELD (GSFC 1.70-C)

James P. Murphy
James G. Marsh

ABSTRACT

A geopotential field complete to degree and order fifteen has been derived by combining fifteen separate determinations of spherical harmonic coefficients. Among the fields combined were ones obtained from Doppler data, optical data, Doppler and optical data, optical and terrestrial data, optical, Doppler and terrestrial data, and small sets of coefficients obtained by methods of resonant satellite geodesy.

Several tests of the combined gravity field were performed. The maximum difference between degree variances, σ_ℓ^2, obtained from this field and the corresponding ones obtained by Kaula in 1966 from free-air gravity anomalies is 4.5 m gal^2. The corresponding maximum difference obtained with the Smithsonian Astrophysical Observatory (SAO) 1966 Standard Earth was 9.9 m gal^2. After special resonant coefficients previously determined for the Geodetic Earth Orbiting Satellite (GEOS) I and II were substituted into the combined field, fits to six-day arcs of precisely reduced optical data were made. The rms of the fit to the GEOS I data arc was 2".3 which was the best fit among eight published fields considered. For GEOS II, the rms fit of 2".9 was second best among the eight fields. The SAO B13.1 (1969) model was used to obtain a fit of 2".3 for this GEOS II arc. For GEOS orbits 1" is approximately equal to 7 m. Some additional improvement to the fits were realized after the resonant coefficients (degree, order) = (13,12) and (13,13) were allowed to adjust.

DERIVATION AND TESTS OF THE GODDARD COMBINED GEOPOTENTIAL FIELD (GSFC 1.70-C)

INTRODUCTION

The potential of the earth at a point with spherical coordinates (r,ϕ,λ), in an earth centered rotating coordinate system may be given by

$$U = \frac{\mu}{r}\left\{1 + \sum_{\ell=2}^{\infty}\sum_{m=0}^{\ell}\left(\frac{a_e}{r}\right)^{\ell} P_{\ell,m}(\sin\phi)\,(C_{\ell,m}\cos m\lambda + S_{\ell,m}\sin m\lambda)\right\}. \tag{1}$$

This form of the potential is the recommended form for axially asymmetric (zonal, tesseral, and sectorial harmonics) cases, Reference 1. In equation (1), μ is the product of the gravitational constant, G, times the mass of the earth, M, and a_e is the mean equatorial radius of the earth. The Legendre associated function, $P_{\ell,m}(\sin\phi)$, is defined by

$$P_{\ell,m}(x) = \frac{1}{2^{\ell}\,\ell!}\,(1-x^2)^{m/2}\,\frac{d^{\ell+m}(x^2-1)^{\ell}}{dx^{\ell+m}}. \tag{2}$$

Instead of using the spherical harmonic coefficients $C_{\ell,m}$ and $S_{\ell,m}$, the fully normalized coefficients $\bar{C}_{\ell,m}$ and $\bar{S}_{\ell,m}$ have been adopted for this work. They are related to $C_{\ell,m}$ and $S_{\ell,m}$ coefficients by

$$\bar{C}_{\ell,m} = N_{\ell,m}\,C_{\ell,m} \tag{3}$$

$$\bar{S}_{\ell,m} = N_{\ell,m}\,S_{\ell,m}$$

where

$$N_{\ell,m} = \left[\frac{K(2\ell+1)(\ell-m)!}{(\ell+m)!}\right]^{-1/2}.$$

and where K = 1 for m = 0, and K = 2 for $m \neq 0$.

Combined geopotential fields based upon four individual solutions for the geopotential have been published, Reference 2. The first such field, C, appearing in Reference 2 was obtained by taking an arithmetic mean of these four solutions which were obtained from satellite tracking data. The second field, CA, was obtained by taking field C and combining it with terrestrial gravity data. In this paper Professor Kaula stated that an arithmetic mean of different solutions from satellite data is superior to any single solution and a combination of satellite and terrestrial solutions, such as solution CA, should be superior to either solution alone. He also suggested that such a combination should be made when more solutions are available.

In this paper we will form such a combination solution based upon eleven complete solutions and four partial solutions for the geopotential. This solution is not completely analogous to either of the solutions C or CA of Kaula. It is an arithmetic mean of individual solutions as is solution C; however, the individual solutions are made up of determinations based upon satellite data and ones based upon both satellite and terrestrial data. Thus, this combined solution is an arithmetic mean of solutions of the type C and CA.

INPUT GEOPOTENTIAL FIELDS

The fields used in obtaining the combined geopotential field are of various types. They include fields obtained solely from satellite data. These satellite determined fields include ones obtained from optical observations, Doppler observations, and both optical and Doppler observations. There are also fields represented which were determined from both satellite and terrestrial gravity data. In addition to these two types of fields, various sets of coefficients determined from satellites in resonant orbits were used in obtaining the combined field. The particulars concerning these input fields are contained in Table 1.

Table 1

Gravity Fields used in the Combination Solution

		Derivation of Fields		
Gravity Field	Reference	No. of Satellites	Data Types	Comments
NWL 5E-6	4	3	Navy Doppler	Complete to (7,6)
APL 3.5	5	5	Navy Doppler	Complete to (8,8)
SAO M-1	3	16	Optical	Complete to (8,8)
Köhnlein	6	16	Optical & Terrestrial	Complete to (15,15)
Kaula UCLA 656	7	9	Navy Doppler, Optical & Terrestrial	Complete to (8,8)
Kaula CA	2		Navy Doppler, Optical & Terrestrial	Complete to (7,2)
Kaula K-8	2			Complete to (7,5)
SAO B6.1	8	24	Optical, Range & Range Rate	Complete to (16,16)
SAO B13.1	9	24	Optical, Range, Range Rate & Terrestrial	Complete to (16,16)
Rapp 1967	10	16	Optical & Terrestrial	Complete to (14,14)
Rapp 1968	11	16	Optical & Terrestrial	Complete to (14,14)
Wagner	12	3	Mean Kepler Elements	Resonant Coefficients (2,2), (3,3)
Gaposchkin & Veis	13	2	Optical	Resonant Coefficients (13,12), (14,12), (15,12)
APL	14	3	Navy Doppler	Resonant Coefficients (13,13), (15,13), (17,13)
Goddard	15	1	Optical & Range	Resonant Coefficient (14,13) to be used with APL coefficients in April 1968 for GEOS II

NASA-GSFC T&DS
MISSION & TRAJECTORY ANALYSIS DIVISION
BRANCH 552 DATE 04/08/70
BY Murphy & Marsh PLOT NO 2099

The result of taking the arithmetic mean of these fields appears in Table 2. Note however, that the combined field, GSFC 1.70-C, so obtained was truncated after the terms of fifteenth degree and order. If terms of higher degree were averaged, there would be only a few contributors. A variety of tests conducted using this combined field are discussed in the next section. Tests were made with the remaining geodetic constants (zonals, earth radius, etc.) equal to those adopted for the SAO 1966 Standard Earth, Reference 3. For convenience they are also listed in Table 2.

Table 2

Earth Model

TESSERAL HARMONICS *

N	M	$\bar{C}(N,M)$	$\bar{S}(N,M)$
2	2	2.402	-1.370
3	1	1.391	0.219
3	2	0.834	-0.653
3	3	0.518	1.355
4	1	-0.550	-0.452
4	2	0.316	0.604
4	3	0.915	-0.121
4	4	-0.125	0.212
5	1	-0.037	-0.061
5	2	0.553	-0.248
5	3	-0.357	-0.012
5	4	-0.142	0.117
5	5	0.040	-0.501
6	1	-0.086	0.055
6	2	0.027	-0.329
6	3	0.051	0.079
6	4	-0.090	-0.459
6	5	-0.220	-0.501
6	6	-0.072	-0.261
7	1	0.159	0.039
7	2	0.324	0.089
7	3	0.206	-0.094
7	4	-0.224	-0.043
7	5	0.055	-0.040
7	6	-0.266	0.115
7	7	0.070	0.043
8	1	-0.047	0.028
8	2	0.059	0.020
8	3	-0.012	0.081
8	4	-0.094	0.025
8	5	-0.050	0.021
8	6	-0.038	0.259
8	7	0.040	0.025
8	8	-0.142	0.020
9	1	0.111	-0.014
9	2	0.003	-0.038
9	3	-0.034	-0.030
9	4	0.060	0.053
9	5	-0.044	-0.054
9	6	0.062	0.035
9	7	-0.055	-0.087
9	8	0.218	0.037
9	9	0.012	-0.025
10	1	0.075	-0.054
10	2	-0.067	-0.034
10	3	-0.017	-0.068
10	4	-0.050	-0.125
10	5	-0.045	0.006
10	6	-0.076	-0.060
10	7	0.071	-0.013
10	8	0.079	-0.097
10	9	0.040	-0.044
10	10	0.051	-0.064
11	1	-0.034	-0.027
11	2	0.057	-0.083
11	3	-0.023	-0.103
11	4	-0.000	-0.019
11	5	0.041	-0.006
11	6	-0.044	-0.073
11	7	0.012	-0.101
11	8	0.160	0.014
11	9	-0.016	-0.044
11	10	-0.046	-0.040
11	11	0.083	0.012
12	1	-0.079	-0.047
12	2	0.004	0.046
12	3	0.073	-0.011
12	4	-0.039	-0.095
12	5	-0.002	0.065
12	6	-0.065	0.024
12	7	0.004	0.026
12	8	0.009	0.073
12	9	-0.073	0.043
12	10	-0.002	0.005
12	11	-0.029	-0.011
12	12	-0.025	-0.012
13	1	-0.017	0.011
13	2	-0.031	-0.031
13	3	-0.067	0.024
13	4	-0.025	0.084
13	5	0.083	-0.077
13	6	-0.038	0.054
13	7	0.016	-0.007
13	8	0.047	-0.025
13	9	-0.010	0.009
13	10	0.055	-0.071
13	11	-0.038	0.009
13	12	-0.030	0.072
13	13	-0.098	0.055
14	1	-0.017	0.044
14	2	-0.028	0.009
14	3	0.109	-0.021
14	4	0.032	-0.043
14	5	0.068	-0.039
14	6	-0.033	-0.011
14	7	0.051	-0.015
14	8	-0.032	-0.056
14	9	-0.027	0.054
14	10	0.009	-0.070
14	11	0.081	0.024
14	12	0.017	-0.027
14	13	0.028	0.051
14	14	-0.040	-0.009
15	1	-0.015	-0.057
15	2	0.004	-0.109
15	3	-0.033	0.030
15	4	0.023	0.074
15	5	0.022	0.008
15	6	0.050	-0.053
15	7	0.075	0.053
15	8	-0.030	0.031
15	9	-0.040	0.045
15	10	0.038	0.022
15	11	0.013	0.072
15	12	-0.048	0.032
15	13	-0.045	-0.033
15	14	0.008	-0.013
15	15	-0.005	-0.015

*UNIT EQUALS TEN TO MINUS SIXTH POWER

ZONAL HARMONICS* $\bar{C}(N,0)$

$\bar{C}(2,0)$ =	-484.1733
$\bar{C}(3,0)$ =	0.9623
$\bar{C}(4,0)$ =	0.5497
$\bar{C}(5,0)$ =	0.0533
$\bar{C}(6,0)$ =	-0.1792
$\bar{C}(7,0)$ =	0.0860
$\bar{C}(8,0)$ =	0.0655
$\bar{C}(9,0)$ =	0.0122
$\bar{C}(10,0)$ =	0.0118
$\bar{C}(11,0)$ =	0.0630
$\bar{C}(12,0)$ =	0.0714
$\bar{C}(13,0)$ =	0.0219
$\bar{C}(14,0)$ =	-0.0332
$\bar{C}(15,0)$ =	0.0

SEMI MAJOR AXIS
(METERS)

6378142.00

FLATTENING

1./298.25

GRAVITATIONAL CONSTANT
(METERS**3/SECONDS**2)

3.986009000 14

TESTS AND EVALUATION OF THE COMBINED FIELD

Several tests of this new model have been made. The first pair of these were concerned with the fit to six day arcs of precision reduced optical data for GEOS I and GEOS II. The fits were made without and then with special values for resonant coefficients for the two satellites. For GEOS I the resonant coefficients were those obtained by Gaposchkin and Veis, Reference 13; and for GEOS II the resonant coefficients were those obtained by APL, Reference 14, and Goddard, Reference 15. Characteristics of these two satellite orbits are given in Table 3. In Table 4 there appears a list of resonant coefficients obtained previously for these two satellites. The combined field was then tested in orbit computations with and without resonant terms against some of the fields that were used in deriving it. After these tests were completed, the combined field was truncated in the following manner. All the coefficients of degree greater than eight with the exception of those of order twelve, thirteen, fourteen, and fifteen were deleted from the field. The same orbit determination runs were then repeated for this adjusted field, GSFC 1.70-T.

Table 3

GEOS I and GEOS II Orbit Characteristics

	GEOS I	GEOS II
semi major axis	8077.9 km	7701.1 km
eccentricity	.070	.033
inclination	59°.4	105°.8
argument of perigee	312°.0	194°.8
right ascension of ascending node	266°.1	353°.7
mean anomaly	224°.1	121°.0
epoch	July 11, 1966 $0^h 0^m$	April 28, 1968 $17^h 56^m$
resonant harmonics	12th order	13th order
resonant period	7.3 days	6.5 days
perigee height	1130.6 km	1071.8 km
apogee height	2268.9 km	1574.1 km

NASA GSFC T&DS
MISSION & TRAJECTORY ANALYSIS DIVISION
BRANCH 552 DATE 04/08/70
BY Murphy & Marsh PLOT NO 2101

Table 4

Resonant Coefficients for GEOS Satellites

GEOS I*	GEOS II**
$\bar{C}_{12,12} = -3.1 \times 10^{-8}$	$\bar{C}_{13,13} = -6.53 \times 10^{-8}$
$\bar{S}_{12,12} = .08 \times 10^{-8}$	$\bar{S}_{13,13} = 5.79 \times 10^{-8}$
$\bar{C}_{13,12} = -6.769 \times 10^{-8}$	$\bar{C}_{15,13} = -3.82 \times 10^{-8}$
$\bar{S}_{13,12} = 6.245 \times 10^{-8}$	$\bar{S}_{15,13} = -1.85 \times 10^{-8}$
$\bar{C}_{14,12} = .261 \times 10^{-8}$	$\bar{C}_{17,13} = 6.36 \times 10^{-9}$
$\bar{S}_{14,12} = -2.457 \times 10^{-8}$	$\bar{S}_{17,13} = 1.11 \times 10^{-8}$
$\bar{C}_{15,12} = -7.473 \times 10^{-8}$	$\bar{C}_{14,13} = 7.81 \times 10^{-9}$
$\bar{S}_{15,12} = -1.026 \times 10^{-8}$	$\bar{S}_{14,13} = 8.91 \times 10^{-8}$

* SAO

** APL & GSFC

NASA GSFC T&DS
MISSION & TRAJECTORY ANALYSIS DIVISION
BRANCH 552 DATE 04/08/70
BY Murphy & Marsh PLOT NO 2102

The fits to the data for the six day GEOS I and GEOS II arcs with the GSFC 1.70 C and GSFC 1.70T geopotential fields appear in Table 5. Also presented in Table 5 are fits obtained from previous studies, Reference 16, for the same orbital arcs using some of the complete fields used to derive the combined field. For the orbit computations involving the SAO B13.1 field, the recommended set of zonals, Reference 17, adopted for the 1969 SAO Standard Earth was used. Two points can be made concerning this table. First, after the resonant coefficients for these two satellites are inserted into the field, the fit to the data with the combined field is better than that of any other field for GEOS I, and for GEOS II the fit using the combined field was second only to the SAO B13.1 field. Secondly, after the field is adjusted so that it has only about forty percent of the terms that the original field had, the fit to the data remains about the same.

Table 5

Rms's (Sec's of Arc) of Fitted Orbits for Six Day Arcs of Optical Data from GEOS I and GEOS II when Different Gravity Models are used with and without Resonant Coefficients*

Geopotential Model	GEOS I		GEOS II		Number of Coefficients
	without	with	without	with	
SAO M 1	19.04	2.52	17.36	3.08	108
SAO B13.1	2.56	3.27	3.39	2.29	294
Köhnlein	14.65	2.89	9.41	3.12	236
Rapp 1967	7.81	6.91	11.30	5.48	206
NWL 5E-6	11.82	3.33	27.99	8.08	58
APL 3.5	13.51	6.64	59.41	5.79	74
Kaula 1967	5.80	5.95	16.67	9.32	88
GSFC 1.70C	6.48	2.30	6.67	2.95	236
GSFC 1.70T	6.67	2.43	6.87	3.23	88

*NOTE 1" equals approximately 7 m.

Certain coefficients in the combined field were adjusted using optical data in the six day arcs referred to in Table 5. Other coefficients were adjusted using accelerations from seven twenty-four hour satellites in the Syncom, Intelsat and ATS (Applications Technology Satellite) series of spacecraft. These accelerations had been prepared by Mr. C. Wagner for use in some of his deep resonance studies (see Reference 12, for example) and made available for this work by him. Values of the original and adjusted geopotential coefficients using these data appears in Table 6. The second and third degree sectorial harmonics were improved with the sectorial harmonic of degree four and the tesseral harmonics of degree three order one and degree four order two which are also sensitive for the accelerations held fixed to the values for the coefficients appearing in the combined field.

Table 6

Adjusted Coefficients*

Term	A Priori	Improved	Satellite (S)
$\bar{C}_{2,2}$	2.402	2.434	ATS 1,3,5, INTELSAT 1,2-F3, Syncom 2, 3
$\bar{S}_{2,2}$	-1.370	-1.398	
$\bar{C}_{3,3}$	0.618	0.726	
$\bar{S}_{3,3}$	1.365	1.371	
$\bar{C}_{13,12}$	-0.0675	-0.0703	GEOS I
$\bar{S}_{13,12}$	0.0622	0.0681	
$\bar{C}_{13,13}$	-0.0653	-0.0629	GEOS II
$\bar{S}_{13,13}$	0.0579	0.0586	

* Multiply all coefficients by 10^{-6}

NASA GSFC T&DS
MISSION & TRAJECTORY ANALYSIS DIVISION
BRANCH 552 DATE 04/08/70
BY Murphy & Marsh PLOT NO. 2103

When the twelfth order coefficient was adjusted, a two second of arc fit was obtained for the GEOS I arc. The corresponding improvement to the fit for the GEOS II arc was only a few percent. The RMS error to the twenty-four hour accelerations for the low degree coefficients that are sensitive to these accelerations appears in Table 7 for the SAO 1966 Standard Earth, SAO B13.1, SAO 1969 Standard Earth, GSFC 1.70-C and GSFC 1.70-C with the adjusted sectorial harmonics.

It may be concluded that based upon the results so far, the GSFC 1.70-C field modified with the SAO, APL, and Goddard GEOS I and II coefficients, Table 4, further modified with the adjusted coefficients of Table 7 might be the best field to be presented here for satellite orbit computations. If speed of computation becomes a factor, the analogue of this field based upon GSFC 1.70-T might be used with some small sacrifice in accuracy of computations instead of GSFC 1.70-C.

Table 7

Fits to 24 hr Satellite Accelerations

Geopotential Field	RMS, rad./(sid.da.)^2
1966 SAO Standard Earth	8.5×10^{-7}
SAO B13.1	3.9×10^{-7}
1969 SAO Standard Earth	2.5×10^{-7}
GSFC 1.70-C	3.8×10^{-7}
GSFC 1.70-C + Adjusted Sectorials	1.9×10^{-7}

NASA GSFC T&DS
MISSION & TRAJECTORY ANALYSIS DIVISION
BRANCH 552 DATE 04/08/70
BY Murphy & Marsh PLOT NO. 2103

As a means of further testing the orbital solutions obtained with the GSFC 1.70-C and the modified GSFC 1.70-C gravity models, satellite position differences were computed using the orbits based upon the SAO M-1 (1966) model (modified by GEOS-I and GEOS-II resonant terms) and the more recent SAO B13.1 model as standards.

The position differences were computed at five minute intervals and were resolved into radial, along track, and cross track components. The differences were computed using the unit vectors $\underline{H}$, $\underline{L}$ and $\underline{C}$, respectively which were calculated from the following relationships:

$$\underline{H} = \frac{\underline{R}}{R}$$

$$\underline{L} = \left[\underline{V} - \left(\frac{\underline{R} \cdot \underline{V}}{R^2}\right)\underline{R}\right] \Bigg/ \sqrt{V^2 - \frac{(\underline{R} \cdot \underline{V})^2}{R^2}}$$

$$\underline{C} = \underline{H} \times \underline{L}$$

where $\underline{R}$ is the vector from the geocenter to the satellite,

R is the distance from the geocenter to the satellite, and

$\underline{V}$ is the velocity vector of the satellite.

The RMS of satellite position differences for the respective GEOS-I and GEOS-II orbital arcs are presented in Table 8. The largest position differences were along track for both the GEOS-I and GEOS-II orbits which was not unexpected due to poorly modeled resonance. These along track position differences were reduced significantly when the GSFC 1.70-C model was modified by the Gaposchkin-Veis 12th order coefficients for GEOS-I and the APL and Goddard 13th order coefficients for GEOS-II. As indicated in Table 8, the RMS of the along track position differences between the GEOS I and GEOS II SAO M-1 standard orbits and the orbits computed with the modified GSFC 1.70-C model were on the order of 25 meters. The RMS of the radial and crosstrack position differences were on the order of 10 meters or less for all cases. The comparisons between the orbits computed using the GSFC 1.70-C modified models with the coefficients (13,12) adjusted for GEOS-I and (13,13) adjusted for GEOS-II showed an increase in the along track component of 8 meters for GEOS-I and 1 meter for GEOS-II. This is consistent with the RMS of fits presented in Table 5 and the fact that adjustment of (13,13) for Geos II resulted in very little change to the orbital fit.

Although the RMS of fits for the GEOS-I orbital arc were within .3 arc seconds for the SAO B13.1 orbit and the GSFC 1.70-C orbit (2.56 arc seconds vs. 2.30 arc seconds as shown in Table 5) the trajectory comparison presented in Table 8 shows that the RMS of position differences were on the order of 67 meters.

Table 8
Satellite Position Comparisons
GEOS I July 11-16, 1966
GEOS II April 28-May 4, 1968

Satellite	SAO M 1 (Modified)* vs	RMS Position Difference (meters)				Maximum Difference
		Radial	Crosstrack	Alongtrack	Total	
GEOS I	GSFC 1.70-C	7.0	7.8	82.8	83.4	139.7
GEOS I	GSFC 1.70-C + Gaposchkin and Veis 12th order terms	9.0	6.4	25.8	28.1	71.5
GEOS II	GSFC 1.70-C	10.3	9.3	91.8	92.9	210.8
GEOS II	GSFC 1.70-C + APL (1968) and GSFC (1969) 13th order terms	7.8	8.3	26.9	29.2	75.1
	SAO B13.1 vs					
GEOS I	GSFC 1.70-C + Gaposchkin and Veis 12th order terms	19.9	7.3	59.0	62.7	159.3
GEOS II	GSFC 1.70-C + APL (1968) and GSFC (1969) 13th order terms	20.3	14.3	75.6	78.6	188.2

*Modified with Gaposchkin and Veis 12th order terms for Geos I Comparisons.
Modified with APL (1968) 13th order terms for Geos II Comparisons.

To this point the GSFC 1.70C field has been tested against other fields using several satellites in distant 24hr orbits and the GEOS satellites in their close, resonant and drag free orbits. The next test of this model will involve orbit computations using tracking data from the Orbiting Geophysical Observatory (OGO-4) satellite. Fits to six two day arcs of Minitrack and Goddard Range and Range Rate data using NWL 5E-6, SAO M1, SAO B6.1, and GSFC 1.70C are presented in Table 9.

The analysis of OGO-4 data is of particular interest for a number of reasons. In the first place OGO-4 was not used in deriving any of the models discussed in this paper. This satellite in its near polar close earth orbit (a=7023.4km, e=.03492, I=86.°00) with only modest drag and slight resonance (150 m) is ideal for sampling the total gravity field.

Orbital comparisons similar to the ones made for the GEOS orbits have been also made using the OGO-4 arcs discussed above. In this case we were interested in the overlap region of successive pairs of orbital arcs. The results of these orbital comparisons appear in Table 10 for the NWL 5E-6, SAO M1, SAO B6.1 and GSFC 1.70C models.

Table 9

OGO-4 RMS of Orbital Solutions

Data Arc and Number of Observations	Model	Range (m)	Range-Rate (cm/sec)	Direction Cosines 1 (mils)	m(mils)
8/16/67 and 8/17/67	NWL 5E-6	84	67	1.7	3.4
R=59, RR=59, ℓ =m=27	SAO M1	63	47	.3	3.5
	SAO B6.1	60	45	.3	3.4
	GSFC 1.70-C	54	33	.4	3.3
8/17/67 and 8/18/67	NWL 5E-6	150	109	2.0	4.0
R=55, RR=54, ℓ =m=33	SAO M1	90	57	1.4	3.7
	SAO B6.1	72	49	1.3	3.8
	GSFC 1.70-C	60	28	.9	3.6
8/21/67 and 8/22/67	NWL 5E-6	126	89	1.7	3.4
R=85, RR=82, ℓ =m=38	SAO M1	69	51	1.0	3.3
	SAO B6.1	60	22	.2	1.9
	GSFC 1.70-C	48	27	.6	2.4
8/22/67 and 8/23/67	NWL 5E-6	102	65	.7	3.4
R=101, RR=98, ℓ =m=36	SAO M1	54	51	.7	3.0
	SAO B6.1	66	39	.7	3.0
	GSFC 1.70-C	45	32	.3	2.3
8/26/67 and 8/27/67	SAO M1	81	57	.8	3.1
R=78, RR=78, ℓ =m=34	GSFC 1.70-C	72	50	.8	2.9
8/27/67 and 8/28/67	SAO M1	81	41	.7	3.0
R=98, RR=97, ℓ =m=36	GSFC 1.70-C	75	50	.8	3.0

Table 10

OGO 4 Orbital Comparisons

Overlap Region	Model	RMS Position Difference (meters)				Maximum
		Radial	Crosstrack	Alongtrack	Total	Difference
8/17/67	NWL 5E-6	99.4	407.8	263.2	495.4	785.1
	SAO M1	31.1	298.4	105.7	318.1	484.8
	SAO B6.1	20.4	441.2	131.1	460.7	764.9
	GSFC 1.70C	19.9	79.5	84.7	117.9	254.7
8/22/67	NWL 5E-6	26.4	151.1	151.7	215.8	479.0
	SAO M1	17.7	69.5	247.4	257.6	770.6
	SAO B6.1	30.9	26.7	296.2	299.0	916.9
	GSFC 1.70C	19.1	21.8	166.7	169.2	479.0
8/27/67	SAO M1	20.2	25.5	62.9	70.8	144.5
	GSFC 1.70C	4.4	8.5	28.9	30.5	64.9

The best orbital fits for practically every two day arc were obtained when the GSFC 1.70C model was used. In several instances the RMS fits for the Range data were a factor of two lower than those obtained with the NWL 5E-6 model and the fits to the range rate data were as much a factor of three lower in some cases.

Similar results were obtained from the orbital overlap comparisons. The results presented in Table 10 indicate that the smallest total RMS position differences were obtained for every case when the GSFC 1.70-C model was used. Although in general smaller position differences were obtained for all components, the largest reduction was observed in the crosstrack component with the GSFC 1.70C cross track differences on 8/22/67 a factor of six smaller than those obtained using the NWL 5E-6 model.

Although a study of this nature has not been performed for the OGO-6 satellite data (OGO-6 orbital paramaters are quite similar to those for OGO-4) it is anticipated that the results of such a study would be comparable to those presented in Tables 9 and 10. That is, we would expect the overlap errors to be reduced significantly.

The combined field was compared to terrestrial free-air anomalies and to other geopotential fields through consideration of degree variances. The degree variances computed from the terrestrial data were obtained from Reference 2. The degree variances, σ_ℓ^2 , for the various geopotential fields were obtained from equation (4) which is based upon an analysis of gravity appearing in Reference 18. Thus,

$$\sigma_\ell^2 = \gamma^2 (\ell - 1)^2 \sum_m (\bar{C}_{\ell_m}^2 + \bar{S}_{\ell_m}^2) \tag{4}$$

where γ is the mean acceleration of gravity. These degree variances for the input fields, GSFC 1.70-C gravimetric, and for the SAO 1969 standard earth, Reference 20, appear in Table 11.

In Table 12 there appears an RMS coefficient difference between GSFC 1.70-C and the various other geopotential fields. By both of these methods of comparison GSFC 1.70-C compares very well with Köhnlein's field. Good agreement between GSFC 1.70-C and Kaula CA, SAO B13.1, Rapp 67, and Rapp 68 on the two means of comparison are obtained.

The mean degree variance, $\bar{\sigma}_\ell^2$, is given by equation (5) for a set of non-zonal harmonics. Thus,

$$\bar{\sigma}_\ell^2 = \sum_\ell (\bar{C}_{\ell_m}^2 + \bar{S}_{\ell_m}^2) / 2\, a_\ell \tag{5}$$

where a_ℓ is the number of pairs of non-zonal harmonics of degree ℓ. In Figure 1 a plot of the log of 10^{17} times the mean degree variance for 1.70-C versus the log of the degree is shown.

The rule of thumb that the size of a normalized gravity coefficient of degree ℓ is $10^{-5}/\ell^2$ is adhered to closely by the data points in this figure. The straight line so obtained is in good agreement with one presented in Reference 19 for NWL-8 D by Anderle and Smith.

Finally, a geoid map based upon GSFC 1.70-C and the other constants in Table 2 is given in Figure 2.

Table 11

Degree Variances σ^2_ℓ, (m gal^2)

Degree	NWL 5E6	APL 3.5	SAO M1	Köhnlein	Kaula 656	Kaula CA	Kaula K8	SAO B6.1	SAO B13.1	Rapp 67	Rapp 68	GSFC 1.70C	Gravimetric	SAO 69 S.E.
2	7.9	6.8	7.2	7.2	7.5	7.4	7.5	7.6	7.4	6.8	7.1	7.3	6.3	7.4
3	36.2	25.9	29.0	24.6	26.6	25.8	25.5	28.7	28.1	25.1	25.3	26.8	31.8	40.1
4	21.6	14.4	16.4	14.8	20.6	16.9	17.8	18.3	19.1	14.8	14.9	16.3	18.6	19.2
5	21.7	15.4	18.2	13.5	19.3	9.7	21.1	18.7	15.4	9.0	10.5	12.0	8.4	17.1
6	30.8	24.9	17.9	14.9	49.6	18.8	19.9	15.7	15.1	14.9	12.9	17.4	22.2	15.7
7	32.8	44.9	13.3	10.5	6.1		21.0	13.6	14.3	9.2	7.2	11.9	11.0	17.1
8		28.4	11.7	8.2	2.7		10.4	7.3	8.4	7.6	5.1	5.5	9.2	6.9
9				3.3	3.7			30.9	12.2	7.3	3.5	5.6	10.1	13.0
10				4.6				25.7	11.2	8.3	4.3	6.3		13.8
11				3.4				51.8	25.5	4.2	1.8	7.8		16.0
12				3.2				59.1	15.3	7.3	2.3	5.9		11.4
13				3.3				80.5	18.5	7.0	2.2	8.8		15.9
14				4.9				67.9	27.7	9.9	10.8	8.8		16.1
15				5.3				18.8	20.5			10.8		30.3

Table 12
RMS Coefficient Difference
Between Fields

GSFC 1.70-C and	RMS Difference (unit is 10^{-6})
NWL 5E-6	.163
APL 3.5	.192
SAO M1	.067
Köhnlein	.047
Kaula UCLA 656	.165
Kaula CA	.061
Kaula K8	.179
SAO B6.1	.098
SAO B13.1	.055
Rapp 67	.066
Rapp 68	.052
SAO 69 S.E.	.062

NASA GSFC T&DS
MISSION & TRAJECTORY ANALYSIS DIVISION
BRANCH 552 DATE 04/08/70
BY Murphy & Marsh PLOT NO. 2107

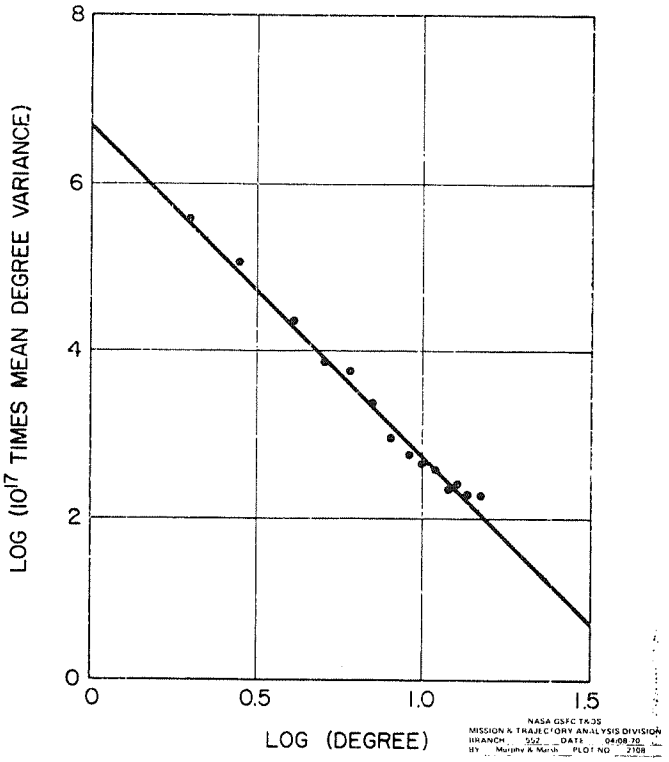

Figure 1. Mean Degree Variances, $\bar{\sigma}_\ell^2 = \sum_m (\bar{C}_{\ell m}^2 + \bar{S}_{\ell m}^2)/2a_\ell$, for GSFC 1.70-C.

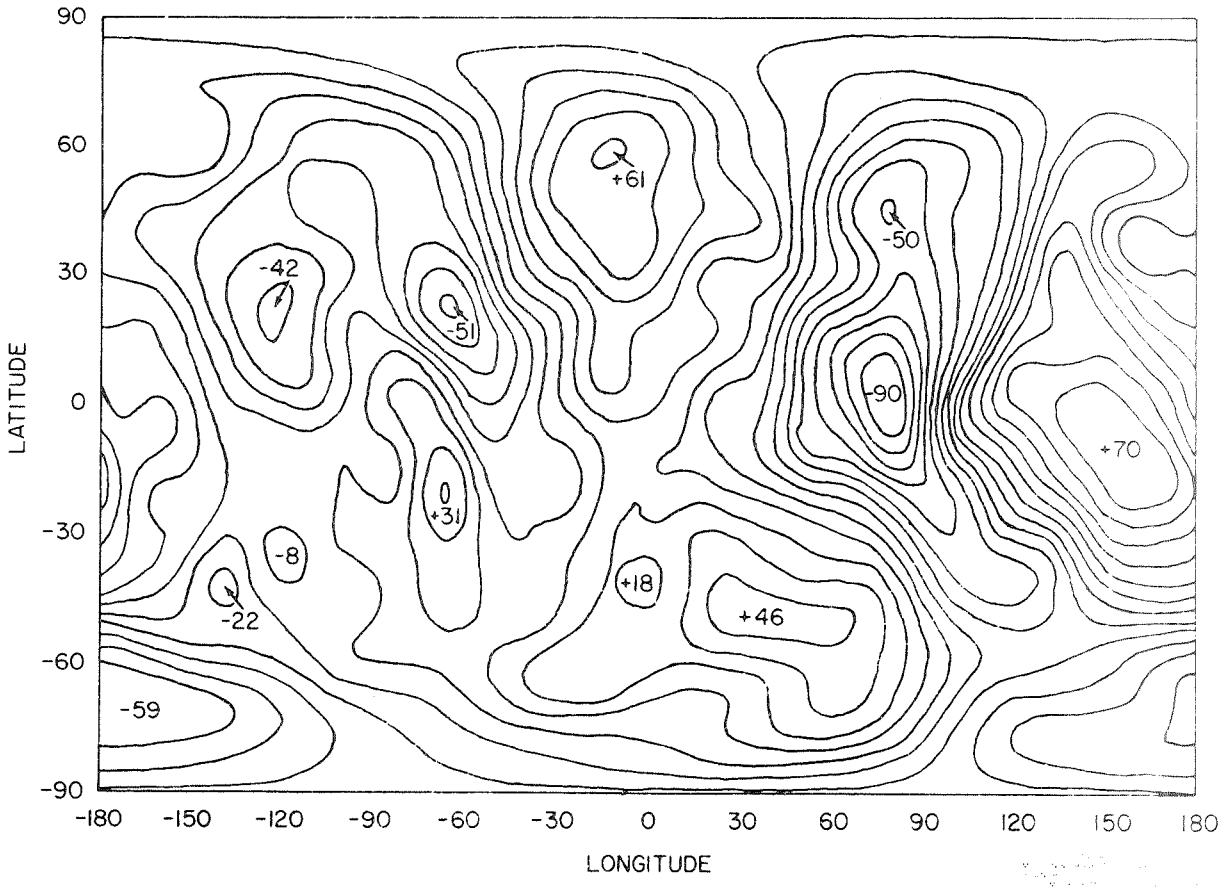

Figure 2. Geoid undulations from GSFC 1.70-C solution in meters.

COMMENT AND CONCLUSIONS

Several possible conclusions with regard to the performance of the combined gravity field for orbit computations can be made.

1. After the proper resonant terms are inserted in the combined field, the fit to the tracking data is as good or better than the fits obtained with any of the fields used in composing it.

2. The truncated field with 60% fewer coefficients fit the data almost as well as any of the fields tested. This implies that a 60% savings in computer time for trajectory integration could be realized over a (15 × 15) field with GSFC 1.70-T for some satellite prediction problems.

3. Adjustments to the resonant coefficients were small for both GEOS-I and GEOS-II. This seems to indicate that the complement of the field with respect to these resonant coefficients represents the gravity field adequately.

4. Comparisons of 1.70-C with other fields from the point of view of satellite position errors, degree variances, and geoid maps are favorable.

5. The tracking data processing carried out in this study was accomplished using the NONAME (orbit and geodetic parameter estimation) system, Reference 21, which includes all satellite perturbations such as lunar-solar gravitation, solar radiation pressure, etc. to the required degree of accuracy.

6. Professor Kaula's conclusion concerning the superiority of the arithmetic mean of different solutions to any single solution has been reexamined using several additional models.

ACKNOWLEDGEMENT

We thank Mr. Carl A. Wagner for making accelerations on several twenty-four hour satellites available to us. We also thank him for help in the analysis of those accelerations with regards to the adjustment of low degree coefficients.

REFERENCES

1. Hagihara, Y., Astronomical Journal, Volume 67, page 108, 1962.

2. Kaula, W. M., Journal of Geophysical Research, Volume 71, No. 22, pages 5303-5314, 1966.

3. Lundquist, C. A., and Veis, G., "Geodetic Parameters for a 1966 Smithsonian Institution Standard Earth," Smithsonian Astrophysical Observatory Special Report No. 200, 1966.

4. Anderle, R. G., "Observations of Resonance Effects on Satellite Orbits Arising from the Thirteenth and Fourteenth-order Tesseral Gravitational Coefficients," Journal of Geophysical Research, Volume 70, No. 10, May 1965.

5. Guier, W. H., and Newton, R. R., "The Earth's Gravitational Field as Deduced from the Doppler Tracking of Five Satellites" Journal of Geophysical Research, Volume 70, No. 18, September 1965.

6. Köhnlein, W., "The Earth's Gravitational Field as Derived from a Combination of Satellite Data with Gravity Anomalies," Smithsonian Astrophysical Observatory Special Report No. 264, pages 57-72, December 1967.

7. Kaula, W. M., Publication No. 656, Institute of Geophysics and Planetary Physics, University of California, Los Angeles, December 1967.

8. Gaposchkin, E. M., Private Communication, U. S. Gov't Memorandum, July 22, 1969.

9. Gaposchkin, E. M., Private Communication, U. S. Gov't Memorandum, October 7, 1969.

10. Rapp, R. H., "The Geopotential to (14,14) from a Combination of Satellite and Gravimetric Data," presented at the XIV General Assembly International Union of Geodesy and Geophysics, International Association of Geodesy, Lucerne, Switzerland, October 1967.

11. Rapp, R. H., "A Global $5^\circ \times 5^\circ$ Anomaly Field," Presented at the 49th Annual American Geophysical Union Meeting, April 1968.

12. Wagner, C. A., "Resonant Gravity Harmonics from 3 1/2 years of Tracking Data on Three 24 Hour Satellites," GSFC Document X-653-67-535.

13. Gaposchkin, E. M., and Veis, G., "Comparisons of Observing Systems and the Results Obtained from Them," Presented at the COSPAR meeting, London, July 1967.

14. Yionoulis, S. M., "Improved Coefficients of the Thirteenth-Order Harmonics of the Geopotential Derived from Satellite Doppler Data at Three Different Orbital Inclinations," Johns Hopkins/Applied Physics Laboratory Report TG-1003, May 1968.

15. Douglas, B. C., Marsh, J. G., Williamson, R. G., "GEOS-II and 13th Order Terms of the Geopotential," GSFC Document X-552-69-291, July 1969.

16. Marsh, J. G., Douglas, B. C., Dutcher, M., "Tests and Comparisons of Gravity Models using Camera Observations of GEOS-I and II, GSFC Document X-552-70-48, February 1970.

17. Gaposchkin, E. M., and Lambeck, K., "New Geodetic Parameters for a Standard Earth," December 1969.

18. Kaula, W. M., Reviews of Geophysics, Volume 5, No. 1, pages 83-107, 1967.

19. Anderle, R. G., and Smith, S. J., The Journal of the Astronautical Sciences Volume 15, No. 1, 1968.

20. Gaposchkin, E. M. and Lambeck, K., "New Geodetic Parameters for a Standard Earth," presented at the American Geophysical Union Fall Meeting, December 1969.

21. O'Neill, B., "NONAME, An Orbit and Geodetic Parameter Estimation System," Prepared under contract number NAS 5-9756-71D, August 1968.

REDUCTION OF ERRORS IN COMPUTED SATELLITE ORBITS DUE TO UNCERTAINTIES IN GRAVITY COEFFICIENTS

R. J. Anderle

Naval Weapons Laboratory
Dahlgren, Virginia

FOREWORD

Satellite observations have been used to determine over 200 terms in the spherical harmonic expansion for the earth's gravity field. This paper was prepared for presentation at a meeting sponsored by the National Aeronautics and Space Administration to review the results of observations of the GEOS II satellite, the last satellite launched specifically for geodetic applications. The paper indicates the contribution the GEOS II satellite made to the computation of precise satellite orbits, the needs for additional satellite observations to continue this work, and the orbit conditions which would contribute best to further refinement of the gravity field.

ABSTRACT

Observation of the GEOS II satellite and extensive related research in satellite geodesy have permitted considerable improvements to be made in the accuracy of computation of satellite orbits. However, computed satellite orbits still do not match satellite observations due to remaining errors in the gravity field. Furthermore, the recent advances made in satellite geodesy suggests additional discoveries are likely. Launch of additional geodetic satellites are therefore highly desirable to permit further advances to be made in this field. The next geodetic satellite would make maximum contribution to satellite geodesy if it were launched at low inclination.

Simulated Effects of Gravity Errors

Surface gravity measurements and satellite observations have shown that the expected size of a fully normalized gravity coefficient of degree N is $10^{-5}/N^2$. Malyevac (1970) showed that, excluding resonance effects, all randomly generated sets of gravity coefficients obeying this decay law would produce effects on computed satellite orbits which are essentially the same in magnitude. It was therefore possible to compute the effect on a satellite orbit of neglecting gravity coefficients above a given degree. The peak effect of such a truncation during a 24 hour span is shown in figure (1) for three satellite altitudes. The computations are based on the assumption that the gravity field up to the point of truncation is known perfectly and that resonance effects are zero. An extensive simulation reported by Anderle, Malyevac and Green (1969) showed that the net effect of truncating the gravity field is less than these figures for orbital conditions at which errors in gravity coefficients determined in the general geodetic solutions compensate for the neglected gravity coefficients.

Observed Effects of Gravity Errors

In the early years of satellite geodesy, residuals in orbit fits were strongly dominated by the effects of uncertainties in the gravity field. In 1966, however, over 200 terms in the expansion for the gravity field were evaluated in the NWL 8D solution yielding orbits for 600 mile polar satellites to an accuracy of better than 10 meters, excluding resonance effects and scale (Anderle etal, 1969).

EFFECT OF NEGLECTED GRAVITY COEFFICIENTS

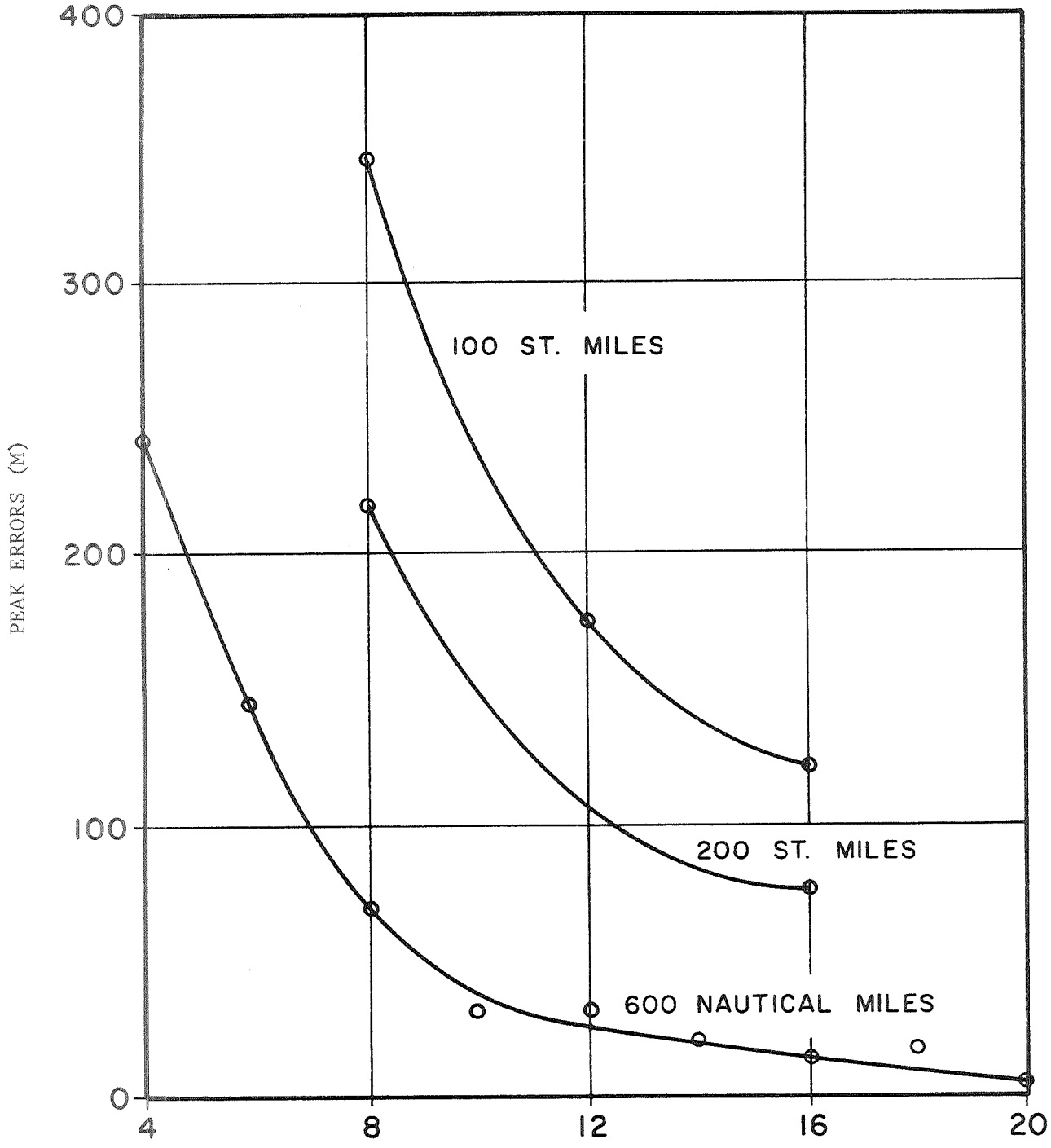

Figure (1)

This solution was subsequently modified to better represent resonance effects on the GEOS II satellite to yield the NWL 8H solution. In late 1969, the solution NWL 9B containing over 400 terms was obtained based on data for all satellites included in the NWL 8 series plus the data for the GEOS II, D1-1 and D1-2 satellites. With random observational errors and effects of gravity errors on high altitude satellites both about 10 meters, evaluation of differences in gravity coefficients with such observations becomes difficult. For example, if differences in noise and geometry among passes are ignored, residuals for polar orbiting satellites are currently found to be 10 to 15 meters. However, if residuals are weighted according to the noise and elevation angle, the root weighted squares are only 7 meters. The effect of the change from the NWL 8H to the NWL 9B gravity field on residuals for a navigation satellite is shown in table 1. A change in root weighted squares of residuals from 7.5 to 7.0 meters could represent an rms of a difference in bias between 0.5 and 2.7 meters depending on the size of the random error or the size of the remaining bias. Although even at worst this error appears to be small, it is only the rms during the time the satellite is observed. The peak error, particularly where the satellite is not observed could be considerably larger. For example, figure (2) compares orbits fit with NWL 9B and NWL 8H gravity coefficients to perfectly distributed simulated observations; an orbit difference of 18 meters is attained at one point during the day even for these well distributed observations. Now data for polar orbiting satellites were used in both the NWL 8H and NWL 9B geodetic solutions. A more critical evaluation of the relative accuracy of the solutions is obtained by comparing their accuracy for satellites not used in their determination.

Table 1

EFFECT OF GRAVITY FIELD ON ALONG-TRACK RESIDUALS

FOR NAVY NAVIGATION SATELLITES

Gravity	Days	Passes	Weighted Residuals (Meters)
NWL 8H	46- 47 1969	123	7.36
NWL 9B			7.01
NWL 8H	154-155 1969	121	5.55
NWL 9B			5.01
NWL 8H	258-259 1969	121	7.76
NWL 9B			6.90

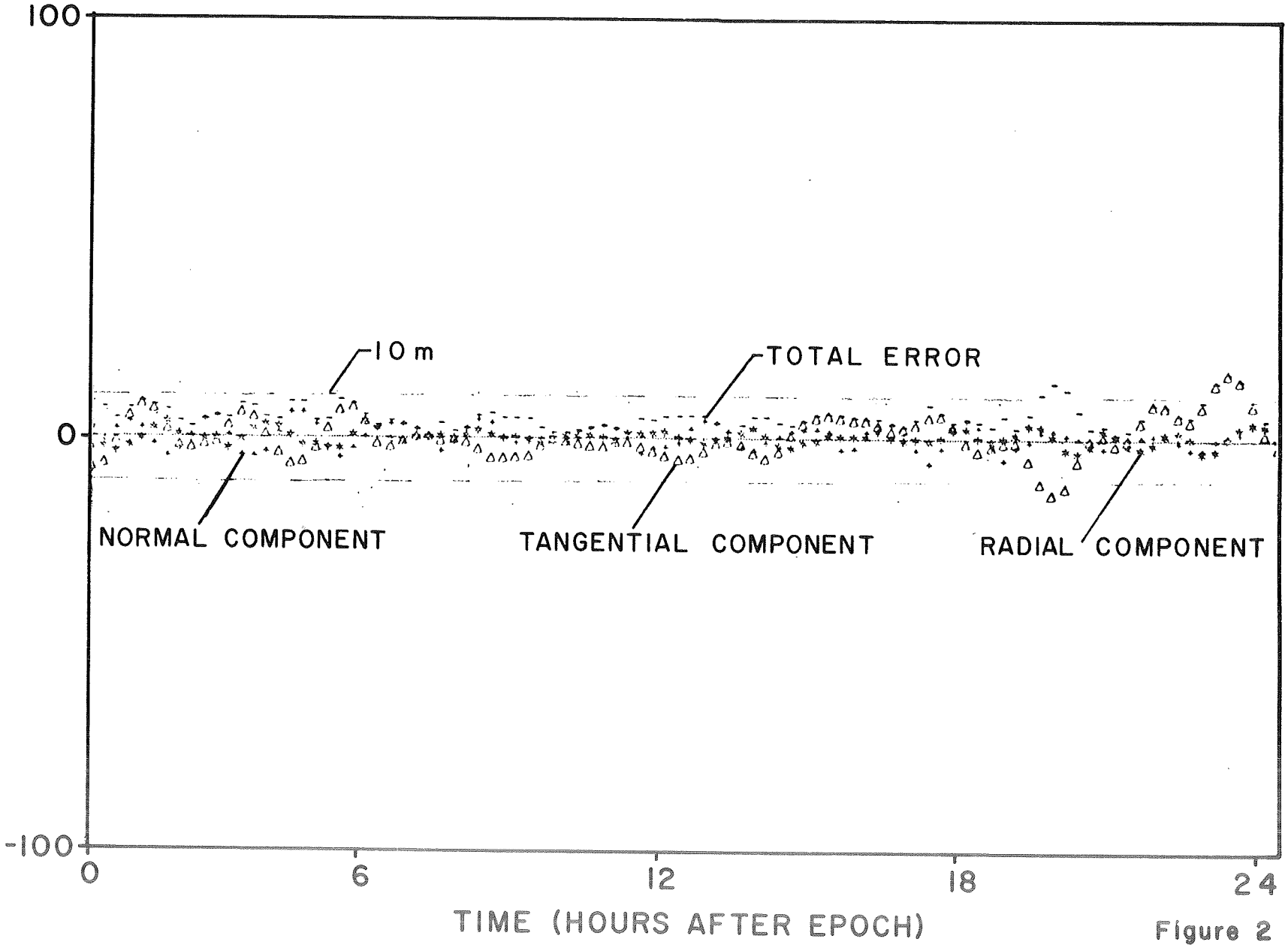
ORBIT COMPARISON FOR 600 N.M. POLAR SATELLITE
NWL 9B VERSUS NWL 8H GRAVITY COEFFICIENTS
100
0
-100
ORBIT DIFFERENCES IN METERS
10 m
TOTAL ERROR
NORMAL COMPONENT
TANGENTIAL COMPONENT
RADIAL COMPONENT
0
6
12
18
24
TIME (HOURS AFTER EPOCH)

Figure 2

One such satellite is 1969-82B, the Timation II satellite, which is in a 70 degree inclination, 900 km circular orbit. Although Doppler observations had been received from only four stations at the time of preparation of this report, the residuals for the NWL 9B gravity set are significantly better than those for the NWL 8H set as shown in table 2. Of course, comparisons for additional time spans and particularly additional stations would be desirable.

Recent Results with Improved Gravity Field

The recent improvements in the accuracy of the computation of the orbits of the navigation satellites have manifested themselves in at least two ways. First, the precision of the computation of the coordinates of the Doppler stations has increased significantly. Table 3 shows that station coordinates determined on the basis of independent groups of about 30 passes agree with each other to at least 2 meters in latitude and height and 4 meters in longitude. While the solutions are subject to common biases, this level of self consistency has never been achieved before for so few passes. A second result of interest is the determination of the position of the earth's pole based on Doppler observations of polar satellites (Anderle, Beuglass 1970). Figures (3) and (4) show the two components of pole position for 1969; the vertical bars give the standard error for the mean of the pole positions determined for each of six orbit computations; except for the displacement of the origin, which is relatively arbitrary, the Doppler solutions agree with the IPMS and BIH values about as well as these astronomical determinations agree with each other. As pointed out by Mueller of Ohio State University, who forwarded the IPMS data, the Doppler and IPMS coordinates on figure (3)

Table 2

RESIDUALS FOR "TIMATION II" SATELLITES 1969-82B

Days 341-342 1969

	Gravity Field	
	NWL 8H	NWL 9B
RMS of Ratios of Residuals to Noise	1.66	1.47
RMS of Along Track Residuals (M)	20	16
RMS of Slant Range Residuals (M)	8	6

TABLE 3

SOLUTION CONSISTENCY

Station	Δ Long (Sec)	Δ Lat (Sec)	Height (M)	Satellite Used	Passes
A	.04	.06	1	30120	32
	.04	.05	0	30130	29
	.05	.06	-1	30140	31
B	-.05	.04	-1	30130	14
	-.03	-.02	-1	30140	21
C	-.11	.06	2	30120	36
	.08	.00	1	30130	29
	.02	.01	2	30140	36
D	-.16	.07	1	30140	37
	-.06	.05	0	30130	41

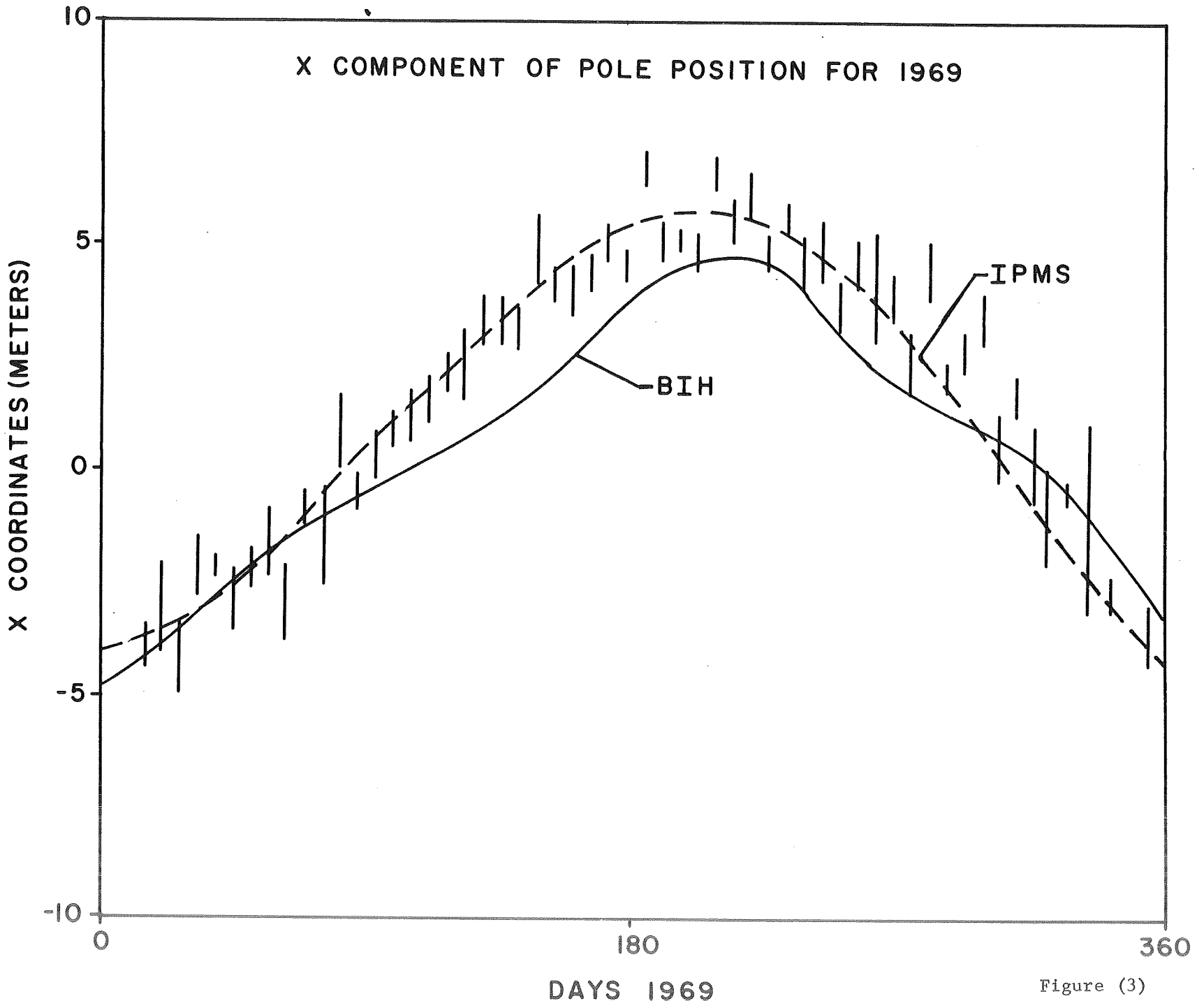
X COMPONENT OF POLE POSITION FOR 1969
X COORDINATES (METERS)
10
5
0
-5
-10
0
180
360
DAYS 1969
IPMS
BIH

Figure (3)

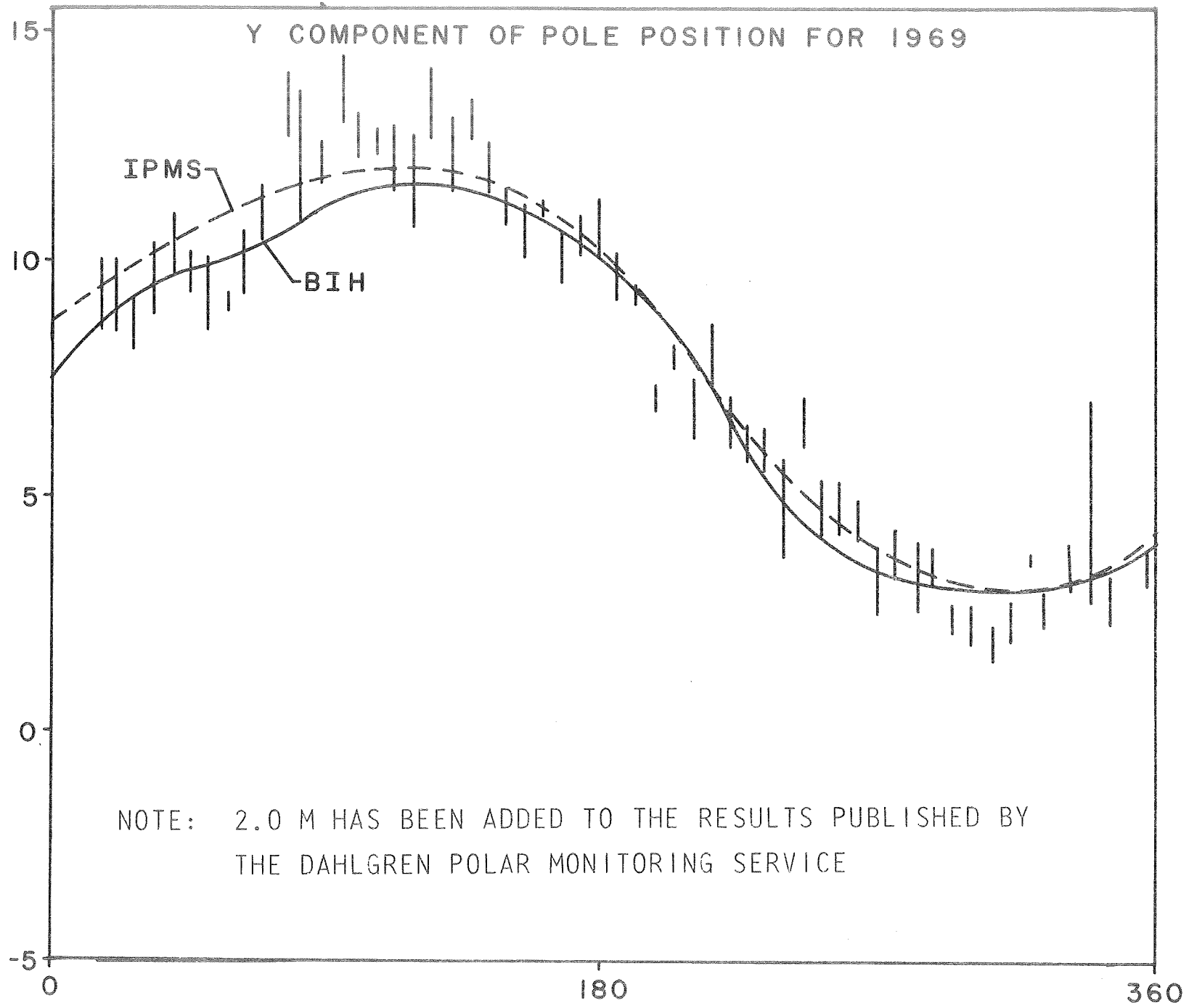
Y COMPONENT OF POLE POSITION FOR 1969
IPMS
BIH
15
10
5
0
-5
Y COORDINATES (METERS)
0
180
360
DAYS 1969
NOTE: 2.0 M HAS BEEN ADDED TO THE RESULTS PUBLISHED BY
THE DAHLGREN POLAR MONITORING SERVICE

Figure (4)

agree better than the BIH and IPMS data.

Selection of Orbital Conditions for Further Refinement of the Gravity Field

Doppler observations of satellites are a very effective means of improving the coefficients of the earth's gravity field because they provide the larger number of passes per day required to analyze high frequency perturbations of the satellite orbit produced by the high order gravity coefficients. Since the perturbations on high altitude (500 mile) satellites are small, the observations must have low noise level so that the gravity effects will be larger than the random errors of measurements. Accurate Doppler observations have been obtained for the following five orbital conditions:

Satellite	Orbital Inclination
NAVSAT	90°
GEOS II	74° R
GEOS I	59°
ANNA IB	50°
BE-C	40°

Howard L. Green of the Naval Weapons Laboratory conducted a simulation to test which of several orbital conditions would yield observations which would most effectively add to our knowledge of the gravity field. At the time the simulation was conducted the computer program used could not form normal equations for more than 237 gravity coefficients. Rather than utilize this capacity to form normal equations complete to 14th degree and order, it was decided that normal equations would be formed for all coefficients through 12th degree and order and for coefficients through 20th degree for orders 0, 1, 2, 10 and 11. In this way, a more complete

set of terms having the effects on the satellite orbit with the same frequency could be studied, and both high and low frequency effects could be studied. (Higher frequency effects for higher order terms will be separated primarily through their resonance effects). Normal equations were formed for two days of simulated observations for each of the five satellites for which precise actual Doppler observations have been made and for the following additional postulated orbital conditions:

Condition	Inclination	Altitude (St.Mi)
1	28°	500/1500
2	80°	500
3	80°	300
4	35°	300

The normal equations included the gravity parameters listed above and the usual station coordinate, orbit constant and instrument bias parameters. "Observations" were weighted according to the inverse variance of observations actually made for the first five satellites. Nominal weights corresponding to good observations were assigned to the postulated satellites. Normal equations for the five available satellites were combined and solved to find the expected accuracy of the determination of the gravity coefficients. Additional solutions were made after adding one or another of the sets of normal equations for the four postulated orbital conditions to those for the five available satellites. Since a solution for so many gravity coefficients with so few orbital conditions is underdetermined, standard deviations of gravity coefficients would be meaningless due to their high correlation. Therefore the eigenvalues for the normal equations were determined. The reciprocal square root of the eigenvalues can be

considered to be standard deviations of gravity coefficients in a new domain, say "Q Space", where the coefficients are decoupled. The pattern of these standard deviations for different combinations of orbital conditions can be easily compared in figures (5a) and (5b). The abscissa starts at the 97th gravity coefficients. This is because 96 gravity coefficients through about 9th degree and order were eliminated from the normal equation by Gaussian elemination before the eigenvalues were determined. This elimination was performed for reasons not pertinent to results presented here. The figures show that, as one would expect, observations on satellites at lower altitudes would reduce the errors in the gravity field more than observations on higher altitude satellites. The figures also show that observations on satellites at lower inclinations would be more valuable than observations on a satellite at an 80 degree inclination. The fact that this result holds the whole range of coefficients is surprising, since it implies that the low inclination satellites will provide valuable information on high as well as low frequency terms. The line labeled $10^{-5}/N^2$ is an approximation of the size of the coefficients predicted by the decay law. The approximation is inexact since it does not apply in this parameter space; but it does confirm the obvious fact that six satellites are inadequate to determine the gravity field through 20th degree, since the standard deviations exceed the decay law around the 190th coefficient.

Summary

Observation of the GEOS II satellite and extensive related research in satellite geodesy have permitted considerable improvements to be made in the accuracy of computation of satellite orbits. However, computed satellite orbits still do not match satellite observations due to remain-

EFFECT OF SATELLITE ORBITAL CONDITION ON
IMPROVEMENT OF GRAVITY COEFFICIENT

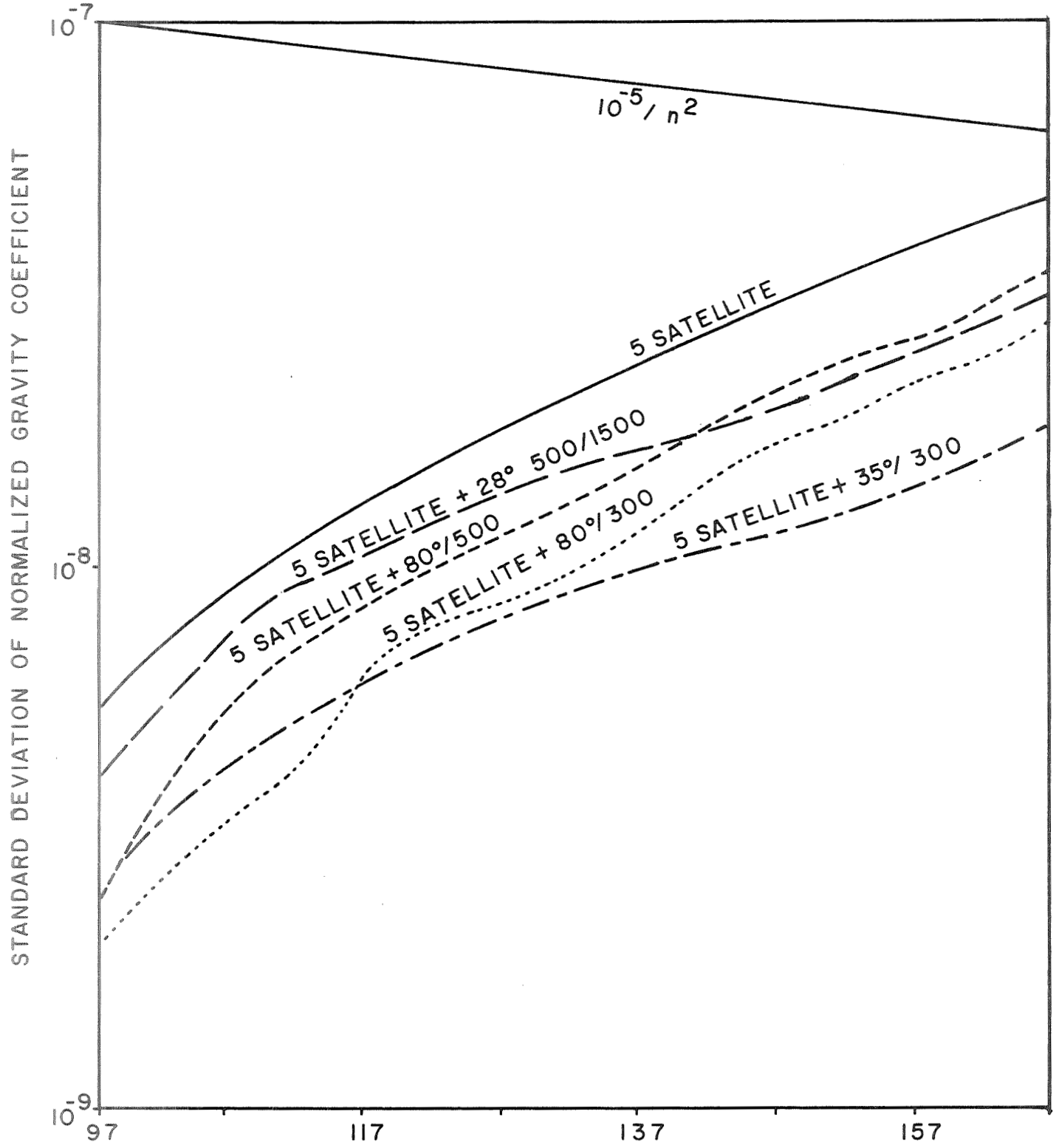

Figure 5(a)

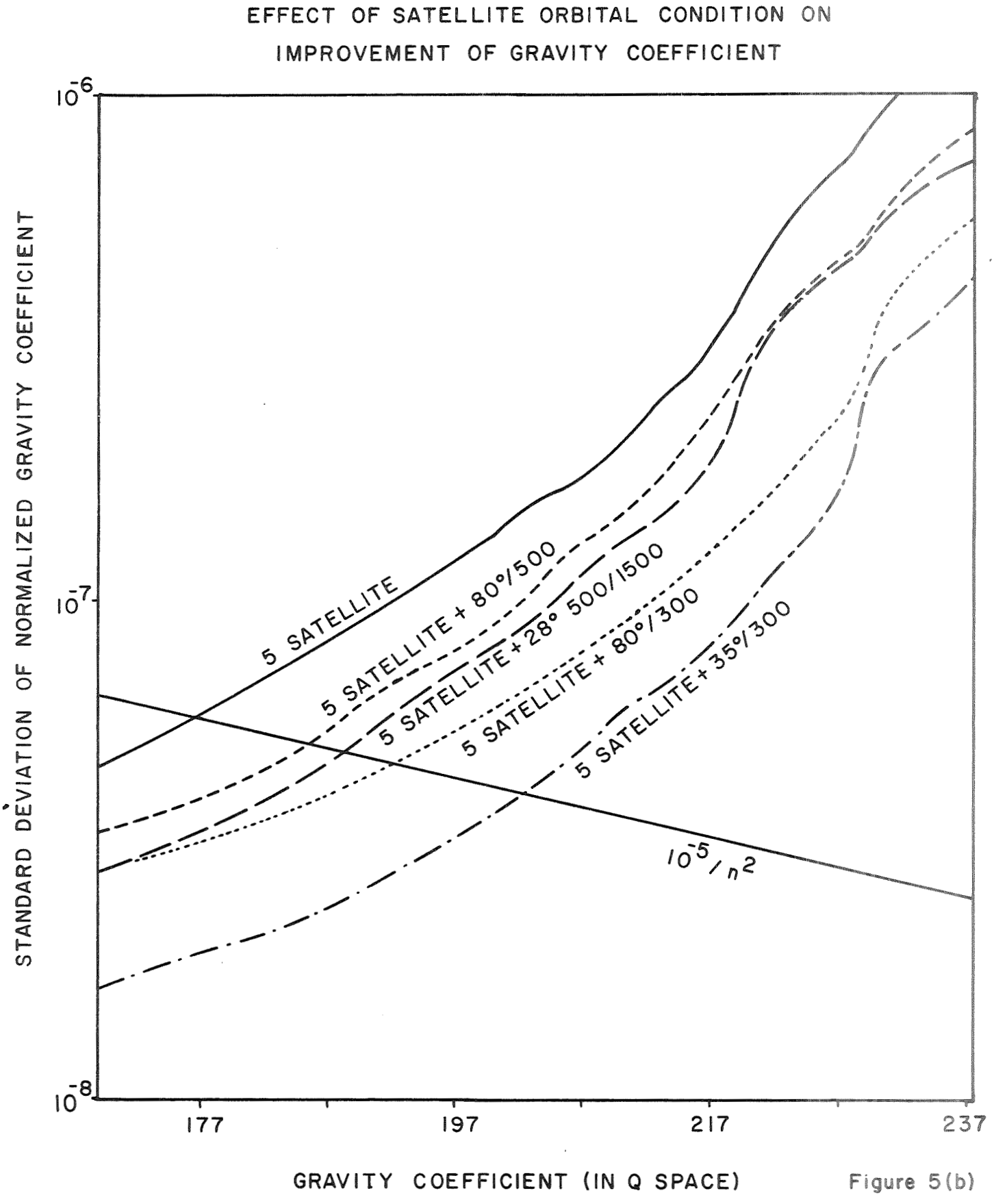
EFFECT OF SATELLITE ORBITAL CONDITION ON
IMPROVEMENT OF GRAVITY COEFFICIENT
STANDARD DEVIATION OF NORMALIZED GRAVITY COEFFICIENT
10^{-6}
10^{-7}
10^{-8}
5 SATELLITE
5 SATELLITE + 80°/500
5 SATELLITE + 28° 500/1500
5 SATELLITE + 80°/300
5 SATELLITE + 35°/300
$10^{-5}/n^2$
177
197
217
237
GRAVITY COEFFICIENT (IN Q SPACE)

Figure 5(b)

ing errors in the gravity field. Furthermore, the recent advances made in satellite geodesy suggests additional discoveries are likely. Launch of additional geodetic satellites are therefore highly desirable to permit further advances to be made in this field. The next geodetic satellite would make maximum contribution to satellite geodesy if it were launched at low inclination.

References:

1. Malyevac, C. A., "Effects of Truncation of Gravity Field on Computed Satellite Orbits", NWL TR-2372, 1970.

2. Anderle, R. J., C. A. Malyevac and H. L. Green, Jr., "Effect of Neglected Gravity Coefficients on Computed Satellite Orbits and Geodetic Parameters", Journal of Spacecraft and Rockets, Vol 6, No. 8 951-954 Aug 1969.

3. Anderle, R. J. and L. K. Beuglass, "Doppler Satellite Observations of Polar Motion", Bulletin Geodesique in press, abstracted in Transactions American Geophysical Union Vol 50, No. 11 Nov 1969.

4. Lundquist, C. A., and G. Veis, "Geodetic Parameter for a 1966 Smithsonian Institution Standard Earth", Smithsonian Astrophysical Observatory Special Report 200.

5. Gaposchkin, E. M., and K Lambeck, "New Geodetic Parameters for a Standard Earth", Smithsonian Astrophysical Observatory preprint of paper presented at Western Regional Meeting of the American Geophysical Union, Dec 1969.

COMPARISON OF GEOPOTENTIAL MODELS FOR GEOS-I EPHEMERIS PREDICTION

L. Wong
R. Prislin

December 1969

Prepared for
National Aeronautics and Space Administration

51st Annual AGU Meeting
April 1970, Washington, D.C.

ACKNOWLEDGMENT

This study was conducted for NASA under contract NASW-1858 from July 15 to December 15, 1969.

The authors wish to thank Mr. J. Rosenberg and Dr. M. Swetnick of the National Geodetic Satellite Program Office for the administration and technical direction of the study. In addition our appreciation is extended to Dr. M. Payne (E.R.C.), Mr. E. Markson (Geonautics), Mr. J. Murphy (NASA), Mr. J. Marsh (Goddard) who contributed helpful suggestions and comments along the way.

We also wish to thank Mr. R. Mercer, R. Gladson, D. Walker, and W. Downs for programming assistance and data extraction.

SUMMARY

A comparison of four geopotential models for the prediction of GEOS-I orbits over time spans of a month is described. The comparison is made on the basis of ephemerides calculated from Baker-Nunn-optical and Tranet-doppler observations over two 6-day arcs in 1966. The magnitude of the errors was found to be strongly dependent on the interaction between geopotential and radiation pressure constant, γ. By assigning the proper value to γ, each of the models could be used for predicting the ephemeris to within 2 km over a month period; in particular, the SAO-M1 and NWL-8D ephemerides were within 1 km. The long-term in-track error consists of a secular component plus a nearly sinusoidal oscillation which has the same period as GEOS. The sinusoidal component is shown to be the differences of two Keplerian orbits having slightly different eccentricities.

Tranet doppler orbits were consistent with optical orbits to within 40-60 meters. Hence, there was no necessity for combining the two sets of observations in a single solution. For a given geopotential model, the prediction errors from the two data types were approximately the same. Also, the sensitivities to geopotential changes were comparable even though the doppler set contains many more observations.

I. INTRODUCTION

The objectives of the current study are (1) to compare the performance of several geopotential models for satellite ephemeris prediction over time intervals on the order of one month and (2) to obtain a rough measure of the prediction error magnitude. The practical applications of the results to satellite operations are rather obvious and need no elaboration. However, past experience has more or less established the axiom that the performance of a given model relative to one satellite geometry is not necessarily applicable to another. It is therefore desirable to consider a variety of representative satellite geometries. This report details the findings from the analysis of GEOS-I observations. The approximate values of the orbital elements are respectively 8700 km, 7500 km, and 60 degrees for apogee, perigee, and inclination.

While the details of the analysis are tedious, the procedure is straightforward. Satellite observations are fitted to a dynamical model over a selected fit span. The resultant state vector at one epoch and the dynamical model then uniquely specifies the state at a future time in accordance with Newton's Laws. The predicted states are then compared with actual observations at given times to obtain the ephemeris errors.

Observations from GEOS-I are of several types. However, only the SAO (Baker-Nunn) optical and Tranet doppler are considered in this analysis. It will be shown that one or the other by itself could serve the purpose of prediction-error evaluation. While the number of doppler observations far exceeded the number of optical, it was found that the sensitivity to geopotential model changes was about the same for both types. Two orbital arcs, one in Jan 1966 and the other in July 1966, were examined. The two spans

were chosen because of good tracking coverage and because they were arcs which had been examined to some extent by other investigators. Marsh (1969); Lerch and Marsh (1969).

II. PROGRAM GENERALITIES

The Aerospace Orbit Program, Trace, was used for the bulk of computations. The program details are lengthy and more or less standard. Hence, only modifications and features related to the present problem will be described.

2.1 Coordinate System

A choice of several coordinate systems applicable to satellite dynamics was available at the beginning of the study. The systems are all geocentric, cartesian; they differ in their reference equator and equinox. The ones considered were:

Agency Using	Reference Equator	Reference Equinox
Smithsonian (SAO)	true of date	mean of 1950.0
Jet Propulsion Lab (JPL)	mean of 1950.0	mean of 1950.0
Naval Weapons Lab (NWL)	mean at midnite of date	mean at midnite of date
Aerospace (A)	true of date	mean at midnite of date

The SAO and Aerospace systems were the simplest considering both optical and doppler data but the frames are not inertial. In order to maintain the highest precision consistent with a 14 digit CDC computer, the JPL frame was chosen. The choice has several advantages with respect to the optical data. First, the optical observations were referred to the 1950.0 system and hence require no further transformation. Second, the lunar-solar ephemeris tapes (JPL DE-19 export tapes) were tabulated in this system and could therefore be used directly after interpolation. It is of course necessary to transform to an earth fixed or terrestrial system for the geopotential and tracker position computations. The transformation is a sequence of rotation matrices:

$$(\text{vector})_{\text{terrestrial}} = \left[S_2\ S_1\ N\ P\right] (\text{vector})_{\text{mean of 1950.0}}$$

S_2, S_1, N, P are respectively matrices of polar motion, sidereal angle rotation, nutation, and precession. The matrix symbols are the same as those used in Veis (1966). However, the matrix elements differ from Veis in that the sine and cosine functions were not replaced by their small angle approximations.

Station coordinates (cartesian) for the Baker-Nunn stations were the same as the ones used by Miller and Caliri (1967) while the doppler tracker positions were obtained from Mr. R. J. Anderle. The latter set was referred to the mean pole of 1965 and had to be rotated into the 1900-1905 system before using. Based on the findings of Gaposchkin (1967) it does not seem worthwhile to make any adjustments between the two tracking networks at this time.

2.2 Time

Atomic time (A.1) was adopted as the basic time system. The doppler time tags (UTC) had to be modified by the difference between UTC and A.1. Timing polynomials developed by Muller (1968) were used. The relations between the several time systems for the two intervals of interest were:

Ephemeris time (ET) = A.1 + 32.15 seconds

$$\text{ET-UTC} = a + b(t)\ ;\quad \text{UT1-ET} = c + d(t) + e(t^2)$$

where

t is seconds from midnite Jan 1, 1950, and

	Jan, 66	July, 66
a =	21.348034	21.359804
b =	.30009928 E-7	.29987399 E-7
c =	-.59641384 E3	-.33881691 E3
d =	.22315531 E-5	.11721046 E-5
e =	-.22236831 E-14	-.11378846 E-14

2.3 Force Model

The trajectory of the satellite is obtained by a numerical integration of the equations of motion, F = ma. The approximate relative magnitudes of the various force terms included are:

Central gravitation term	.5 - .7 g's; 1 g $\simeq$ 10 m/s^2
Harmonics beyond C_{20}	5×10^{-6}
Lunar-solar; resonance term	1.5×10^{-7}
Radiation pressure	6×10^{-9}
Atmospheric drag	3×10^{-11}

The expansion of the geopotential, V, has the form

$$V = \frac{GM}{a} \sum_{n,m} \left(\frac{a}{r}\right)^{n+1} (C_{nm} K^c_{nm} + S_{nm} K^s_{nm})$$

where K^c_{nm}, K^s_{nm} are spherical harmonics, C_{nm} and S_{nm} are fully normalized model coefficients (Kaula, 1966). The adopted value of GM is the one derived from lunar probes 398601.3 km^3/sec^2. This GM is consistent with the adopted station coordinates for both doppler and optical networks.

Lunar-solar and radiation pressure accelerations were obtained using the export version of the JPL ephemeris tapes, DE-19. The radiation pressure term has magnitude a_{rp} given by:

$$a_{rp} = \gamma\, g\, \delta$$

$$\gamma = \frac{kC_p A}{w}$$

δ = 1 when satellite is illuminated

= 0 when satellite is eclipsed by earth (cylindrical shadow was assumed)

C_p is the solar pressure constant, A the effective area, w/g the satellite mass and k the reflectivity factor. In the Trace program, the quantity γ (dimensionless, γ = radiation pressure acceleration in units of g's) is a parameter which could be differentially corrected.

The magnitude of the drag term is

$$a_d = q\alpha g\ ; \qquad \alpha \equiv \left(\frac{C_D A'}{w}\right)$$

where q is the dynamic pressure, A' the cross sectional area for drag, and C_d the drag coefficient. The differentially correctable parameter in Trace is α. From the Lockheed-Jacchia density model with mean Jan (2-8), 1966 value for the 10 cm flux density of 80 x 10^{-22} w/m^2/hz reported by the Ottawa Observatory, the density and deceleration ranges were found to be: (the maxima in density and a_d do not occur at the same time)

	density (kg/m^3)	a_d(m/sec^2)
maximum	10^{-15}	3 x 10^{-13}
minimum	1.5 x 10^{-16}	5 x 10^{-15}

based on the values A' = 1.23 m^2, C_D = 2, and w/g = 175 kg. The cross sectional area for drag and radiation pressure need not be the same since

the satellite is asymmetrical and the attitude angle with respect to velocity (drag) is different from that relative to the heliocentric direction. However assuming A = A', nominal values for γ and α are respectively 5.75×10^{-9} g's/g and .0014 m^2/nt.

2.4 Differential Correction Elements

The parameters employed in differential correction are the f, g elements widely used for low eccentricity orbits by Aeronutronic and others. In terms of the classical elements a, e, i, Ω, ω, M (mean anomaly), the f and g set is defined by:

$$a_f = e \cos(\omega + \Omega) \qquad a_g = e \sin(\omega + \Omega)$$

$$n = \frac{\sqrt{\mu}}{a^{3/2}} \quad \text{(mean motion in degrees/sec)}$$

$$L = \omega + \Omega + M \text{ (deg)}$$

$$\chi = \frac{\sin i \sin \Omega}{1 + \cos i} \qquad \psi = \frac{\sin i \cos \Omega}{1 + \cos i}$$

The set was chosen because the corrections were linear for all cases likely to be encountered. Convergence was generally obtained in 2 to 3 iterations starting from the elements given in SAO Report 264. Analytical partials were available, but were not used, since the variational equations were more accurate and added little to the overall running time.

III. COMPUTER RESULTS

Many orbit determination runs were made during the test. They may be loosely grouped as follows.

a. Estimate initial state and γ ($\gamma = \frac{kC_p A}{w}$; see page 6)

optical observations

doppler observations

b. Estimate initial state, fixed γ - optical observations

The groups could be further divided into January and July arcs.

3.1 Data Spans and Data Corrections

Data spans of 1 day, 3 days, and 6 days were examined in trial orbit determination runs. Convergence of the solution for the initial state vector was readily attained for all three intervals; when γ was also estimated, convergence was easy for the 3 and 6 day spans but was exceedingly difficult to achieve over a one day interval. The standard deviations of γ from the estimate were $\sigma_\gamma = 1.6 \times 10^{-8}$; 5×10^{-10}, 1.7×10^{-10} for arcs of 1, 3, and 6 days respectively. The final fit span was chosen to be 6 days which is approximately equal to the beat period of the 12th order resonance. The first and last optical observation times were:

	Start			Stop			Number of Observations
	d	hr	m	d	hr	m	
January arc	2	6	4	8	12	46	140
July arc	10	2	48	16	1	11	928

Observing stations in January included 9001, 2, 4,5, 6, 7, 8, 10, 11, 23, 50, 425 and 426; in July, they were: 9001, 2, 4, 6, 7, 8, 9, 10, 11, 12, 23, and 425 (Geonautics, 1969; also Lerch, 1969).

The optical data as received from the NASA data bank were used directly without modification. The following corrections were made internally in the Trace Program: parallactic refraction - (Veis, 1960); diurnal aberration - (Smart, 1962); light transit time. The latter correction is the largest of the three.

Doppler observations over essentially the same time spans came from seven trackers including Anchorage, Samoa, Hawaii, Las Cruces, Lasham England, Howard County, and McMurdo Sound. The observation-time tags were converted from UTC to A.1 to conform with the SAO system. In the Trace program, corrections were applied for light time, tropospheric refraction, time dilatation, gravitational shift, and a frequency bias.

3.2 Test Models

Four selected geopotential models plus some hybrid combinations were tested. The four are: NWL 5E6, NWL 8D, SAO M1, and Kohnlein (1967). The first two were derived solely from doppler tracking, the third from optical and the fourth contains both satellite and terrestrial data. In the models listed in table 1,

- the symbol K69 designates the 20 zonal harmonics (degrees 2 through 21) published by Kozai in 1969, M1+K69 signifies the M1 model with the original 13 (degrees 2 through 14) zonal terms replaced by Kozai's new zonals;
- R signifies the 9 pairs of resonant and near resonant coefficients in the M1 model of order 11 through 15,
- the 8D and Kohnlein models have their own resonant coefficients and the original terms were not altered. The Kohnlein model used in our tests is a hybrid consisting of Kohnlein's tesseral harmonics through degree 15 plus the Kozai-69 zonals rather than the Kozai-67 values given in SAO Report 264.

- the number in parenthesis designates the number of pairs of coefficients in each model.

Model coefficients are given in Appendix I.

3.3 Optical Data Fits - Variable γ

The long term prediction errors turn out to be a function of the interplay between drag, radiation pressure, and the resonant harmonics. Solutions in which the drag parameter α was estimated along with γ invariably failed to converge. Over the 6 day span, the correlation coefficient, $\rho_{\alpha\gamma}$, was found to be .994 and the standard error $(\sigma_\alpha/\alpha) \simeq 2$. The strong correlation is caused by the similarity of the sensitivity curves shown in figure 1. Both curves are essentially quadratic in time over the fit interval. Since there were some questions on the validity of atmospheric models beyond 1000 km altitude, the drag force was deleted in the first set of runs. The effects of drag will be discussed in a later section. The fact that the drag effects could be almost entirely absorbed by radiation pressure is evidenced by the RMS fits to the data. We had, fitting over 6 days of optical data, using the M1 model:

RMS residual without drag force - 2.44 arc sec

RMS residual with drag force - 2.48 arc sec.

Table 1 summarizes some results of fitting the optical data with variable γ. Orbital elements are listed in Appendix II. The M1 model not only fitted the observations best for both January and July arcs but also obtained the smallest prediction error of the 4 basic models tested.

Principal cause of the M1 superiority is the group of resonant and near resonant terms.* The along-track perturbations caused by the largest terms as derived by Gaposchkin-Veis (GV) are shown in figure 2. In addition to the effects shown $S_{12,12}$, $S_{15,12}$, $C_{13,13}$, $S_{13,13}$, all contribute on the order of 100 meters at the end of six days. By augmenting the 5E6 model with the GV resonant harmonics, performance approaching the M-1 results was achieved. These improvements had also been observed by Marsh for the APL and Kohnlein potentials (Marsh, 1969) and we decided not to repeat the experiment with the Kohnlein model.

Table 1

RMS Residuals of Optical Data and Estimates of γ

		RMS (sec)		γ (10^{-9}) - Nominal 5.75	
Case	Model	Jan	July	Jan	July
1	M1 (68)	2.44	2.21 2.02	4.397	6.02 2.00 (3 day arc)
1A	M1 + K69 (75)	2.52		4.396	
2	NWL 5E6 (32)	6.66	6.00	20.52	23.05
2A	5E6 + R (41)	2.50		5.38	
2B	5E6 + R + K69 (55)	2.52	2.72	4.94	5.33
3	NWL 8D (111)	2.59	3.36	-2.38	-.27
4	Kohnlein + K69 (137)	4.28	6.76	-8.33	33.16

*The primary resonance is order 12. However terms of order 13 are also significant. The 5E6 model plus 12th order terms alone fitted to 3.2 seconds and to 2.5 seconds with the 13th order terms added.

In general, the results for the July arc are very similar to the January span. One notable exception is the degradation of RMS for the Kohnlein model. Modifications arising from the use of the Kozai-69 zonals in the January arc were so slight that the corresponding M1 case in the July span was omitted.

The remarkable feature of the results in table 1 is the large variability of γ relative to the standard error $\sigma_\gamma = 1.7 \times 10^{-10}$ for a 6 day arc. Again the primary cause was the resonant harmonics. Figure 2 shows the similarities between the effects of the resonant terms and α and γ. When allowed to vary, γ assumes a value which absorbs errors in the resonant terms or the absence thereof as in the case of 5E6. The wide variations between models relative to σ_γ is a good illustration of the fact that the standard deviation obtained from a covariance matrix based on random observation errors is quite meaningless in the presence of model errors.

The nominal value of γ, $\gamma_N \simeq 5.75 \times 10^{-9}$ g's/g, is in fair agreement with cases 1, 1A, 2A, and 2B of table 1. One concludes that a reasonable estimate of γ is obtained provided that the model contains the Gaposchkin-Veis coefficients which is perhaps not too surprising since GEOS-I data was prominent in the derivation of these terms.

3.3.1 Prediction Errors

Thirty day ephemerides were calculated for several of the cases listed in table 1 from the converged state vectors and γ (see Appendix II). At approximately 5-day intervals, each predicted ephemeris was compared against an orbit derived from a 1-day fit of observations localized about the times of comparison. The localized orbits were derived only once using the M-1 model, i.e., we did not repeat the local orbit determination with different

geopotential models. Comparison times were chosen to be close to times of actual observations and the differences are regarded as prediction errors -- assuming that errors in the localized orbits are small. The difference vectors are resolved into in-track, cross-track and radial components. Each component has a nearly sinusoidal variation with period equal to the orbital period of GEOS. The in-track component also has a secular part which increases quadratically with time. The secular parts over a 30-day span for four geopotential models are shown in figure 3. The range is from -24 km for the 5E6 to +22 km for 8D with M1 and the modified 5E6 in between at 7.5 and 6.5 km respectively. These trends were attributed to erroneous estimates of the initial state and γ -- particularly the latter, induced by the gravity model.

3.4 Optical Data Fits - Fixed γ

A least squares fit of the prediction error ϵ at 30 days in figure 3 to the value of γ resulted in the linear equation

$$\epsilon = 15950 - 2007\gamma \quad \text{(meters)} \tag{1}$$

which implies that $\gamma_m = 7.944(10^{-9})$ should result in essentially zero secular error at the end of the prediction interval. The data fits were repeated for the various potential models with γ set equal to γ_m. The RMS residual for these are given in table 2. Equation (1) was obtained from the long-term prediction errors in the January arc. However, the derived value was used for both January and July arcs. Interestingly, the fit to the July data with γ_m was even better than the January arc. Converged solution vectors for $\gamma = \gamma_m$ are also given in Appendix II. These were used to

generate 1-month trajectories and calculate prediction errors as described in the preceding section. Figures 4 through 10 show various components of the prediction error at approximately 5-day intervals for one orbit (120 minutes). These figures show the near-sinusoidal nature of the error. As one might expect, the secular trends in the in-track component were very much reduced for all of the models -- even 5E6 which does not contain resonant harmonics. With a few exceptions, the errors were less than 1.5 km over a 30-day interval -- the M1 prediction errors were less than 600 m for the January arc and 1 km in the July arc.

Table 2

RMS Residual of Optical Data with Fixed γ

	$\gamma = 7.944(10^{-9})$ $\alpha = 0$		$\gamma = 9.907(10^{-9})$; $\alpha = .0014\ m^2/nt$
Model	Jan	July	Jan
M1	3.52	2.30	3.67
5E6	11.16	7.82	11.15
5E6 + R	3.11	3.05	
5E6 + R + K69	3.27	2.85	
8D	7.81	4.32	
Kohnlein	12.35	10.80	

3.4.1 Comments on Prediction Error

Let ϵ be the secular prediction error at time t. We have for a variable γ,

$$\epsilon = \left(\frac{\partial \epsilon}{\partial n} \frac{\partial n}{\partial v} + \frac{\partial \epsilon}{\partial \gamma} \frac{\partial \gamma}{\partial v} + \frac{\partial \epsilon}{\partial v} \right) \delta v \qquad (2)$$

where n is the Keplerian mean motion at initial epoch, v the vector of geopotential coefficients. The quantities $\frac{\partial \epsilon}{\partial n}$, $\frac{\partial \epsilon}{\partial \gamma}$, $\frac{\partial \epsilon}{\partial v}$ are partial derivatives evaluated about the nominal orbit, $\frac{\partial n}{\partial v}$, $\frac{\partial \gamma}{\partial v}$ are functions of the least squares normal matrix which in turn depends on the type and distribution of observations as well as the track interval. The fact that ϵ satisfies equations (1) and (2) implies

$$\frac{\partial \epsilon}{\partial v} \delta v = - \frac{\partial \epsilon}{\partial n} \frac{\partial n}{\partial v} \delta v \qquad (3)$$

and

$$\epsilon = \frac{\partial \epsilon}{\partial \gamma} \left(\frac{\partial \gamma}{\partial v} \right) \delta v \qquad (4)$$

Equation (3) expresses the condition that any direct error caused by the geopotential model is canceled by a change in the calculated mean motion. One would expect this to be the case if the track interval is long enough to allow a unique determination of the "true" period and the separation of quadratic effects due to γ from linear effects due to n. A change in potential

would then cause a change in the size of the orbit, i.e., semi major axis, such that the "true" period remains unaltered. The variations of n due to variations* in a between models are on the order of 5×10^{-8} deg/sec (see Appendix II). Over a 30 day period, the in-track displacement from such a change amounts to about 18 km - much larger than the observed shifts when γ is held fixed. The point is that the mean motion calculated from the Kepler formula $n = \sqrt{\mu}/a^{3/2}$ is not the true mean motion. The latter does not depend on the potential model if it is well determined from the observations.

The principal error is given by equation (4). It is nearly quadratic with time and depends on the model only via the aliasing effects of γ. If γ (and/or α) were held constant, there should be very little dependence of the long-term error on the geopotential model. This is what we observed in figures 4 through 10. In-track differences between models are on the order of 1-2 km over the 30 days and 100-300 meters for the radial and cross-track components. The largest error encountered was 3000 meters for the July arc using the 5E6 model. These residual errors and the sinusoidal oscillations are ascribable to model differences. In summary the maximum prediction errors with $\gamma = \gamma_m$ were:

Model	January Arc	July Arc
M1 8D 5E6 + R + K69	600 (m)	1200
5E6	1500	3000
Kohnlein	1800	--

*Using the usual relation $\frac{\delta n}{n} = -\frac{3}{2}\frac{\delta a}{a}$

The sinusoidal variations over a single revolution in figures 4 to 10 suggests that the errors might be describable as differences between Keplerian orbits. The differentials of the 3 components to first order in eccentricity are: (Moulton, 1914, p. 171)

$$\delta I = r(\delta M + 2\delta e \sin M) \qquad \text{in-track} \qquad (5)$$

$$\delta r = \delta a - a\delta e \cos M \qquad \text{radial} \qquad (6)$$

$$\delta c \simeq r(\sin u\, \delta i + \sin i \cos u\, \delta\Omega) \qquad \text{cross-track} \qquad (7)$$

where M is the mean anomaly; u the argument of latitude; δM is the mean value at each date about which the sine wave varies; δa, the change in major axis - generally less than 10 meters. From (5) and (6), we observe that the amplitude of the in-track oscillation should be twice the amplitude of the radial oscillation and the two should be 90 degrees out of phase. Comparison of figures 4 and 7 shows that this is <u>indeed</u> the case - that the oscillations are describable as differences of Kepler orbits having slightly different eccentricities.

There is, however, one deviation. The positions of apogee and perigee marked on figures 4 and 7 indicate a phase angle such that the observed differences are actually given by:

$$\delta I = r\left[\delta M + 2\delta e \sin(M+\varphi)\right] \quad \text{and} \quad \delta r = \delta a - a\delta e \cos(M+\varphi).$$

The phase angle φ is a non-Keplerian quantity introduced by the fine structure in the potential. For Keplerian orbits, φ should be zero. It is interesting that φ remains more or less constant throughout a given arc. This is true for each of the models tested although there are variations in the degree of constancy. In contrast the cross-track or out-of-plane errors do not seem to maintain a constant phase pattern as well as the in-plane components do.

3.5 Doppler Data

Use of doppler data was somewhat more difficult than optical because of the large volume and the necessity for including a frequency bias parameter on each pass. The NASA data tapes were edited and sampled at a rate of 2 points per minute.

Tropospheric corrections were calculated from Hopfield's (1963) model. A more recent model is available but probably not necessary at this time; also we do not have the necessary meteorological inputs for the later model. The surface refractivity was assumed to be a nominal 350×10^{-6}. The efficacy of the correction is illustrated by the residuals in figure 11. Over an 18 hour span containing 450 observations, we obtained

RMS (with tropospheric correction) = .0120 hz $\simeq$ 3.3 cm/sec

RMS (without correction) = .0163 hz $\simeq$ 4.5 cm/sec

Both the January and July arcs contained approximately 3000 points from 167 and 168 passes respectively. Convergence was generally attained in 1 or 2 iterations. The RMS of residuals obtained from fitting with various models is given in table 3 (1 hz = 2.8 m/sec).

Table 3

RMS Residuals for Doppler Observations

	RMS (hz)		Estimated γ	
Model	Jan	July	Jan	July
M1	$1.55(10^{-2})$	2.21	$4.65(10^{-9})$	5.98
5E6	3.83		20.47	
5E6 + R	1.76		4.80	
8D	1.73		-3.80	

The ratio in the quality of fit between the models 5E6 and M1 is about 2.5 for doppler and 2.7 for optical (see table 1).

Orbits obtained from doppler were similar to those from optical in nearly all aspects. For example, the long term prediction errors of doppler solutions essentially coincided with corresponding curves in figure 3. Some differences of ephemerides over the fit interval are shown in figure 13. The amplitudes are less than 40 meters for cases with good agreement and 60 meters for the poorer ones.

Initially, the plan was to fit optical and doppler data separately and then combine the two with the appropriate weights such that the former wouldn't be overwhelmed by the numerical preponderance of the latter. However, the excellent consistency between the two sets of data made this combination unnecessary. For the purposes of testing geopotential models, one or the other set would do. The remaining could be used as a redundancy check. Since the doppler data was more cumbersome to manipulate, most of the tests were made using the optical.

Actually, the disparity in weight is not overly heavy in favor of the doppler. Comparing some standard deviations from the covariance matrix of estimation, we have for the elements defined in 2.4, the values listed in Table 4.

Table 4

Standard Deviation of Estimation

	Jan			July	
	$\sigma_{optical}$	$\sigma_{doppler}$		$\sigma_{optical}$	$\sigma_{doppler}$
		Estimate state & bias	Estimate state only		state & bias
a_f	$4.5(10^{-7})$	1.1	.75	2.4	1.4
a_g	$3.2(10^{-7})$	.75	.51	.72	1.3
n(deg/sec)	$2.3(10^{-10})$	1.3	.84	1.2	2.2
L(deg)	$5.6(10^{-5})$	2.2	1.4	2.6	3.8
χ	$4.6(10^{-7})$	2.7	1.9	1.1	3.7
ψ	$2.8(10^{-7})$	1.9	1.5	.78	3.0
γ	$2.0(10^{-10})$	1.5	.82	1.5	3.7

Hence, while the doppler has considerably more weight in January the reverse is true in July where the angular observations are numerically comparable and have a better geographical distribution. The above comparison is one instance where the covariance matrix seems to serve a useful purpose. There is some absorption of model induced errors by the frequency biases. For example fixing the biases at the values derived from the M1 model and combining observations with the orbit based on 5E6 resulted in an RMS of .0639 hz instead of the .0383 given in table 3. The RMS change of 38 biases from station 14 (Anchorage) in changing from M1 to 5E6 was .049 hz and the mean was .01 hz. The mean is perhaps not too meaningful because the changes were systematic. See figure 12.

The degradation in the standard errors of the initial state vector caused by the necessity to estimate biases is small -- about a factor of 1.5. Typical values are given in table 3 under the column "state only."

3.6 Drag

While the drag force is more than two orders of magnitude smaller than radiation pressure, the perturbations are not in the same proportion because the integrated effects over an orbit are different. Over time periods of a month, both perturbations are essentially quadratic. Introducing the drag force (nominal α = .0014 m^2/nt, and Lockheed-Jacchia atmosphere extended) into the orbit computation resulted in the following changes to the cases listed under table 1.

Model	RMS Residuals (Jan) (arc sec)	Estimate of γ
M1	2.46	6.11
5E6	6.68	22.00
5E6 + R + K69	2.52	6.67
8D	2.58	-.70

In other words, the RMS fit remained essentially unchanged while all of the values of γ increased by about 1.5 - 1.7 (10^{-9}). Prediction errors calculated from the M1 model had a mean value at the end of the 30 day interval of 7.65 km - nearly the same as the corresponding case without drag. Using the value of 2007 meters for each 10^{-9} increment in γ obtained in (1), the value of γ which would remove the secular trend in the presence of drag is $\gamma'_{md} = 9.921(10^{-9})$. Upon reevaluating the prediction errors again with $\gamma = \gamma'_{md}$, the mean (over one

period) prediction errors at the dates given in figure 4 were found to be as follows:

Date	Mean error (m)
Jan. 15	-390
20	-550
25	-580
31	-480
Feb 6	180

The net effect of drag is to increase the value of γ_m by 2×10^{-9} and leave all else about the same. In view of the many variables in density models at high altitudes, it was decided not to pursue the drag effects further at this time.

IV. CONCLUSIONS AND REMARKS

With regards to the first question mentioned in the introduction, it can be said that the M1 model predicts GEOS-I ephemeris with smaller errors than the other unmodified models; that when the 5E6, 8D or Kohnlein models are augmented by the Gaposchkin resonant harmonics, they perform almost as well as M1.

The question of the prediction error magnitude depends on the manner in which one chooses the radiation pressure and drag parameters. Assuming nominal values of α and γ, and holding these fixed while estimating the initial state results in errors of about 7-8 km after 30 days. This is also the magnitude obtained by solving for γ over a 6-day arc using a geopotential model which contains the Gaposchkin-Veis resonance terms. Solving for γ in the presence of other resonant coefficients or omitting the term altogether could introduce 25-30 km discrepancies after 1 month.

Finally, by a careful selection of γ (with or without drag) the prediction error could be reduced to a level of 1-2 km. The question is: how does one find the "proper" value of γ?

One possibility is to perform measurements on a laboratory model. Since the satellite is asymmetrical, the cross sectional area to radiation is changing as a function of time. A careful modeling of the cross-section and the reflectivity could result in a better approximation to the true γ. Over time periods of a month and longer, it appears worthwhile to introduce a time-dependent area into dynamical calculations.

A second approach is to use an aposteriori estimate from the prior month to predict for the next month. For example, the best estimate of γ

from the January arc (as derived in section 3.4) could be used for February predictions and the best adjusted value from February would be used for March, etc. In place of the method in 3.4, γ could be estimated directly by using a longer fit span. Over time spans of 3 weeks to a month, there should be little aliasing of potential model errors into γ. The drag influence is comparatively small and should, in any case, be absorbed by γ. It does not seem unreasonable to expect errors of less than 1 km after a month with current models. The experiments in this paragraph are interesting ones to try out on GEOS type orbits, particularly GOES-II which seems to fit the M1 model considerably worse than GEOS-I (Marsh, 1969).

Since all four models are capable of predicting an ephemerides accurate to 1-2 km after a month (within this range, the quality rating is M1, 8D, 5E6+R, 5E6, Kohnlein), the choice of a "preferred" model evolves from other factors. One criterion which has some practical considerations is that of computation time. The time required to calculate a 36 day ephemeris for various models are:

Model	Central processor time on CDC 6600 computer
5E6	640 (sec)
5E6+R	700
M1	800
8D	1000
Kohnlein	1060

Evidently, there are some significant savings to be gained from using the smaller models.

The test models augmented by the Gaposchkin-Veis resonance terms perform very well with respect to the GEOS-I orbit. Whether the same applies to other orbital geometries can only be determined from further investigations.

Appendix 1. Normalized Geopotential Coefficients x 10^6

	M1		5E6		Kozai-69
n,m	C	S	C	S	C
2 0	-484.1736		-484.194		-484.166
3 0	.9623		.984		.9593
4 0	.5497		.507		.5310
5 0	.06332		.045		.0693
6 0	-.1792		-.219		-.1392
7 0	.08598		.105		.0932
8 0	.06548				.0286
9 0	.01216				.0229
10 0	.01178				.0772
11 0	-.06297				-.0421
12 0	.0714				.0084
13 0	.02194				.0236
14 0	-.03324				.0136
15 0					.0312
16 0					-.0325
17 0					-.0143
18 0					.0380
19 0					.0355
20 0					.0008
21 0					-.0221
2 1			.016	.062	
2 2	2.379	-1.351	2.446	-1.519	
3 1	1.936	.266	2.148	.274	
3 2	.734	- .538	.978	- .906	
3 3	.561	1.62	.585	1.625	
4 1	-.572	- .469	-.495	- .575	
4 2	.330	.661	.274	.671	
4 3	.851	- .19	1.030	- .247	
4 4	-.053	.23	-.413	.336	
5 1	-.079	- .103	.032	- .119	
5 2	.631	- .232	.637	- .328	
5 3	-.520	.007	-.389	- .124	
5 4	-.265	.064	-.549	.148	
5 5	.156	- .592	.215	- .594	
6 1	-.047	- .027	-.085	.192	
6 2	.069	- .366	.129	- .457	
6 3	-.054	.031	-.020	- .134	
6 4	-.044	- .518	-.193	- .316	
6 5	-.313	- .458	-.093	- .786	
6 6	-.040	- .155	-.324	- .360	
7 1	.197	.156	.331	.083	
7 2	.364	.163	.350	- .195	
7 3	.250	.0180	.323	.045	
7 4	-.152	- .102	-.467	- .244	
7 5	.076	.054	.055	.021	

Appendix 1. Normalized Geopotential Coefficients* (Cont)

	M1		5E6		Kozai-69
n,m	C	S	C	S	C
7 6	-.209	.063	-.477	- .244	
7 7	.055	.096			
8 1	-.075	.065			
8 2	.026	.03			
8 3	-.037	.004			
8 4	-.212	- .012			
8 5	-.053	.118			
8 6	-.017	.318			
8 7	-.0087	.031			
8 8	-.248	.102			
9 1	.117	.012			
9 2	-.004	.035			
9 9	-.065	.0909			
10 1	.105	- .126			
10 2	-.105	- .042			
10 3	-.065	.030			
10 4	-.074	- .111			
11 1	-.053	.015			
12 1	-.163	- .071			
12 2	-.103	- .0051			
12 12	-.031	.0008			
13 12	-.06848	.0657			
13 13	-.059	.077			
14 01	-.015	.0053			
14 11	.0002	- .0001			
14 12	.00261	- .02457			
14 14	-.014	- .003			
15 9	-.0009	- .0018			
15 12	-.07473	- .01026			
15 13	-.058	- .046			
15 14	.0043	- .0211			

Appendix II. Initial State Vector Solutions

Classical Elements Referenced to Mean Equator Equinox of 1950.0

January Arc Epoch: Jan 2, 6^h 0^m 0^s; 1966

γ Estimated

Model	a (km)	e	i (deg)	Ω (deg)	w (deg)	Mo (deg)	γ (10^{-9})
M1	8066.861	.0714389	59.33152	332.19532	186.97039	276.43146	4.397
5E6	.853	369	155	524	7758	2461	20.528
5E6+R	.850	382	157	527	7196	2957	5.386
5E6+R+K69	.850	417	156	533	7288	2898	4.940
8D	.855	369	161	51[illegible]	6871	3259	-2.385
Köhnlein	.863	283	144	552	6770	3425	-8.331

γ Fixed (5.75 E-9)

M1	8066.861	.0714383	59.33150	332.1[illegible]534	186.96[illegible]80	276.43183	
5E6	.854	354	165	516	6962	2331	
5E6+R	.850	384	155	528	7154	2984	
8D	.854	380	153	527	7017	3368	
Köhnlein	.862	301	131	563	6410	3596	
M1 - with drag	.861	401	151	531	7017	3156	

July Arc Epoch: July 10, 0^h 0^m 0^s; 1966

γ Estimated

M1	8078.395	.0705325	59.30662	268.16625	311.18022	235.64625	6.021
5E6	.403	328	659	608	8404	4356	23.055
5E6+R	.399	359	672	625	7911	4689	5.329
8D	.394	363	668	631	8182	4464	- .266
Köhnlein	.392	260	656	634	8433	4406	33.161

γ Fixed

M1	8078.395	.0705319	59.30662	268.16625	311.18078	235.64589
5E6	.401	378	64	607	7968	4636
5E6+R	.400	367	68	614	8083	4543
8D	.395	336	66	632	8419	4312
Köhnlein	.390	345	64	631	7705	4874
M1 - doppler	.395	325	62	625	8022	4625

Figure 1. Perturbations from Drag and Radiation Pressure

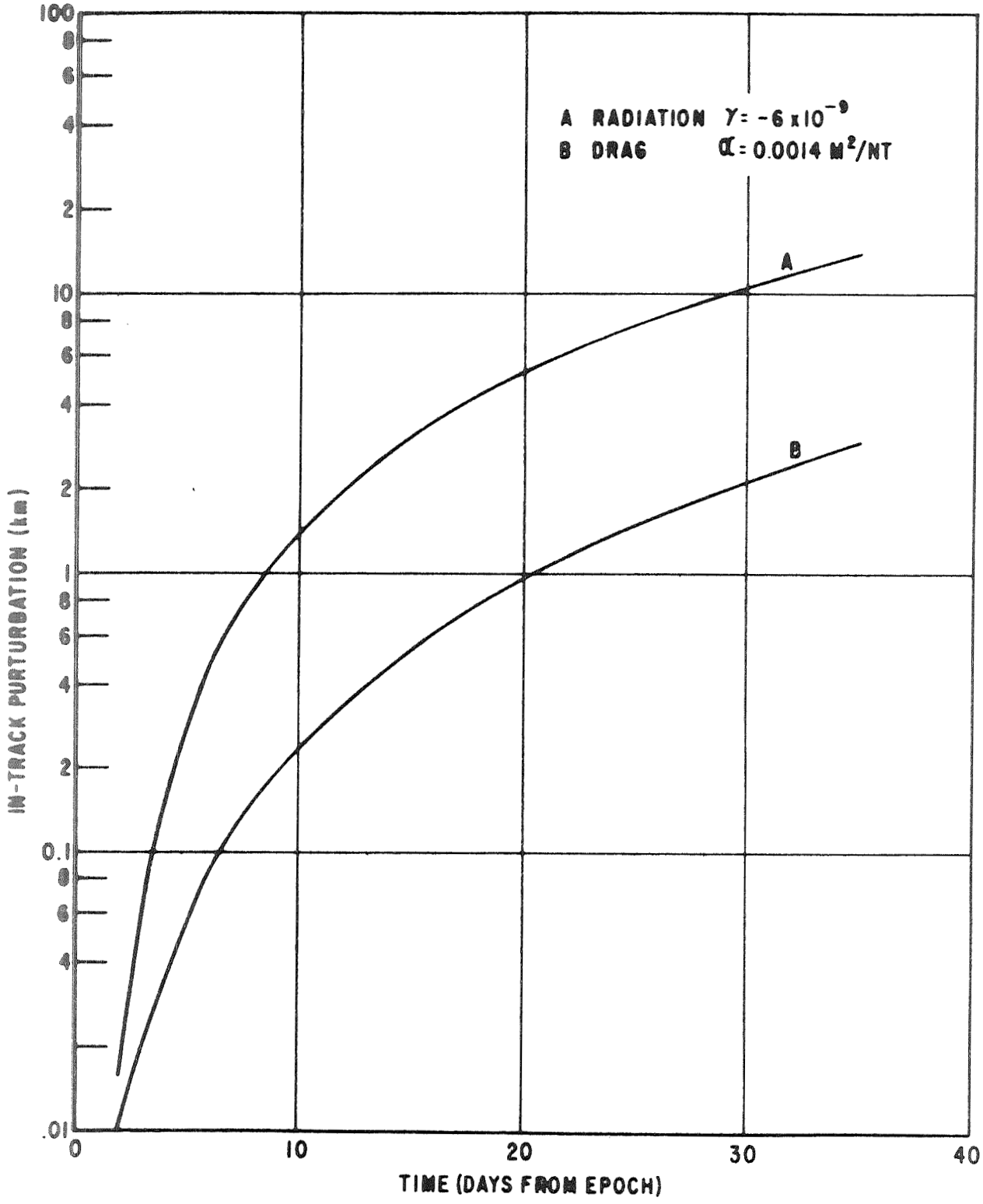

Figure 2. Perturbations from Resonant Harmonics

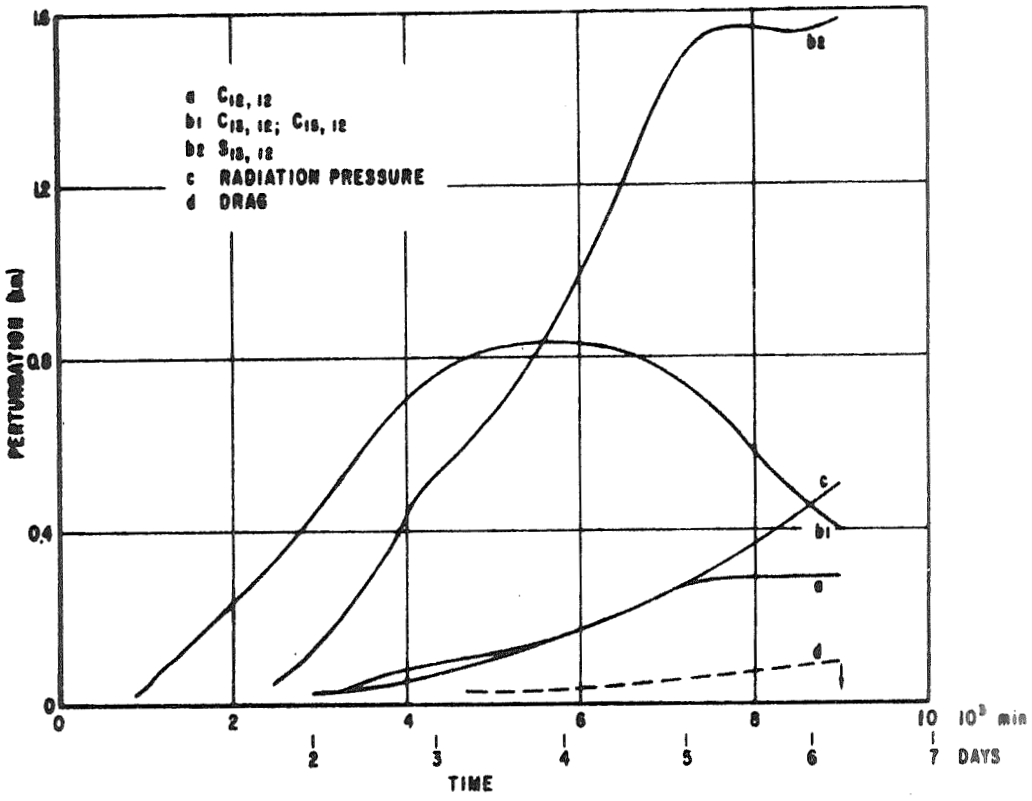

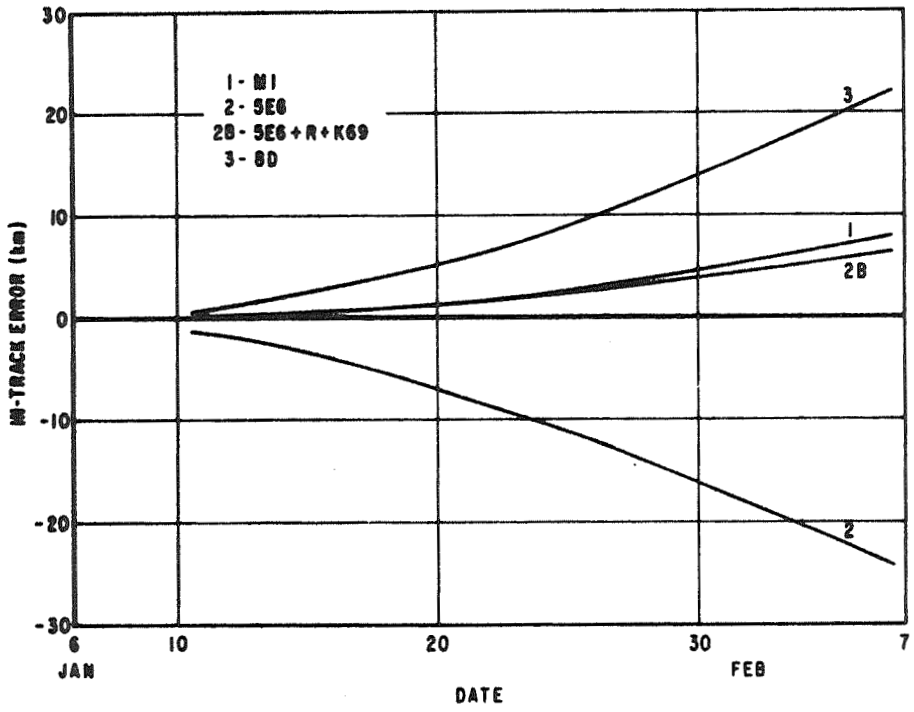

Figure 3. In-track Prediction Errors with Estimated γ

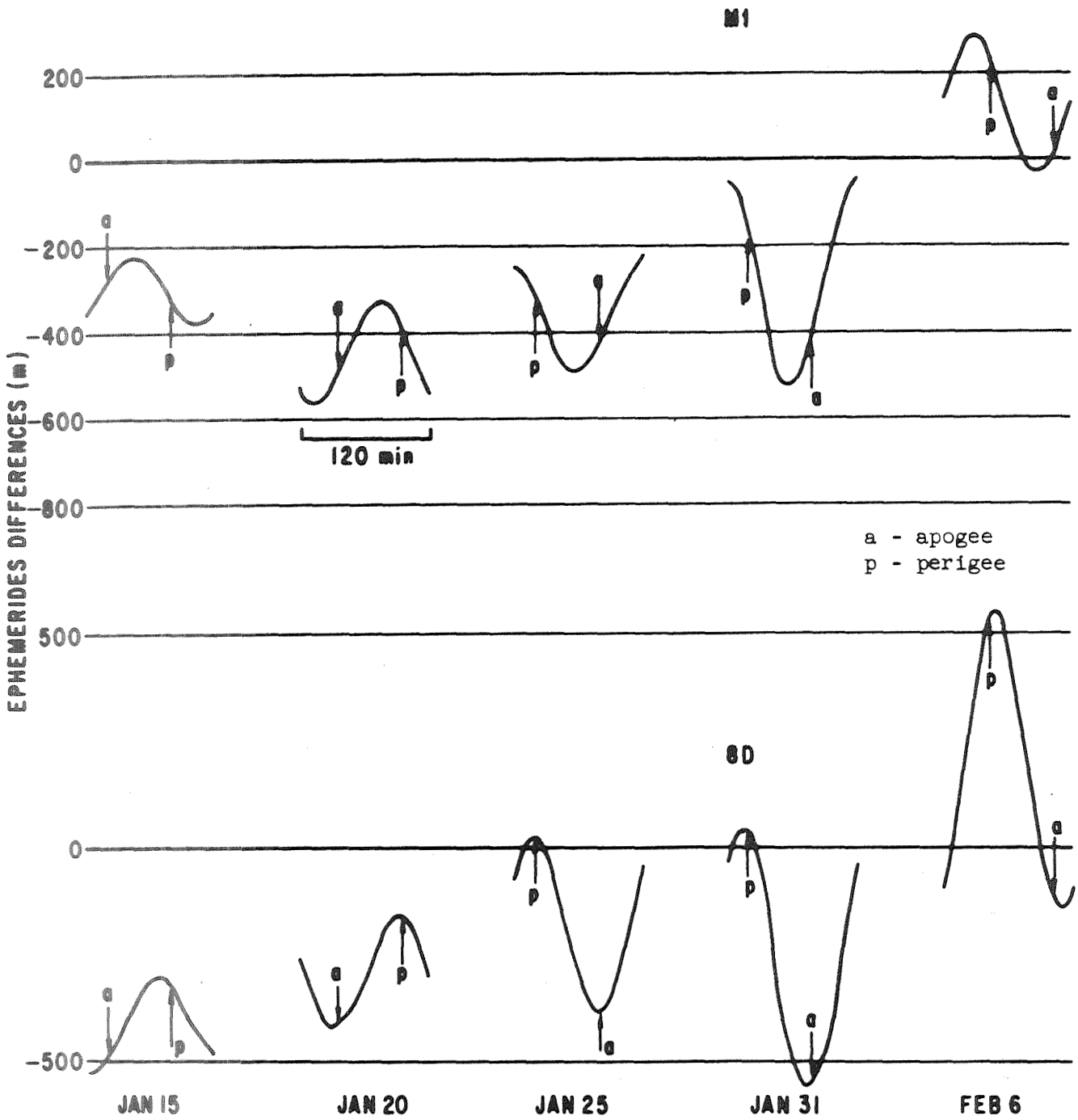

Figure 4. In-track Ephemeris Difference - M1, 8D - January Arc

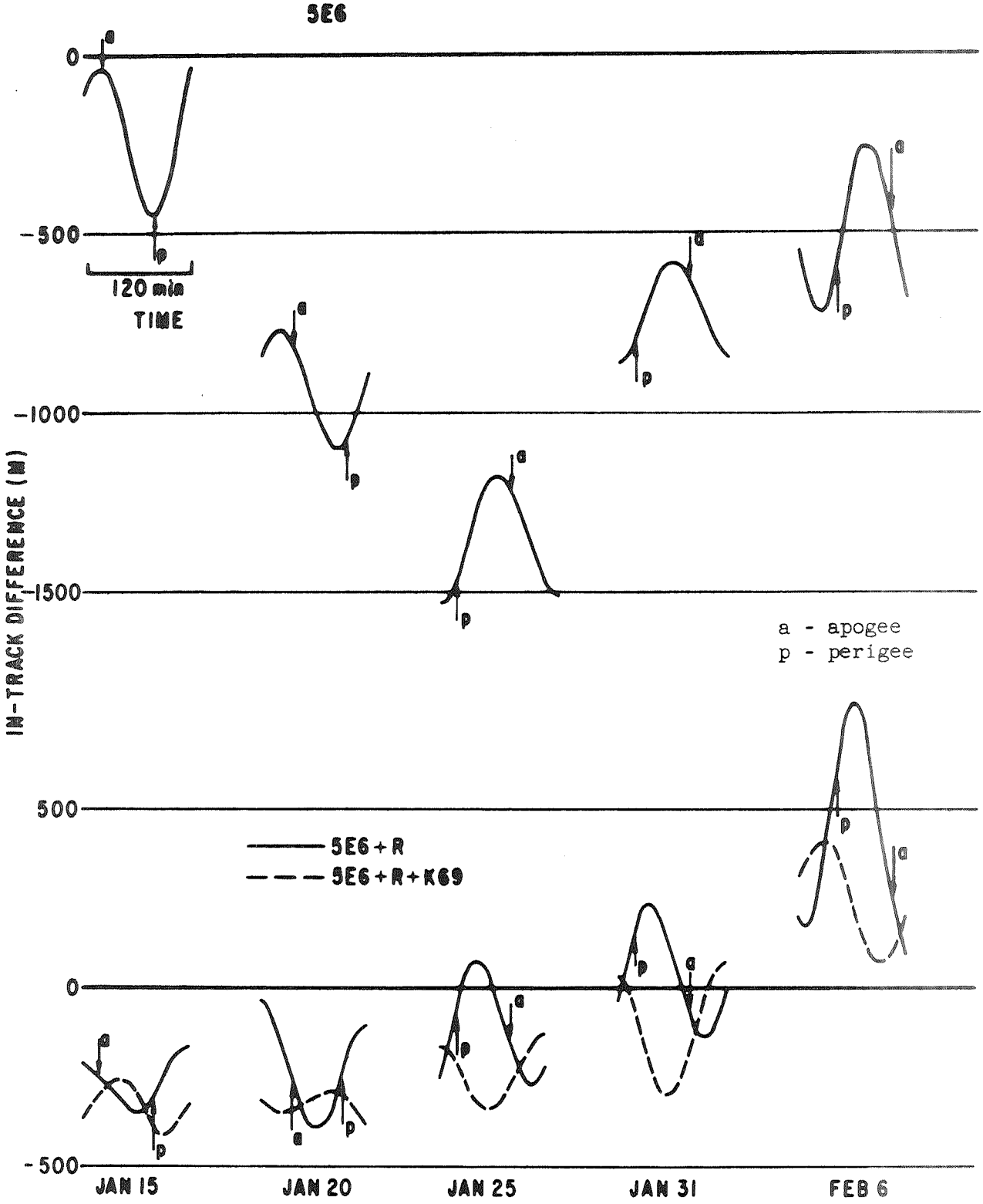

Figure 5. In-track Ephemeris Difference - 5E6, 5E6+R - January Arc

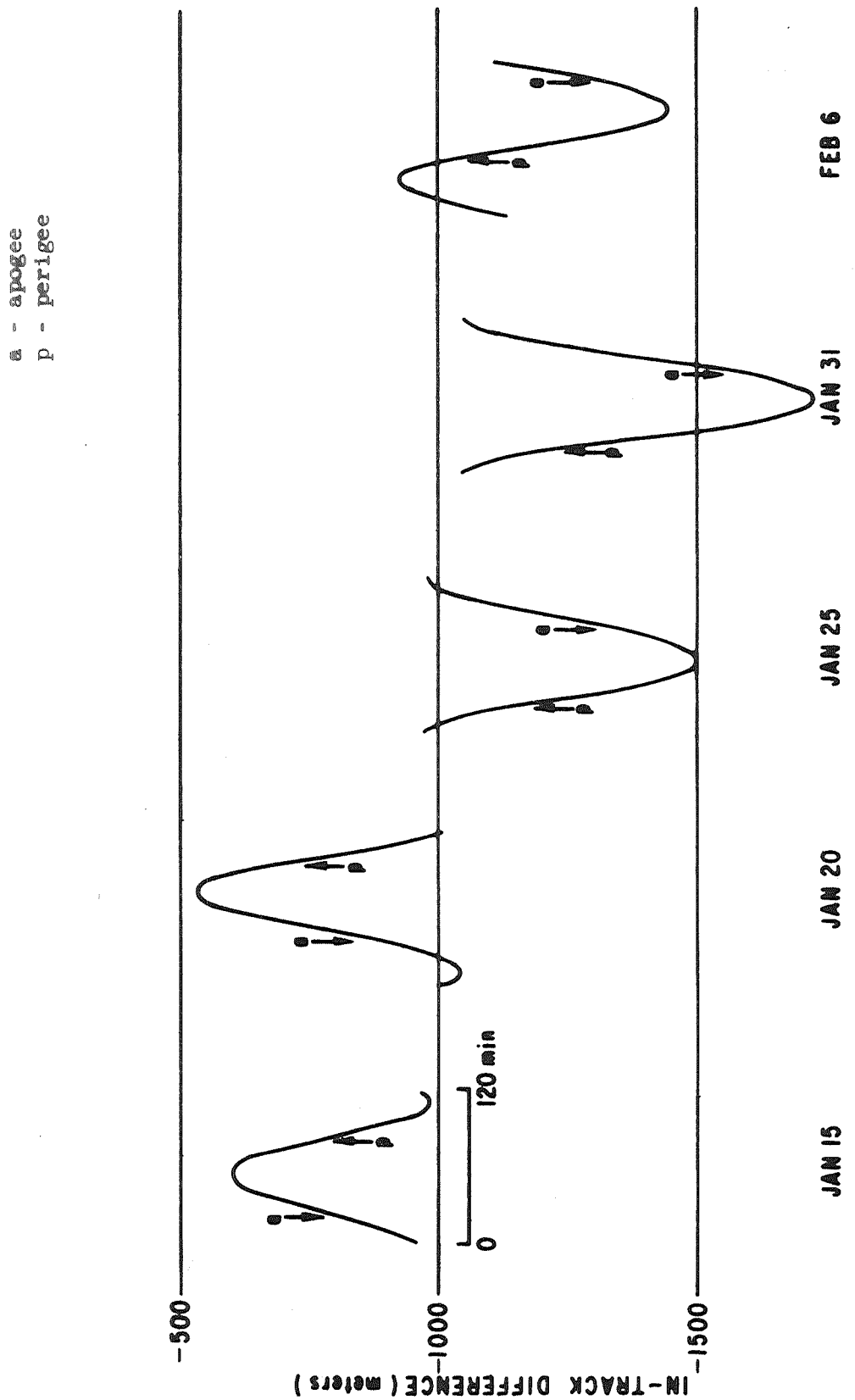

Figure 6. In-track Ephemeris Difference - Kohnlein - January Arc

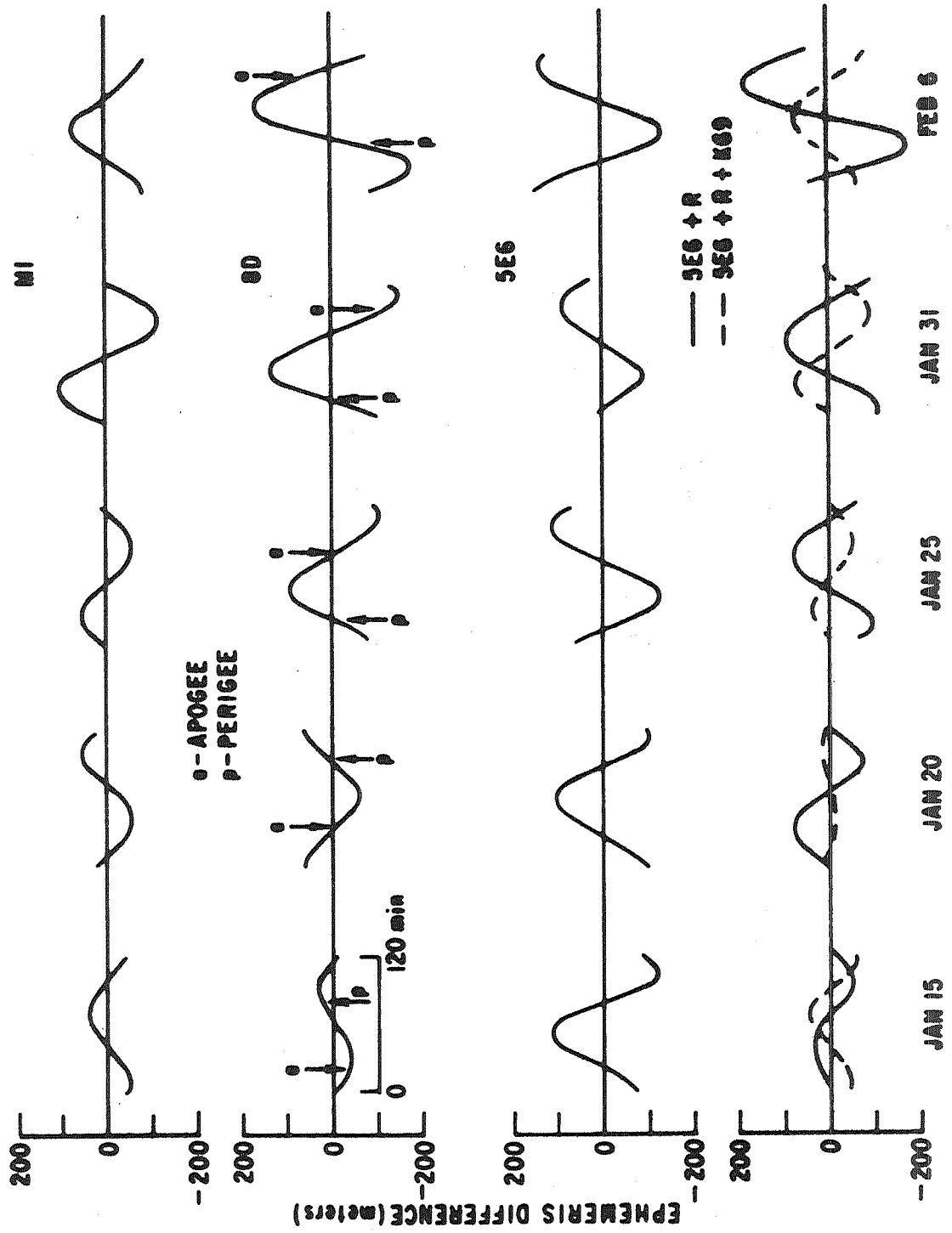

Figure 7. Radial Ephemeris Differences - January Arc

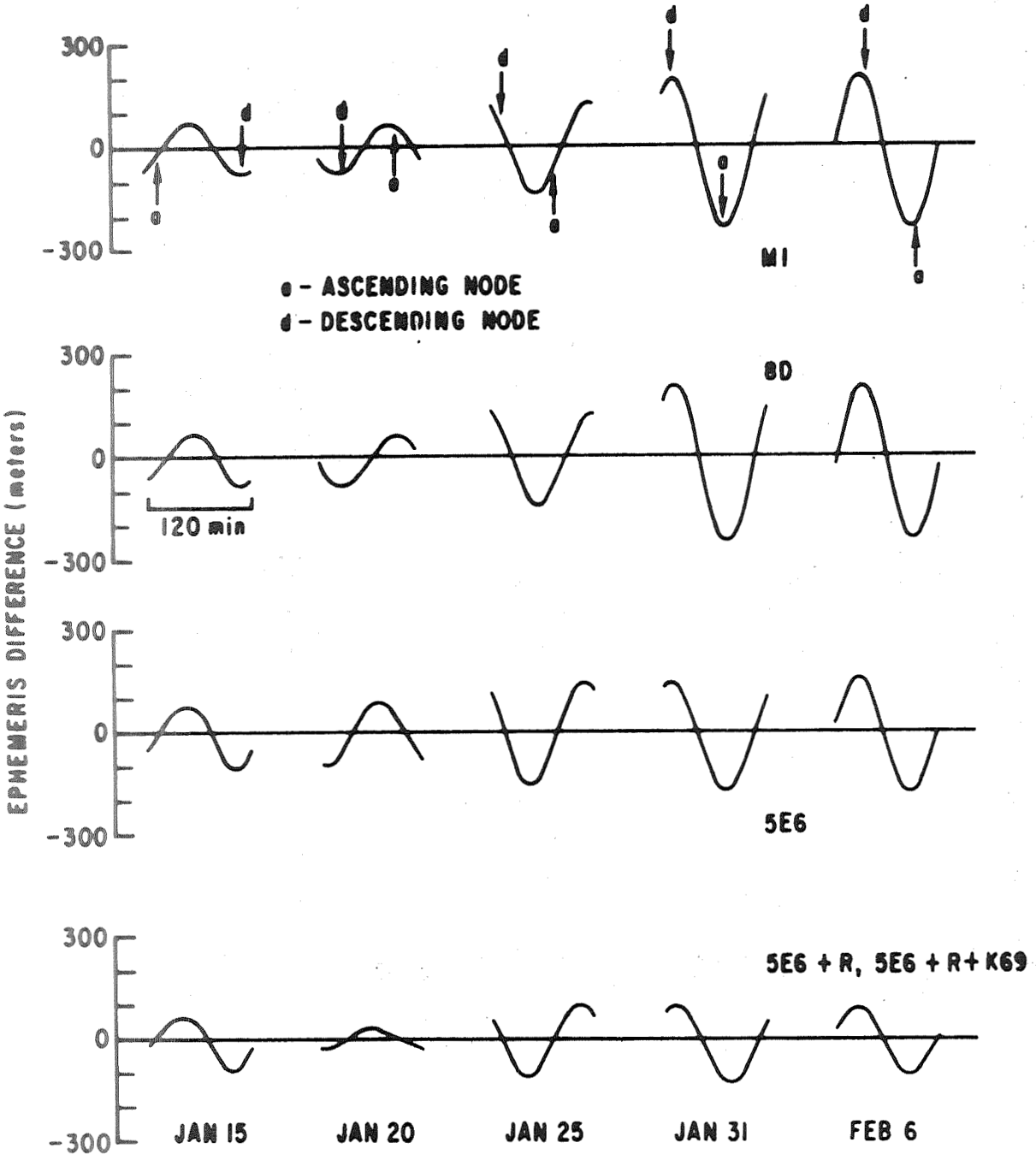

Figure 8. Cross-track Ephemeris Differences - January Arc

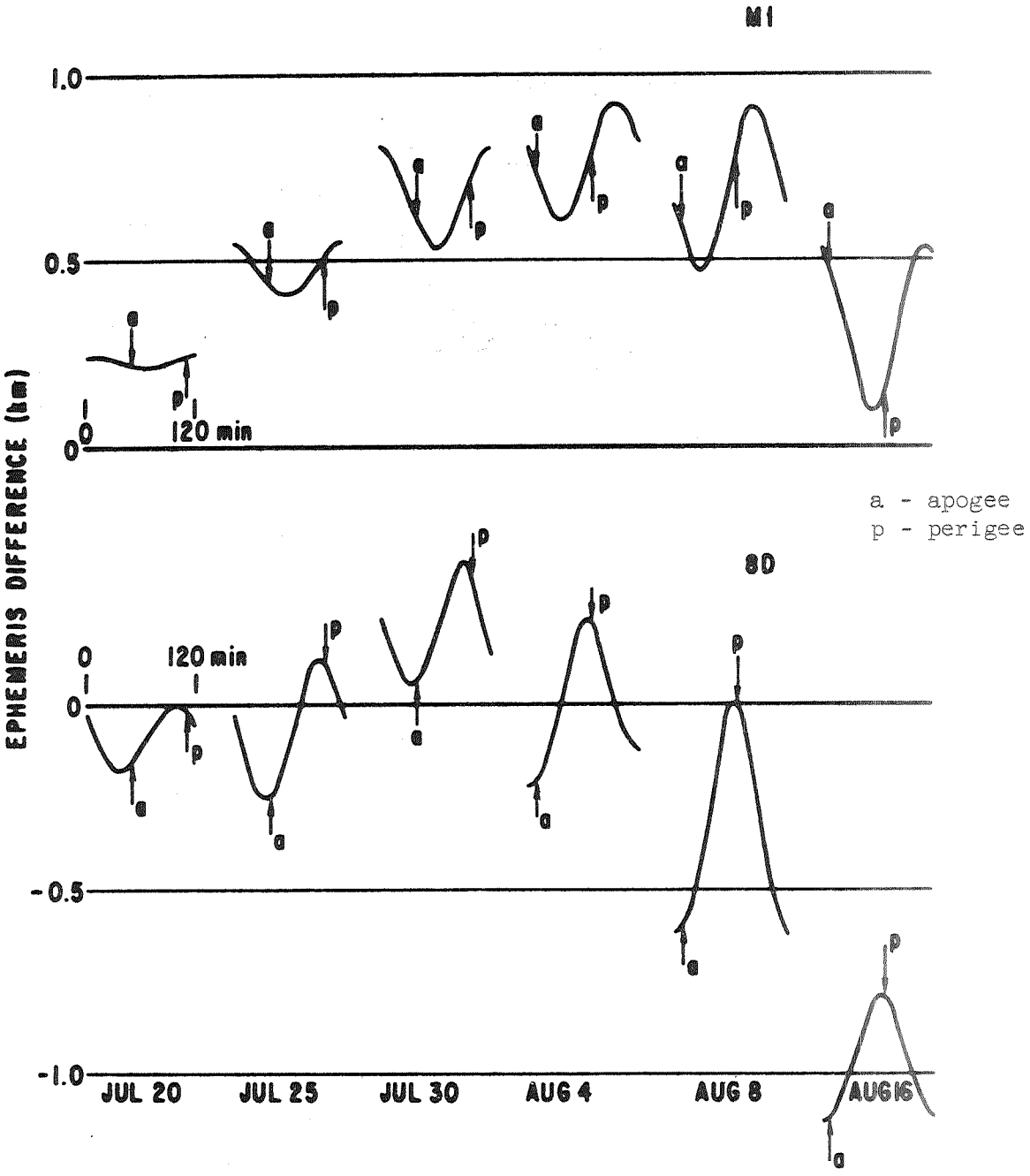

Figure 9. In-track Ephemeris Differences - M1, 8D - July Arc

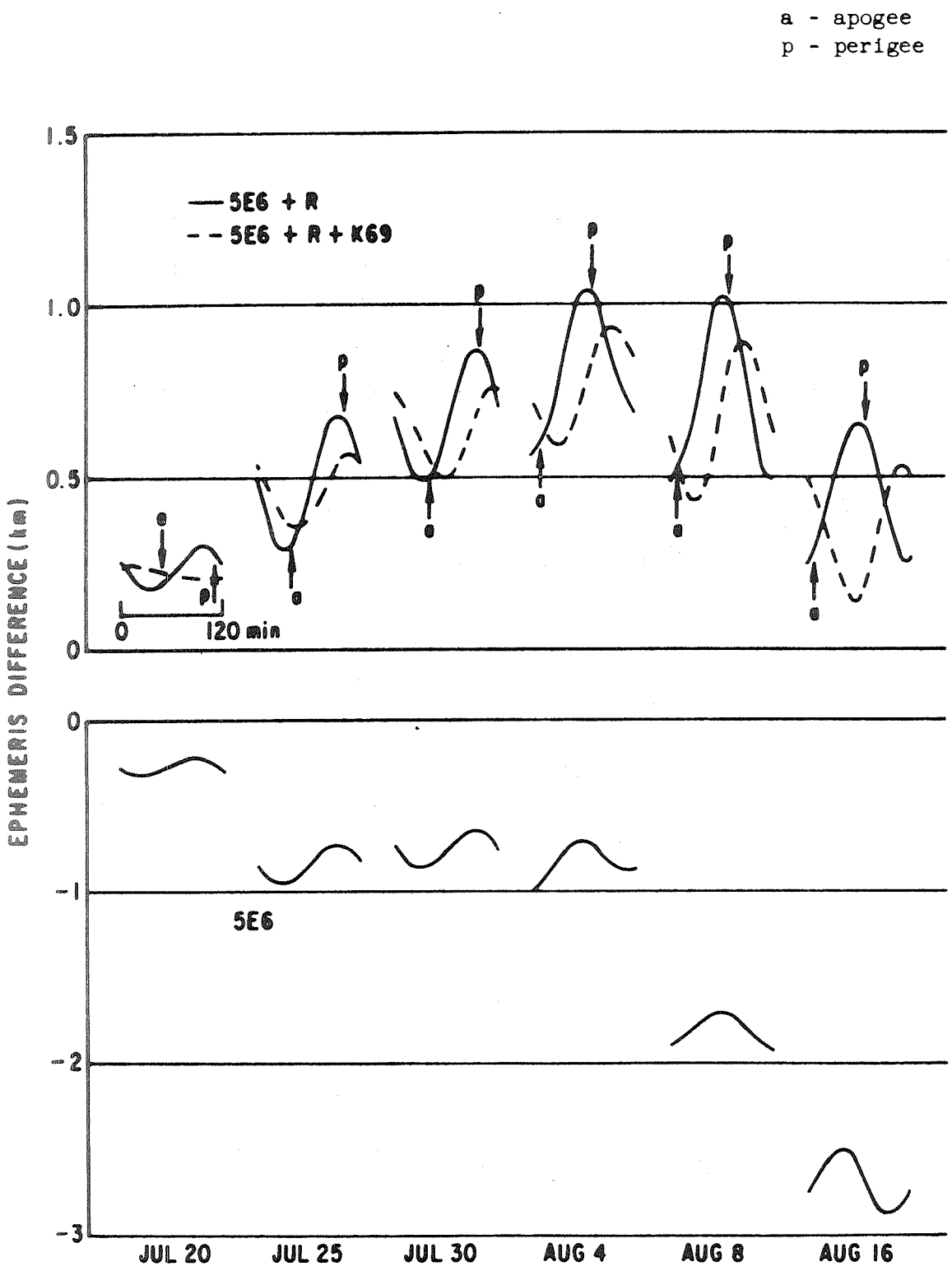

Figure 10. In-track Ephemeris Differences - 5E6, 5E6+R - July Arc

Figure 11. Typical Tranet Doppler Residuals

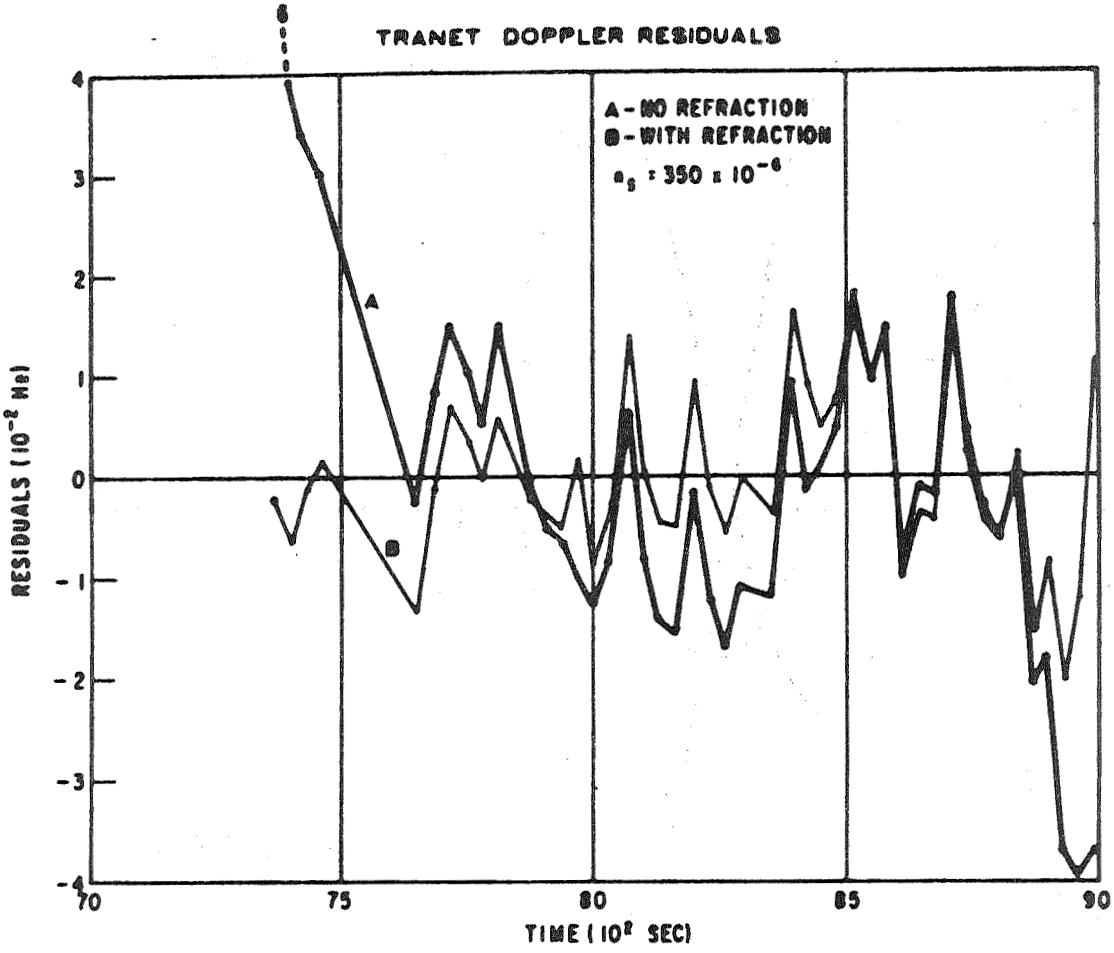

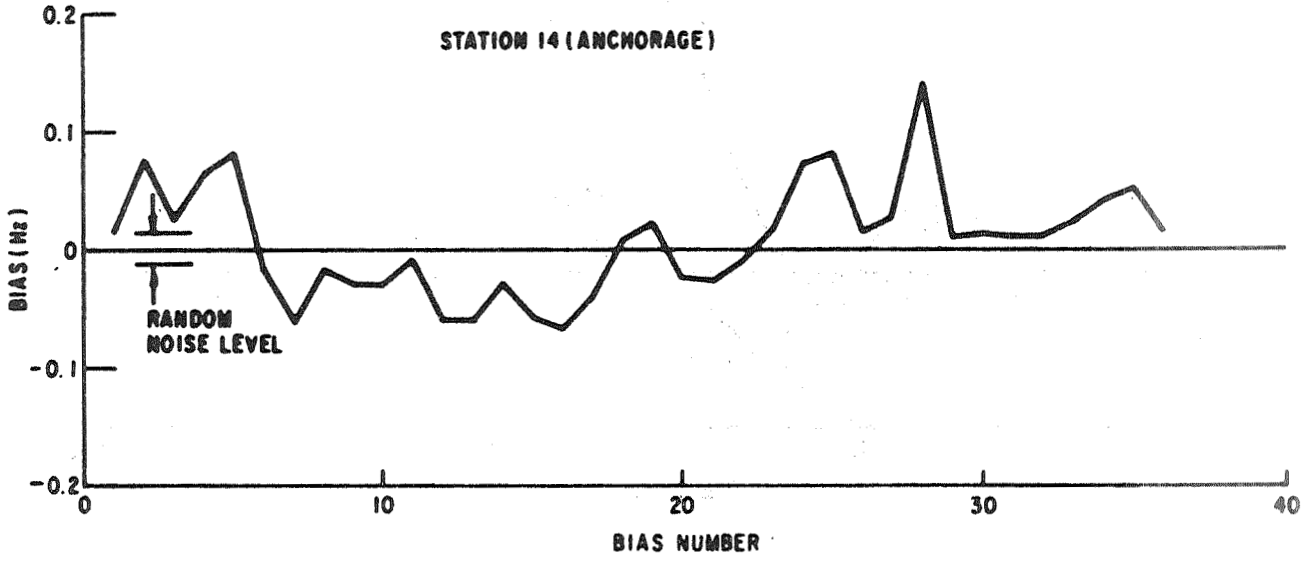

Figure 12. Differences in Tranet Biases - M1 vs 5E6 Model

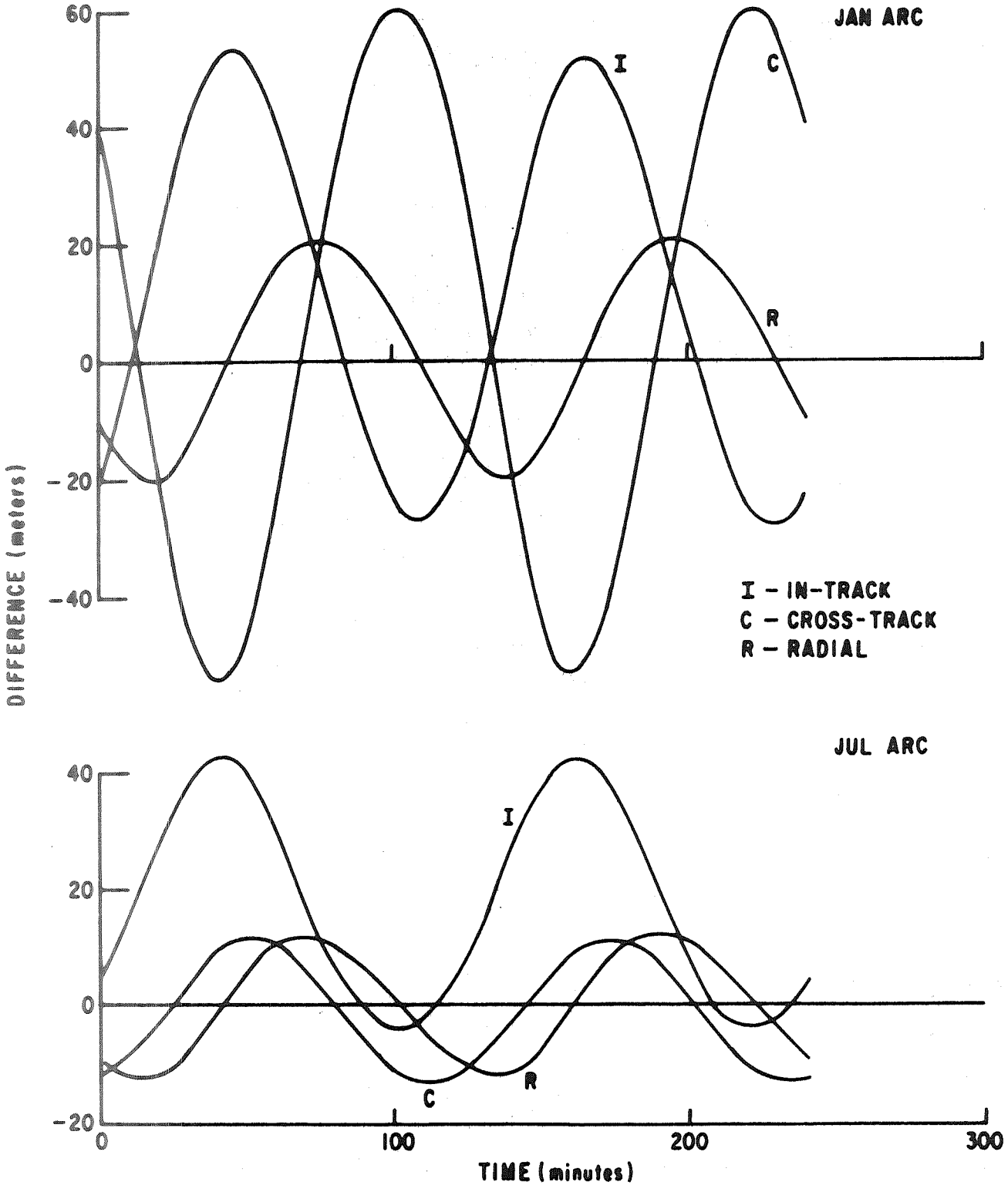

Figure 13. Differences Between Doppler and Optical Orbits

REFERENCES

1. Gaposchkin, E. M. Dynamical Determination of Station Locations Using GEOS I Data. SAO Report 264, 1967, p. 25.

2. Geodetic Satellites Observation Station Directory, Geonautics, Inc., July 1969.

3. Hopfield, H. S. "The Effect of Tropospheric Refraction on the Doppler Shift of a Satellite Signal," JGR, Vol. 68, Sept. 1963, p. 5157.

4. Kaula, W. M. Theory of Satellite Geodesy. Blaisdell Co., 1966, p. 7.

5. Kohnlein, W. The Earth's Gravitational Field as Derived from a Combination of Satellite Data with Gravity Anomalies. SAO Report 264, 1967, p. 57.

6. Kozai, Y. Revised Zonal Harmonics in the Geopotential. SAO Report 295, 1969.

7. Lerch, F., Marsh, J. G., and O'Neill, B. Gravity Model Comparison Using GEOS I Long Arc Orbital Solutions. NASA TN D-5035, June 1969.

8. Marsh, J. G., and O'Neill, B. Orbital Analysis and Prediction for GEOS Satellites Using Different Sets of Geopotential Coefficients. 50th AGU Paper, 1969.

9. Miller, B., and Caliri, P. J. GEOS I Orbital Elements and Observations. SAO Report 264 edited by C. A. Lundquist, 1967, p. 151.

10. Moulton, F. R. An Introduction to Celestial Mechanics. MacMillan Co., 1914, p. 171.

11. Muller, P. M. Constants and Related Information for Astrodynamic Calculations. JPL Tech Report 32-1306, 1968, pp. 10-19.

12. Smart, W. M. Spherical Astronomy. Cambridge University Press, 1962, p. 191.

13. Veis, G. "Geodetic Uses of Artificial Satellites," Smithsonian Contributions to Astrophysics, Vol. 3, No. 9, 1960, p. 121.

14. _____. SAO Report 200, 1966, pp. 9-43.

SECTION II

GEOMETRIC GEODESY

NASA STADAN, SPEOPT, AND LASER TRACKING STATION POSITIONS DERIVED FROM GEOS-I AND GEOS-II PRECISION REDUCED OPTICAL AND LASER OBSERVATIONS

By

J.G. Marsh
NASA Goddard Space Flight Center
Greenbelt, Md., USA

B.C. Douglas
C.F. Martin
Wolf Research and Development Corporation
Riverdale, Md., USA

ABSTRACT

Coordinates for 23 NASA STADAN and SPEOPT optical and 2 NASA laser tracking sites have been dynamically estimated from GEOS-I and II data. To strengthen the solutions, SAO Baker-Nunn optical data were also used with the SAO station coordinates held fixed at their 1969 C6 values. Multiple 2-day arcs were used to minimize model error effects.

An analysis of model error effects and comparison of results with these of SAO suggest an uncertainty of perhaps 5m north-south (latitude) and east-west (longitude) for most stations in North America. Height for the NAD sites, and latitude, longitude, and height elsewhere are uncertain by 10-15m in most cases.

SECTION 1.
INTRODUCTION

The GEOS-I and II satellites, extensively observed by a wide variety of tracking systems with good geographic coverage, provide an unusual opportunity for satellite geodesy. Literally tens of thousands of precision-reduced optical observations in the period 1966-69 are available, along with many thousands of passes of laser and electronic data. Our initial analyses were designed to provide accurate coordinates for NASA optical and laser sites.

The GEOS-I and II satellite orbital specifications are presented in Table 1. The orbits are complementary to one another, in that combined GEOS-I and II solutions provide excellent geometry for station recovery. Resonance is a problem for the GEOS-satellites, but can be dealt with either by adjusting resonant geopotential coefficients[1] or by using multiple short orbital arcs.

Our approach to the station estimation problem was dynamical using Cowell's method to solve the equations of motion. The orbital solutions included an equal amount of SAO Baker-Nunn data in addition to the STADAN-SPEOPT Minitrack Optical Tracking System (MOTS) observations. This served to greatly strengthen the solutions, particularly for those stations with limited data.

TABLE 1

ORBITAL ELEMENTS OF GEOS I AND II

	GEOS I	GEOS II
Epoch	January 2, 1966	April 28, 1968
Apogee Height	2273 Kilometers	1569 Kilometers
Perigee Height	1116 Kilometers	1077 Kilometers
Eccentricity	0.07	0.03
Inclination	59.4 Degrees	105.8 Degrees
Anomalistic Period	120.3 Minutes	112.1 Minutes

Mission Trajectory Determination Branch
Mission & Trajectory Analysis Division
Goddard Space Flight Center

The Baker-Nunn station positions were held fixed at their 1969[2] values referred to the C6 Earth. Thus the SAO 1969 gravity[2] model was used for all analyses. This model appears to be the best available. However, unmodeled long-period perturbations approaching 50 m (due to resonance) and additional short periodic errors exist.

To estimate the errors of our positions, we analyzed the effects of gravity model error, SAO station position error, and error in GM. The position uncertainty produced by the assumed gravity model error was generally 5-15 m. Other effects, including data noise, account for 2-3 m position error. These good results, in some cases obtained with GEOS-I data alone, are the direct result of the high quality data and good coverage afforded by the satellite-borne flashing lights.

SECTION 2.
SELECTION OF OPTICAL DATA

Figure 1 shows the geographic distribution of the SAO Baker-Nunn and STADAN/SPEOPT sites. Note the concentration of the STADAN/SPEOPT sites in North America, in contrast to the worldwide distribution of SAO positions.

We attempted to obtain station observation geometry that would minimize model error effects. This requires passes on all sides of the station and in opposing directions. Unfortunately for the case of GEOS-II data this latter requirement could not be met because the data was taken only on South-North passes. Figure 2 shows the geometry of the passes for an ideal case, the Edinburg, Texas site. The length of the lines indicates the pass lengths. Coverage of the extent shown in Figure 2 was not available in all cases, but was sufficient in nearly every case to obtain an accurate position.

Table 2 presents the number of observations used for each site. We examined 140 two day arcs containing approximately 60,000 observations. About 13,000 STADAN/SPEOPT observations and an equal number of SAO Baker-Nunn points in 60 two day arcs were used in the determination.

Tables 3, 4, and 5 give the SAO 1969[2, 3], gravity model and station coordinates adopted for our work. An evaluation (Marsh and Douglas, 1970)[4] of gravity models has demonstrated the general superiority of the SAO 1969 model. However, significant errors still exist in this model. Figure 3 shows apparent timing errors for range data from the Rosman, N.C. GRARR site computed from a 5 1/2 day GEOS-II optical reference orbit. Note that

Figure 1

TRACKING STATION POSITIONS

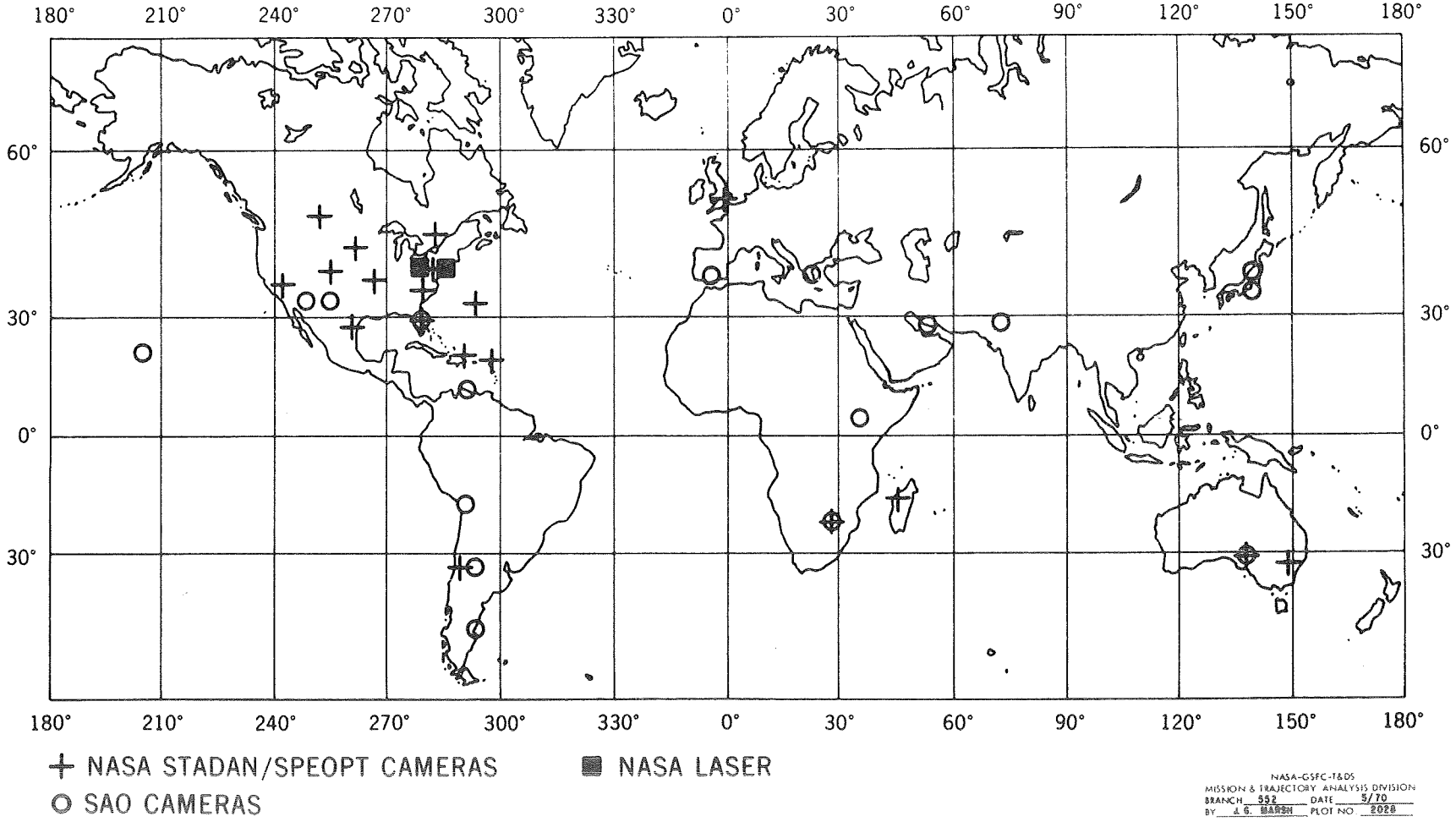

Figure 2

SUBSATELLITE PLOT OF GEOS I AND GEOS-II PASSES
EDINBURG, TEXAS

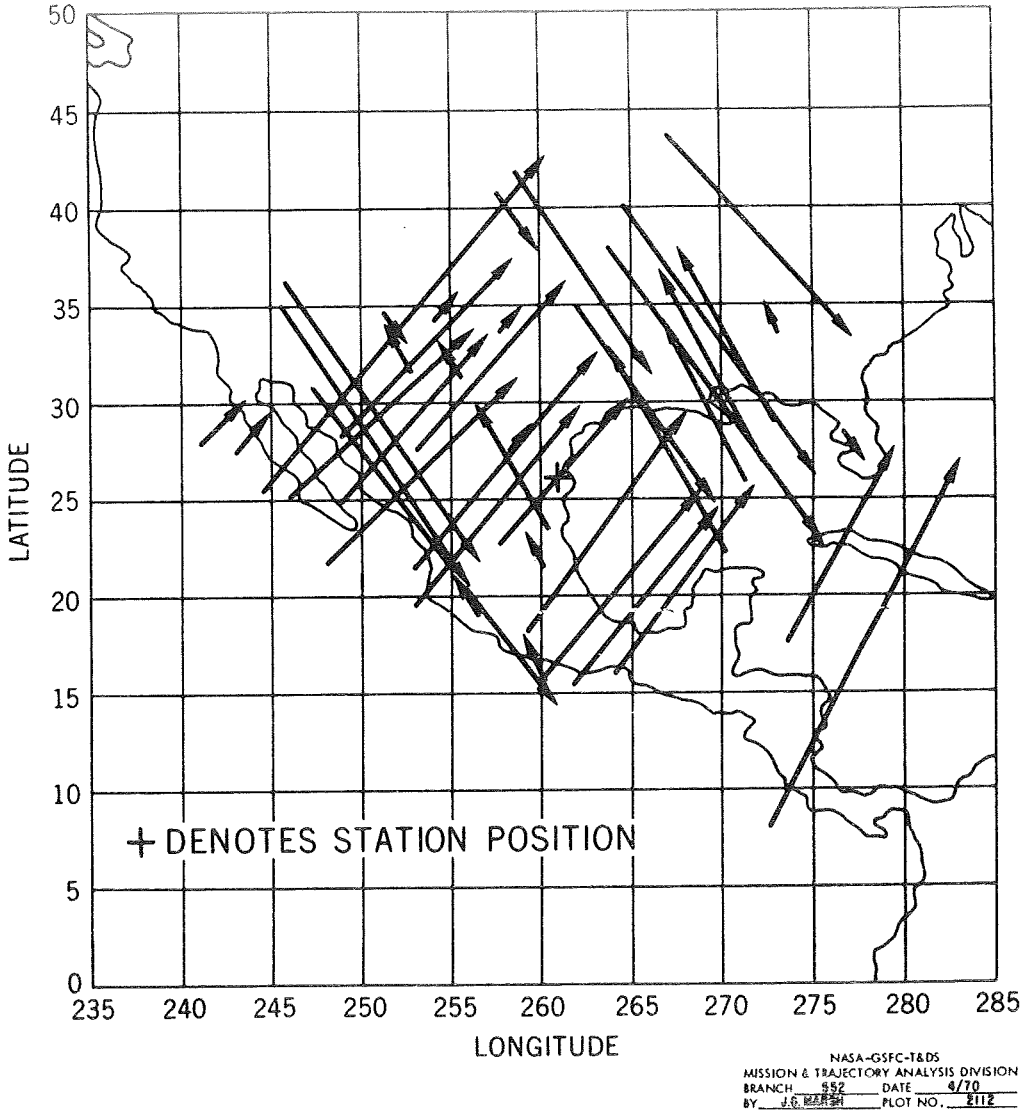

TABLE 2

NUMBER OF OPTICAL OBSERVATIONS PER STATION USED IN DYNAMICAL ESTIMATION

STATION		OBSERVATIONS	STATION		OBSERVATIONS
BLOSSOM POINT, MD.	(1021)	650	TANANARIVE, MADAGASCAR	(1043)	339
FT. MYERS, FLA.	(1022)	680	UNIV. OF N. DAKOTA, N. D.	(7034)	548
WOOMERA, AUSTRALIA	(1024)	152	EDINBURG, TEXAS	(7036)	1109
SANTIAGO, CHILE	(1028)	264	COLUMBIA, MO.	(7037)	1540
MOJAVE, CAL.	(1030)	932	BERMUDA	(7039)	448
JOHANNESBURG, UN. OF SO. AFR.	(1031)	623	SAN JUAN, P. R.	(7040)	475
ST. JOHNS, NEWFOUNDLAND	(1032)	179	GREENBELT, MD.	(7043)	158
E. GRAND FORKS, MINN.	(1034)	542	DENVER, COLO.	(7045)	573
WINKFIELD, ENGLAND	(1035)	400	JUPITER, FLA.	(7072)	516
ROSMAN, N. C.	(1037, 1042)	1015	SUDBURY, ONTARIO	(7075)	699
ORRORAL, AUSTRALIA	(1038)	482	KINGSTON, JAMAICA	(7076)	388

NASA-GSFC-T&DS
MISSION & TRAJECTORY ANALYSIS DIVISION
BRANCH 552 DATE 5/70
BY J. G. MARSH PLOT NO. 2031

Table 3. SAO-1969 Tesseral Harmonics

C0202	2.4161E-06	S0202	-1.3659E-06				
C0301	1.9751E-06	S0301	2.5549E-07	C0302	8.9005E-07	S0302	-6.4170E-07
C0303	6.9020E-07	S0303	1.4064E-06	C0401	-5.3491E-07	S0401	-4.8013E-07
C0402	3.2699E-07	S0402	7.0318E-07	C0403	9.9574E-07	S0403	-1.5147E-07
C0404	-8.8849E-08	S0404	3.3282E-07	C0501	-5.9419E-08	S0501	-9.9010E-08
C0502	6.0220E-07	S0502	-3.4210E-07	C0503	-4.1258E-07	S0503	-7.7774E-08
C0504	-2.6947E-07	S0504	6.7363E-08	C0505	1.3107E-07	S0505	-5.8964E-07
C0601	-1.0058E-07	S0601	3.3353E-08	C0602	6.0756E-08	S0602	-3.5467E-07
C0603	2.3195E-08	S0603	4.6183E-08	C0604	-4.0534E-09	S0604	-4.1423E-07
C0605	-2.0651E-07	S0605	-5.1784E-07	C0606	7.7062E-08	S0606	-7.9660E-09
C0701	2.5891E-07	S0701	1.1812E-07	C0702	3.0927E-07	S0702	1.5165E-07
C0703	2.0950E-07	S0703	-2.5571E-07	C0704	-2.1772E-07	S0704	-9.9535E-08
C0705	5.8836E-10	S0705	8.0903E-08	C0706	-2.6138E-07	S0706	1.0723E-07
C0707	1.5936E-07	S0707	-8.6695E-08	C0801	2.8995E-08	S0801	3.3769E-08
C0802	3.1768E-08	S0802	7.9006E-08	C0803	-6.5467E-08	S0803	2.5892E-08
C0804	-1.7457E-07	S0804	7.6981E-08	C0805	-3.8947E-08	S0805	5.8609E-08
C0806	-5.6676E-08	S0806	2.5440E-07	C0807	3.9788E-08	S0807	9.3092E-08
C0808	-8.4590E-08	S0808	4.8844E-08	C0901	1.4748E-07	S0901	-1.3452E-08
C0902	-6.5813E-09	S0902	-7.1488E-08	C0903	-9.3300E-08	S0903	-1.0329E-07

C0904	5.6475E-08	S0904	1.1735E-07	C0905	-6.2122E-09	S0905	2.4203E-08
C0906	3.5025E-08	S0906	2.2871E-07	C0907	-5.9879E-08	S0907	-1.2904E-07
C0908	2.3234E-07	S0908	7.6310E-08	C0909	-7.0411E-08	S0909	9.4418E-08
C1001	1.0988E-07	S1001	-1.1190E-07	C1002	-1.3689E-08	S1002	-1.0385E-07
C1003	-2.4944E-08	S1003	-1.4725E-07	C1004	-6.3531E-08	S1004	-6.5758E-08
C1005	-5.5523E-08	S1005	-1.5747E-07	C1006	-7.0152E-08	S1006	-1.9470E-07
C1007	6.9152E-08	S1007	6.1804E-08	C1008	6.9300E-08	S1008	-8.8606E-08
C1009	-9.2577E-09	S1009	3.2702E-08	C1010	1.3206E-07	S1010	-3.9516E-08
C1101	1.9718E-08	S1101	1.7416E-08	C1102	3.5409E-08	S1102	-8.3246E-08
C1103	-7.2398E-08	S1103	-1.4168E-07	C1104	-3.4533E-08	S1104	5.8623E-08
C1105	2.9488E-08	S1105	1.7339E-07	C1106	6.8275E-08	S1106	6.0137E-08
C1107	4.4653E-08	S1107	-1.9444E-07	C1108	9.9838E-08	S1108	-3.7787E-08
C1109	1.6166E-07	S1109	-4.6015E-08	C1110	-1.2633E-07	S1110	-1.1490E-08
C1111	1.0851E-07	S1111	-3.5434E-08	C1201	-5.8686E-08	S1201	-2.3105E-08
C1202	1.5920E-08	S1202	7.6958E-08	C1203	4.9759E-08	S1203	6.4893E-08
C1204	-2.4201E-08	S1204	-5.7292E-08	C1205	2.1686E-09	S1205	4.5293E-08
C1206	-8.6279E-08	S1206	-6.9239E-08	C1207	-2.4601E-09	S1207	1.1372E-07
C1208	-4.5992E-08	S1208	6.1974E-08	C1209	-1.6950E-07	S1209	8.6866E-08
C1210	-2.2905E-08	S1210	1.0180E-08	C1211	-4.1035E-08	S1211	-4.5052E-08
C1212	-1.8989E-08	S1212	-6.0304E-08	C1301	-6.2655E-08	S1301	1.8464E-08
C1302	-6.2746E-08	S1302	2.0472E-08	C1303	4.8867E-08	S1303	-3.8613E-08
C1304	-2.5277E-08	S1304	1.1241E-07	C1305	1.5942E-07	S1305	-3.6076E-08
C1306	-2.6708E-08	S1306	1.0018E-07	C1307	1.9903E-08	S1307	-1.2315E-08
C1308	-4.0852E-08	S1308	-2.8897E-08	C1309	9.8415E-08	S1309	7.1015E-08
C1310	8.6950E-08	S1310	-1.8175E-08	C1311	-3.0466E-08	S1311	8.2538E-08
C1312	-5.5883E-09	S1312	9.1888E-08	C1313	-7.0369E-08	S1313	7.2809E-08
C1401	-1.0963E-08	S1401	5.0787E-08	C1402	5.7579E-08	S1402	-5.3880E-08
C1403	9.8439E-09	S1403	-1.1248E-08	C1404	6.1209E-09	S1404	-1.0658E-07
C1405	-1.0088E-07	S1405	-3.5727E-08	C1406	-4.9692E-08	S1406	-5.8748E-08
C1407	-6.9174E-08	S1407	7.6868E-09	C1408	4.8643E-09	S1408	-4.1410E-08
C1409	-1.0896E-08	S1409	1.1561E-07	C1410	6.0335E-08	S1410	-4.2580E-08
C1411	2.8078E-08	S1411	-1.5272E-07	C1412	1.0683E-08	S1412	-5.9781E-08
C1413	5.3563E-08	S1413	5.0528E-08	C1414	-5.3994E-08	S1414	-1.1646E-08
C1501	-8.8807E-09	S1501	3.2392E-08	C1502	-6.3852E-08	S1502	-2.6915E-08
C1503	1.2258E-08	S1503	-4.6661E-10	C1504	2.2243E-08	S1504	1.2379E-07
C1505	7.7119E-08	S1505	4.3820E-08	C1506	1.1696E-07	S1506	-1.3911E-07
C1507	1.9585E-07	S1507	3.9890E-08	C1508	-1.3430E-07	S1508	-4.9333E-08
C1509	3.2748E-08	S1509	5.4493E-09	C1510	-4.1753E-08	S1510	-1.0768E-08
C1511	-4.0045E-08	S1511	1.7610E-07	C1512	5.4810E-09	S1512	1.8854E-08
C1513	-3.8086E-08	S1513	9.2215E-10	C1514	1.2490E-08	S1514	-2.8153E-08
C1515	3.6230E-09	S1515	-1.0808E-08	C1601	-1.9620E-08	S1601	7.3004E-08
C1602	2.5614E-08	S1602	4.1595E-08	C1603	-3.9732E-08	S1603	4.5346E-08
C1604	-1.3082E-08	S1604	2.5548E-08	C1605	-6.8038E-08	S1605	1.2917E-08
C1606	-7.8209E-08	S1606	-4.0015E-08	C1607	9.0352E-08	S1607	4.3458E-09
C1608	-7.8992E-08	S1608	1.2284E-08	C1609	1.5532E-08	S1609	-1.1203E-07
C1610	-1.2047E-08	S1610	1.8863E-08	C1611	1.1710E-08	S1611	-1.1563E-07
C1612	2.2785E-08	S1612	-3.4986E-08	C1613	3.6574E-08	S1613	2.2980E-08
C1614	-6.0552E-09	S1614	-2.3051E-08	C1615	-3.3634E-08	S1615	6.7563E-10
C1616	-3.5086E-08	S1616	1.2329E-08	C1712	7.9168E-08	S1712	1.4437E-08
C1713	3.3464E-08	S1713	4.4817E-09	C1714	-1.7868E-08	S1714	2.9766E-08
C1812	6.3896E-09	S1812	5.9120E-09	C1813	9.3048E-09	S1813	-2.6794E-08
C1814	-2.5884E-08	S1814	-4.9653E-08	C1912	6.3336E-08	S1912	7.2476E-10
C1913	3.6630E-08	S1913	-5.3030E-08	C1914	-3.7025E-09	S1914	-2.3541E-08
C2013	6.2126E-08	S2013	4.0822E-08	C2014	1.2752E-08	S2014	-1.3875E-08
C2113	4.3091E-09	S2113	-1.0273E-08	C2114	5.3341E-08	S2114	-5.9833E-09
C2214	-4.8469E-09	S2214	2.1719E-08				

TABLE 4

ZONAL HARMONICS AND RELATED CONSTANTS

J(2) =	1.08262800E-03	J(3) =	-2.5380E-06
J(4) =	-1.5930E-06	J(5) =	-2.3000E-07
J(6) =	5.0200E-07	J(7) =	-3.6200E-07
J(8) =	-1.1800E-07	J(9) =	-1.0000E-07
J(10) =	-3.5400E-07	J(11) =	2.0200E-07
J(12) =	-4.2000E-08	J(13) =	-1.2300E-07
J(14) =	-7.3000E-08	J(15) =	-1.7400E-07
J(16) =	1.8700E-07	J(17) =	8.5000E-08
J(18) =	-2.3100E-07	J(19) =	-2.1600E-07
J(20) =	-5.0000E-09	J(21) =	1.4400E-07

$GM = 3.986013 \times 10^{20}\ cm^3\ sec^{-2}$

$a_e = 6.378155 \times 10^{6}\ m$

$c = 2.997925 \times 10^{10}\ cm\ sec^{-1}$

TABLE 5

SAO STATION COORDINATES

Station Name	Number	Geodetic Latitude (deg min sec)	East Longitude (deg min sec)	Height Above Ellipsoid (meters)
Organ Pass, New Mexico	9001	32 25 24.8	253 26 48.4	1613
Pretoria, Union of South Africa	9002	-25 57 36.7	28 14 52.2	1559
San Fernando, Spain	9004	36 27 46.6	353 47 36.8	47
Tokyo, Japan	9005	35 40 22.6	139 32 16.2	80
Naini Tal, India	9006	29 21 34.6	79 27 27.2	1862
Arequipa, Peru	9007	-16 27 57.1	288 30 24.1	2479
Shiraz, Iran	9008	29 38 13.4	52 31 10.7	1555
Curacao, Antilles	9009	12 5 24.8	291 9 44.2	-30
Jupiter, Florida	9010	27 1 14.1	279 53 13.1	-29
Villa Dolores, Argentina	9011	-31 56 35.4	294 53 36.6	629
Maui, Hawaii	9012	20 42 25.7	203 44 33.6	3028
Island Lagoon, Australia	9023	-31 23 27.0	136 52 43.3	135
Mt. Hopkins, Arizona	9021	31 41 2.9	249 7 13.4	2337
Dodairi, Japan	9025	36 0 19.9	139 11 31.2	879
Addis Ababa, Ethiopia	9028	8 44 51.5	38 57 33.2	1877
Comodoro Rivadavia, Argentina	9031	-45 53 13.0	292 23 9.5	188
Dionysos, Greece	9091	38 4 44.6	23 55 57.8	466

Figure 3

APPARENT TIMING ERRORS FOR ROSMAN PASSES OF RANGE DATA BASED UPON GEOS-II ORBITAL ARC APRIL 28 TO MAY 4, 1968

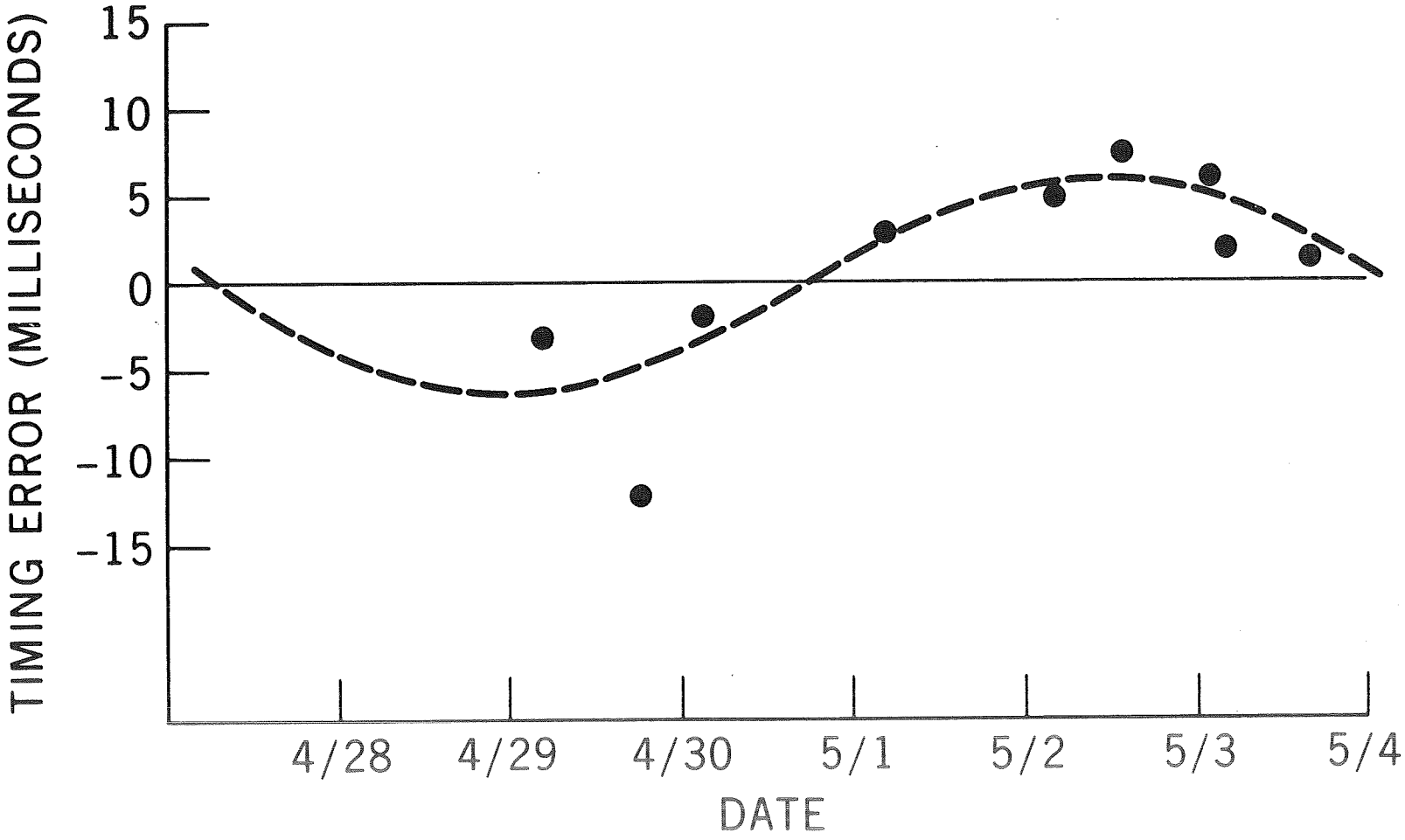

NASA-GSFC-T&DS
MISSION & TRAJECTORY ANALYSIS DIVISION
BRANCH 552 DATE 4/70
BY J.G.MARSH PLOT NO. 2117

the satellite alternately leads and lags in its orbit by up to 6 or more milliseconds. The 6+ day period of this oscillation is of course the same as the beat period of GEOS-II and is thus a result of inadequately modeled resonance. However, our choice of two day arcs effectively eliminated unmodeled resonance as a significant factor. We obtained good solutions through the use of many of these relatively short arcs.

SECTION 3.
RESULTS FOR OPTICAL STATIONS

Table 6 presents our C-6 center of mass positions for 23 STADAN and SPEOPT sites.

The errors in our coordinates were estimated by the method of error analysis outlined in the appendix. We considered errors in the gravity model, the SAO station positions, and error in GM. The error in the gravity model was taken to be the difference between the SAO 66 and SAO 69 gravity models through (8,8) plus 20% error chosen for the resonant terms. This error of resonant terms is about 2 times that indicated by Figure 3, but an error of this size proved to have little effect because of the short arcs (2 days) used. The error assumed for the low degree and order terms is also pessimistic, in that it implies that the SAO 1969 model is not improved over the SAO 1966 model for $(\ell,m) < (8,8)$.

The SAO station position error was taken to be 10 m in each coordinate which is probably pessimistic. It will be seen that an error of this magnitude has little effect on our estimates of station position. The gravity model error assumed through (8,8) was by far the most important.

Table 7 shows the relative contributions to error in latitude, longitude and height of the assumed gravity model error through (8,8) and the assumed 10 meter (each coordinate) SAO station position error. The contribution of SAO station error is nearly constant and only a few meters. The gravity model error effects are particularly large for the GEOS-II stations where inferior coverage was obtained.

TABLE 6

STADAN-SPEOPT STATION COORDINATES

Station Name	Number	Geodetic Latitude (deg min sec)	East Longitude (deg min sec)	Height Above Ellipsoid (meters)
Blossom Pt., Md.	1021	38° 25' 49".9	282° 54' 48".5	-49
Fort Myers, Fla.	1022	26° 32' 53".2	278° 8' 4".1	-45
Woomera, Aust.	1024	-31° 23' 26".2	136° 52' 14".9	123
Santiago, Chile	1028	-33 8' 59".0	289° 19' 53".7	711
Goldstone, Calif.	1030	35° 19' 47".9	243° 5' 58".8	876
Johannesburg, S. Africa	1031	-25° 53' 1".7	27° 42' 26".1	1535
St. Johns, Newfoundland	1032	47° 44' 29".3	307° 16' 46".1	48
E. Grand Forks, Minn.	1034	48° 1' 21".7	262° 59' 19".3	212
Winkfield, Eng.	1035	51° 26' 46".4	359° 18' 7".9	88
Rosman, N.C.	1037	35° 12' 7".4	277° 7' 41".4	852
Orroral, Aust.	1038	-35° 37' 33".0	148° 57' 14".7	946
Rosman, N.C.	1042	35° 12' 7".3	277° 7' 40".7	850
Tananarive	1043	-19° 0' 32".6	47° 17' 59".3	1360
E. Grand Forks, Minn.	7034	48° 1' 21".6	262° 59' 19".4	191
Edinburg, Texas	7036	26° 22' 46".5	261° 40' 7".1	5
Columbia, Mo.	7037	38° 53' 36".3	267° 47' 40".8	213
Bermuda	7039	32° 21' 50".0	295° 20' 35".3	-28
San Juan, P.R.	7040	18° 15' 28".6	294° 0' 23".5	-21
Greenbelt, Md.	7043	39° 1' 15".8	283° 10' 18".7	-26
Denver, Col.	7045	39° 38' 48".1	255° 23' 38".3	1746
Jupiter, Florida	7072	27° 01' 14".3	279° 53' 12".7	-39
Sudbury, Canada	7075	46° 27' 21".6	279° 3' 10".3	222
Kingston, Jamaica	7076	18° 4' 34".5	283° 11' 27".0	403

TABLE 7

EFFECTS OF ASSUMED SAO STATION POSITION AND GRAVITY MODEL ERROR ON STATION COORDINATES

Station Name	Number	Latitude (meters)		Longitude (meters)		Height (meters)	
		Gravity	Stations	Gravity	Stations	Gravity	Stations
Blossom Point, Md.	1021	6	1	7	1	3	1
Ft. Myers, Fla.	1022	10	2	3	3	8	1
Woomera, Aust.	1024	2	2	1	2	6	1
Santiago, Chile	1028	8	2	8	1	8	1
Goldstone, Calif.	1030	1	2	7	2	5	1
Johannesburg, S. Afr.	1031	8	1	8	1	2	1
St. Johns, Newfoundland	1032	19	1	4	1	8	1
E. Grand Forks, Minn.	1034	2	2	3	1	4	1
Winkfield, U.K.	1035	12	1	15	1	3	1
Rosman, N.C.	1037	13	2	8	2	11	1
Orroral, Aust.	1038	29	5	7	1	3	1
Rosman, N.C.	1042	7	2	6	1	8	1
Tananarive, Madagascar	1043	13	1	9	1	12	1
East Grand Fork, Minn.	7034	1	1	3	1	7	1
Edinburg, Texas	7036	6	2	6	2	9	1
Columbia, Mo.	7037	7	1	2	2	9	1
Bermuda	7039	16	2	5	2	4	1
San Juan, P.R.	7040	16	2	11	2	5	1
Greenbelt, Md.	7043	8	1	14	1	4	1
Denver, Colo.	7045	1	2	9	2	7	1
Jupiter, Fla.	7072	2	1	1	1	3	1
Sudbury, Ontario	7075	2	1	5	2	7	1
Kingston, Jamaica	7076	14	2	7	1	8	1

Table 8 compares our results for some MOTS stations with those obtained by Lambeck (1969) by a different (geometrical) method. The agreement in latitude and longitude is very satisfying, and suggests that our estimate of gravity model error was indeed pessimistic. The systematically much larger difference in height was not expected from gravity model error, and hence requires further investigation.

TABLE 8

DIFFERENCES BETWEEN SAO AND GODDARD STATION COORDINATES ON THE SAO C-6 STANDARD EARTH

STATIONS		LATITUDE Secs of Arc (Meters)		LONGITUDE Secs of Arc (Meters)		Ht. Meters
EDINBURG, TEXAS	(7036)	0.11	(3)	0.02	(0)	-17
COLUMBIA, MO.	(7037)	0.25	(7)	0.05	(1)	-14
BERMUDA	(7039)	0.24	(7)	-0.22	(-6)	-16
SAN JUAN, P.R.	(7040)	0.21	(6)	-0.04	(-1)	-11
DENVER, COLO.	(7045)	0.02	(1)	-0.02	(-1)	-20
SUDBURY, ONTARIO	(7075)	0.20	(6)	-0.32	(-7)	- 2
KINGSTON, JAMAICA	(7076)	0.43	(13)	-0.02	(0)	-27
E. GRAND FORKS, MINN.	(1034)	0.37	(11)	-0.16	(-3)	- 5
ROSMAN, N.C.	(1042)	0.04	(-1)	-0.05	(1)	- 5
GODDARD	(7050)	0.30	(9)	0.10	(3)	-14
AVERAGE		6 Meters		1 Meter		-13 Meters

NASA-GSFC-T&DS
MISSION & TRAJECTORY ANALYSIS DIVISION
BRANCH 552 DATE 5/70
BY J. G. MARSH PLOT NO. 2029

SECTION 4.
LASER STATION ESTIMATION

The ultimate goal of our work is to obtain solutions from combined laser, optical, and electronic data. The combined solutions should be much stronger, and many more control points for datum orientations will be obtained.

As an initial attempt to obtain combined solutions, we have obtained positions for the Goddard Space Flight Center and Wallops Island laser tracking sites from combined optical and laser data. Five two day arcs were used for the Wallops site and seven two day arcs were used for Goddard Space Flight Center. The C6 positions derived are given in table 9 , below.

Station	Geodetic Latitude	E. Longitude	Height (meters) Above Ellipsoid
Goddard (7050)	39°01'14".5	283°10'18".3	-9
Goddard (SAO det.) (7050)	39°01'14".2	283°10'18".2	+5.
Wallops Island (7052)	37°51'35".9	284°29'24".1	-65

TABLE 9
LASER SITE LOCATIONS

The solution for the Wallops laser site contained about 2,000 optical observations and 800 laser ranges. The a priori standard deviation assumed was two seconds for optical data and 3m for range data. The rms fit for the right ascension and declination measurements in the converged solution was 1.9 seconds of arc. The rms of fit for range measurements was 2.7 m. Similar results were obtained for the Goddard laser solution. This latter solution contained 1,800 optical observations and 1250 laser observations. In both cases, only about 1/5 of the available laser data in each pass was used.

Table 9 also shows the SAO[1] result for the Goddard laser site. As before, the most serious discrepancy is in height, and our height is again lower. A check of the shifts for conversion of North American Datum coordinates to center of mass coordinates shows that both SAO and Goddard have inconsistancies between laser and optical solutions for heights approaching 10 m, in addition to the previously noted difference in height obtained for the same optical stations.

SECTION 5.
CONCLUSIONS

We conclude that the use of multiple short (2 day) orbit arcs is a valid means of determining accurate station positions. Gravity model error effects, particularly resonance, are minimized by the use of short arcs. Also, the solution is less complex because periods where observations are sparse or absent are excluded. The strength of the solution lies in the use of multiple arcs with passes on all sides of the station.

Comparison of SAO optical and laser results, and our optical and laser results shows systematic differences in station height, but very close agreement in latitude and longitude. Thus, our latitude and longitude uncertainties estimated from gravity model error are pessimistic, being larger than indicated by the agreement between ourselves and SAO. The existence of the large systematic difference in height between Goddard and SAO optical solutions, indicates that further analysis is required. The need for combined solutions consisting of both angle and scale data is also underscored.

SECTION 6
THE GODDARD 1970 DIRECTORY OF TRACKING STATION COORDINATES

There is a great need for a unified set of station coordinates for the complete spectrum of tracking instruments. To this end, we have used our positions and the SAO Baker-Nunn positions as control points to obtain shifts from local to center of mass coordinates (SAO C-6) for more than 100 sites including Minitrack, C-Band, Unified S-Band, Laser, and many others. This directory, to be published by NASA in the summer of 1970, will in most cases provide positions accurate to 20 m or better. These coordinates will provide a highly accurate means for many orbit analyses and will serve as an accurate starting point for future investigations.

APPENDIX

ERROR ANALYSIS

The ORAN (Orbital Analysis) computer program used for this study was designed for computing the effects of random and systematic errors on minimum variance orbit determinations. Systematic errors can be in the form of either adjusted or unadjusted parameters, with the effects of the latter broken down into effects of the individual error sources. The program computes the effects of the unadjusted parameters on both the recovered parameters and the orbit, with the orbital effects propagated from epoch to any desired prediction time.

The program is configured for multiple arcs, with some error model parameters such as station positions constrained to be common to all arcs, and other parameters, such as measurement biases, which differ from arc to arc.

Force model errors can arise from uncertainties in geopotential coefficients through degree and order 20. Uncertainties in up to 44 individual coefficients can be carried, and any of these may be either adjusted or their unadjusted effects propagated. Alternately, or in addition, the force model error can be carried as the differences between complete gravity models in which case the restriction to 44 parameters does not apply. The SAO, APL, and NWL models are built into the program and the differences between any two of these three, or any complete model supplied as input, are available as force model errors. Note that the gravity model difference is treated as a single parameter, and 43 geopotential parameters may also be considered as adjustable. Of course, adjusting a geopotential coefficient removes it from the model difference set.

Mathematically, the unmodeled error propagation is based on the following observations. The minimum variance orbit determination uses the basic equation

$$\delta 0 \quad A\delta a + e \tag{1}$$

to relate discrepancies ($\delta 0$) between measured and calculated observations to discrepancies (δa) between true and a priori estimates of the set of parameters to be recovered. The set δa includes the six orbital elements but may also include other parameters. The matrix A is the set of partial derivatives of the measurements with respect to the adjustable parameters, and e is a vector of measurement "noise." When the least squares criterion is used to solve (1) for

the best estimate of a, the result is

$$\delta\hat{a} = (A^TWA)^{-1}A^TW\delta O, \tag{2}$$

where W is the matrix of measurement weights. For the solution to be minimum variance, the weight matrix must be chosen such that

$$W^{-1} = E(ee^t). \tag{3}$$

That is, W must be the inverse of the variance covariance matrix of measurement noise. In the normal data reduction programs, W is generally so chosen because it actually is measurement random error, in which case W is rather accurately expressed as a diagonal matrix.

For various reasons, the set of parameters adjusted in data reduction programs is only a subset of those parameters having some error. For example, our knowledge of geopotential coefficients is by no means complete. Yet a truncated model is always (of necessity) used, and the error in all coefficients used is ignored in all variance computations. Because the net effect is that e is not random yet contains definite systematic components, we can obtain a more accurate representation of the measurement discrepancy vector by expressing e as

$$e = K\gamma + \epsilon, \tag{4}$$

where γ is a set of errors in parameters previously ignored, K is the matrix of partial derivatives of the measurements with respect to these parameters, and ϵ is the vector of measurement random noise upon which W is still based. Substitution of (4) into (1) gives

$$\delta O = A\delta a + K\gamma + \epsilon. \tag{5}$$

If the weight matrix for the measurements is based on ϵ and is the same as that used in the data reduction program, it follows that the solution for $\delta\hat{a}$ actually being obtained is not that given by (2), but actually is a "biased" solution given by

$$\delta\hat{a} \quad (A^TWA)^{-1}A^TW(\delta O - K\gamma). \tag{6}$$

From this relation, we may obtain by differentiation the effects of "unit" values of the set of γ parameters,

$$\frac{\partial \delta\hat{a}}{\partial \gamma} \quad - (A^TWA)^{-1}A^TWK. \tag{7}$$

It follows that if the matrix K can be obtained, the effects of unit values of the γ parameters are obtained by substituting K for the δO vector used in the data reduction program. A priori estimates of errors in the γ parameters lead to an estimate of the magnitudes of the effects on recovered parameters, and the trajectory, of each γ parameter.

Uncertainties in the γ's are generally uncorrelated. If their correlations are known or can otherwise be accounted for, an estimate of the total or overall accuracy of the orbital solution is readily obtainable. For this study, errors in station locations, GM, and the geopotential were considered.

ACKNOWLEDGEMENTS

We wish to acknowledge the important contributions to this work of P. Ruttkay and S. Klosko.

REFERENCES

1. Douglas, B.C., Marsh, J.G., "GEOS-II and 13th Order Terms of the Geopotential," Celestial Mechanics, Volume 1, 1970, pp. 479-490.

2. Gaposchkin, E.M. and Lambeck, K., "New Geodetic Parameters for a Standard Earth," presented at the Fall Meeting of the American Geophysical Union, San Francisco, California, December 1969.

3. Koyai, G., "Revised Values for Coefficients of Zonal Spherical Harmonics in the Geopotential," Smithsonian Astrophysical Observatory Special Report No. 295, 1969.

4. Marsh, J.G., Douglas, B.C., and Dutcher, M., "Tests and Comparisons of Gravity Models Using Camera Observations of GEOS I and II," NASA Document No. X-552-70-48, February 1970.

NAD Survey Adjustments From Short Arcs Using GEOS I Observations

by

F. M. Loveless, Jr. and J. J. Lynn
DBA Systems, Inc.

and

John H. Berbert
NASA/Goddard Space Flight Center

Presented at the

GEOS II Review Conference
Goddard Space Flight Center

June 22-24, 1970

NAD Survey Adjustments From Short Arcs Using GEOS I Observations

by

F. M. Loveless, Jr. and J. J. Lynn
DBA Systems, Inc.

and

John H. Berbert
NASA/Goddard Space Flight Center

In way of introduction, a brief history of the NAD Survey Adjustments from Optical Short Arcs performed by DBA Systems for Goddard Space Flight Center (GSFC) since early 1968 will be given.

The original work was done by Duane Brown in 1968 (Reference 1) and he presented the results of a 17 Station Network of MOTS and PC-1000 Cameras participating on 38 short arcs. In this report, he stressed the importance of short arc technique of recovering station coordinates without constraining baselines to enforce scale; scale being derived dynamically with the proper choice of well distributed short arcs, a good value of the gravitational parameter μ, and the position of the origin station known.

In furtherance of this study, work was performed by J. J. Lynn (Reference 2) to investigate the practical value of deriving scale by orbital dynamics. He used the same 38 short arcs as Brown had previously, but restricted the tracking network to 13 MOTS sites. The PC-1000 stations were deleted due to a suspected error in the data preprocessing. The purpose of the study was to determine the effects of (1) errors in gravity parameter, μ, and (2) errors in the assumed position of the fixed station, on the precise determination of the positions of the 13 MOTS stations on or near the North American Continent. This was accomplished by making several reductions with varying values of μ, and by perturbing the Cartesian Coordinates of the origin station by 50 meters in each component, one at a time.

As a by-product of Lynn's study, it was hoped that the survey recoveries would be sufficiently improved to provide the best possible Optical Reference Orbits for use in the Systems Intercomparison Study. To this end, the study will continue with plans to increase the data set by adding peripheral MOTS stations, SAO stations, and Air Force PC-1000 sites.

The most recent results were obtained in April 1970. This was a repeat of the survey recovery on the NAD that Lynn had reported earlier. The fact that about 10 percent of the MOTS GEOS I observations that were placed in the National Space Sciences Data Center (NSSDC), had to be reprocessed prompted this rerunning. The error in the MOTS data was reported in January 1969 by D. W. Harris, (Reference 3). This error occurred in the reduction procedure when the camera was pointed at or near the stations local meridian and affected about 350 plates. The reduction program at New Mexico State University (NMSU) was corrected and the plates were reprocessed and submitted to NSSDC in mid-1969. The corrected data was not available from the NSSDC until mid-October 1969, however, due to timing differences in the two data sets which necessitated some program changes.

As a matter of curiosity, a comparison was made between the data that was in error and the data that was used in the 38 Short Arcs. The data had undergone several levels of editing over the years and it was assumed that most of the bad data had been deleted. It was discovered, however, that of the 311 plates used in the 38 short arcs, 28 were listed as being in error. This represented almost 10 percent of the data and it was decided to rerun the survey recovery with the corrected data.

The new NAD survey corrections, Table 2, were evaluated on the basis of the deviations of the corrections from those of the earlier recovery, given in Table 1. These earlier results are presented graphically in Figures 1 and 1A. The differences in the two recoveries are given in Table 3. These differences are represented graphically in Figures 3, 3A, 4, and 4A. The dot represents the earlier corrected surveys and the triangle represents the latest survey corrections, the latter using the corrected MOTS data. The general trend in the new recovery was a movement toward the origin station (Columbia). From the earlier recovery, a change in scale (increase of 3.9 parts per

million)was obtained. The new results would indicate a decrease in this value to 1.9 parts per million. The 1.9 parts per million increase over the initial NAD scale could be accounted for by two dynamic effects. One is the error in the gravitational parameter, μ, and the other is the uncertainty of the origin station with respect to the center of mass of the earth.

Short arc dynamic scaling is dependent on the error, $\Delta\mu$, in the gravitational parameter, μ, and in the uncertainty of the station designated as origin with respect to the center of mass of the earth. Kaula (1965) has shown that the proportional error in scale, $\Delta s/s$, due to error $\Delta\mu$ in the gravitational parameter μ is given by

$$\frac{\Delta s}{s} = \frac{1}{3}\frac{\Delta\mu}{\mu} \quad .$$

In the report published by Lynn (Reference 2), he reported that the change in scale of -2.2 parts per million from a solution that used a value for μ of 3.986013×10^{14} m^3/sec^2 to one that used a μ value of 3.986032×10^{14} m^3/sec^2. The reductions were identical except for the μ values used, a difference ($\Delta\mu$) of -4.75 parts per million. According to Kaula's formula, this would translate to a proportional scale error of -1.58 parts per million, leaving only -.6 parts per million unaccounted for.

In earlier reductions, pronounced proportional scale changes have also been seen when the height of the origin station was perturbed. In all of these cases, the origin station was essentially at the center of short arc passes. A perturbation of 50 meters in Columbia's Y-component of position produced a 13 parts per million scale change. From what has been observed, a 20 meter error in the center of mass could result in a possible proportional scale error of 5 parts per million. This 20 meters is consistent with the uncertainty in the center of mass for some of the better earth models. In the tracking systems evaluation studies, a criteria of 5 meters uncertainty for the tracking station positions has been set. The 20 meter uncertainty in the center of mass would restrict us to a network within a million meters of the origin which would rule out the North American peripheral sites. If the uncertainty in the center of mass of the earth is reduced to 10 meters (one of the goals of the National Geodetic Satellite Program), then the proportional scaling error would be down to 2.5 parts per

million, allowing short arc survey recovery to a 5 meter accuracy for a network extending 2 million meters from the origin.

Of particular interest in the survey recoveries was the 29 meter eastward adjustment of the Bermuda site. The same trend has also been noted by other investigators.

In conclusion, we found that the use of the corrected MOTS data did affect the overall solution as shown in Table 4, and reduced the scale by one-half. Of the differences in the two sets of results, 75 percent of the station adjustments were still within the 6 meters estimated uncertainty of the positions.

Table 1

Earlier Results

Stations	Inital Survey NAD-27			Corrections to Given NAD-27 Survey			Standard Deviation			Corrections Referred to Mean Corrections		
	φ (geodetic)	λ	h(meters) (geodetic)	ΔE	ΔN (meters)	ΔV	ΔE	ΔN (meters)	ΔV	$\Delta E-\Delta\bar{E}$	$\Delta N-\Delta\bar{N}$ (meters)	$\Delta V-\Delta\bar{V}$
GSFMA	39°01'15.010"	-283°10'19.930"	54.5	1.8	17.7	-4.3	3.6	2.3	3.3	-2.4	10.8	-1.2
BPOMA	38°25'49.630"	-282°54'48.230"	5.5	6.2	-4.6	7.0	4.9	4.0	5.4	2.0	-11.5	10.2
JU4MA	27°01'13.170"	-279°53'12.490"	25.7	5.1	1.7	-11.3	3.3	3.5	3.3	.9	-5.2	-8.2
FTMMA	26°32'51.890"	-278°08'03.930"	19.6	6.2	8.0	-2.9	2.7	3.1	2.6	2.1	1.1	.3
BERMA	32°21'48.830"	-295°20'32.560"	21.0	33.0	10.1	-.4	5.7	3.5	4.1	28.8	3.2	2.7
*COLMA	38°53'36.070"	-267°47'42.120"	271.7	0	0	0	0	0	0	-4.2	-6.9	3.1
DENMA	39°38'48.030"	-255°23'41.190"	1796.1	-2.4	7.6	1.4	3.3	2.0	2.8	-6.5	.7	4.5
EDIMA	26°22'45.440"	-261°40'09.030"	67.1	-2.9	4.6	6.5	2.6	3.4	3.0	-7.0	-2.3	9.6
GFOMA	48°01'21.400"	-262°59'21.560"	253.9	-4.6	15.5	.5	2.3	2.7	2.5	-8.8	8.6	3.6
JAMMA	18°04'31.980"	-283°11'26.528"	485.9	12.0	12.9	-16.4	3.9	5.1	4.1	7.8	6.0	-13.3
MOJMA	35°19'48.090"	-243°06'02.730"	905.4	-10.9	3.0	7.9	5.6	2.5	3.4	-15.0	-3.9	11.0
PURMA	18°15'26.220"	-294°00'22.170"	58.7	5.1	8.2	-21.0	4.8	4.9	4.7	.9	1.4	-17.9
ROSMA	35°12'06.930"	-277°07'41.010"	914.0	5.4	4.6	-7.6	3.0	2.3	3.2	1.3	-2.3	-4.5
	MEAN			4.2	6.9	-3.1	3.5	3.0	3.3	0.0	0.0	0.0

*Adopted Origin of Survey

Short Arc Optical Survey
The GEOS North American Network
(MOTS, GEOS I Observations)

● Initial NAD Position
▲ Adjusted Position

East-North Corrections
(Mean Corrections Removed)

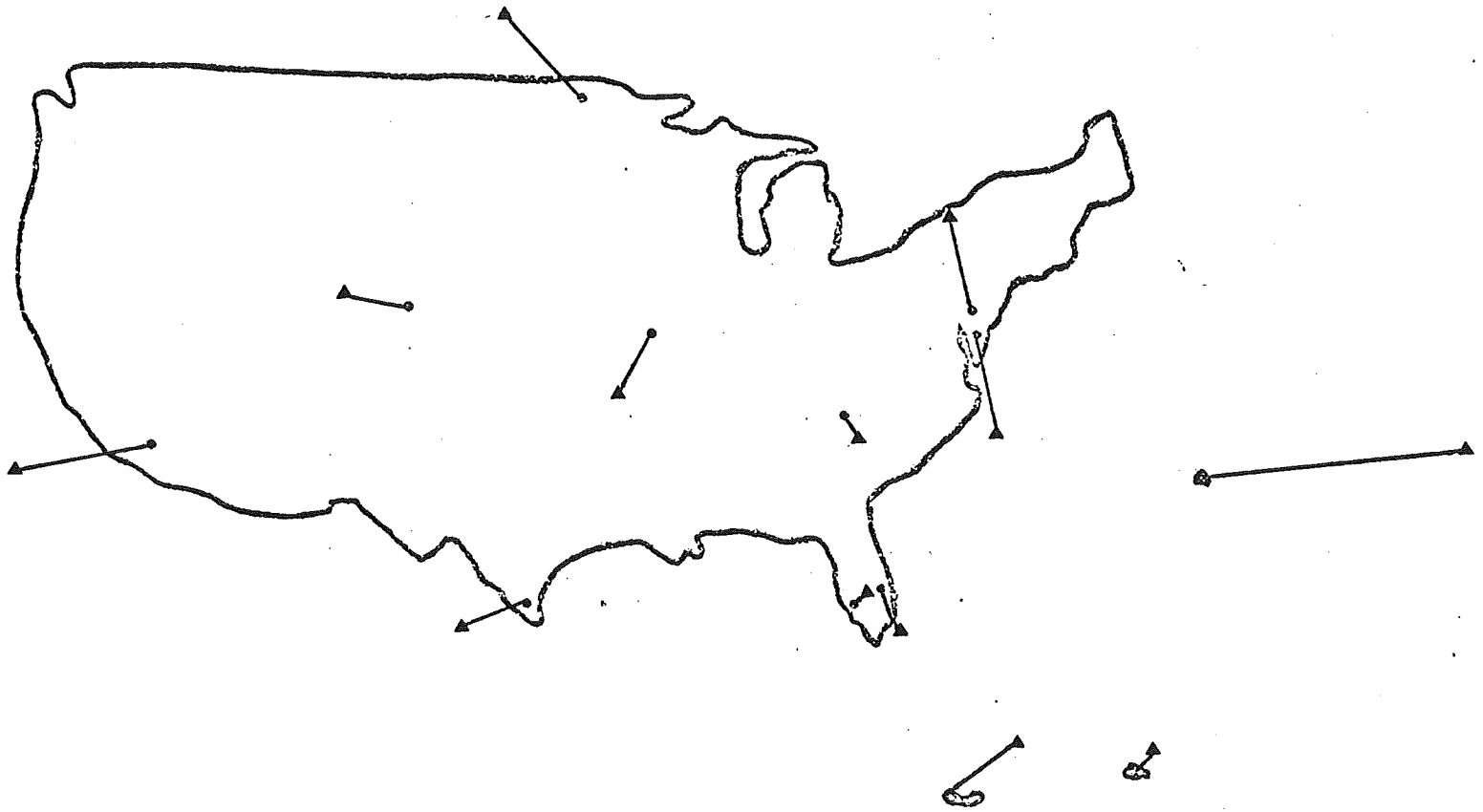

Vector Scale

1 inch = 20 meters

Figure 1

Short Arc Optical Survey
The GEOS North American Network
(MOTS, GEOS I Observations)

● Initial NAD Position
▲ Adjusted Position

East-Vertical Corrections
(Mean Corrections Removed)

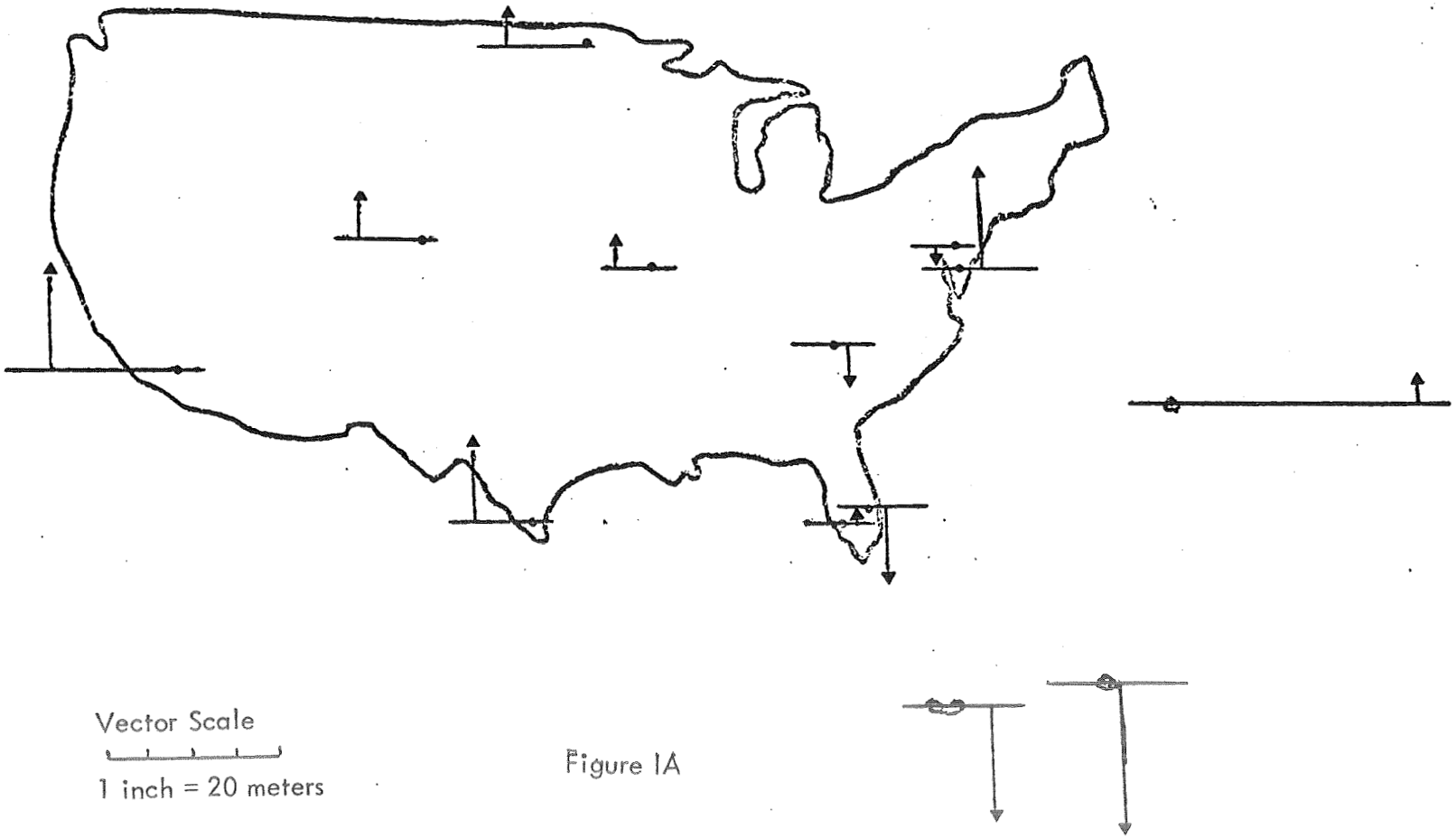

Vector Scale

1 inch = 20 meters

Figure 1A

Table 2

Corrected Data, Edited
(meters)

	Corrections			Standard Deviations			Corrections with Mean Removed		
	ΔE	ΔN	ΔV	ΔE	ΔN	ΔV	$\Delta E-\overline{\Delta E}$	$\Delta N-\overline{\Delta N}$	$\Delta V-\overline{\Delta V}$
GSFMA	-5.7	13.3	-.1	3.9	2.5	3.6	-8.1	7.0	3.5
BPOMA	6.4	-7.2	12.8	5.2	4.5	5.9	3.9	-13.5	16.4
JU4MA	1.7	3.4	-9.3	3.7	3.8	3.6	-.7	-3.0	-5.7
FTMMA	2.2	8.3	-7.6	3.0	3.4	2.8	-.2	2.0	-4.0
BERMA	31.0	2.6	.7	6.2	3.8	4.3	28.6	-3.7	4.3
COLMA	0	0	0	0	0	0	-2.4	-6.3	3.6
DENMA	-2.7	4.6	4.2	3.9	2.4	3.2	-5.1	-1.7	7.8
EDIMA	-3.5	8.1	2.4	3.0	3.8	3.2	-5.9	1.8	6.0
GFOMA	-2.5	11.2	2.2	2.5	3.0	2.8	-4.9	4.9	5.8
JAMMA	8.2	16.5	-26.6	4.2	5.4	4.3	5.8	10.2	-23.0
MOJMA	-7.5	4.4	7.4	6.2	2.8	3.7	-9.9	-1.9	11.0
PURMA	-1.2	11.8	-28.1	5.2	5.3	5.0	-3.6	5.5	-24.5
ROSMA	5.1	4.9	-4.8	3.2	2.4	3.5	2.6	-1.4	-1.2
Mean	2.4	6.3	-3.6	3.9	3.3	3.5	0.0	0.0	0.0

Table 3

East, North and Up Corrections After Reprocessing

Minus Corrections Before Reprocessing

(Table 2 Results Minus Table 1 Results)
(meters)

	$\Delta E_{New} - \Delta E_{Old}$	$\Delta N_{New} - \Delta N_{Old}$	$\Delta V_{New} - \Delta V_{Old}$
GSFMA	-7.5	-4.4	4.3
BPOMA	.2	-2.6	5.8
JU4MA	-3.3	1.7	2.1
FTMMA	-4.0	.3	-4.7
BERMA	-2.0	-7.5	1.1
COLMA	0.0	0.0	0.0
DENMA	- .3	-3.0	2.9
EDIMA	- .6	3.5	-4.1
GFOMA	2.1	-4.3	1.7
JAMMA	-3.8	3.6	-10.1
MOJMA	3.4	1.4	- .5
PURMA	-6.3	3.6	-7.1
ROSMA	- .4	.4	2.8
Mean	-1.7	- .6	- .5

Table 4

East, North and Up Corrections (With Means Removed)

After Reprocessing Minus Corrections Before Reprocessing

(Table 2 Results Minus Table 1 Results)
(meters)

	$\Delta(\Delta E-\Delta\bar{E})$	$\Delta(\Delta N-\Delta\bar{N})$	$\Delta(\Delta V-\Delta\bar{V})$
GSFMA	-5.7	-3.8	4.7
BPOMA	1.9	-2.0	6.3
JU4MA	-1.6	2.2	2.5
FTMMA	-2.3	.9	-4.3
BERMA	- .3	-6.9	1.6
COLMA	1.7	.6	.5
DENMA	1.4	-2.4	3.3
EDIMA	1.1	4.1	-3.6
GFOMA	3.7	-3.7	2.2
JAMMA	-2.0	4.2	-9.7
MOJMA	5.1	2.0	- .0
PURMA	-4.5	4.1	-6.6
ROSMA	1.3	.9	3.3
Mean	0.0	0.0	0.0

Corrected Positions Before and After
MOTS Data Reprocessing

East-North Differences

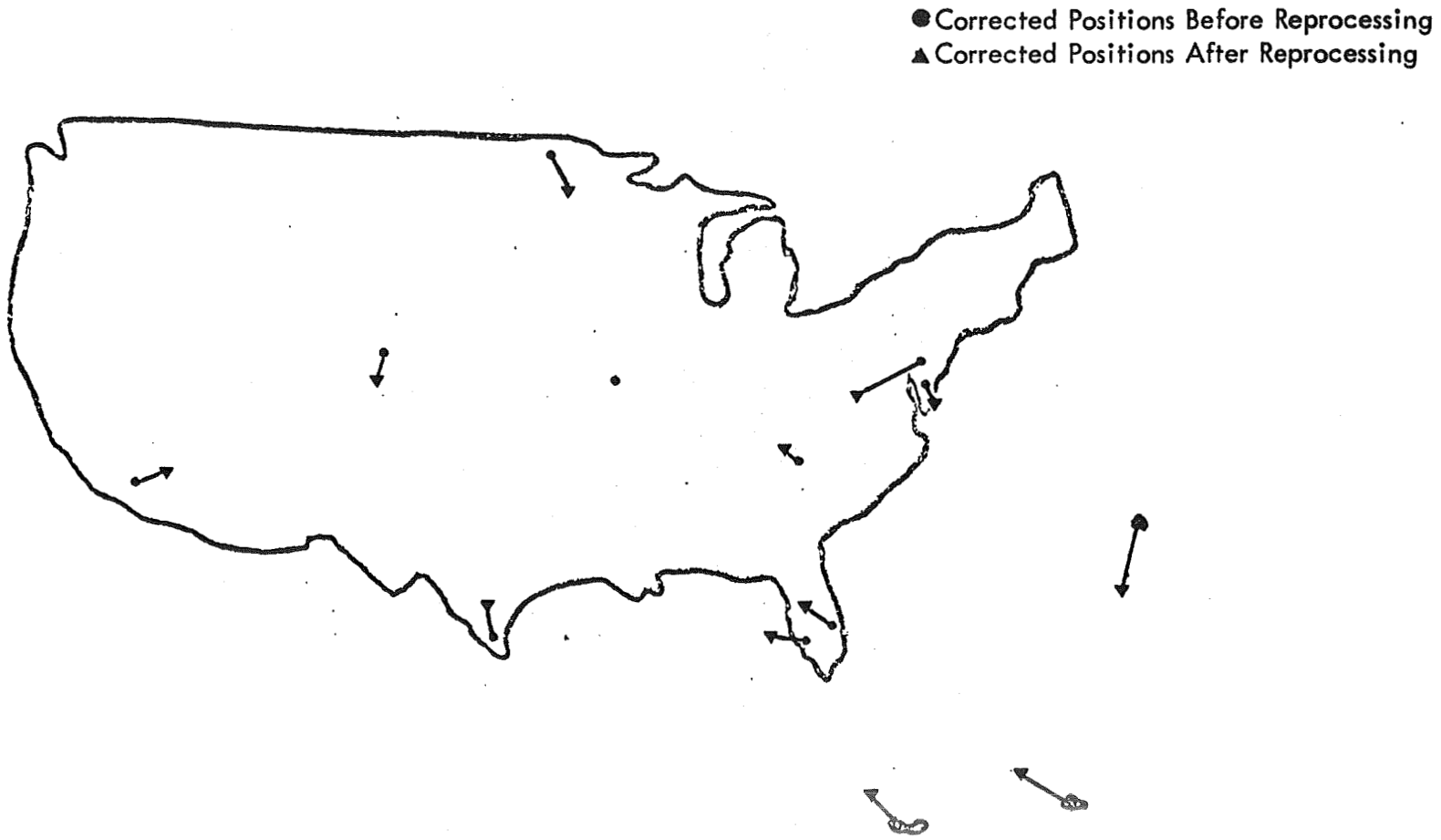

Vector Scale

1 inch = 20 meters

Figure 2

Corrected Positions Before and After
MOTS Data Reprocessing

East-Vertical Differences

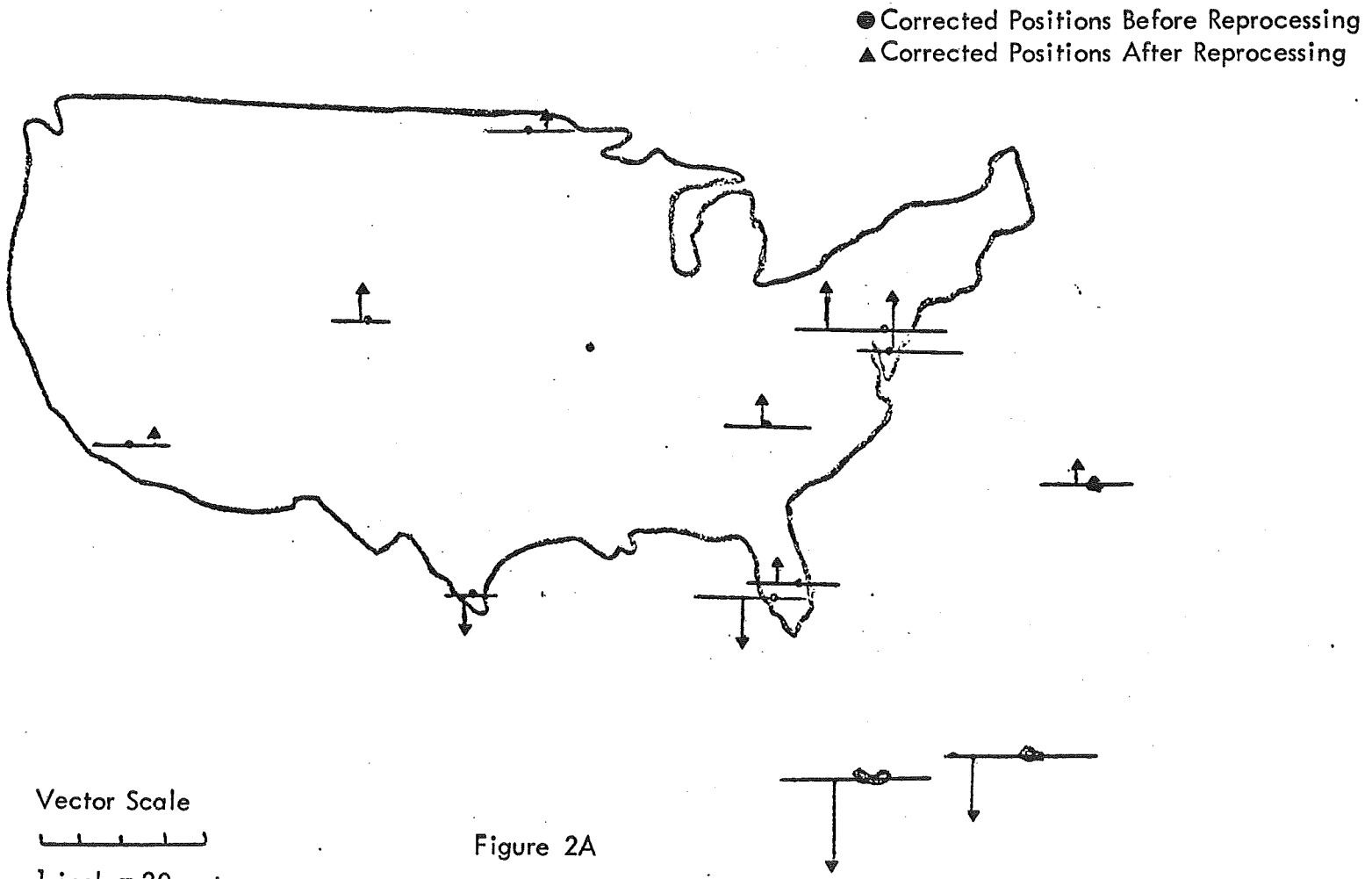

Figure 2A

Corrected Positions Before and After
MOTS Data Reprocessing

East-North Differences
(Mean Corrections Removed)

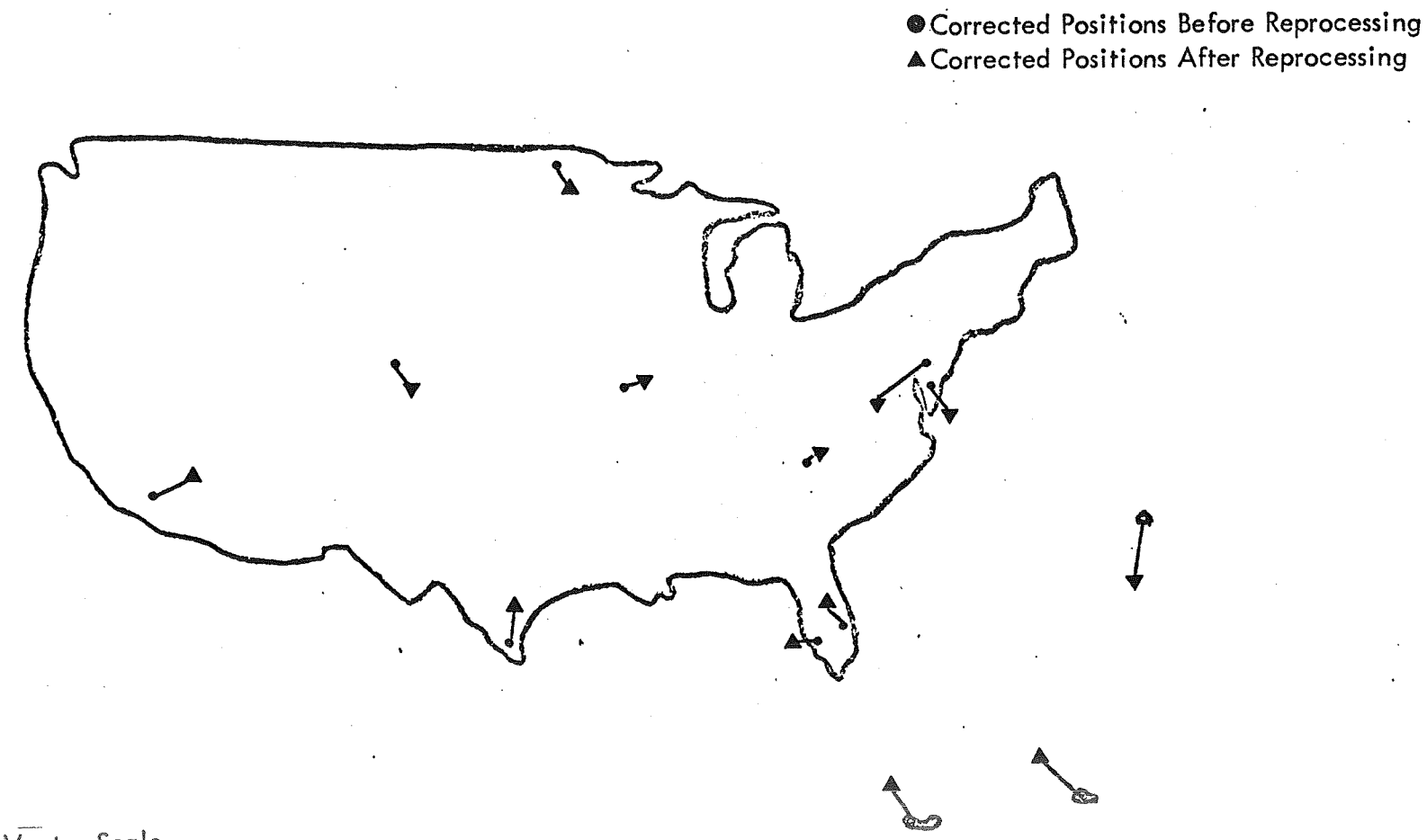

Figure 3

Corrected Positions Before and After
MOTS Data Reprocessing

East-Vertical Differences
(Mean Corrections Removed)

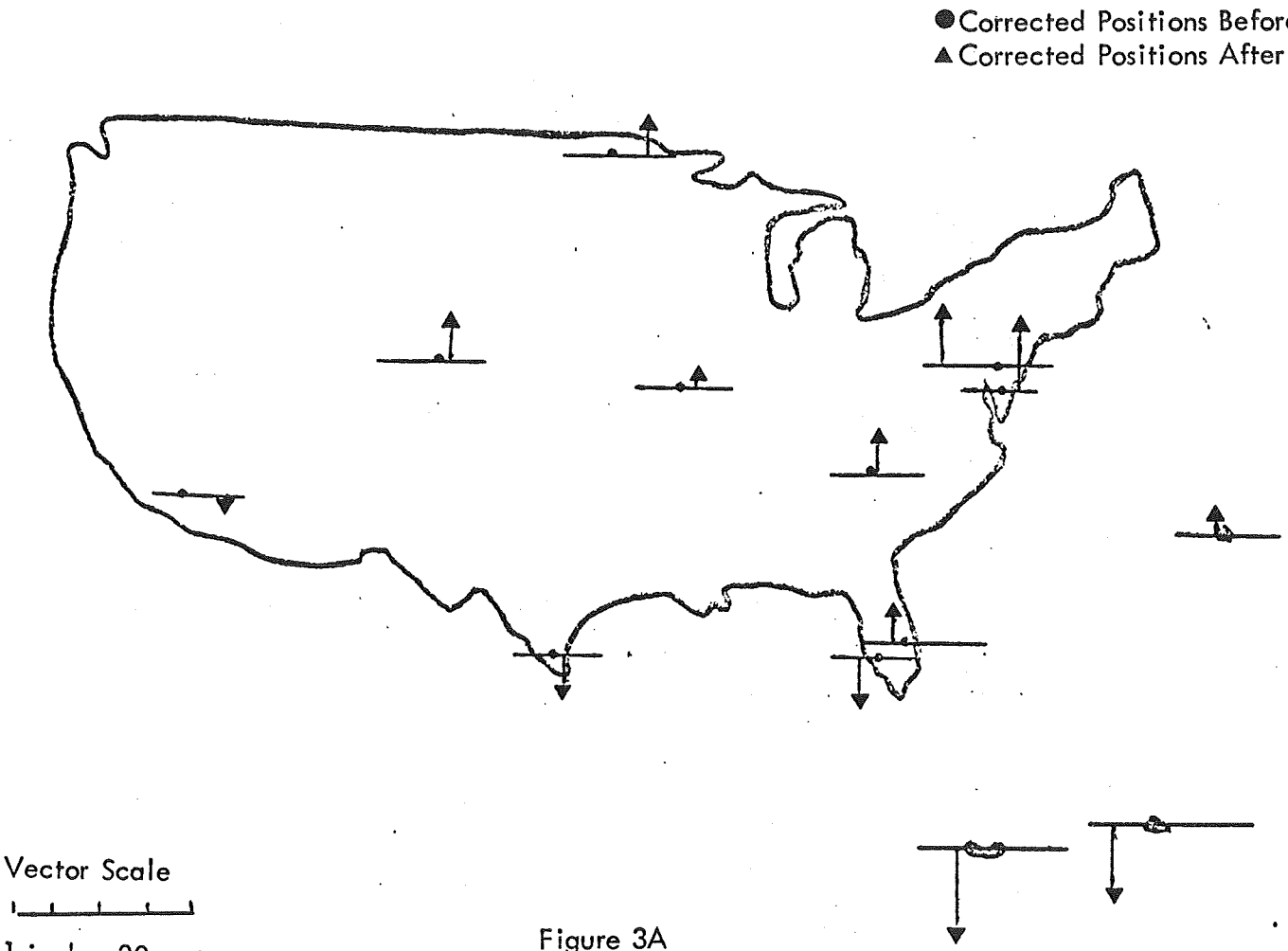

Figure 3A

REFERENCES

[1] Brown, D. and J. H. Berbert, November 1968. Short Arc Optical Survey of the North American Tracking Network. NASA X-550-68-439. Also presented to Fall meeting of AGU, December 1968.

[2] Lynn, J. J., 1969. Short Arc Optical Survey of the North American Optical Tracking Network. Presented at the "Symposium on Astrodynamics and Related Planetary Sciences", April 1969, and at the "Twelfth Plenary Meeting, Committee on Space Research", May 1969, Prague, Czechoslovakia.

[3] Harris, D. W., January 1969. NASA-GSFC GEOS I MOTS Optical Validation Report. NASA X-514-69-83.

AFCRL-70-0090
FEBRUARY 1970
ENVIRONMENTAL RESEARCH PAPERS, NO. 315

TERRESTRIAL SCIENCES LABORATORY PROJECT 7600
AIR FORCE CAMBRIDGE RESEARCH LABORATORIES
L. G. HANSCOM FIELD, BEDFORD, MASSACHUSETTS

Improvement of the GEOS-1 North American Tracking Network From Multiple Short Arc Geodetic Adjustments

GEORGE HADGIGEORGE

OFFICE OF AEROSPACE RESEARCH
United States Air Force

Abstract

Combinations of 171 passes were employed in a short arc geodetic adjustment to improve the survey coordinates of 29 observing stations. The recovery of the station positions and their standard errors along with other geodetic parameters are presented. The results of this adjustment show a mean standard error of approximately 3.5 meters, and corrections to NAD survey coordinates basically consistent with the observation network with the origin at Hunter AFB.

AFCRL-70-0090
FEBRUARY 1970
ENVIRONMENTAL RESEARCH PAPERS, NO. 315

IMPROVEMENT OF THE GEOS-1 NORTH AMERICAN TRACKING NETWORK FROM MULTIPLE SHORT ARC GEODETIC ADJUSTMENTS

by

George Hadgigeorge

Errata

Table 5 Page 22

Reads: $\sigma_{\Delta x}$ $\sigma_{\Delta y}$ $\sigma_{\Delta x}$

Should Read: $\sigma_{\Delta x}$ $\sigma_{\Delta y}$ $\sigma_{\Delta z}$

Table 6 Page 23

Reads: 7043 39° 01′ 51″.327
Should Read: 7043 39° 01′ 15″.327

Table 6 Page 23

Reads: 3648 x = 832334.77 y = -5349731.00
Should Read: 3648 x = 832594.33 y = -5349690.56

AIR FORCE CAMBRIDGE RESEARCH LABORATORIES
OFFICE OF AEROSPACE RESEARCH
L.G. HANSCOM FIELD
UNITED STATES AIR FORCE
BEDFORD, MASSACHUSETTS

Contents

Illustrations

Tables

Improvement of the GEOS-1 North American Tracking Network From Multiple Short Arc Geodetic Adjustments

1. INTRODUCTION

The development of the Short Arc Geodetic Adjustment (SAGA) program has provided satellite geodesy with another very accurate reduction tool. This program, we believe, is one of the most advanced reduction programs yet developed for precise geodetic positioning by means of satellite observations. It can handle any combination of directional or ranging observations. Specifically, these are:

(1) Optical (active, passive, and continuous trace): PC-1000, MOTS, BAKER-NUNN, BC-4.

(2) Electronic: Geodetic SECOR, GEOCEIVER, LASER, RADAR.

Each observation parameter may be subject to systematic errors governed by an error model having either unknown coefficients or statistically constrained coefficients. In the optical case the angular elements of external orientation α, ω, κ may be subjected to slight adjustments that are consistent with their actual accuracies. The orientation accuracy is typically 0.5" of arc in α, ω, and 2.0" in κ. The exercise of orientation error-model constraints is particularly important in chopping shutter observations. A conventional reduction of a large quantity of chopping shutter observations per plate, with the existence of systematic error in orientation, would lead to an unduly optimistic error propagation. In a chopping operation (as opposed to a flashing light), allowances should be made for

(Received for publication 7 January 1970)

uncertainties in inter-station timing synchronization. The inter-station timing bias simulates the case of non-synchronization between stations observing a common satellite pass. The electronic error model accommodates biases in zero set, timing, frequency (satellite oscillator), frequency (ground oscillator), frequency drift and refraction. SAGA will accept as many as 4 observation intervals from the various systems. This allows observation drop-out with a new zero setting of ranges, and re-orientation of the optical system.

2. DUMMY CAMERA PROJECTION

Generally, plate coordinates and associated projective parameters are not available to the user. Hence one may resort to what may be termed the "dummy camera method" in order to construct, from the given angles, sets of plate coordinates that are approximately equivalent to those actually measured.

Optical observations are converted from right ascension and declination to plate coordinates (x, y). First convert right ascension and declination to azimuth (A_j) and elevation (E_j). Assume the middle observation (azimuth and elevation) to be the direction of the principal axis of the camera. The external orientation elements (α, ω, κ) become:

$$\alpha = A_m, \quad \omega = E_m \text{ and let } \kappa = 0 .$$

For the ith station and time t_j compute the local hour angle of the jth observation as follows. Let

$$t_s = t_G + 1.00273791\, t_j - \lambda - \alpha$$

where

t_G = Greenwich hour angle at t = 0 (apparent),

t_j = observing time (universal) in angular measurement from Greenwich (radians),

λ = longitude of station (West) and

α = right ascension of observation.

Then

$$\sin E = \sin\phi \sin\delta + \cos\phi \cos\delta \cos(t_s),$$

$$\cos E = (1 - \sin E)^{1/2},$$

$$\sin A = -\cos\phi \sin(t_s)/\cos E \text{ and}$$

$$\cos A = (\sin\delta - \sin\phi\sin E)/(\cos\phi\cos E) .$$

Then

$$A_j = \tan^{-1}(\sin A/\cos A) \text{ and}$$

$$E_j = \tan^{-1}(\sin E/\cos E) .$$

Use midpoint A_j, E_j to compute the local orientation matrix:

$$\begin{bmatrix} \hat{A} & \hat{B} & \hat{C} \\ \hat{A}' & \hat{B}' & \hat{C}' \\ \hat{D} & \hat{E} & \hat{F} \end{bmatrix}_j = \begin{bmatrix} -\cos\alpha & \sin\alpha & 0 \\ -\sin\alpha\sin\omega & -\cos\alpha\sin\omega & \cos\omega \\ \sin\alpha\cos\omega & \cos\alpha\cos\omega & \sin\omega \end{bmatrix}_j$$

Then

$$\begin{bmatrix} l \\ m \\ n \end{bmatrix}_j = \begin{bmatrix} \sin A\ \cos E \\ \cos A\ \cos E \\ \sin E \end{bmatrix}_j$$

and

$$\begin{bmatrix} u \\ v \\ w \end{bmatrix}_j = \begin{bmatrix} \hat{A} & \hat{B} & \hat{C} \\ \hat{A}' & \hat{B}' & \hat{C}' \\ \hat{D} & \hat{E} & \hat{F} \end{bmatrix} \begin{bmatrix} \ell \\ m \\ n \end{bmatrix}_j$$

The plate coordinates for the jth point are:

$$\hat{x} = cu_j/w_j$$

$$\hat{y} = cv_j/w_j .$$

Let $(\hat{x}_a\ \hat{y}_a)$, $(\hat{x}_b, \hat{y}_b)$ denote the coordinates of the first and last points on the trace. Let κ denote the angle between the line joining these two points and the $\hat{x}$ axis. Then compute.

$$\sin\kappa = -(\hat{y}_b - \hat{y}_a)/r_{ab}$$

$$\cos\kappa = (\hat{x}_b - \hat{x}_a)/r_{ab}$$

where

$$r_{ab} = \left[(\hat{x}_b - \hat{x}_a)^2 + (\hat{y}_b - \hat{y}_a)^2\right]^{1/2}$$

The new x, y coordinates are:

$$\begin{bmatrix} x \\ y \end{bmatrix}_j = \begin{bmatrix} -\cos\kappa & \sin\kappa \\ \sin\kappa & \cos\kappa \end{bmatrix} \begin{bmatrix} \hat{x} \\ \hat{y} \end{bmatrix}_j$$

The rotation of the local orientation into the master frame is accomplished by:

$$\begin{bmatrix} A & B & C \\ A' & B' & C' \\ D & E & F \end{bmatrix} = \begin{bmatrix} -\cos\kappa & \sin\kappa & 0 \\ \sin\kappa & \cos\kappa & 0 \\ 0 & 0 & 1 \end{bmatrix} \begin{bmatrix} \hat{A} & \hat{B} & \hat{C} \\ \hat{A}' & \hat{B}' & \hat{C}' \\ \hat{D} & \hat{E} & \hat{F} \end{bmatrix} \begin{bmatrix} 0 & 1 & 0 \\ -\sin\phi & 0 & \cos\phi \\ \cos\phi & 0 & \sin\phi \end{bmatrix} \begin{bmatrix} \cos\lambda & -\sin\lambda & 0 \\ \sin\lambda & \cos\lambda & 0 \\ 0 & 0 & 1 \end{bmatrix}$$

The coordinates x_j, y_j and the master orientation matrix serve as input to the main program.

For the short arc adjustment theory see AFCRL 69-0080.

3. RANGE ERROR MODEL

The error model adopted for ranging systems is of the form

$$\delta r = a_0 + a_1 \tau + a_2 \tau^2 + a_3 r + a_4 \dot{r} + a_5 \csc E$$

in which

r, $\dot{r}$ = range and range rate at time τ ($\tau = 0$ at epoch)

E = local elevation angle

a_0, a_1, a_2, a_3, a_4, a_5 = error coefficients accounting for systematic errors in zero set, frequency offset (between satellite and ground station oscillators), frequency drifts, frequency bias, interstation timing bias and residual tropospheric refraction.

The model was derived to apply specifically to Geoceiver observations, but is applicable to ranging systems in general when appropriate constraints are placed on the error coefficients.

4. OPTICAL ERROR MODEL

Systematic errors in optical observations are assumed to be governed by error models of the form:

$$\delta x = a_0 f_1 + a_2 f_2 + a_3 f_3 + a_4 f_4 + a_5 f_5$$
$$\delta y = a_0 f'_1 + a_2 f'_2 + a_3 f'_3 + a_4 f'_4 + a_5 f'_5$$

where

$$f_1 = -(c^2 + x^2)/c \qquad f'_1 = xy/c$$
$$f_2 = xy/c \qquad f'_2 = (c^2 + y^2)/c$$
$$f_3 = y \qquad f'_3 = -x$$
$$f_4 = x/c \qquad f'_4 = y/c$$
$$f_5 = \dot{x} \qquad f'_5 = \dot{y}$$

in which

x, y = plate coordinates of satellite image

$\dot{x}$, $\dot{y}$ = rate of change of plate coordinates

c = nominal focal length of camera.

The optical error coefficients a_0 through a_5 account for the combined effects of biases in the angular elements of orientation of the camera, the elements of interior orientation (coordinates of principal point and focal length), and interstation timing. They also account for any linear drift in the direction of the camera axis throughout the exposure.

5. DATA PREPROCESSING

Prior to the short arc geodetic reduction, all of the optical and electronic observations were run through a data preprocessor. The optical observations were corrected for polar motion, and all of the observational times given in UTC were corrected to UT1. For random-measurement residuals evaluation, all optical observations were fit to a general conic section equation of the form

$$a' x^2 + 2b' xy + c' y^2 + 2d' x + 2e' y + 1 = 0$$

where x and y are the plate coordinates.

By virtue of redefining the swing angle κ so that the x-axis coincides approximately with the trace of the satellite and by virtue of the approximately linearity of the trace, the above expression is dominated by the term in y. It is thus convenient to re-express the equation as

$$y = ax^2 + 2bxy + cy^2 + 2dx + e$$

in which $a = -a'/2e'$, $b = -b'/2e'$, etc. Since the approximate linearity of the trace assures that b and c will be very small, we may safely regard the error of measurement as being restricted to the y-coordinate on the left-hand side of the above equation. Accordingly, the least squares solution for the conic coefficients is given by

$$(abcde)^T = \left(\sum_{i=1}^{n} B_i^T B_i \right)^{-1} \left(\sum_{i=1}^{n} B_i^T y_i^o \right)$$

in which y_i^o denotes the measured value of the y coordinate of the ith point on the trace (i = 1, 2, e.....n) and

$$B_i = (x_i^2 \quad 2x_i y_i^o \quad y_i^{o2} \quad 2x_i \quad 1) .$$

and the observational residuals are determined from

$$V_i = y_i^o - (ax_i^2 + 2bx_i y_i^o + cy_i^{o2} + 2dx_i + e) .$$

The plots of the conic residuals along with the rms error for all of the optical observations used in this reduction are given in Appendix A. Plates with three observations or less are not included in Appendix A.

6. RESULTS OF THE SHORT ARC REDUCTION

To demonstrate the capabilities and flexibility of the Short Arc Geodetic Adjustment computer program we reduced a net consisting of optical and ranging observations. These involved the PC-1000, MOTS, SECOR and Laser. One-hundred and seventy-one (171) orbits were chosen that provided good geometry

with the 29 station network for accurate station position determination (Figure 1 and Table 1).

Prior to the reduction, observational times given in UTC were corrected to UT1, and corrections were applied to all right ascensions and declinations to account for polar motion.

The optical observations were assumed subject to orientation biases of 1 second of arc in α, ω, 2 seconds of arc in κ, and inter-station timing bias of 0.1 ms for all passes. The random error of the optical observation was 3 microns in plate x- and y-coordinates. The orbit parameters were completely relaxed to 1×10^4 meters in position, and 5 meters/second in velocity. The laser range measurements were assumed to be subject to a systematic range bias of 10 meters with a random noise of 5 meters, while the SECOR measurements were subject to a systematic range bias of 30 meters with a random noise of 5 meters (Table 2). For station positions and position errors input, see Table 3. Thirteen (13) orbits

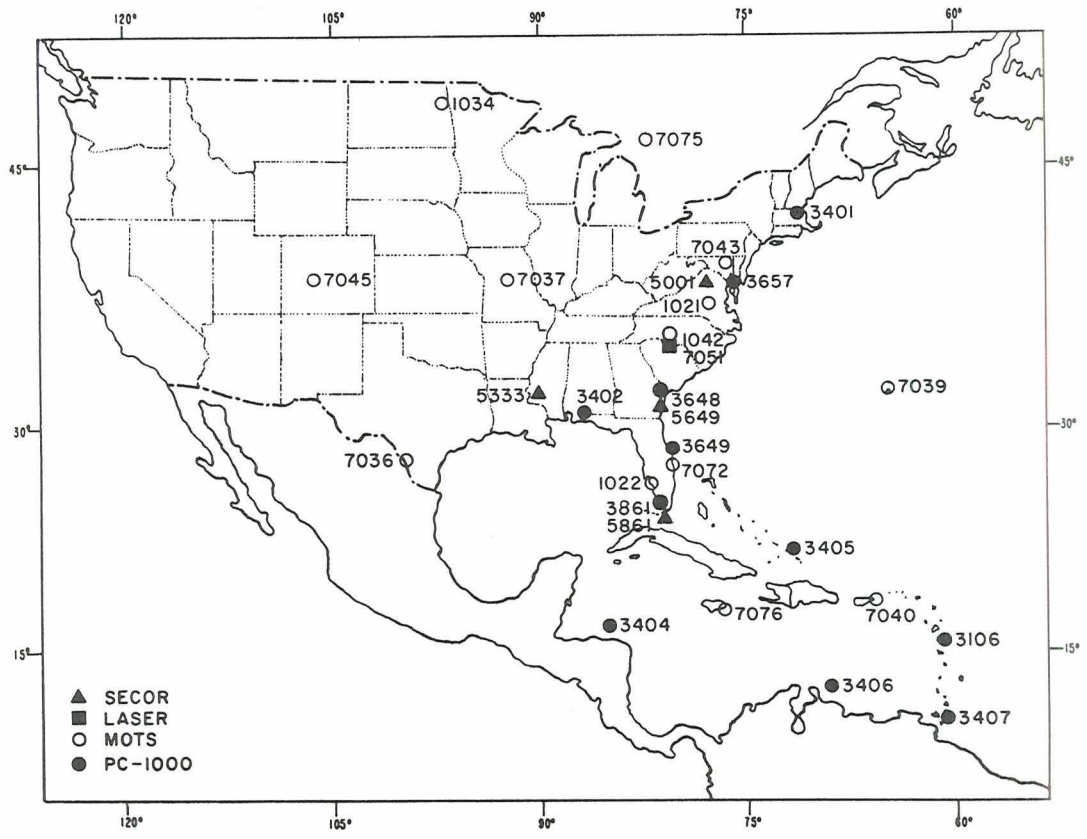

Figure 1. GEOS-1 Tracking Network

Table 1. Sequences Observed by Each Station

Orbit No.	5001	5333	5649	5861	7051	3405	3402	3657	3106	3861	3401	7040	1022	1034	1042	7037	7036	7039	7075	3648	3649	3404	3406	3407	1021	7043	7045	7072	7076	Time of Observation	
																														Date	GMT
1												2	2		1											1				18 Dec 65	0034
2												3	3		1	2		2	1											25 Jun 66	0812
3															1	1									1					20 Dec 65	0259
4						1		1		1			2			1						1							1	21 Dec 65	0928
5													1				1												1	24 Dec 65	0942
6												1			1										1			2		27 Dec 65	0749
7														2		2		1	4											3 Aug 66	0657
8										1								1												1 Jan 66	0605
9							1			1										1	1		1							2 Jan 66	0610
10							2														1							1		2 Jan 66	0811
11													2			1		2												3 Jan 66	0615
12											1					1							1							4 Jan 66	0620
13								1		1															1	1				5 Jan 66	0623
14						1									1		1													8 Jan 66	0635
15								1							1										1					10 Jan 66	0440
16						1	1	1												1										11 Jan 66	0445
17								1			1															1				12 Jan 66	0244
18							1	1	1		1		2		1															12 Jan 66	0449
19										1	1		1								1									13 Jan 66	0452
20						1			1				1																	14 Jan 66	0500
21						1					1					1									1	1				15 Jan 66	0256
22						1		1	1							1	1				1		1		1			1		15 Jan 66	0502
23					L*							1			1			2												19 Nov 66	0945
24						1				2							1				1							1		16 Jan 66	0506
25							1					1	2								1									17 Jan 66	0305
26										1			1															1		17 Jan 66	0512
27								1		2	1			2		1								1				1		18 Jan 66	0302
28										1	1			1		2					1									19 Jan 66	0310
29						1		1						1												1				22 Jan 66	0319
30										1			1	1		2				1										24 Jan 66	0329
31									1			1		2		2								1	1	1				25 Jan 66	0129

*L - Laser Obs.
*S - SECOR Obs.

Table 1 (Continued)

Orbit No.	5001	5333	5649	5861	7051	3405	3402	3657	3106	3861	3401	7040	1022	1034	1042	7037	7036	7039	7075	3648	3649	3404	3406	3407	1021	7043	7045	7072	7076	Time of Observation	
																														Date	GMT
32									1		1		1	2		2		1				1	1							26 Jan 66	0131
33								1	1			1	1	1		2	1	1				1								28 Jan 66	0142
34					L							1	1				1	2												10 Aug 66	0742
35													1	1			2				2		1							31 Jan 66	0153
36						1			2														1	1						4 Feb 66	0019
37														1			1										1			4 Feb 66	0214
38										2			1								1							1		9 Feb 66	0036
39					L								1				1		1											29 Jul 66	0215
40													3								2					1				20 Feb 66	1029
41								1					2		1						2							1		26 Feb 66	0853
42								1					3								1					1		2		27 Feb 66	0854
43							1	1								1	1													1 Mar 66	0903
44													1				1									1		1		2 Mar 66	0912
45						2	1			1								1					1							5 Mar 66	0720
46					L											2		1	2											9 Sep 66	0124
47													2		1	1												1		8 Mar 66	0935
48						1	1	1				1	1												1	1				9 Mar 66	0737
49													2		1	2	1	1	2											20 Oct 66	0723
50												1						1					3		1	1				10 Mar 66	0745
51												2			1			3												23 Jul 66	0152
52									1		1				1													2	1	12 Mar 66	0540
53													2	1														2	1	12 Mar 66	0744
54																											2		1	13 Mar 66	0751
55								1											1									1		26 Apr 66	0506
56												1		1		2	2	3	2											11 Jul 66	0510
57													1				2													15 Mar 66	0800
58													1													1		2	1	16 Mar 66	0557
59													2														1	2		16 Mar 66	0807
60													1			2	1									1			2	17 Mar 66	0601
61																1	3									1				17 Mar 66	0804
62													3			3										1	1		1	19 Mar 66	0613

Table 1. (Continued)

Orbit No.	5001	5333	5649	5861	7051	3405	3402	3657	3106	3861	3401	7040	1022	1034	1042	7037	7036	7039	7075	3648	3649	3404	3406	3407	1021	7043	7045	7072	7076	Time of Observation	
																														Date	GMT
63										2		1	1		1			3					1			1		1		20 Mar 66	0411
64													3		2	3												1		20 Mar 66	0617
65											1		4		2											2				21 Mar 66	0412
66													2	3	3											1	1			21 Mar 66	0621
67										1	2		3				1						1					2		22 Mar 66	0418
68													3				2											1		22 Mar 66	0625
69																1	2	1												4 Mar 66	0918
70									2	1																				15 Apr 66	0157
71															2	2										2				25 Mar 66	0645
72													2	2													1			26 Mar 66	0438
73																3	3	2	2											12 Jul 66	0513
74													2	3	1															27 Mar 66	0448
75														3	1	3											1			27 Mar 66	0647
76														3	2	2														28 Mar 66	0446
77													1	2	1		1													30 Aug 66	0442
78									1					3	1		1									2	1			29 Mar 66	0450
79									1														2	1						30 Mar 66	0042
80				S	S*		1		2														1			1				30 Mar 66	0246
81								1	1																					31 Mar 66	0251
82																							2							1 Apr 66	0049
83														1	1	1										1				2 Apr 66	0310
84						2		2												1			1	1						29 Jan 66	0149
85		S	S	S																										12 Apr 66	0145
86							1			2			1		2											1				11 Apr 66	0134
87	S	S	S																											13 Apr 66	0818
88	S	S	S	S																										14 Apr 66	0823
89	S	S	S	S																										15 Apr 66	0152
90										1			2									1				1		1	1	15 Apr 66	0836
91							1															1				2			1	17 Apr 66	0838
92							1		1				1		2													1		18 Apr 66	0842
93							1		1		1									1										11 Apr 66	0812

Table 1. (Continued)

Orbit No.	5001	5333	5649	5861	7051	3405	3402	3657	3106	3861	3401	7040	1022	1034	1042	7037	7036	7039	7075	3648	3649	3404	3406	3407	1021	7043	7045	7072	7076	Time of Observation	
																														Date	GMT
94							1	1	1		1																			12 Jan 66	0449
95													1	1		2	2										1			24 Oct 66	0736
96														1		1	1										1			5 Sep 66	0309
97							3			2			1			1														22 Apr 66	0656
98													2			2													1	22 Apr 66	0858
99										2			2									1							1	23 Apr 66	0906
100												1	1	1													2			24 Apr 66	0653
101	S	S	S												1	1												1		25 Apr 66	0502
102												1	2					1				1					1			25 Apr 66	0710
103	S	S	S	S																										26 Apr 66	0502
104	S	S	S	S																										12 Apr 66	0816
105	S	S	S	S																										25 Apr 66	0707
106												1	3																2	27 Apr 66	0715
107	S	S	S																											18 Apr 66	0633
108													2	1															2	29 Apr 66	0520
109													2					1										1	1	30 Apr 66	0525
110													2							2		1							2	30 Apr 66	0732
111		S	S	S																										16 Apr 66	0202
112								2				2		1		2		1										2		3 May 66	0325
113												1		1													1	1		3 May 66	0530
114												2	2	1		3		3								1				4 May 66	0327
115												1		1	2	2									1		2			4 May 66	0534
116														2											1		1			5 May 66	0539
117									1			2		2	2												1		2	6 May 66	0340
118														3												1	2		1	6 May 66	0540
119														1		1											2		1	7 May 66	0551
120													3				1								1				1	8 May 66	0352
121													1			1	3										2		1	8 May 66	0550
122														2	2		3		1										1	9 May 66	0353

Table 1. (Continued)

Orbit No.	5001	5333	5649	5861	7051	3405	3402	3657	3106	3861	3401	7040	1022	1034	1042	7037	7036	7039	7075	3648	3649	3404	3406	3407	1021	7043	7045	7072	7076	Time of Observation	
																														Date	GMT
123													3	1		2	2		1											10 May 66	0355
124															2				3						1					11 May 66	0155
125													1		3		2		2						1					11 May 66	0359
126													2						2								2		2	13 May 66	0410
127												2	2						2										1	15 May 66	0215
128													2		1	3											1		1	15 May 66	0416
129												3	3						2			2			1				2	16 May 66	0221
130													1	1			1										2			16 May 66	0423
131												2	2				2								1				1	17 May 66	0226
132	S	S	S	S																										14 Mar 66	1029
133	S	S	S	S																										2 Mar 66	0512
134													1			2	2												1	22 May 66	0245
135													3			2	3					1								19 May 66	0233
136												1			1				1						3				2	23 Jun 66	0758
137													2			2	3										2			28 Jun 66	0817
138																2			1						1	1			2	4 Jul 66	0642
139														1		2	1								1		1			4 Jul 66	0848
140														2			2										3			5 Jul 66	0848
141															2	2									2		3			9 Jul 66	0703
142														3		2	3								1	1				10 Jul 66	0704
143														3	2	2	1		2						2					11 Jul 66	0713
144												1						2	2											15 Jul 66	0324
145													3	2		3			1								1			7 Sep 66	0312
146												1				2	2	2							1					18 Jul 66	0329
147														3		2	2								1					18 Jul 66	0534
148														1		2	2	1								1				19 Jul 66	0334
149														3		1	2								1					19 Jul 66	0539
150													1	2			1		1						2					20 Jul 66	0342
151													2		1	2														6 Oct 66	1031

Table 1. (Continued)

Orbit No.	5001	5333	5649	5861	7051	3405	3402	3657	3106	3861	3401	7040	1022	1034	1042	7037	7036	7039	7075	3648	3649	3404	3406	3407	1021	7043	7045	7072	7076	Time of Observation	
																														Date	GMT
152													1		2	3	2		1											22 Jul 66	0348
153											2									1			1							24 Jul 66	0357
154													1	2	1		2		3								1			25 Jul 66	0359
155														2	1	3	2		2								2			26 Jul 66	0403
156																	3								1					27 Jul 66	0412
157														1	1		2										1			31 Jul 66	0851
158													1			2			2						1	1				2 Aug 66	0902
159													1	2											3	1				17 Oct 66	0912
160													1	2		2										1				7 Aug 66	0715
161																1		2							2		1			11 Aug 66	0523
162														2		2									2		1			20 Oct 66	0922
163														2		2	1										3			14 Aug 66	0741
164													2	2			1										1			21 Oct 66	0724
165															2	1	1									1				16 Aug 66	0547
166												1	1					2							2		1			17 Aug 66	0556
167														1			1	2	1											17 Aug 66	0758
168													1	2			2										3			19 Aug 66	0604
169													2	2	2		1	1	2								1			19 Aug 66	0604
170															2		1										2		1	22 Aug 66	0614
171								2	1											1	1			1						6 Feb 66	0019
Total	11	13	13	10	4	13	18	23	21	26	17	40	136	95	66	113	89	46	47	9	16	11	19	6	41	35	57	36	38		

*L - Laser Obs.
*S - SECOR Obs.

Table 2. Input Errors of the Observed Parameters

Optical

Orientation:

$\sigma_\alpha = 1.$
$\sigma_\omega = 1.$ in Arc Seconds
$\sigma_\kappa = 2.$

Timing (Inter Station):

$\sigma_t = 1 \times 10^{-4}$ seconds (active)

Measurement:

$\sigma_x = 3$ microns
$\sigma_y = 3$ microns } Plate coordinates

$\sigma_c = 10$ microns (Focal length)
$\sigma_\tau = 1 \times 10^{-4}$ seconds (Interval timing)

Electronic

Laser:

$\sigma_a = 10$ meters (Zero Set)
$\sigma_r = 5$ meters (Random Range)
$\sigma_\tau = 1 \times 10^{-4}$ seconds (Interval timing)

SECOR:

$\sigma_a = 30$ meters (Zero Set)
$\sigma_r = 5$ meters (Random Range)
$\sigma_\tau = 1 \times 10^{-4}$ seconds (Interval timing)

Initial Conditions

Position: $\sigma_x = \sigma_y = \sigma_z = 10,000$ meters
Velocity: $\sigma_{\dot{x}} = \sigma_{\dot{y}} = \sigma_{\dot{z}} = 5$ meters/second

Table 3. Geodetic Coordinates and Standard Errors of Observing Sites, NAD 27

	LATITUDE			LONGITUDE (E)			HEIGHT	STANDARD ERROR		
STATION	Deg	Min	Sec	Deg	Min	Sec	Meters	$\sigma\phi''$	σ_λ''	σ_h(M)
*3648	32	00	05.868	278	50	46.359	18	0	0	0
**5649	32	00	04.040	278	50	43.170	20	0	0	0
**5001	38	59	37.697	282	40	16.705	129	.160	.200	5.0
**5333	33	25	32.342	269	05	10.784	44	.180	.200	6.0
**5861	25	29	21.175	279	37	39.354	22	.150	.170	5.0
***7051	35	11	46.595	277	07	26.231	886	.120	.140	4.0
3405	21	25	47.050	288	51	14.030	8	.260	.260	8.0
3402	30	46	49.350	271	44	52.372	80	.140	.160	5.0
3657	39	28	18.971	283	55	44.565	5	.180	.230	6.0
3106	17	08	51.680	298	12	37.410	8	.360	.360	11.0
3861	25	30	24.690	279	36	42.688	16	.150	.170	5.0
3401	42	27	17.530	288	43	35.030	88	.250	.330	8.0
7040	18	15	26.216	294	00	22.174	59	.320	.320	10.0
1022	26	32	51.891	278	08	03.926	20	.140	.150	5.0
1034	48	01	21.403	262	59	21.561	255	.330	.480	10.0
1042	35	12	06.926	277	07	41.008	916	.120	.140	4.0
7037	38	53	36.068	267	47	42.120	273	.230	.280	7.0
7036	26	22	45.443	261	40	09.033	66	.280	.310	10.0
7039	32	21	48.834	295	20	32.560	21	.260	.300	8.0
7075	46	27	20.988	279	03	10.354	280	.260	.370	8.0
3649	27	01	13.160	279	53	12.690	26	.160	.140	5.0
3404	17	24	16.570	276	03	29.870	83	.260	.260	8.0
3406	12	05	22.110	291	09	43.760	23	.350	.350	11.0
3407	10	44	32.780	298	23	23.670	269	.400	.400	12.0
1021	38	25	49.630	282	54	48.230	7	.170	.140	5.0
7043	39	01	15.010	283	10	19.930	55	.170	.140	5.0
7045	39	38	48.030	255	23	41.190	1796	.340	.270	10.0
7072	27	01	13.170	279	53	12.490	26	.160	.140	5.0
7076	18	04	31.980	283	11	26.530	486	.260	.250	8.0

*Origin of Survey
**SECOR Stations
***Laser Station

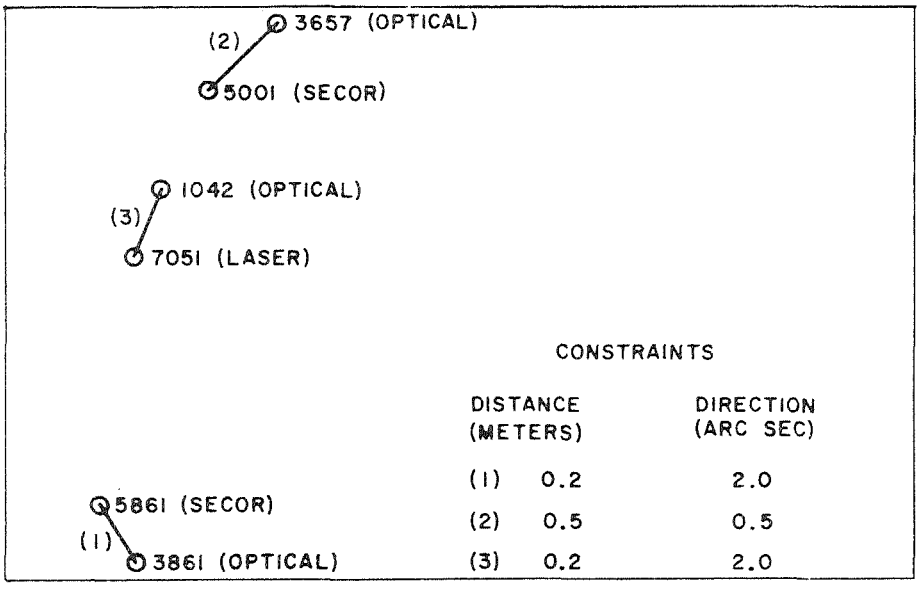

Figure 2. Constrained Relationships between SECOR, Laser and Optical Stations

were observed by four SECOR stations, two of which were observed simultaneously with optical stations. Since the majority of the SECOR orbits were not observed simultaneously with optical observations, two baseline constraints were applied between the two SECOR and the two optical co-located stations (see Figure 2) for the incorporation of the SECOR stations in the overall station network.

Laser range measurements from one station were obtained on four orbits in conjunction with optical observations. Since the number of laser orbits observed were not enough to improve station initial position again a baseline constraint was applied between the Laser and optical co-located station (Figure 2), and thus it was possible to incorporate it in the overall network.

Table 4 reflects the strength of each orbit into the overall solution. The standard error of the orbit determination reflects the degree of contribution of that pass to the overall tracking network. The accuracy of the satellite position (x, y, z) is largely dependent on the intersection angle of station observations and the accuracy of the measurements. For instance, orbits 8, 26, 38, 99, 107, 111, and 133 are weak in satellite position determination since the geometry and the number of stations observing each pass were marginal. The determination of satellite velocity vectors ($\dot{x}$, $\dot{y}$, $\dot{z}$) improves significantly as the number of stations and the length of the short arc observed increases. For instance, the determination of the velocity vectors of orbits 3, 5, 8, 15, 16, 17, 26, and 37 was poor since the arcs observed in each orbit were very small (24 seconds of time).

Table 4. Standard Errors of Recovered Orbital Parameters (Meters)

Orbit No.	σ_x	σ_y	σ_z	$\sigma_{\dot{x}}$ m/sec	$\sigma_{\dot{y}}$ m/sec	$\sigma_{\dot{z}}$ m/sec	Different Time Intervals Observed
1	38	13	17	.135	.050	.059	2
2	9	12	7	.027	.031	.024	3
3	16	8	33	.710	.291	1.329	1
4	5	5	8	.037	.023	.038	2
5	7	8	11	.359	.305	.478	1
6	13	7	16	.050	.030	.057	2
7	13	14	35	.026	.030	.050	4
8	58	49	148	.515	.322	.828	2
9	18	9	50	.065	.032	.127	2
10	14	20	24	.197	.208	.336	2
11	8	7	11	.051	.050	.053	2
12	10	12	9	.121	.125	.533	2
13	22	43	11	.239	.361	.328	2
14	9	22	14	.037	.279	.060	2
15	8	15	24	.453	.822	1.170	1
16	6	8	11	.359	.363	.581	1
17	29	17	58	1.040	.631	1.886	1
18	4	7	7	.042	.045	.047	2
19	10	12	13	.103	.088	.048	3
20	6	14	13	.153	.298	.152	2
21	6	8	18	.244	.081	.603	2
22	5	7	5	.023	.041	.024	2
23*	8	10	8	.020	.024	.020	4
24	6	8	9	.030	.052	.040	3
25	14	9	44	.072	.054	.187	2
26	54	95	35	1.576	2.885	1.062	1
27	10	9	20	.017	.015	.033	3
28	7	12	19	.034	.058	.084	2
29	53	12	55	.076	.036	.097	3
30	34	14	28	.071	.041	.065	2
31	9	10	32	.022	.027	.081	3
32	8	8	13	.012	.012	.021	4
33	8	8	11	.013	.015	.020	4
34*	33	27	33	.031	.025	.039	3
35	16	10	16	.026	.020	.027	4
36	12	9	10	.046	.064	.049	3
37	20	10	12	.945	.487	.646	1
38	149	23	47	.327	.296	.496	2
39*	6	8	7	.030	.023	.021	2
40	35	49	23	.082	.062	.071	3
41	32	52	15	.107	.334	.179	3
42	44	36	26	.088	.040	.065	3
43	21	38	13	.052	.085	.084	3
44	34	44	32	.384	.564	.417	2
45	16	16	10	.043	.103	.121	2

* Simultaneous Optical and Laser
** Simultaneous Optical and SECOR
*** SECOR

Table 4 (Continued)

Orbit No.	σ_x	σ_y	σ_z	$\sigma_{\dot{x}}$ m/sec	$\sigma_{\dot{y}}$ m/sec	$\sigma_{\dot{z}}$ m/sec	Different Time Intervals Observed
46*	7	8	8	.024	.023	.027	4
47	43	17	24	.078	.038	.077	3
48	25	11	17	.077	.051	.065	2
49	12	19	14	.032	.050	.038	4
50	11	7	12	.038	.033	.038	4
51	14	16	18	.033	.036	.060	4
52	24	13	17	.073	.057	.058	3
53	46	24	18	.072	.046	.032	4
54	22	14	13	.249	.374	.213	2
55	12	20	27	.090	.648	.263	2
56	12	15	9	.021	.028	.020	4
57	38	15	25	.296	.163	.625	2
58	51	16	21	.090	.052	.088	3
59	18	10	15	.104	.111	.567	2
60	20	11	10	.044	.027	.030	4
61	35	23	17	.060	.036	.049	4
62	16	9	10	.034	.027	.039	4
63	15	7	7	.030	.030	.028	3
64	20	12	10	.041	.032	.038	3
65	36	15	20	.051	.037	.036	4
66	16	11	9	.037	.031	.033	3
67	15	8	7	.033	.023	.024	3
68	23	14	18	.054	.037	.104	3
69	28	22	42	.081	.096	.094	3
70	15	48	38	.067	.543	.894	2
71	22	17	41	.080	.062	.206	2
72	19	13	11	.057	.047	.040	3
73	8	17	9	.018	.029	.020	4
74	31	18	18	.066	.042	.047	3
75	29	26	15	.051	.046	.040	3
76	28	17	15	.052	.041	.048	3
77	13	45	34	.037	.170	.099	4
78	21	14	13	.043	.028	.035	3
79	37	21	22	.422	.137	.238	2
80	18	31	14	.036	.048	.026	3
81**	10	14	10	.023	.025	.028	3
82	24	21	15	.075	.046	.038	3
83	51	21	45	.492	.194	.473	2
84	17	9	16	.028	.022	.028	4
85***	87	53	52	.168	.127	.120	1
86	10	45	11	.030	.067	.072	2
87***	40	67	24	.069	.131	.087	1
88***	23	43	20	.039	.057	.043	1
89***	67	17	29	.052	.044	.035	1
90	22	33	18	.077	.123	.081	2
91	59	61	52	.192	.207	.176	2
92	20	25	35	.068	.099	.119	2
93	15	16	23	.059	.083	.128	2
94	5	10	8	.140	.225	.301	2
95	18	10	7	.042	.023	.021	3

Table 4 (Continued)

Orbit No.	σ_x	σ_y	σ_z	$\sigma_{\dot{x}}$ m/sec	$\sigma_{\dot{y}}$ m/sec	$\sigma_{\dot{z}}$ m/sec	Different Time Intervals Observed
96	21	21	33	.195	.222	.104	3
97	6	13	18	.035	.061	.057	3
98	22	16	13	.065	.063	.038	3
99	147	71	35	.466	.251	.131	2
100	14	16	26	.040	.044	.051	3
101**	10	12	14	.070	.025	.020	1
102	10	12	12	.036	.065	.039	3
103***	53	47	14	.111	.053	.073	1
104***	54	62	26	.077	.150	.086	1
105***	25	17	18	.047	.049	.033	1
106	32	14	34	.070	.043	.075	3
107***	74	88	17	.140	.129	.117	1
108	12	20	19	.035	.075	.040	3
109	17	26	54	.058	.087	.132	2
110	29	11	11	.164	.093	.076	2
111***	91	53	40	.172	.073	.106	1
112	10	12	23	.019	.030	.041	4
113	21	10	32	.026	.016	.049	3
114	6	6	19	.015	.019	.034	4
115	18	8	22	.064	.026	.064	3
116	24	9	27	.173	.045	.103	3
117	13	12	22	.031	.028	.055	4
118	18	10	17	.061	.018	.029	4
119	51	23	16	.163	.074	.062	3
120	14	15	28	.038	.049	.060	3
121	27	16	29	.039	.021	.045	4
122	16	9	19	.042	.033	.048	4
123	16	10	22	.026	.022	.034	4
124	14	15	38	.040	.066	.061	3
125	17	15	18	.032	.028	.030	3
126	22	10	15	.052	.019	.029	4
127	17	10	17	.030	.022	.026	4
128	28	20	21	.052	.026	.036	4
129	13	8	12	.023	.017	.021	4
130	38	14	16	.062	.033	.048	4
131	15	10	15	.028	.017	.028	4
132***	41	41	42	.051	.119	.079	1
133***	139	91	60	.190	.047	.132	1
134	21	17	19	.049	.029	.038	3
135	15	9	15	.037	.023	.030	3
136	10	17	8	.026	.036	.021	4
137	12	16	11	.024	.033	.030	4
138	9	15	10	.034	.032	.034	4
139	7	20	26	.033	.066	.076	4
140	13	25	12	.030	.047	.042	4
141	9	18	10	.023	.039	.037	3
142	11	19	10	.019	.034	.022	4
143	7	13	9	.018	.028	.028	4
144	10	19	24	.042	.052	.067	3
145	13	16	18	.022	.036	.033	4
146	11	21	14	.025	.043	.030	3

Table 4 (Continued)

Orbit No.	σ_x	σ_y	σ_z	$\sigma_{\dot{x}}$ m/sec	$\sigma_{\dot{y}}$ m/sec	$\sigma_{\dot{z}}$ m/sec	Different Time Intervals Observed
147	20	21	13	.035	.037	.027	4
148	12	26	11	.037	.066	.028	4
149	22	20	13	.038	.035	.027	4
150	15	17	13	.040	.034	.037	4
151	6	12	5	.047	.060	.052	2
152	10	14	7	.025	.026	.026	4
153	24	44	31	.057	.062	.035	4
154	10	11	9	.020	.023	.024	4
155	13	13	10	.021	.023	.022	4
156	36	19	19	.069	.046	.065	4
157	17	8	22	.150	.067	.177	3
158	9	12	27	.040	.047	.091	4
159	12	9	16	.035	.037	.030	4
160	15	14	10	.037	.032	.033	4
161	10	10	33	.046	.022	.062	4
162	22	14	43	.087	.063	.069	4
163	14	9	9	.030	.020	.025	3
164	15	22	33	.030	.026	.047	4
165	10	16	8	.041	.065	.034	2
166	13	13	28	.024	.017	.033	4
167	15	14	22	.041	.026	.035	4
168	14	23	21	.039	.042	.040	3
169	8	10	14	.032	.028	.033	4
170	13	19	30	.031	.040	.050	4
171	24	13	15	.045	.029	.036	4

* Simultaneous Optical and Laser
** Simultaneous Optical and SECOR
*** SECOR

The corrections to the NAD survey coordinates and the propagated errors (Table 5) are consistent with the observation network with the origin at Hunter AFB. The propagated errors of 2 to 3 meters for the continental U.S. stations and 3 to 6 meters for the Caribbean stations reflect the internal network accuracies and illustrate the strength of this particular solution. The recovery of some stations was weaker than others due to poor geometry and limited observations from that station. (See Table 6 for short-arc adjusted GEOS-I station coordinates - NAD 27.)

A typical recovered bias in optical orientation α, ω, and κ was 0.2 arc seconds. The largest recovered bias was 1.5 arc seconds. Recovered biases in the laser measurements ranged from 2 to 15 meters, and SECOR range biases ranged from 4 to 35 meters. The random noise was approximately 1 to 2 meters for Laser and 1 to 5 meters for SECOR measurements.

7. CONCLUSION

In view of the various instrumentations and observing modes used in this reduction, it is apparent that this program could be used with any type optical and/or ranging system presently employed for global tracking. The GEOCEIVER was given some special consideration in the error model of range measuring systems. Terms for frequency biases and frequency drift were designed to accommodate errors introduced by the satellite and ground oscillators.

The reduction can be exercised to take into account any specified uncertainty in synchronization. Thus when timing offsets or inter-station biases are known to worthwhile precision (say one millisecond or better), the reduction would automatically propagate their residual uncertainties rigorously through the reduction, even though no practical improvements were to result in their recovery.

SAGA accommodates adjustments to the Earth's center of mass and has the capability of treating the coordinates of the adopted center of mass as constrained parameters. This means that in sufficiently strong tracking networks of continental extent, the possibility emerges of improving the location of the Earth's center of mass relative to the origin of the adopted datum. The results presented were obtained with the center of mass known perfectly. This network is concentrated on a small section of the earth's surface and the geometry with respect to the center of mass is very weak. Further studies will be undertaken with emphasis placed on orbital geometry and observing station locations relative to the center of mass.

This multiple short arc reduction reflects the potential of this program for accurate geodetic studies, and for improvement of continental and inter-continental

Table 5. Results from Short Arc Adjustment

Corrections to NAD Coordinates (Meters)					Standard Error (Meters)		
Station No.	Name	Δ_x	Δ_y	Δ_z	$\sigma_{\Delta x}$	$\sigma_{\Delta y}$	$\sigma_{\Delta x}$
*3648	Hunter	0	0	0	0	0	0
*5649	Hunter	0	0	0	0	0	0
5001	Herndon	-1.01	6.93	2.10	2.81	3.90	2.54
5333	Greenville	9.12	-3.53	4.63	3.36	4.84	3.95
5861	Homestead	2.26	2.52	-0.75	2.30	2.55	2.33
7051	Rosman	-0.72	-4.16	-2.91	2.96	2.85	2.03
3405	Grand Turk	-5.08	1.15	-12.98	4.39	5.24	4.68
3402	Semmes	2.31	-0.50	-1.99	3.40	3.57	3.52
3657	Aberdeen	-3.32	3.12	2.21	2.40	3.67	2.54
3106	Antigua	8.15	20.15	10.60	5.03	5.32	5.19
3861	Homestead	2.23	2.44	-0.70	2.30	2.54	2.33
3401	Bedford	-13.58	5.61	7.83	3.64	5.62	4.20
7040	Puerto Rico	-3.26	8.16	-2.58	3.60	4.05	4.09
1022	Ft. Meyers	0.75	-3.57	-0.17	1.91	2.22	2.15
1034	Grand Forks	-2.05	-5.97	6.35	2.84	3.16	3.27
1042	Rosman	0.13	-3.43	-2.91	2.00	2.18	2.03
7037	Columbia	-0.66	-9.00	-4.33	2.39	2.42	2.43
7036	Edinburg	-3.13	-10.86	0.59	3.21	2.92	2.94
7039	Bermuda	19.79	5.55	10.76	3.53	3.74	3.39
7075	Sudbury	5.11	1.97	8.66	3.13	3.61	3.62
3649	Jupiter	2.83	2.30	-1.64	3.00	3.57	3.38
3404	Swan Is.	-4.86	6.99	-1.44	4.93	4.88	4.94
3406	Curacao	-18.13	-0.53	3.92	4.83	5.83	5.34
3407	Trinidad	-28.85	0.15	-32.15	6.58	7.16	7.66
1021	Blossom Pt.	0.28	0.59	-1.52	2.27	2.94	3.07
7043	Greenbelt	-3.82	9.39	4.52	2.31	3.14	3.05
7045	Denver	-0.97	-8.94	3.21	3.55	3.53	3.41
7072	Jupiter	-0.59	-1.81	-3.28	2.49	2.96	3.09
7076	Jamaica	2.46	2.12	5.28	3.47	4.03	3.90
	RMS				3.28	3.78	3.52

* Origin of Survey

Table 6. Short Arc Adjusted Geos-I Station Coordinates, NAD 27

Station	GEODETIC							RECTANGULAR		
	Latitude			Longitude (E)			Height	x	y	z
	Deg.	Min.	Sec.	Deg.	Min.	Sec.	Meters	Meters	Meters	Meters
3648	32	00	05.868	278	50	46.359	18.0	832334.77	-5349731.00	3360414.47
5649	32	00	04.040	278	50	43.170	20.0	832516.59	-5349734.63	3360367.78
5001	38	59	37.892	282	40	16.704	124.7	1088886.63	-4843080.19	3991669.31
5333	33	25	32.404	269	05	11.133	49.2	-84963.42	-5328097.19	3493299.63
5861	25	29	21.182	279	37	39.421	19.5	963495.79	-5679880.38	2727945.13
7051	35	11	46.438	277	07	26.169	887.4	647208.98	-5178467.88	3656001.72
3405	21	25	46.687	288	51	13.865	.4	1919524.80	-5621243.75	2315603.91
3402	30	46	49.285	271	44	52.433	79.3	167292.27	-5482121.94	3244861.09
3657	39	28	19.104	283	55	44.444	03.2	1186822.94	-4785337.44	4032706.97
3106	17	08	52.141	298	12	37.961	-2.3	2881879.78	-5372309.13	1868357.20
3861	25	30	24.694	279	36	42.759	13.6	961794.02	-5679310.13	2729706.56
3401	42	27	17.924	288	43	34.526	85.8	1513167.78	-4463167.78	4282883.00
7040	18	15	26.224	294	00	22.179	49.6	2465086.66	-5535074.00	1985343.41
1022	26	32	51.833	278	08	03.907	22.9	807882.52	-5652139.19	2833328.25
1034	48	01	21.390	262	59	21.465	263.4	-521681.81	-4242203.50	4718549.38
1042	35	12	06.782	277	07	40.986	916.9	647539.05	-5178086.63	3656531.13
7037	38	53	35.774	267	47	42.103	277.1	-191261.40	-4967437.13	3983079.88
7036	26	22	45.297	261	40	08.958	76.0	-828467.56	-5657614.25	2816640.03
7039	32	21	49.069	295	20	33.311	29.3	2308245.38	-4873752.19	3394394.00
7075	46	27	21.208	279	03	10.585	285.3	692650.55	-4347223.63	4600306.69
3649	27	01	13.137	279	53	12.792	23.4	976304.88	-5601545.50	2880069.72
3404	17	24	16.595	276	03	29.715	75.3	642535.59	-6054102.19	1895516.58
3406	12	05	22.275	291	09	43.168	17.8	2251843.66	-5817042.81	1327008.58
3407	10	44	31.834	298	23	22.817	249.6	2979940.41	-5513660.63	1180971.64
1021	38	25	49.599	282	54	48.235	05.3	1118061.02	-4876471.44	3942791.88
7043	39	01	51.327	283	10	19.835	49.8	1130737.78	-4831478.31	3993956.97
7045	39	38	47.922	255	23	41.233	1804.7	-1240450.92	-4760388.19	4048807.53
7072	27	01	13.048	279	53	12.435	25.8	976295.78	-5601550.50	2880068.31
7076	18	04	32.157	283	11	26.604	486.1	1384189.69	-5905824.56	1966372.75

surveys. The mean standard error of 3.5 meters is a tremendous improvement to the NAD survey coordinates and especially for the ETR tracking stations down as far as Trinidad. Further reductions will be undertaken utilizing GEOS-II observations now available to the geodetic community. The incorporation of the GEOS-II data into this adjustment will strengthen the results considerably.

Acknowledgments

This paper results from the excellent support of AFCRL's Analysis and Simulation Branch personnel, and cooperation of AFCRL's Computer Processing Branch. The consultation and programming assistance offered by Mr. Jerry Trotter of DBA Systems, Inc. deserves special mention.

Bibliography

Anderle, R.J., Orbit Computation Reports, U.S. Naval Weapons Laboratory.

Berbert, J.H. (1969) GEOS station position solutions comparisons. Presented to the Annual Fall Meeting of the DIA MC&G Conference.

Brown, D.C. and Trotter, J.E. (1967) Precise Determination of Geodetic Positions by the Method of Continuous Traces, AFCRL 67-0558.

Brown, D.C. and Trotter, J.E. (1969) SAGA, A Computer Program for Short Arc Geodetic Adjustment of Satellite Observations, AFCRL 69-0080.

Eckhardt, D.H. (1966) Tests of a method for making geodetic ties by observing a satellite optical beacon, J. Spacecraft and Rockets Vol. 3, (No. 12).

Hadgigeorge, G. and Trotter, J.E. (1969) Numerical results from short arc geodetic adjustments using combinations of directional and/or ranging observations from GEOS-I satellite. Presented at the Annual Meeting of the American Geophysical Union.

Iliff, R.L. and Hadgigeorge, G. (1969) Daytime ground-to satellite laser ranging experiments, Applied Optics Journal.

Mueller, I.I., Reilley, J.P. and Schwarz, C.R. (1969) The North American datum in view of GEOS I observations. Presented at National Fall Meeting of the AGU.

NASA/Goddard Space Flight Center (1969) Geodetic Satellites Observation Station Directory, Compiled by Geonautics, Inc.

NASA/Goddard Space Flight Center, National Space Science Data Center.

Addition to AFCRL-70-0090

Environmental Research Papers, No. 315

SECOND NETWORK ADJUSTMENT

In order to minimize dynamic errors induced by the displacement of earth's center of mass relative to the center of the spheroid another reduction was attempted. In this reduction the given NAD-27 coordinates of all stations were transformed to Mercury Datum prior to the adjustment. After the adjustment was completed, the new coordinates were transformed back to NAD-27. The results are shown on Table 7. A comparison between Tables 6 and 7 reveals that high quality determination of station locations may be sensitive to uncertainties in the coordinates of the earth's center of mass. If the station locations are referred to a datum whose origin does not coincide with the center of mass of the earth, then either the first order coefficients of the geopotential should be constrained appropriately or the station locations transformed before the adjustment to a spheroid whose origin coincides with the center of mass of the earth.

Table 7. Short Arc Adjusted Geos-I Station Coordinates, NAD 27

Station No.	GEODETIC			RECTANGULAR		
	Latitude	Longitude (E)	Height(M)	x (M)	y (M)	z (M)
3648	32°-00'-05"87	278°-50'-46"36	18	832594	-5349691	3360414
5649	32 -00 -04.04	278 -50 -43.17	20	832516	-5349734	3360367
5001	38 -59 -37.79	282 -40 -16.63	127	1088886±3	-4843084±4	3991669±3
5333	33 -25 -32.28	269 -05 -11.00	48	-84968±3	-5328099±5	3493294±4
5861	25 -29 -21.21	279 -37 -39.39	20	963495±2	-5679881±3	2727946±2
7051	35 -11 -46.48	277 -07 -26.13	885	647208±3	-5178465±3	3656001±2
3405	21 -25 -46.65	288 -51 -13.84	1	1919524±4	-5621245±5	2315603±5
3402	30 -46 -49.29	271 -44 -52.35	80	167290±3	-5482123±4	3244861±4
3657	39 -28 -19.15	283 -55 -44.43	1	1186822±2	-4785335±4	4032706±3
3106	17 -08 -52.08	298 -12 -37.92	-2	2881879±5	-5372311±5	1868356±5
3861	25 -30 -24.72	279 -36 -42.74	14	961794±2	-5679310±3	2729707±2
3401	42 -27 -17.95	288 -43 -34.44	86	1513166±4	-4463727±6	4282883±4
7040	18 -15 -26.16	294 -00 -22.15	49	2465086±4	-5535074±4	1985341±4
1022	26 -32 -51.84	278 -08 -03.88	23	807882±2	-5652140±2	2833327±2
1034	48 -01 -21.22	262 -59 -21.53	265	-521681±3	-4242208±3	4718547±3
1042	35 -12 -06.78	277 -07 -40.93	916	647538±2	-5178087±2	3656530±2
7037	38 -53 -35.76	267 -47 -42.09	278	-191262±2	-4967439±2	3983080±2
7036	26 -22 -45.27	261 -40 -08.93	76	-828469±3	-5657615±3	2816639±3
7039	32 -21 -49.07	295 -20 -33.19	29	2308242±3	-4873753±4	3394394±3
7075	46 -27 -21.04	279 -03 -10.53	288	692650±3	-4347229±4	4600304±4
3649	27 -01 -13.14	279 -53 -12.76	24	976304±3	-5601546±4	2880070±3
3404	17 -24 -16.56	276 -03 -29.70	77	642535±5	-6054104±5	1895516±5
3406	12 -05 -22.14	291 -09 -43.13	20	2251843±5	-5817046±6	1327005±5
3407	10 -44 -31.74	298 -23 -22.73	251	2979939±7	-5513663±7	1180969±8
1021	38 -25 -49.59	282 -54 -48.18	6	1118060±2	-4876472±3	3942792±3
7043	39 -01 -15.31	283 -10 -19.79	50	1130737±2	-4831479±3	3993956±3
7045	39 -38 -47.85	255 -23 -41.34	1806	-1240448±4	-4760392±4	4048807±3
7072	27 -01 -13.03	279 -53 -12.41	24	976295±2	-5601550±3	2880067±3
7076	18 -04 -32.10	283 -11 -26.00	485	1384189±4	-5905824±4	1966371±4

ANALYSIS OF GEODETIC SATELLITE (GEOS I) OBSERVATIONS IN NORTH AMERICA

by

Ivan I. Mueller
Charles R. Schwarz
James P. Reilly

Department of Geodetic Science
The Ohio State University, Columbus

ABSTRACT

GEOS I observations made at thirty optical and four SECOR stations were analyzed in the geometric and short-arc modes for the purpose of detecting systematic distortions in the North American Datum. The results indicate that the NAD at its origin (Meades Ranch, Kansas) requires an easterly rotation in azimuth and a westerly rotation in the prime vertical plane, both in the magnitude of one second of arc to fit the satellite data. There is also evidence of the need for a reduction in scale of about 1:200 000.

To be published in the Bulletin Géodésique, June 1970

6/69
1/70-rev.

1. INTRODUCTION

During the lifetime of the GEOS I satellite a large number of optical and electronic observations were made from stations located on the North American Datum (NAD). The NAD coordinates of most of these stations have been determined through precise geodetic ground ties to the first-order triangulation network. In this report an attempt is made to determine the coordinates of these stations from the available satellite observations and possible distortions present in the North American Datum. The coordinates were determined both from simultaneous observations (geometric mode) and from observations distributed along the orbital path (short-arc mode).

The observation stations involved are shown in Fig. 1. All coordinate computations (and results) are relative to the NAD coordinates (and variances) of Columbia, Missouri, the station nearest to the origin of the NAD: Meades Ranch, Kansas. On the other hand, the parameters, defining the distortions of the NAD with respect to the satellite determined system, refer to Meades Ranch.

2. OBSERVATIONS

The observations utilized in the calculations were taken by the U.S. Air Force using the PC-1000 cameras (15 stations), by NASA/Goddard Space flight Center using mostly MOTS 40 cameras (15 stations), and by the U.S. Army Topographic Command (TOPOCOM) SECOR ranging system (4 stations). The optical observations were processed as described in [1] and deposited in the National Space Science Data Center (NSSDC) by the agencies responsible for data reduction. The SECOR data was directly obtained from U.S. Army TOPOCOM, where it was processed as given in [2].

The principle tool used for screening the optical data was the individual event adjustment. The observations are grouped by event (i.e., individual flash) and an adjustment is performed for the three components of the satellite position. The a posteriori variance of the observation of unit weight is computed and compared to a test value. If the computed variance is greater than the test value, the entire event (flash) is deleted from the data sample. The purpose of the individual event adjustment is to detect blunders in the observational data, since these will generally cause large residuals and consequently a large a posteriori unit variance. On the other hand, the residuals and a posteriori unit variance also include some contribution from the errors in the station positions, which are held fixed during the event adjustment. Thus the test is efficacious only if the station positions are fairly well known. In the case of the MOTS and PC-1000 observations, the station positions were considered to be quite well known a priori. We expected the approximate station coordinates to be sufficiently accurate that their errors would seldom contribute more than a second of arc to any of the residuals in the individual event adjustments.

Altogether about 5000 MOTS and 2000 PC-1000 observations were investigated. We expected to find that the data had been thoroughly screened before it was deposited in the Data Center, so that it would not be necessary for us to delete any observations at all. However, the individual event adjustments showed that the unit variance was unacceptably large in a sizable number of cases. The values of the a posteriori unit variance fell over a wide range; only in some cases was this value large enough to indicate an obvious blunder, while in other cases this value indicated that the data probably contained a blunder of small magnitude. We were able to identify the actual observation containing the blunder in a few cases by examining the residuals of the individual event adjustment and in other cases by examining

the residuals of the orbital mode adjustment, but in most cases the offending observation could not be identified and it was necessary to delete the whole event. We were not able to detect any correlation between bad observations or events and the tracking stations, so that we could not ascribe the existence of bad events to large errors in the coordinates of any station. On the other hand, we often found that all, or at least several, of the flashes of a sequence yielded poor event adjustments, which indicated the existence of an error in the plate reduction for at least one of the plates involved. Since we did not have access to the raw data and the plate reductions, we were not able to follow the possibility further.

The data suspected of containing blunders amounted to about 10% of the MOTS data and about 30% of the PC-1000 data. The PC-1000 data was the most troublesome, not only because of the large amount of suspected data but also because the value of the unit variance often fell into the "doubtful" range; the values of the a posteriori standard deviation of unit weight for the individual event adjustments were fairly continuously spread from 0" to 30". We were willing to accept that an individual event could yield a standard deviation of as much as 6" or even 10" due to the normal sample fluctuation of accidental errors. However, it seemed that a value greater than this amount indicated the probable presence of a small blunder that would be identifiable with sufficient investigative effort. In the case of the MOTS data, the a posteriori standard deviations were usually either less than 6" or greater than 20", thus allowing a fairly clear separation of good and erroneous data.

Since we were not in a position to search for the cause of the apparent blunders in the data, we were not able to determine which events actually contained small blunders and which only appeared bad due to normal sample fluctuation. If we were to consider the small blunders to be part of the population of accidental errors, the population standard deviation of the data would be so large as to render it practically useless for geodetic purposes. This meant that it was necessary for us to accept, a priori, some value for the

standard deviation of the data and to rely on statistical methods to detect and delete suspect data.

Based on previous experience, we decided to ignore the standard deviations of the observations given on the data cards, since these were completely unrealistic, and to accept a value of 2".0 as the standard deviation of all optical observations, both MOTS and PC-1000. This value was used as the standard deviation for the declination and for the right ascension times the cosine of the declination. If this value is the true standard deviation of the accidental errors in the data, then the expected value of the a posteriori unit variance of an individual event adjustment is one. This statistic is distributed as chi-square so that we were able to construct a confidence interval in which it was expected to fall. Our final decision was to use a rejection criterion of 10, rejecting all events for which the unit variance was greater than this value. Since most of the event adjustments involved only two plates, and thus four observations and one degree of freedom, this rejection criterion corresponded in most cases to a probability level of .99843. I.e., if the hypothesis that the true standard deviation is 2".0 is correct, then only 0.157% of the events are deleted by this test when they are actually good events. This is a small price to pay for the rejection of most of the small blunders.

When combined with the a priori standard deviation of 2".0, this rejection criterion corresponds to an observational standard deviation of 6".3 for the sample of observations contained in the event. Thus the screening criterion used for optical data may be phrased as the rejection of all events for which the observational standard deviation, estimated from the individual event adjustment with the starting coordinates held fixed, is greater than 6".3. As expected, this rejection criterion resulted in an overall unit variance of close to one, as seen in the results of the simultaneous adjustments of all nondeleted optical data (NA-1 and NA-2 solutions).

The SECOR range data had already been extensively screened during the processing described in [2]. Therefore it was not necessary to delete any range data. In a preliminary adjustment the SECOR data was adjusted alone. This adjustment indicated that the observational standard deviation of the SECOR data was 3.5 m. This value was used to form the weights for the SECOR observations in the combinations of the optical and range data (NA-5 and NA-6 solutions).

3. NETWORK ADJUSTMENT

3.1 Geometric Adjustment

The network adjustment in the geometric (simultaneous) mode was carried out as described in [1], with minor modifications. Four adjustments (NA-1, NA-2, NA-5, and NA-6) are presented here with characteristics as follows:

NA-1 Only MOTS and PC-1000 data was used. The coordinates of Columbia, Missouri (7037), were given a weight of 10 (which kept the station coordinates effectively fixed). The scale was determined by imposing a chord constraint between Homestead, Florida (3861) and Greenbelt, Maryland (7043). These two stations were on the precise traverse of the U.S. Coast and and Geodetic Survey (USCGS). This chord distance is 1,531,562.9 m and was constrained to ±2 m (1: 750,000), as estimated by the USCGS.

NA-2 Same as NA-1 but the coordinates of Columbia, Missouri, were given a weight of 0.11 (which corresponds to the standard deviation computed by Simmons' formula [4]).

NA-5 The SECOR data was included along with the MOTS and PC-1000 data. The coordinates of Columbia, Missouri, were given a weight of 0.11. There was no chord constraint; the scale was determined from the SECOR ranges.

NA-6 Same as NA-3 but the chord distance, (3861) - (7043), was constrained in the same way as in the NA-1.

Information pertaining to these adjustments is included in Table 1. The final adjusted coordinates are given in Table 2. The values in the columns of the four solutions are corrections to be added to the NAD coordinates (taken from [3]) of the stations.

Table 1

General Information on the Geometric Adjustments

	NA-1	NA-2	NA-5	NA-6
No. of PC-1000 stations	15	15	15	15
No. of MOTS stations	15	15	15	15
No. of SECOR stations	—	—	4	4
σ (a priori)	2"	2"	optical:2".0 range: 3.5 m	optical:2".0 range: 3.5 m
Rejection criteria	6".3	6".3	optical:6".3 range: none	optical:6".3 range: none
Weight assigned to coordinates of Columbia, Mo.	10	0.11	0.11	0.11
Chord constraint between Homestead and Greenbelt (1,531,562.9 m)	1:750,000	1:750,000	—	1:750,000
Relative positions of the 4 SECOR stations and the 4 collocated PC-1000 stations constrained by adding 999 to the diagonal elements of the corresponding 3 x 3 matrices	—	—	X	X
No. of ground stations	30	30	34	34
No. of spatial chord equations	1	1	0	1
No. of degrees of freedom	4220	4220	5182	5183
Quadratic sum of all the residuals (VPV)	3951.4	3951.4	4956.4	4962.6
Standard deviation of unit weight	1.0	1.0	1.0	1.0

Table 2

Coordinates of the North American GEOS I Tracking Stations from the Geometric Adjustment

Station	Name		NAD	σ	NA-1	σ	NA-2	σ	NA-5	σ	NA-6	σ
7075	Sudbury, Ontario	X	692646.1	6.0	0.7	4.8	0.7	5.6	- 19.0	7.0	- 2.7	5.7
	MOTS 40	Y	-4347225.8	5.0	9.6	5.8	9.6	6.4	- 4.0	7.1	7.5	6.5
		Z	4600298.3	4.9	8.6	5.0	8.6	5.8	- 5.0	6.6	6.7	5.9
1032	St. Johns, Newfoundland	X	2602802.5		-81.8	68.8	-81.8	68.8	-145.5	70.9	-90.3	69.5
	MOTS 40	Y	-3419301.2		-10.7	97.3	-10.7	97.4	- 49.1	98.9	-12.2	98.5
		Z	4697477.3		-43.8	37.8	-43.8	37.9	- 59.2	38.4	-46.3	38.3
3334	Greenville, Miss.	X	- 84957.5	4.1	10.3	15.8	10.3	16.1	- 20.9	8.6	0.8	6.5
	PC-1000	Y	-5328100.8	3.1	-13.0	13.0	-13.0	13.3	- 6.1	10.7	- 5.9	10.7
		Z	3493285.2	3.7	-38.9	10.4	-38.9	10.8	3.0	9.4	-11.6	8.6
3902	Cheyenne, Wyo.	X	-1234668.8	2.9	39.2	31.7	39.2	31.9	61.2	32.5	42.7	32.2
	PC-1000	Y	-4651355.3	2.4	15.3	34.6	15.3	34.7	7.6	35.1	14.6	35.1
		Z	4174612.3	2.5	-40.2	11.5	-40.2	11.8	- 43.1	12.0	-39.4	11.9
1033	College, Alaska	X	-2299238.0	10.7	6.3	15.0	6.3	15.3	52.2	18.4	12.9	15.3
	MOTS 40	Y	-1445840.4	11.0	19.3	73.3	19.3	73.3	- 58.6	75.9	7.2	74.0
		Z	5751629.0	7.8	-20.1	40.0	-20.1	40.2	- 58.3	41.4	-25.4	40.5
3400	Colorado Springs, Colo.	X	-1275173.6	2.7	-21.5	15.5	-21.5	15.8	3.3	16.8	-16.9	15.9
	PC-1000	Y	-4798165.6	2.3	-21.1	11.6	-21.1	12.0	- 24.0	12.2	-20.6	12.1
		Z	3994037.6	2.4	7.0	8.0	7.0	8.5	7.6	8.6	8.3	8.6
3903	Herndon, Va.	X	1089023.7	6.4	- 7.3	11.6	- 7.3	11.9	- 31.0	9.5	-10.0	7.8
	PC-1000	Y	-4843194.9	5.1	113.7	13.9	113.7	14.2	58.5	9.5	47.0	9.0
		Z	3991564.7	5.6	- 3.1	9.9	- 3.1	10.3	- 15.8	8.1	-26.1	7.7
7039	Bermuda Island	X	2308230.2	8.8	18.9	8.5	18.9	9.0	- 36.9	14.9	9.6	8.8
	MOTS 40	Y	-4873765.5	7.2	31.9	5.4	31.9	6.1	30.7	6.2	32.0	6.2
		Z	3394389.0	8.3	- 8.5	5.4	- 8.5	6.2	4.4	6.8	- 6.1	6.2

all units are in meters

Table 2 (continued)

Station	Name		NAD	σ	NA-1	σ	NA-2	σ	NA-5	σ	NA-6	σ
3405	Grand Turk	X	1919530.5	9.2	- 6.2	7.6	- 6.2	8.1	-53.0	12.8	-13.9	8.0
	PC-1000	Y	-5621245.2	6.6	27.8	5.8	27.8	6.5	42.4	7.2	30.5	6.5
		Z	2315617.1	9.0	-28.0	7.4	-28.0	8.0	8.9	11.2	-21.9	7.9
3407	Trinidad	X	2979925.0	11.4	- 5.3	11.4	- 5.3	11.7	-75.9	19.1	-16.9	11.6
	PC-1000	Y	-5513746.9	9.2	94.7	7.1	94.7	7.6	107.2	8.1	97.5	7.7
		Z	1180994.8	12.1	-25.1	12.0	-25.1	12.3	36.8	18.1	-15.2	12.2
3648	Hunter AFB, Ga	X	832594.6	6.3	2.8	5.1	2.8	5.9	-23.2	7.5	- 2.9	5.4
	PC-1000	Y	-5349690.7	4.6	17.5	4.9	17.5	5.7	33.1	5.7	24.2	5.2
		Z	3360414.7	5.7	- 1.2	5.3	- 1.2	6.0	13.0	6.6	- 4.4	4.9
3404	Swan Island	X	642541.2	8.5	-20.0	5.1	-20.0	5.9	-38.4	7.1	-23.1	5.9
	PC-1000	Y	-6054109.5	5.4	48.8	5.9	48.8	6.6	73.6	8.4	53.4	6.6
		Z	1895518.2	8.2	- 5.1	7.6	- 5.1	8.2	40.5	12.7	2.0	8.0
3657	Aberdeen, Md.	X	1186826.8	6.6	- 7.3	5.2	- 7.3	5.9	-37.9	8.8	-12.3	5.9
	PC-1000	Y	-4785340.8	5.3	20.8	5.2	20.8	6.0	17.0	6.1	21.0	6.0
		Z	4032705.0	5.7	4.3	4.0	4.3	4.9	3.4	5.0	4.4	5.0
3406	Curacao	X	2251837.6	10.7	- 1.0	8.2	- 1.0	8.7	-55.8	14.3	-10.8	8.5
	PC-1000	Y	-5817069.3	7.8	24.5	5.8	24.5	6.5	43.5	7.7	27.7	6.5
		Z	1327016.0	11.0	11.8	10.1	11.8	10.5	70.5	16.3	21.6	10.4
7076	Jamaica, B.W.I.	X	1384188.1	9.1	4.0	6.5	4.0	7.1	-30.9	10.2	- 1.9	7.0
	MOTS 40	Y	-5905826.8	6.1	15.4	6.9	15.4	7.5	36.7	8.7	19.3	7.5
		Z	1966367.6	8.9	9.1	8.0	9.1	8.5	53.4	12.7	16.3	8.4
1021	Blossom Point, Md	X	1118061.3	6.5	- 7.3	5.0	- 7.3	5.8	-36.4	8.5	-12.1	5.7
	MOTS 40	Y	-4876472.4	5.1	20.9	4.4	20.9	5.2	19.0	5.3	21.0	5.3
		Z	3942793.7	5.6	0.0	3.9	0.0	4.8	1.0	4.9	0.7	4.9
3402	Semmes, Ala.	X	167291.0	5.2	- 1.3	4.0	- 1.3	4.9	- 9.0	5.3	- 2.5	5.0
	PC-1000	Y	-5482121.9	3.8	20.2	4.1	20.2	5.0	31.6	5.6	22.0	5.0
		Z	3244863.3	4.7	- 1.5	4.5	- 1.5	5.4	15.7	6.4	2.2	5.4

Table 2 (continued)

Station	Name		NAD	σ	NA-1	σ	NA-2	σ	NA-5	σ	NA-6	σ
3401	L. G. Hanscom Field, Mass. PC-1000	X	1513184.2	7.4	-14.5	5.9	-14.5	6.6	-52.4	10.4	-20.9	6.5
		Y	-4463730.2	6.2	33.1	5.9	33.1	6.6	22.4	7.1	32.0	6.7
		Z	4282975.7	6.3	3.4	4.1	3.4	5.0	- 3.4	5.3	2.4	5.1
3106	Antigua Island PC-1000	X	2881872.3	10.6	0.2	10.1	0.2	10.5	-68.2	17.9	-11.1	10.3
		Y	-5372329.3	8.5	29.4	5.1	29.4	5.8	39.2	6.2	31.8	5.9
		Z	1868346.8	11.1	19.7	7 9	19.7	8.5	66.2	13.0	27.2	8.3
3861	Homestead AFB, Fla. PC-1000	X	961792.9	7.4	8.6	4.6	8.6	5.5	-14.6	7.4	5.6	5.3
		Y	-5679312.7	5.1	22.2	3.9	22.2	4.9	37.7	6.0	24.4	4.9
		Z	2729707.6	7.0	3.2	4.1	3.2	5.0	29.7	7.5	7.7	4.9
7040	San Juan, P. R. MOTS 40	X	2465090.5	10.1	- 2.6	8.7	- 2.6	9.2	-61.6	15.5	-12.4	9.0
		Y	-5535082.5	7.7	15.5	5.1	15.5	5.9	28.5	6.5	18.2	5.9
		Z	1985346.2	10.3	- 4.1	7.1	- 4.1	7.7	39.8	12.1	3.0	7.6
7043	GSFC, Greenbelt, Md. PTH-100	X	1130742.6	6.5	- 2.4	4.9	- 2.4	5.7	-31.1	8.6	- 5.9	5.6
		Y	-4831487.8	5.2	36.1	4.6	36.1	5.4	32.1	5.6	36.7	5.5
		Z	3993952.9	5.6	2.2	4.2	2.2	5.1	2.1	5.2	5.9	5.1
7045	Denver, Colo. MOTS 40	X	-1240449.5	2.6	12.1	5.2	12.1	6.0	34.8	7.8	15.2	6.0
		Y	-4760379.7	2.2	1.4	4.2	1.4	5.1	- 3.7	5.3	0.4	5.2
		Z	4048804.6	2.4	7.1	4.2	7.1	5.1	5.6	5.2	7.0	5.2
1042	Rosman, N. C. MOTS 40	X	647539.6	5.5	- 9.8	3.8	- 9.8	4.8	-28.4	6.2	-13.0	4.8
		Y	-5178083.5	4.2	14.7	3.3	14.7	4.4	19.3	4.6	15.6	4.5
		Z	3656534.4	4.9	- 1.6	3.7	- 1.6	4.7	5.5	5.0	- 0.2	4.8
7072	Jupiter, Fla. MOTS 40	X	976297.2	7.2	- 0.2	4.6	- 0.2	5.4	-26.0	7.7	- 4.6	5.4
		Y	-5601549.2	5.0	13.1	4.1	13.1	5.1	27.5	5.9	15.7	5.1
		Z	2880071.8	6.7	- 2.1	4.5	- 2.1	5.4	22.1	7.5	1.9	5.4
7036	Edinburg, Tex. MOTS 40	X	- 828463.9	5.3	2.7	3.9	2.7	4.9	15.6	5.7	4.1	4.9
		Y	-5657604.0	3.8	- 3.3	4.1	- 3.3	5.1	12.8	6.1	- 0.2	5.1
		Z	2816639.7	5.0	4.6	5.0	4.6	5.7	30.8	8.0	9.1	5.7

Table 2 (continued)

Station	Name		NAD	σ	NA-1	σ	NA-2	σ	NA-5	σ	NA-6	σ
1034	E. Grand Fork, Minn.	X	- 521678.9	4.3	2.3	3.0	2.3	4.2	9.7	4.5	3.4	4.2
	MOTS 40	Y	-4242198.1	3.7	1.1	4.2	1.1	5.1	-14.8	6.2	- 1.3	5.1
		Z	4718543.6	3.5	1.3	4.0	1.3	4.9	-15.0	6.1	- 1.1	4.9
1030	Mojave, Calif.	X	-2357214.3	5.7	- 0.9	8.2	- 0.9	8.7	46.4	13.5	6.0	8.6
	MOTS 40	Y	-4646475.7	4.8	7.1	4.0	7.2	4.9	- 0.3	5.2	5.8	5.0
		Z	3668134.6	5.2	- 4.5	4.2	- 4.5	5.1	2.5	5.3	- 3.2	5.1
7037	Columbia, Mo.	X	- 191260.6	3.0	0.0	0.3	0.0	2.9	0.0	2.9	0.0	2.9
	MOTS 40	Y	-4967428.4	2.5	0.0	0.3	0.0	2.9	0.0	2.9	0.0	2.9
		Z	3983084.5	2.7	0.0	0.3	0.0	2.9	0.0	2.9	0.0	2.9
1022	Ft. Myers, Fla.	X	807883.1	7.3	2.0	3.9	2.0	4.8	-20.2	6.7	- 1.8	4.8
	MOTS 40	Y	-5652136.5	5.1	10.7	3.6	10.7	4.7	26.2	5.7	13.5	4.7
		Z	2833327.2	6.8	1.1	4.2	1.1	5.1	26.3	7.4	5.2	5.1
5861	Homestead, Fla.	X	963494.7	7.4					-14.6	7.4	5.5	5.3
	SECOR	Y	-5679883.1	5.1					37.7	6.0	24.4	4.9
		Z	2727946.1	7.0					29.7	7.5	7.7	4.9
5001	Herndon, Va.	X	1088888.6	6.4					-31.0	9.5	-10.0	7.8
	SECOR	Y	-4843087.3	5.1					58.5	9.5	47.0	9.0
		Z	3991667.5	5.6					-15.8	8.1	-26.1	7.7
5333	Stoneville, Miss.	X	- 84972.0	4.1					-20.9	8.6	0.8	6.5
	SECOR	Y	-5328093.9	3.1					- 6.1	10.7	- 5.9	10.7
		Z	3493295.3	3.7					3.0	9.4	-11.6	8.6
5649	Hunter AFB, Ga.	X	832516.7	6.3					-23.2	7.5	- 2.9	5.4
	SECOR	Y	-5349734.8	4.6					33.1	5.7	24.2	5.2
		Z	3360367.9	5.7					13.0	6.6	- 4.4	4.9

3.2 Short-Arc Orbital Mode Adjustment

In addition to the geometric solutions described in the previous section, one adjustment was performed in the short-arc mode using the program described in [5]. Only the optical tracking stations were involved in this adjustment since no timing information was available for the SECOR observations. The results of this adjustment are given in Table 3.

The orbital arcs used in the short-arc adjustment were limited to about ten minutes. These arcs are too short to afford a strong determination of the scale of the network through the adopted value of the GM. Therefore, scale was furnished by constraining the spatial chord distance between Homestead, Florida, and Greenbelt, Maryland, as had been done in the geometric adjustments. This distance and its a priori uncertainty were computed again from the geodetic coordinates of these two stations on the Cape Canaveral datum (i.e., the USCGS high-precision traverse).

The geocentric coordinates of Columbia, Missouri were constrained in order to define the origin of the coordinate system. These geocentric coordinates together with their associated covariance matrix were taken from [6]:

$$X = -191\,290\,\text{m} \pm 3.8$$
$$Y = -4967\,274\,\text{m} \pm 4.1$$
$$Z = 3983\,255\,\text{m} \pm 4.1$$

The differences between the NAD coordinates and the short-arc solution coordinates of Columbia were (NAD - short arc):

$$dx = 32.1\ \text{m}$$
$$dy = -158.8\ \text{m}$$
$$dz = -171.3\ \text{m}$$

In order to be able to compare the short-arc solution coordinates to the NAD coordinates, these shifts were added to the short-arc solution. The resulting coordinate differences appear under the heading "Orbital" in Table 3. The uncertainty of these coordinates was obtained by quadratically removing the

uncertainties of the geocentric coordinates (3.8 m, 4.1 m, 4.1 m) of Columbia from the standard deviations of the short-arc solution, and quadratically adding the uncertainties of the NAD coordinates of Columbia (3.0 m, 2.5 m, 2.7 m).

The geometric mode adjustment that most nearly resembles the orbital mode adjustment in terms of data used and constraints applied is the one designated NA-2. The short-arc solution and the standard deviation between the two was computed by removing the variance of the coordinates of Columbia from the variances of the two solutions and adding the resulting variances. These also appear in Table 3. From the table it is evident that the agreement between the geometric adjustment and the short-arc adjustment is satisfactory at all stations, except at San Juan, Puerto Rico; St. Johns, Newfoundland; and College, Alaska. The blame should probably be placed on the insufficient amount of data available and/or on the poor geometry.

Table 3

Coordinates of the North American GEOS I Optical Tracking Stations from the Short-Arc Orbital Mode Adjustment

Station	Name		NAD	Orbital	σ	Orbital - NA-2	σ
7075	Sudbury, Ontario	X	692 646.1	5.5	6.1	4.8	7.1
	MOTS 40	Y	-4347 225.8	13.7	6.1	4.1	8.2
		Z	4600 298.3	14.0	5.4	5.4	6.9
1032	St. Johns, Newfoundland	X	2602 802.5	170.4	87.4	252.2	111.1
	MOTS 40	Y	-3419 301.2	621.9	275.1	632.6	291.8
		Z	4697 477.3	-475.6	231.2	431.8	234.2
1033	College, Alaska	X	-2299 238.0	94.1	24.5	87.8	28.6
	MOTS 40	Y	-1445 840.4	820.0	31.5	800.7	79.7
		Z	5751 629.0	-546.3	51.0	-526.2	64.7
3903	Herndon, Va.	X	1689 023.7	- 13.8	13.8	- 6.5	17.7
	PC-1000	Y	-4843 194.9	94.5	16.1	- 19.2	21.2
		Z	3991 564.7	13.8	11.6	16.9	15.0
7039	Bermuda	X	2308 230.2	16.9	11.7	- 2.0	14.1
	MOTS 40	Y	-4873 765.5	31.7	6.1	- 0.2	7.9
		Z	3394 389.0	- 3.4	6.3	5.1	8.0
3405	Grand Turk	X	1919 530.5	- 30.8	10.9	- 24.6	12.9
	PC-1000	Y	-5621 245.2	9.5	8.0	- 18.3	9.7
		Z	2315 617.1	7.4	11.1	- 20.6	13.1
3407	Trinidad	X	2979 925.0	- 50.2	17.1	- 46.9	20.4
	PC-1000	Y	-5513 746.9	100.0	10.5	5.3	12.5
		Z	1180 994.8	3.9	18.4	29.0	21.8

all units are in meters

Table 3 (continued)

Station	Name		NAD	Orbital	σ	Orbital - NA-2	σ
3648	Hunter AFB, Ga.	X	832 594.6	4.9	6.9	2.1	8.0
	PC-1000	Y	-5349 690.7	7.7	6.2	- 9.8	7.6
		Z	3360 414.7	3.2	4.9	7.1	8.5
3404	Swan Island	X	642 541.2	-17.9	8.2	2.1	9.2
	PC-1000	Y	-6054 109.5	45.3	8.8	- 3.5	10.4
		Z	1895 518.2	26.9	11.8	32.0	13.4
3657	Aberdeen, Md.	X	1186 826.8	- 7.4	7.6	- 0.1	8.6
	PC-1000	Y	-4785 340.8	19.1	8.5	1.7	9.8
		Z	4032 705.0	5.8	6.1	1.5	6.8
3406	Curacao	X	2251 837.6	-22.7	11.8	-21.7	14.1
	PC-1000	Y	-5817 069.3	37.0	9.0	12.5	10.6
		Z	1327 016.0	28.1	15.6	16.3	18.4
7076	Jamaica, B.W.I.	X	1384 188.1	-17.1	8.8	-21.1	10.4
	MOTS 40	Y	-5905 826.8	- 1.8	8.3	-17.2	10.6
		Z	1966 367.6	31.7	10.3	22.6	12.8
1021	Blosson Point, Md.	X	1118 061.3	-17.3	7.5	-10.0	8.5
	MOTS 40	Y	-4876 472.4	9.4	5.5	-11.5	6.7
		Z	3942 793.7	6.6	5.0	6.6	5.8
3402	Semmes, Ala.	X	167 291.0	- 8.0	6.5	- 6.7	7.0
	PC-1000	Y	-5482 121.0	20.2	6.2	0.0	7.1
		Z	3244 863.3	-10.0	7.6	8.5	8.5

Table 3 (continued)

Station	Name		NAD	Orbital	σ	Orbital - NA-2	σ
3401	L. G. Hanscom Field, Mass.	X	1513 184.2	-28.7	8.9	-14.3	10.2
	PC-1000	Y	-4463 730.2	5.8	9.5	-27.3	11.0
		Z	4282 875.7	21.3	6.2	17.9	7.0
3016	Antigua Island	X	2881 872.3	-27.1	15.9	-27.3	18.6
	PC-1000	Y	-5372 329.3	26.5	11.4	- 2.9	12.3
		Z	1868 346.8	56.2	14.9	36.5	16.7
3861	Homestead AFB, Fla.	X	961 792.9	12.2	6.9	3.6	7.7
	PC-1000	Y	-5679 312.7	11.9	5.6	-10.3	6.6
		Z	2729 707.6	9.4	6.1	6.2	7.0
7040	San Juan, P.R.	X	2465 090.5	-43.8	12.4	-41.2	14.8
	MOTS 40	Y	-5535 082.5	- 9.7	6.5	-25.2	8.1
		Z	1985 346.2	36.2	10.2	40.3	12.2
7043	GSFC, Greenbelt, Md.	X	1130 742.6	7.8	7.1	10.2	8.0
	PTH-100	Y	-4831 487.8	46.4	6.3	10.3	7.6
		Z	3993 952.9	- 5.9	6.1	8.1	7.0
7045	Denver, Colo.	X	-1240 449.5	- 2.8	6.4	-14.9	7.7
	MOTS 40	Y	-4760 379.7	10.2	5.0	8.8	6.2
		Z	4048 804.6	7.6	5.6	0.5	6.5
1042	Rosman, N.C.	X	647 539.6	- 2.1	6.2	7.7	6.6
	MOTS 40	Y	-5178 083.5	21.6	4.6	6.9	5.3
		Z	3656 534.4	-12.4	5.5	-10.8	6.1

Table 3 (continued)

Station	Name		NAD	Orbital	σ	Orbital - NA-2	σ
7072	Jupiter, Fla.	X	976 297.2	-16.4	6.5	-16.2	7.3
	MOTS 40	Y	-5601 549.2	-11.7	5.0	-24.8	6.2
		Z	2880 071.8	-11.7	6.4	- 9.6	7.5
7036	Edinburg, Tex.	X	- 828 463.9	- 6.4	5.1	- 9.1	5.7
	MOTS 40	Y	-5657 604.0	-11.3	5.7	- 8.0	6.8
		Z	2816 639.7	5.6	7.2	1.0	8.4
1034	E. Grand Forks, Minn.	X	- 521 678.9	- 2.9	4.2	- 5.2	4.2
	MOTS 40	Y	-4242 198.1	11.6	5.4	10.5	6.5
		Z	4718 543.6	7.4	5.1	6.1	6.0
1030	Mohave, Calif.	X	-2357 214.3	-35.6	10.2	-34.7	12.7
	MOTS 40	Y	-4646 475.7	15.1	5.0	8.0	6.1
		Z	3668 134.6	-15.7	5.8	-11.3	6.7
7037	Columbia, Mo.	X	- 191 260.6	0.0	3.0	0.0	0.0
	MOTS 40	Y	-4967 428.4	0.0	2.5	0.0	0.0
		Z	3983 084.5	0.0	2.7	0.0	0.0
1022	Ft. Myers, Fla.	X	807 883.1	4.9	5.8	2.9	6.2
	MOTS 40	Y	-5652 136.5	2.6	4.9	- 8.1	5.8
		Z	2833 327.2	7.4	6.4	6.3	7.3

General Information:

No. of unknown stations	30
No. of observations	6247
No. of orbital arcs	86
Degrees of freedom	5641
Standard deviation of the observation of unit weight	1.0

The chord distance between Homestead, Fla., and Greenbelt, Md., as obtained from their Cape Canaveral Datum coordinates (USCGS high precision traverse) was constrained to one part in 750,000.

4. IMPLICATIONS REGARDING THE NORTH AMERICAN DATUM

4.1 Coordinate Transformations

The general relationship between a right-handed coordinate system defined by a certain geodetic datum (geodetic system, e.g., NAD) and one which is defined by the origin in the geocenter, the Z axis in the direction of the CIO, and the X axis in the plane of the Greenwich Mean Astronomic Meridian as defined by the Bureau International de l'Heure (average terrestrial system) [7] is as follows:

$$\begin{vmatrix} X \\ Y \\ Z \end{vmatrix} = \begin{vmatrix} dx_o \\ dy_o \\ dz_o \end{vmatrix} + \begin{vmatrix} x_o \\ y_o \\ z_o \end{vmatrix} + M \begin{vmatrix} x - x_o \\ y - y_o \\ z - z_o \end{vmatrix} + \epsilon \begin{vmatrix} x - x_o \\ y - y_o \\ z - z_o \end{vmatrix}$$

where

X, Y, Z	are the coordinates of a point in the average terrestrial system
x, y, z	are the coordinates of the same point in the geodetic system
M	is the rotation matrix of three rotations $(\theta_x, \theta_y, \theta_z)$ to rotate the geodetic system parallel to the average terrestrial system
x_o, y_o, z_o	are the geodetic coordinates of a point P which is kept fixed during the rotation
dx_o, dy_o, dz_o	are the coordinates of the origin of the geodetic system in the average terrestrial system, after the former has been made parallel with respect to the latter
ϵ	is the scale factor

In practice three main systems have been proposed:

(1) Bursa [8] and Wolf [9] select the point P at the origin of the geodetic coordinate system (i.e., $x_o = y_o = z_o = 0$) and rotate about the axes x, y, z.

(2) Molodensky [10] selects the point P at the origin of the geodetic datum (e.g., at Meades Ranch on the NAD) and rotates about axes parallel to x, y, z.

(3) Veis [11] selects the point P at the origin of the geodetic datum and rotates about axes pointing to the geodetic zenith (z), to the south (x), and to the east (y) in the geodetic horizon.

In our case, since we are not concerned with translations, (1) and (2) are equivalent, and the transformation parameters are restricted to three rotation angles (either in the Bursa/Molodensky or Veis systems) and to the scale factors (all referred to the origin at Meades Ranch). These are determined from the satellite-determined coordinates (X, Y, Z) and the NAD coordinates (x, y, z) of the tracking stations.

The rotation angles are defined as customary: In the right-handed coordinate systems they are positive for counterclockwise rotation as viewed looking toward the origin from the positive end of the rotation axis. For example, in the Veis system, when θ_x is positive the rotation is from the east to the west in the prime vertical plane; when θ_y is positive the rotation is from the north to the south in the meridian plane; and when θ_z is positive the rotation is from the east to the west in the horizon plane (in azimuth).

4.2 Results

In order to detect systematic differences between the satellite-determined station coordinates from the NA-2 solution and the NAD coordinates, transformation parameters (rotations and the scale) were computed from a least squares adjustment utilizing a developed form of the transformation equation above [12]. The stations were considered independent from each other and

only those were used for which it was possible to verify that the NAD coordinates were based on direct ground ties to the first-order triangulation net. Nineteen stations were used in three solutions:

(1) 14 stations in the eastern half of the U. S.

(2) 5 stations in the western half of the U. S.

(3) 19 stations in both the eastern and western halves of the U. S.

The first two solutions were made to detect possible differences between the two halves since they were adjusted separately in the original NAD adjustment. The results are summarized in Table 4. It seems evident that the western data is insufficient to allow meaningful quantitative conclusions. However, it seems evident that there are distortions present. The eastern parameters, on the other hand, indicate a need for a rotation of the NAD coordinate system in the order of one second in azimuth (to the east) and one in the order of two seconds in the prime vertical plane (to the west), together with a possible reduction in scale in the order

Table 4

Datum Transformation Parameters: NA-2 - NAD

		Eastern Half (14 stations)*	Western Half (5 stations)**	Combination (19 stations)
Veis	θ_z (")	-1.2 ± 0.4	0.4 ± 0.9	-0.9 ± 0.3
	θ_y (")	-0.2 ± 0.5	0.2 ± 1.2	-0.2 ± 0.4
	θ_x (")	2.0 ± 0.6	-1.4 ± 1.2	1.2 ± 0.3
Molo-densky	θ_z (")	-2.4 ± 0.5	1.4 ± 1.1	-1.5 ± 0.3
	θ_y (")	-0.3 ± 0.5	0.5 ± 1.1	0.0 ± 0.3
	θ_x (")	-0.3 ± 0.5	0.3 ± 1.2	-0.2 ± 0.4
	ϵ ($\times 10^{-6}$)	-1.3 ± 2.1	0.0 ± 4.7	-1.8 ± 1.6

*Eastern stations: 1021, 1022, 1034, 1042, 3334, 3401, 3402, 3648, 3657, 3861, 3037, 7043, 7072, 7075

**Western stations: 1030, 3400, 3902, 7036, 7045

of 1×10^{-6} (i.e., the NAD distances are too large). Applying these transformation parameters to the NAD would make it conform better to the satellite data. It is likely, however, that these small systematic distortions do not arise from actual systematic errors in the observations but are due rather to errors in the data reduction and adjustment methods utilized in the original NAD adjustment.

Table 5 shows the transformation parameters computed from the NA-5 solution. The resulting rotations are of the same order of magnitude as before, but the scale reduction is about a factor of 15 larger. The latter obviously is the influence of the scale enforced through the SECOR ranges which were put in with a standard deviation of 3.5 m, corresponding on the average to approximately 1: 850,000. (The average range was 3000 km.)

Table 5

Datum Transformation Parameters: NA-5 – NAD

		Eastern Half	Western Half	Combination
Veis	θ_z (")	- 1.1 ± 0.5	0.4 ± 1.0	- 0.9 ± 0.3
	θ_y (")	- 0.2 ± 0.6	0.1 ± 1.4	- 0.2 ± 0.5
	θ_x (")	2.3 ± 0.6	- 1.6 ± 1.3	1.2 ± 0.3
Molo-densky	θ_z (")	- 2.5 ± 0.6	1.5 ± 1.2	- 1.5 ± 0.3
	θ_y (")	- 0.6 ± 0.5	0.7 ± 1.2	- 0.1 ± 0.3
	θ_x (")	- 0.3 ± 0.5	0.2 ± 1.3	- 0.2 ± 0.5
	ϵ ($\times 10^{-6}$)	-22.9 ± 2.3	-23.6 ± 5.6	-23.3 ± 1.8

Table 6 shows the transformation parameters from the NA-6 solution. The rotations are again of the same magnitude. The overriding effect of the chord constraint over SECOR is evident from the $\sim 1{:}4.5$ ratio of the ϵ's taken from the NA-5 and NA-6 solutions.

Table 6

Datum Transformation Parameters: NA-6 - NAD

		Eastern Half	Western Half	Combination
Veis	θ_z (")	-1.2 ± 0.4	0.4 ± 0.9	-0.9 ± 0.3
	θ_y (")	-0.2 ± 0.5	0.2 ± 1.2	-0.2 ± 0.4
	θ_x (")	2.2 ± 0.6	-1.4 ± 1.2	1.3 ± 0.3
Molo-densky	θ_z (")	-2.5 ± 0.5	1.3 ± 1.1	-1.6 ± 0.3
	θ_y (")	-0.4 ± 0.5	0.6 ± 1.1	-0.1 ± 0.3
	θ_x (")	-0.3 ± 0.5	0.2 ± 1.2	-0.2 ± 0.4
	ϵ ($\times 10^{-6}$)	-4.8 ± 2.1	-3.6 ± 4.7	-5.2 ± 1.6

5. CONCLUSIONS

Adopting the NA-6 geometric solution as a standard (since it is based on most of the available data), it seems evident that at least the eastern half of the NAD coordinate system contains inherent systematic distortions expressed by the rotations at Meades Ranch

$\theta_x = 2''.2 \pm 0.6$ (in the prime vertical plane to the west)

$\theta_z = 1''.2 \pm 0.4$ (in azimuth to the east)

and by the scale factor

$\epsilon = 4.8 \times 10^{-6} \pm 2.1$ (NAD distances need to be reduced)

No quantitative conclusion should be drawn on the western half since the available data (the number of stations) seems insufficient.

The same parameters corresponding to the whole NAD coordinate system are

$\theta_x = 1''.3 \pm 0.3$ (rotation in the prime vertical to the west)

$\theta_z = 0''.9 \pm 0.3$ (rotation in azimuth to the east)

$\epsilon = 5.2 \times 10^{-6} \pm 1.6$ (NAD distances need to be reduced)

More details of these calculations may be found in [13].

Acknowledgement

This research was partially supported by NASA Grant No. NGR 36-008-093.

REFERENCES

[1] Mueller, I. I. "Global Satellite Triangulation and Trilateration," Bulletin Géodésique, No. 87, pp. 53-71, 1968.

[2] Peat, Richard P. A Method for Adjusting Simultaneous Range Observations on an Orbiting Geodetic Electromagnetic Satellite. The Ohio State University, MSc thesis, 1967.

[3] NASA/Goddard Space Flight Center. Geodetic Satellite Observation Station Directory. Compiled by Geonautics, Inc., July 1968.

[4] Simmons, L. G. "How Accurate is First Order Triangulation?" The Journal, Coast & Geodetic Survey, April 1950, No. 3, pp. 53-56.

[5] Schwarz, Charles R. The Use of Short Arc Orbital Constraints in the Adjustment of Geodetic Satellite Data. The Ohio State University Department of Geodetic Science Report No. 118, December 1968.

[6] Lambeck, Kurt. "A Spatial Triangulation Solution for a Global Network and the Position of the North American Datum Within It." Presented at the Annual Meeting of the American Geophysical Union, April 1969.

[7] Mueller, Ivan I. Spherical and Practical Astronomy As Applied to Geodesy. New York: Frederick Ungar Publishing Co., Inc., 1969.

[8] Bursa, Milan. "On the Determination of the Direction of the Minor Axis of the Reference Ellipsoid and the Plane of the Initial Geodetic Meridian from Observations of Artificial Earth Satellites," Studia Geophysica et Geodaetica, Vol. 9, No. 1, pp. 14-22, 1965.

[9] Wolf, Helmut. "Geometric Connection and Re-Orientation of Three-Dimensional Triangulation Nets," Bulletin Géodésique, No. 68, pp. 165-169, 1963.

[10] Molodensky, M., V. Yeremeyev and M. Yurkina. Methods for Study of the External Gravitational Field and Figure of the Earth. Jerusalem: Israel Program for Scientific Translations, 1962.

[11] Veis, G. "Geodetic Uses of Artificial Satellites," Smithsonian Contributions to Astrophysics, Vol. 3, No. 9, Smithsonian Institution, Washington, D. C., 1960.

[12] Badekas, John. Investigations Related to the Establishment of a World Geodetic System. The Ohio State University Department of Geodetic Science Report No. 124, 1969.

[13] Mueller, Ivan I., James P. Reilly and Charles R. Schwarz. The North American Datum in View of GEOS I Observations. The Ohio State University Department of Geodetic Science Report No. 125, 1969.


1033
1032
1034
7075
3401
5001
7043
3903
3657
1021
3902
7045
3400
7037
7039
1030
1042
5649
5333
3646
3334
3402
7036
7072
1022
5861
3865
3405
7040
3106
7076
3404
3407
3406
North American GEOS-I Tracking Network
PC-1000
SPEOP
SECOR
SCALE
LAMBERT'S AZIMUTHAL EQUAL-AREA PROJECTION

Fig. 1

EXPERIMENTS WITH WILD BC-4 PHOTOGRAPHIC PLATES

by
Charles R. Schwarz
Ivan I. Mueller
James P. Veach
Daniel H. Hornbarger

Department of Geodetic Science
The Ohio State University
Columbus

Presented at the GEOS-2 Review Conference
NASA Goddard Space Flight Center
June 22-24, 1970

1. Introduction

Studies at The Ohio State University have been concerned not only with the various ways the BC-4 data in the Data Center might be utilized, but also with the various ways the plate reduction itself might be performed for BC-4 or similar plates. These investigations were generally directed toward three broad questions:

1) Must the photogrammetric method of plate reduction be used, or is it possible to obtain satisfactory results by using the astrometric method of plate reduction for a limited area of the plate, a far cheaper procedure?

2) Are better results obtained by using the measured satellite images as independent observations or by using a polynomial curve fit to the measured images? How much information is lost by using only a single fictitious image from a polynomial rather than all the individual images?

3) Can the smoothing effect of a polynomial curve fit be performed more appropriately and with better results by imposing short arc orbital constraints on the adjustment of the measured images?

The first two of these questions are considered in this paper.

2. Astrometric vs. Photogrammetric Plate Reductions

The purpose of this investigation was to find out whether the astrometric technique could be used for the plates taken by the Wild BC-4 camera [303 mm focal length, $33^{\circ} \times 33^{\circ}$ field]: what kind of systematic effects need to be removed a priori or how large a portion of the plate can be reduced without a priori corrections. Three BC-4 plates were used for this investigation although the results for only one are discussed in this paper. The results of the photogrammetric adjustments were used as the standard to which the various astrometric adjustments were compared. The results support previous knowledge and as such are not startling. However, they do graphically demonstrate the kind of systematic distortions that remain after an astrometric adjustment when such a large field of view is used.

2.1 The Photogrammetric Reduction

The distribution of stars and satellite images on the plate is shown in

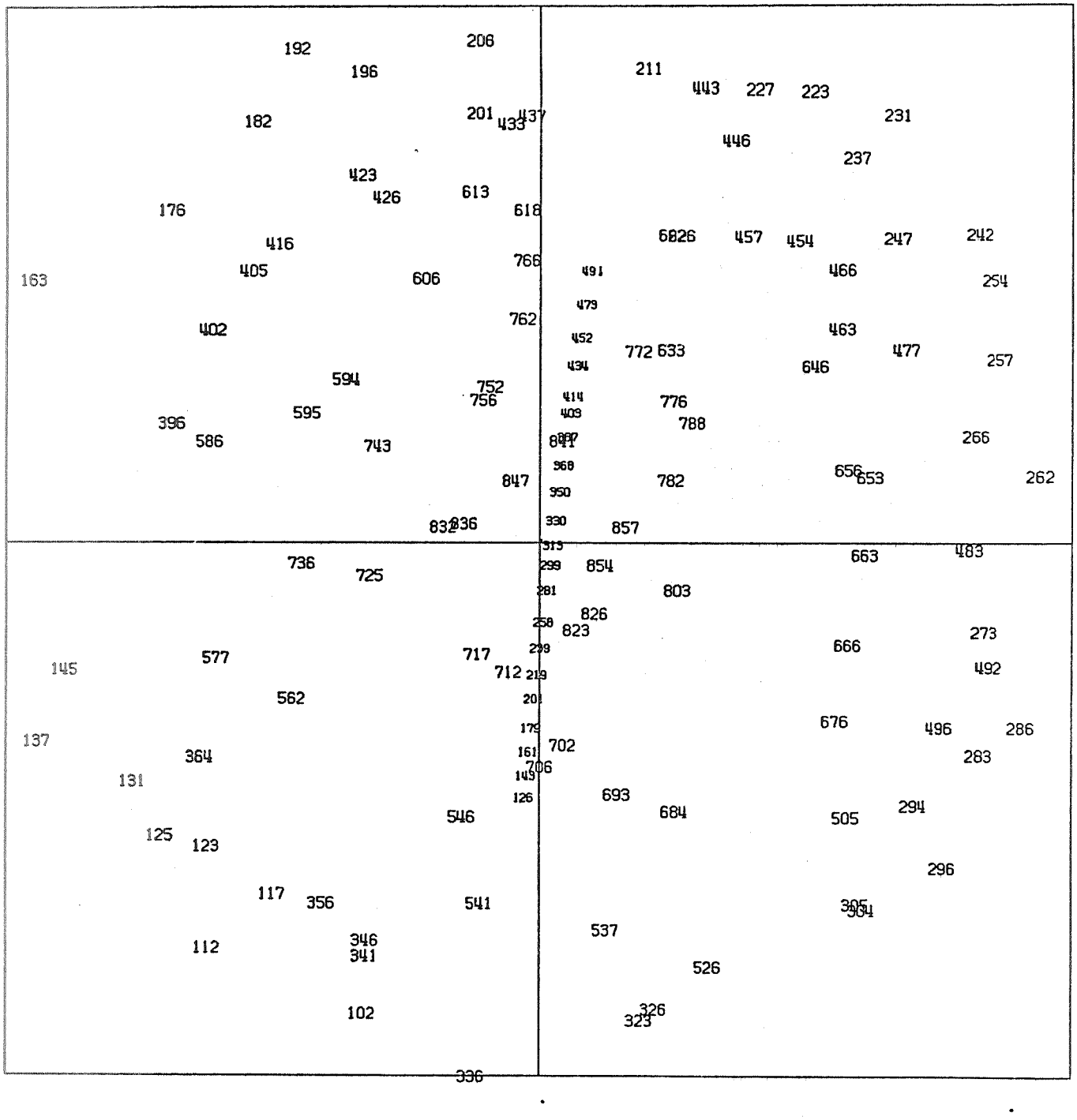

Fig. 1. Plate 6132
Observed Star and Satellite Locations

Fig. 1. The ESSA photogrammetric adjustment utilized 16 unknowns: three angles for orientation; one angle for non-perpendicularity of the comparator axes; the two coordinates of the photogrammetric principle point, or center of the plate; a scale constant for each axis, five parameters to describe radial distortion, and three parameters to describe tangential distortion. The coefficients of the refraction model were not carried as unknowns in this case. The residuals of photogrammetric adjustment are shown in Fig. 2.

2.2 The Astrometric Reduction

In contrast to the photogrammetric reduction in the astrometric technique generally no physical interpretation is attempted except the implicit relationship between the plane of the photograph and a plane tangent to the celestial sphere. The models tested contain six or more plate constants that are coefficients in linear or higher order equations relating object and image space. These constants are not arranged to correct for specific systematic errors (except in the case of a translation term), but they are expected to absorb certain portions of the combination of various systematic errors, such as astronomical refraction, annual and diurnal aberration, errors resulting from unknown orientation of the tangent plane, and even lens distortions in some cases. The astrometric technique is simple in concept and is easy to apply. If accuracies comparable to those from the photogrammetric technique could be obtained, i.e., if the same systematic errors could be removed, its economical aspects would make it extremely appealing.

The following astrometric models were tested:

Model 1: Projective Equations

$$x = \frac{A\xi + B\eta + C}{a\xi + b\eta + 1}$$

$$y = \frac{D\xi + E\eta + F}{a\xi + b\eta + 1}$$

8 (6 independent) plate constants

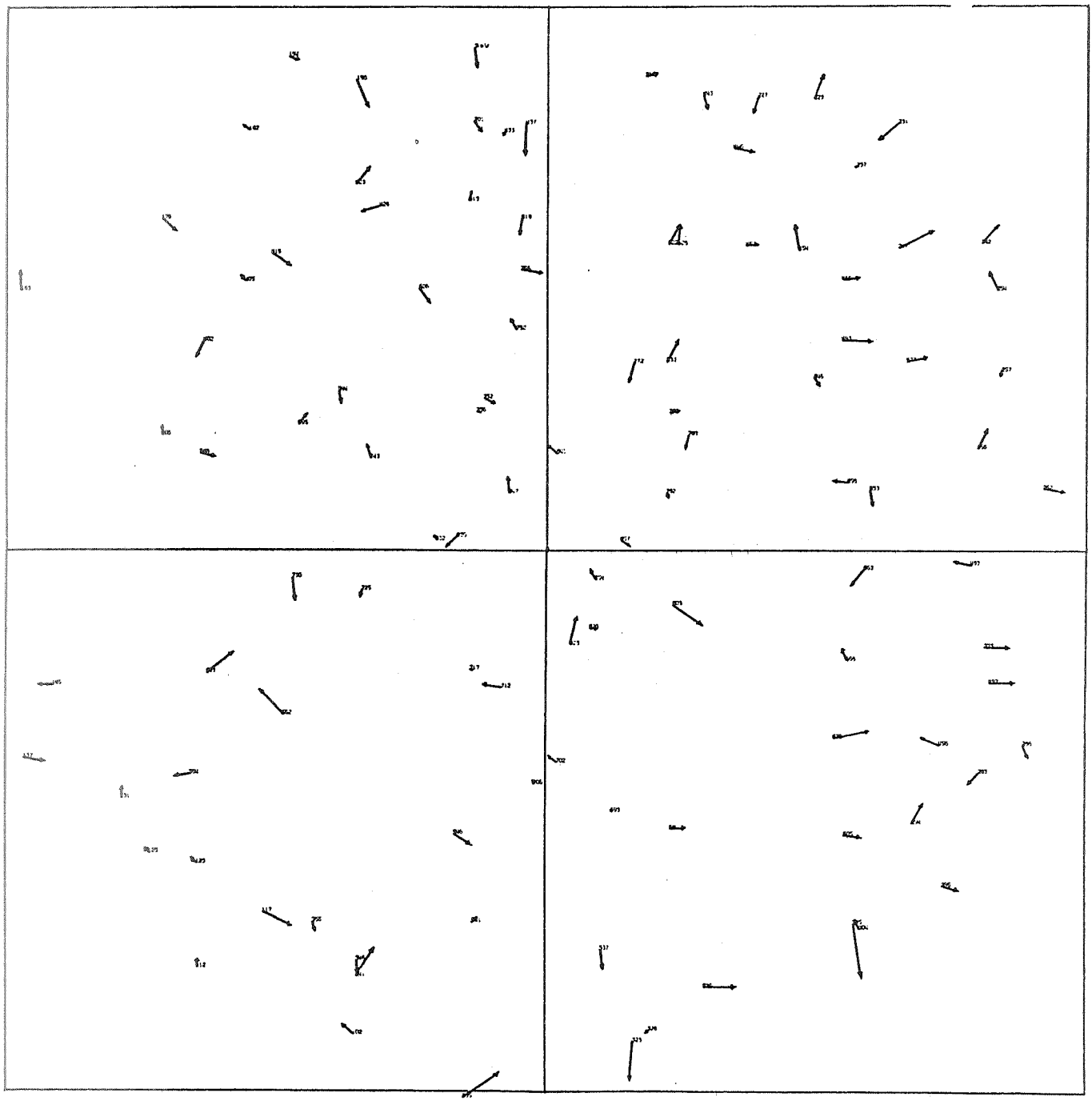

Fig. 2. Plate 6132
Residuals for ESSA Photogrammetric Reduction
m_o = 2.80 microns

Model 2:

$$x = A + B\xi + C\eta + D\xi^2 + E\xi\eta + F\eta^2 + G\xi^3 + H\xi^2\eta + P\xi\eta^2 + Q\eta^3$$

$$y = A' + B'\xi + C'\eta + D'\xi^2 + E'\xi\eta + F'\eta^2 + G'\xi^3 + H'\xi^2\eta + P'\xi\eta^2 + Q'\eta^3$$

20 plate constants

Model 3:

$$x = A\xi + B\eta + C$$

$$y = D\xi + E\eta + F$$

6 plate constants

In this exercise the quantities x and y represent the measured (uncorrected) plate coordinates; ξ and η are the standard coordinates computed from the apparent positions of the reference stars corrected for diurnal aberration and astronomical (Garfinkel) refraction.

In all the astrometric reductions the measured plate coordinates were considered observed quantities and the standard coordinates were regarded as known. All observed coordinates had equal weights. The same image is used to be the origin of the plate coordinate system as the origin of the standard coordinate system.

2.3 Tests and Results

Many tests of the various astrometric models were performed. The following results are of interest:

1) The Projective Equation model was applied to the entire plate area. This involved 106 reference star images. The standard error of unit weight after reduction was 7.81μ. Fig. 3 shows the residual plot. Sizeable systematic errors obviously remain after reduction. The radial distortion effect is especially clear.

2) It was desired to find out how great the effects of decentering distortion were in regard to Model 1. Therefore, decentering distortion was removed from the measured coordinates. Still remaining, then, were radial distortion effects and the nonperpendicularity of the comparator axes. The reductions were

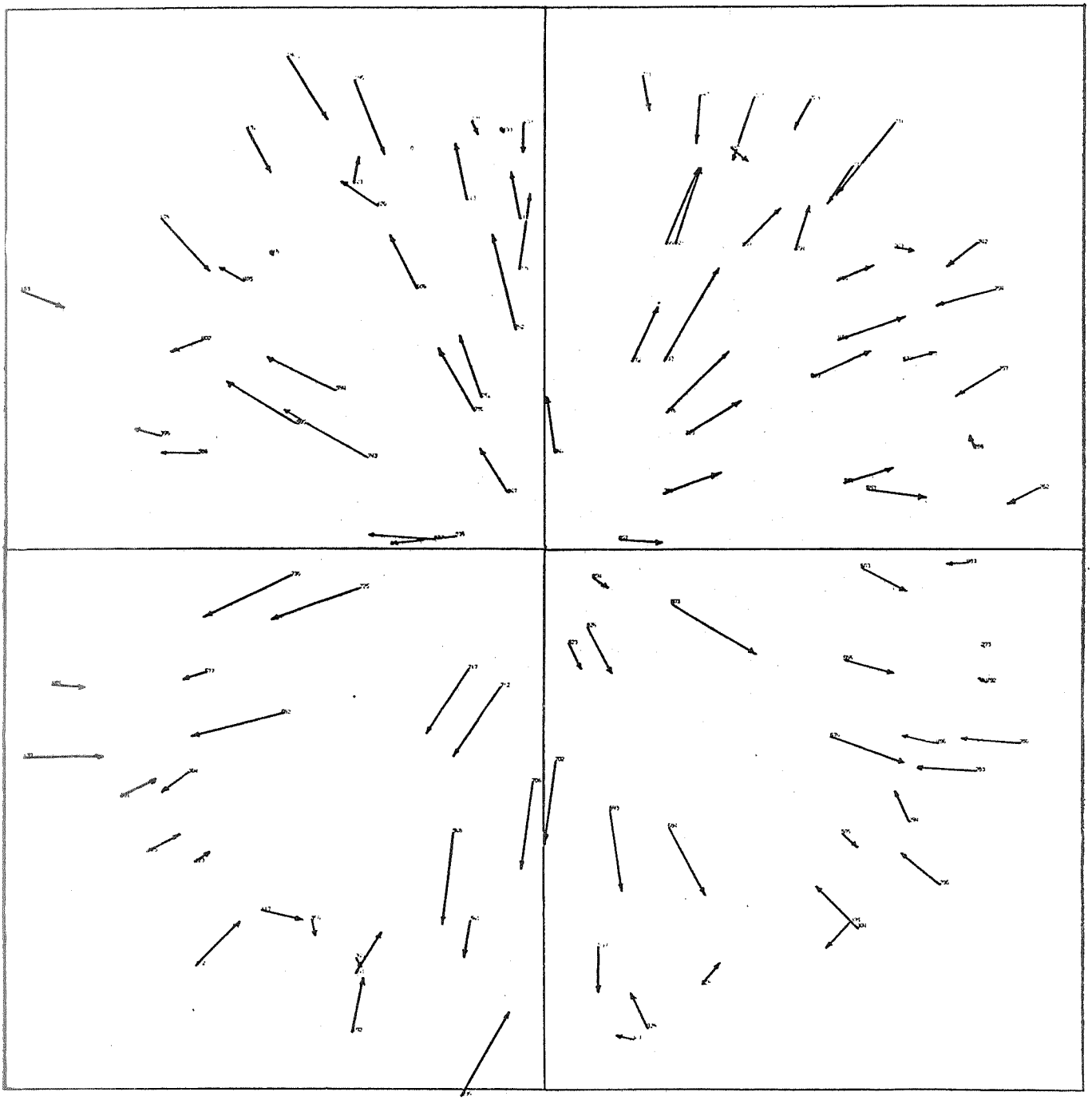

Fig. 3. Plate 6132
Residuals
Projective Equations Applied to Actual Measured Coordinates
$m_o = 7.81$ microns

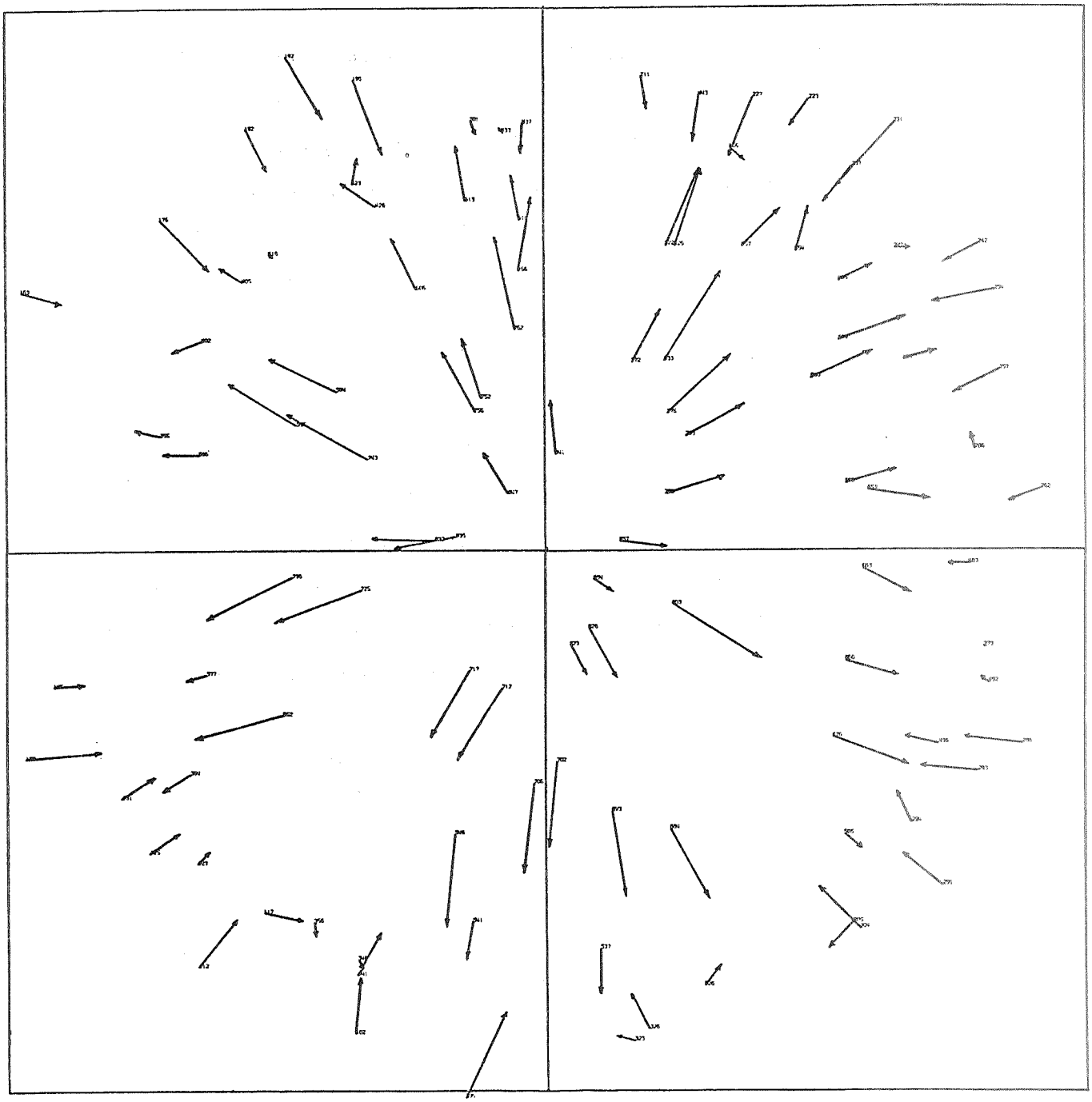

Fig. 4. Plate 6132
Residuals
Projective Equations Applied After Decentering
Distortion is Removed from Measured Coordinates
$m_o = 7.77$ microns

performed as in 1). The change in the plotted residuals compared to those in Fig. 3 appeared to be minimal. The standard error of unit weight was 7.77μ.

3) This time all distortions (including nonperpendicularity of the comparator axes, although this effect is also almost negligible) were removed a priori from the measured coordinates. The reductions were performed as in 1). The residuals are shown in Fig. 5. These, as expected, are almost identical to the residuals of the photogrammetric reduction (Fig. 2). The standard error of unit weight was 2.62μ.

4) We now investigated the largest area to which the projective equations could be applied without precorrecting the image coordinates for lens distortions. After some preliminary investigation, the maximum allowable distortion was set at 16μ. This limit was found to be reached at a radius of about 4 cm. Applying the projective equations to such a restricted area around the center of the plate, the residuals were found to be apparently random and the standard error of unit weight was 3.24μ. When the area was decreased to a circle of 3.4 cm radius, the standard error decreased to 2.40μ, which is even better than that from the photogrammetric adjustment. Fig. 6 shows the residual plot for the 3.4 cm circle. The small magnitude of the residuals, their apparent randomness, and the low standard error of unit weight indicate that the projective equations are applicable in this area without pre-correcting the measured coordinates for lens distortions.

5) The long Turner's method (polynomial out to cubic terms) was applied to the whole plate. The residuals are shown in Fig. 8. They appear moderately random, with a standard error of 3.80. This model is linear in the unknowns, but already contains more unknown parameters (20) than the photogrammetric model.

6) The short Turner Method (linear terms only) was found to be usable only within a circle whose radius is not much bigger than 2 cm. However, if the area is made small enough to produce residuals that are both small and random, then very few usable stars are found in that area (Fig. 9).

From these experiments, we concluded that no astrometric method could

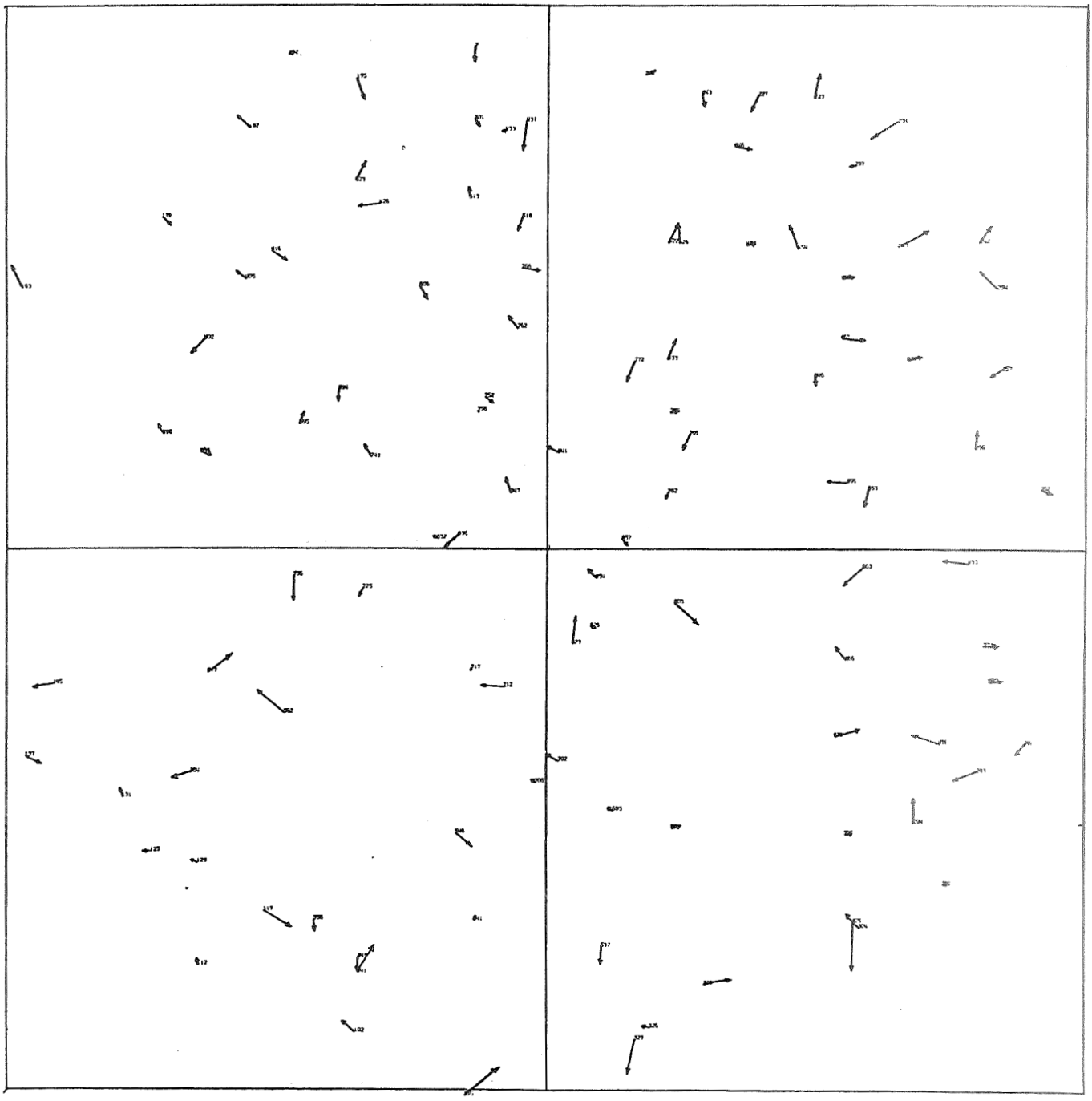

Fig. 5. Plate 6132
Residuals
Projective Equations Applied After All Lens
Distortions are Removed from Measured Coordinates
m_o = 2 62 microns

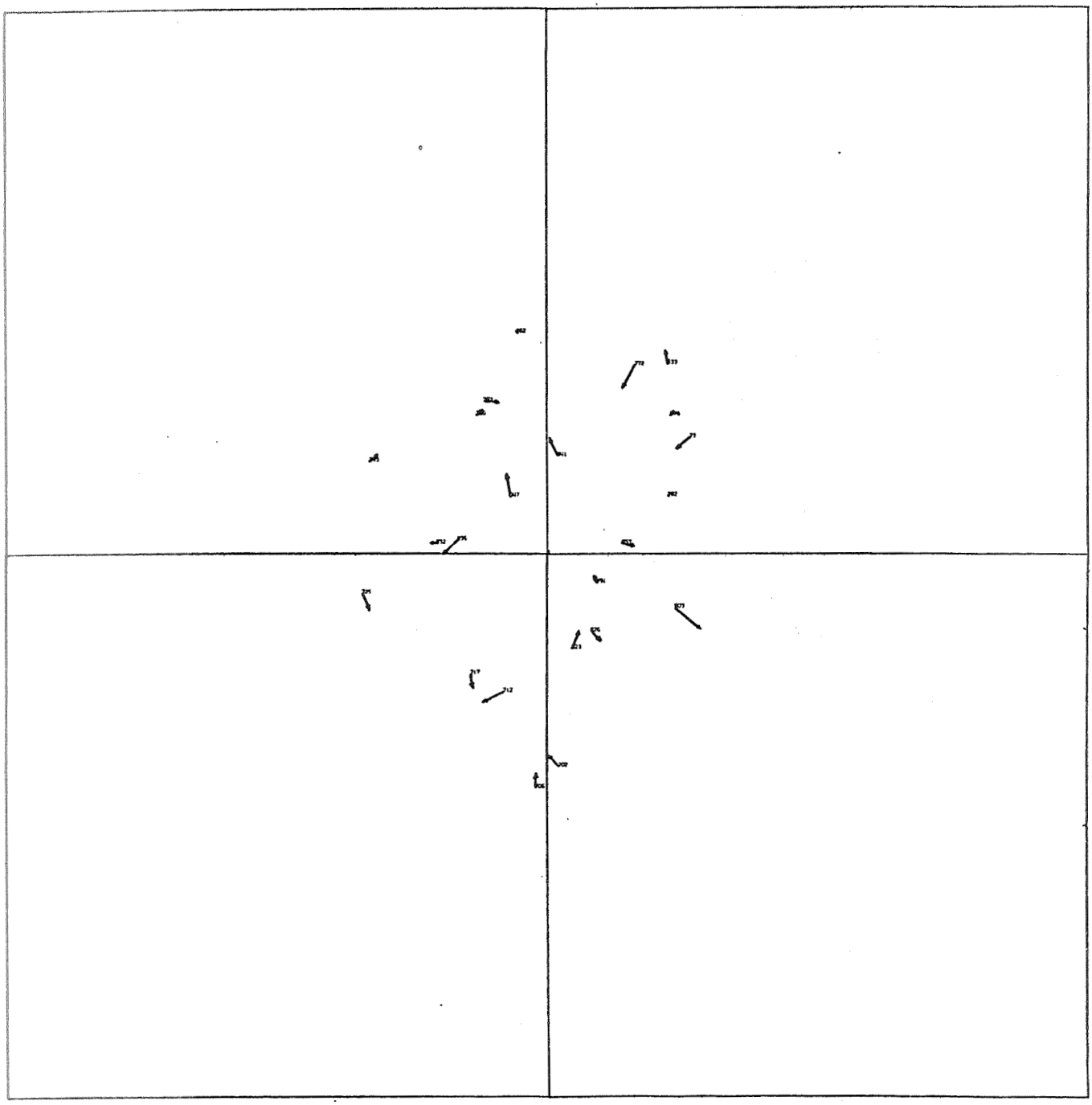

Fig. 6. Plate 6132
Residuals
Projective Equations Applied To Stars Within
3.4 Centimeters of the Plate Center
m_o = 2.37 microns

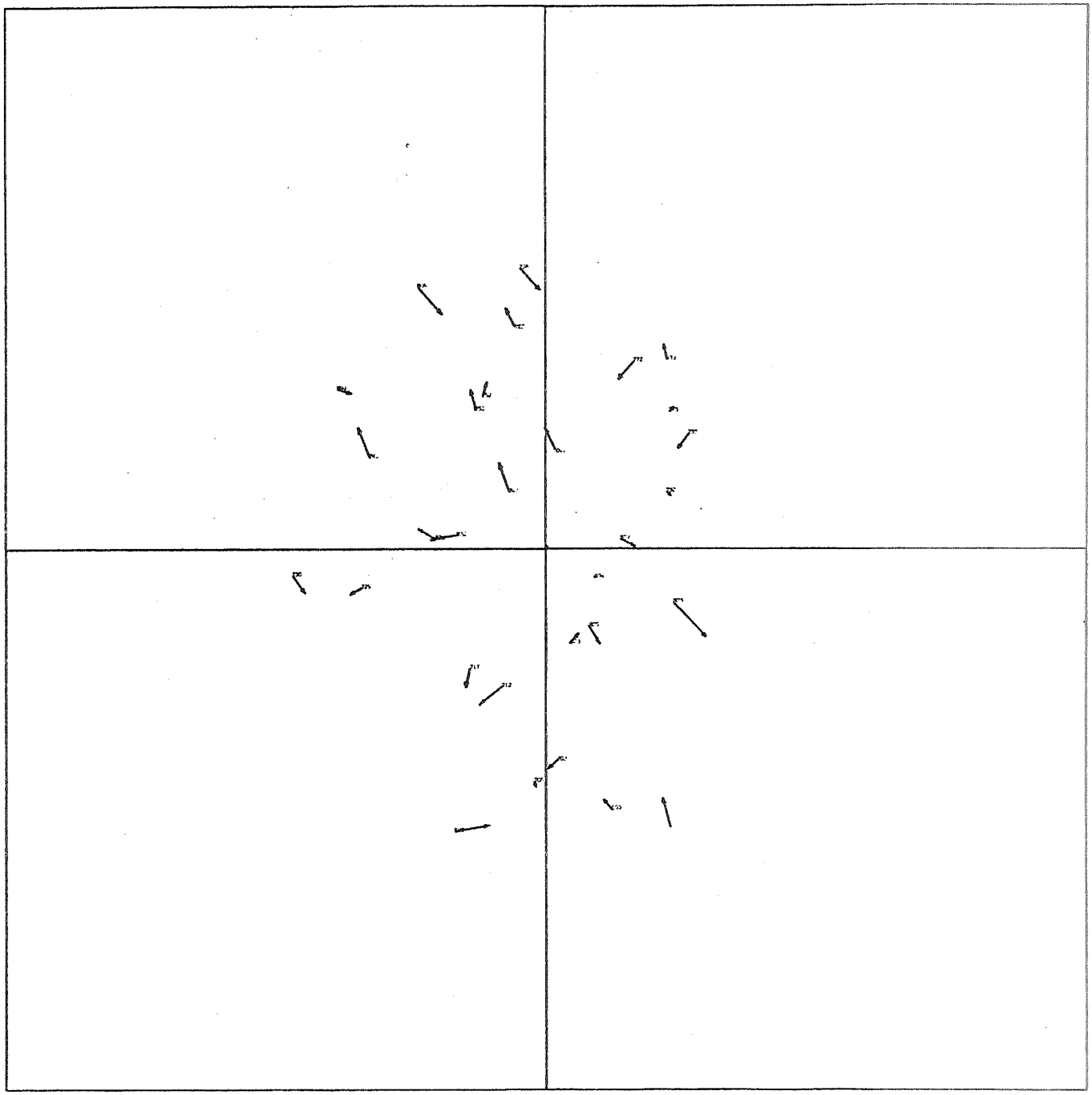

Fig. 7. Plate 6132
Residuals
Projective Equations Applied To Stars Within
4 Centimeters of the Plate Center
m_o = 3.24 microns

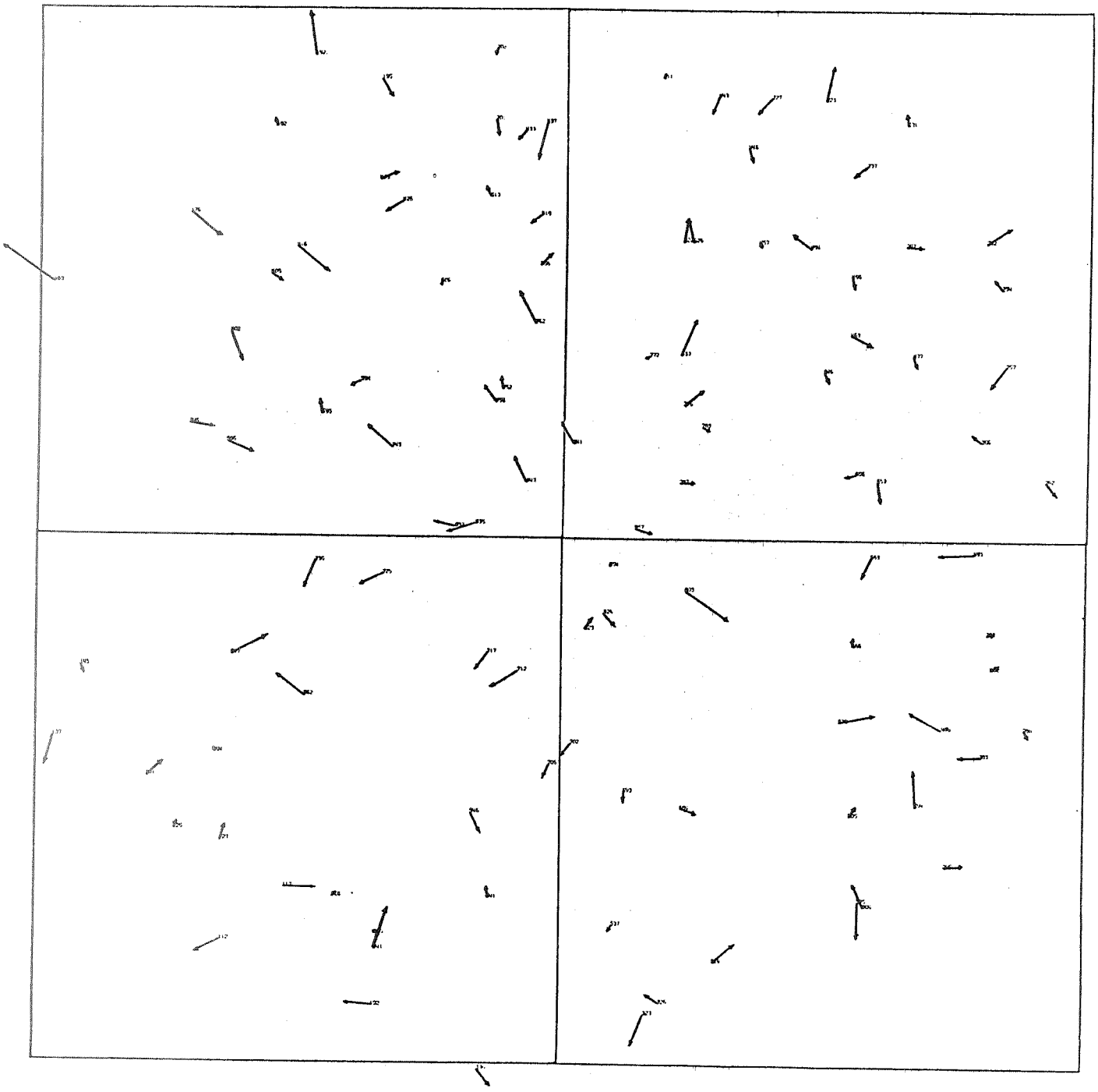

Fig. 8. Plate 6132
Residuals
Long Turner's Method Applied To Entire Plate
m_o = 3.39 microns

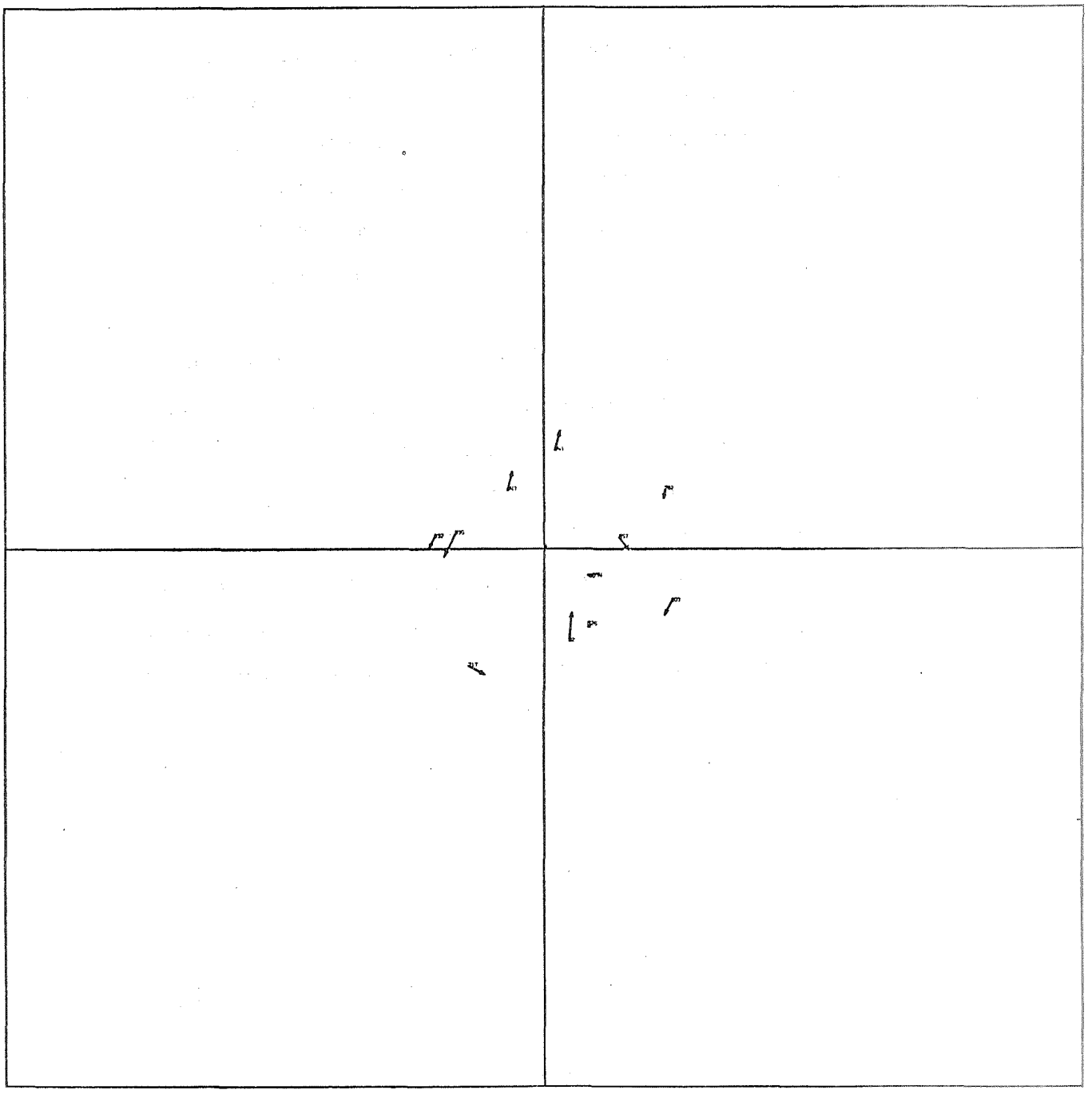

Fig. 9. Plate 6132
Residuals
Short Turner's Method Applied To Stars Within
2.8 Centimeters of the Plate Center
m_o = 2.59 microns

be appropriately used to reduce the entire area of a BC-4 plate. However, if the lens distortion parameters are known and fairly constant for a given camera, then the projective equations (with two conditions) could be used after the measured coordinates have been corrected for lens distortion effects and the apparent stellar coordinates are corrected for diurnal aberration and refraction. If it is not necessary to recalibrate the camera after each exposure, it appears that the projective equations could be applied by means of the procedure just described to obtain results practically equal to those which a complete photogrammetric reduction would provide. If no a priori corrections are made for lens distortions but still the apparent stellar coordinates are corrected for diurnal aberration and refraction, then a confined area not greater than 4 cm (about 8°) in radius from the plate center can still be reduced with good results.

As a final check we reduced each plate astrometrically, using the projective equations, using only stars within 6 degrees of the plate center, and not applying any corrections for lens distortions. The plate constants obtained were then used to compute the direction of a satellite image near the center of the plate. These directions are compared to those obtained by ESSA with the photogrammetric reduction in Table 1.

Table 1

Photogrammetric and Astrometric Coordinates of a Satellite Image Near the Plate Center

PHOTOGRAMMETRIC					ASTROMETRIC
Plate		Hr/Deg	Min	Sec	Sec
2559	α	8	53	38.178	38.169
	δ	60	59	44.06	43.76
5205	α	3	24	4.863	4.857
	δ	53	20	43.16	43.39
6132	α	18	38	52.552	52.611
	δ	55	19	22.36	22.30

The mean departure of an astrometric coordinate from the photogrammetric was only $0.''2$ (0.3 μ) when using the actual measured stars coordinates as input. The maximum departure is $0.''5$, still well below the accidental measurement error level.

3. Multiple Satellite Images Astrometrically

The close agreement between the astrometric and photogrammetric satellite directions at the center of the plate was expected. We next attempted to extend the astrometric reduction to areas away from the plate center.

Two sets of satellite images were chosen, one spaced at 24-second intervals and the other at 17-second intervals. On each plate, astrometric reductions were performed using only stars in the area around each image. Each of those sets of plate constants were then used to compute the direction of the satellite image at the center of the area. Areas of 6° and $3.^\circ8$ radius were used (Figs. 10 and 11).

Considerable overlap of these plate areas is evident. For satellite images at 24-second intervals, there is double and triple overlap of plate areas for the 6° circles, but only double overlap for the $3.^\circ8$ circles. In the case of the 17-second intervals, there is even quadruple overlap of the 6° circles. Since we want to obtain satellite directions that are as independent as possible, we want to eliminate using the same set of stars in two or more reductions as much as possible. This implies the use of widely spaced satellite images and small circular plate areas to minimize overlap of the plate areas. On the other hand, this criterion must be balanced with the need to obtain a reasonable number of stars in each area.

The satellite directions obtained by the astrometric reductions are compared to the directions obtained by the ESSA photogrammetric reductions in Table 2.

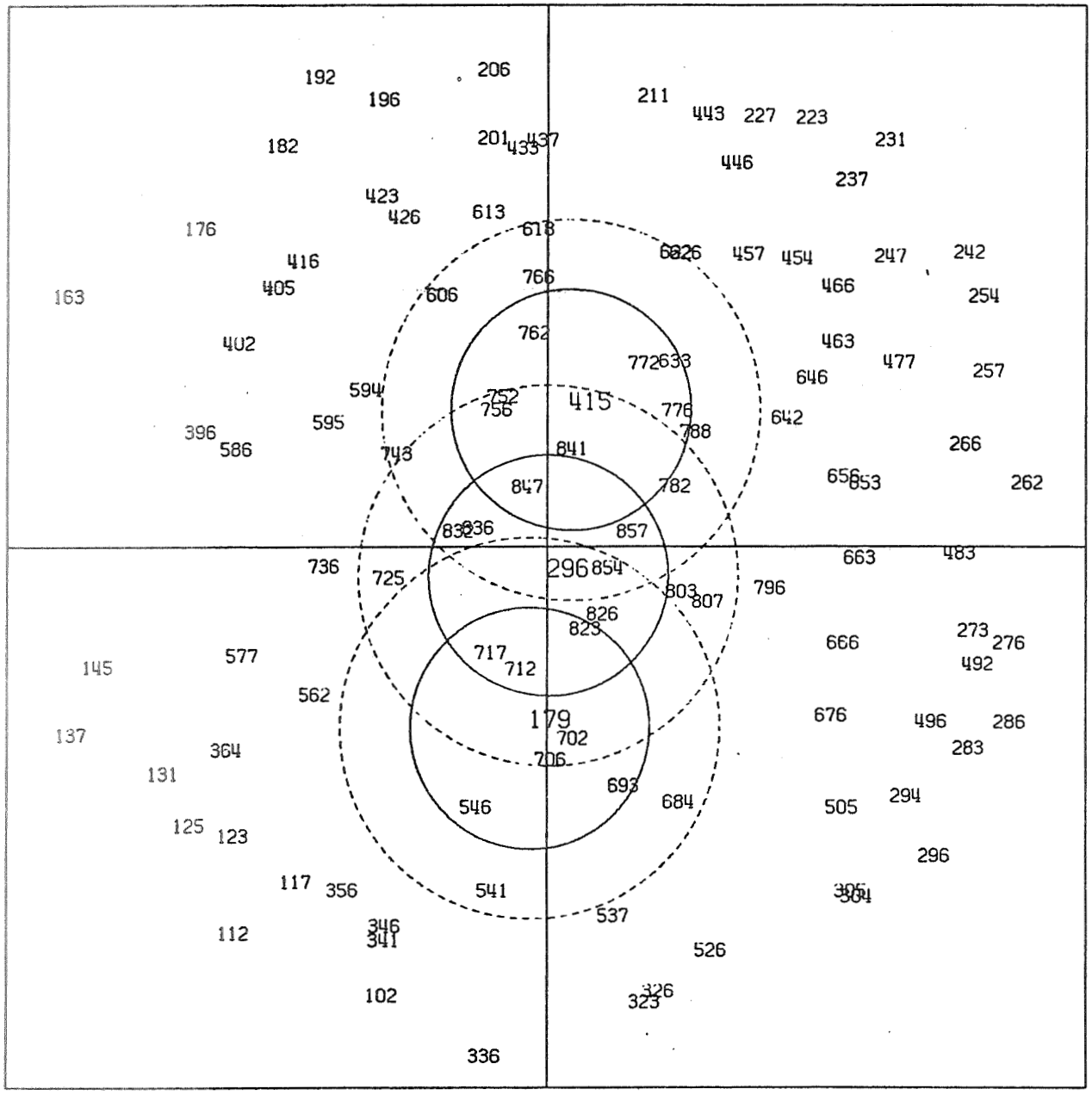

Fig. 10. Plate 6132
Set I Satellite,
24[s] Intervals 3.8° and 6° Circles

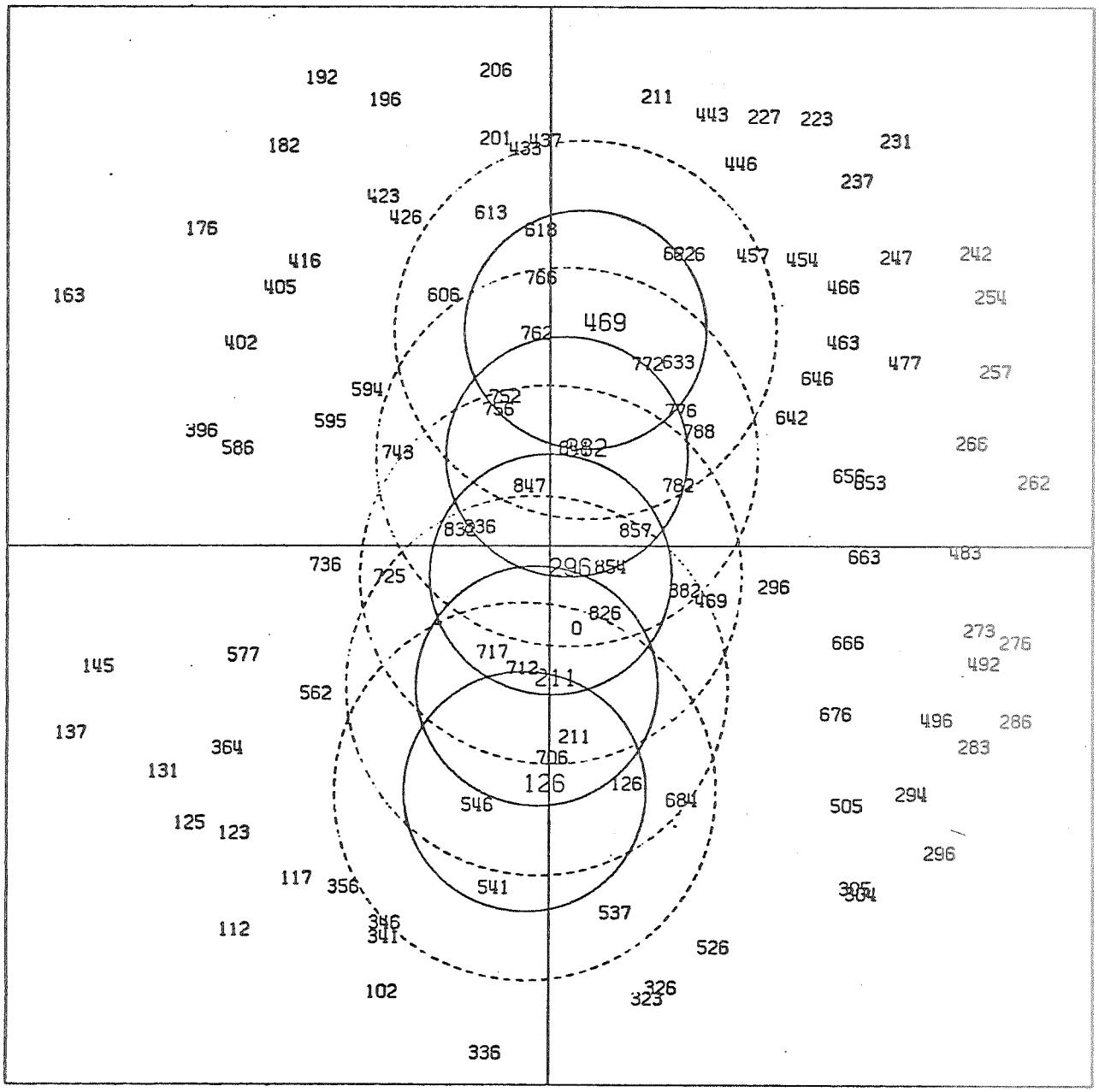

Fig. 11 Plate 6132: Set II Satellite, 17° Intervals
3.8° and 6° Circles

Table 2

Photogrammetric and Astrometric Satellite Directions

Plate 6132

	Right Ascension					Declination				
	Photogrammetric			Astrometric		Photogrammetric			Astrometric	
Set I	h	m	sec	3.8	6.0	°	'	"	3.8	6.0
179	18	05	12.282	-.003	+.054	54	47	50.89	-0.15	+0.20
296	18	38	52.557	+.042	+.054	55	19	22.35	+0.34	-0.06
415	19	16	11.981	-.069	-.105	55	09	26.22	+0.30	+0.34
Set II										
126	17	51	11.497	-.105	+.029	54	22	53.63	+0.49	+0.09
211	18	14	2.952	+.110	+.093	54	59	57.31	+0.63	-0.28
296	18	38	52.557	+.042	+.054	55	19	22.35	+0.34	-0.06
382	19	05	36.885	-.071	-.063	55	16	58.05	-0.16	-0.09
469	19	33	43.956	-.085	-.178	54	48	27.63	+0.37	+0.56

Standard deviations of the differences between the astrometric and photogrammetric coordinates were computed for all plates and are shown in Table 3.

Table 3

Standard and Mean Deviations of the Astrometric from the Photogrammetric Coordinates (numbers in parentheses exclude central image on each plate)

STANDARD DEVIATIONS

	Right Ascension (sec of time)							
	Plate 2559		Plate 5205		Plate 6132		All Plates	
	3°.8	6°.0	3°.8	6°.0	3°.8	6°.0	3°.8	6°.0
Set I	.075	.222	.069	.110	.057	.092	.091	.163
Set II	.138	.232	.076	.038	.096	.110	(.099)	(.213)
	Declination (sec of arc)							
	Plate 2559		Plate 5205		Plate 6132		All Plates	
	3°.8	6°.0	3°.8	6°.0	3°.8	6°.0	3°.8	6°.0
Set I	.85	.41	1.05	.80	.34	.28	.71	.62
Set II	1.03	.81	.78	.92	.48	.32	(.65)	(.66)

The standard errors of unit weight arising from the astrometric adjustment were evaluated for the different plate areas. Tabulated in Table 4 for the satellites of Set I are the standard errors for 6° and 3°.8 radius circles. Included also is the same statistic computed when all known lens distortions were removed from the star coordinates and the adjustment performed for the entire plate.

Table 4

Standard Errors of Unit Weight
($\pm\mu$)

Plate	Image	6°0	3°8	Entire Plate
2559	58	3.22	2.93	3.06
	179	3.27	3.50	
	296	2.60	2.29	
	415	1.95	1.84	
	534	4.45	2.89	
5205	179	3.54	2.73	3.34
	296	3.22	2.85	
	415	3.34	3.08	
6132	179	1.92	2.24	2.26
	296	2.41	2.26	
	415	2.09	2.16	

It was theorized that the smaller plate areas might give better satellite directions than the larger. The experimental results do not seem to have supported this. The poorer distribution and fewer stars may have over-come any advantages of the smaller plate area, or possibly the area was still too large for the astrometric model to successfully accommodate the lens distortions. The standard errors of unit weight do not indicate a lack of accommodation however.

Of more importance is the fact that the smaller plate area did not produce results any less accurate than the larger. Thus the fewer number of stars used did not significantly affect the satellite directions.

The conclusion is that the smaller plate areas are preferable for the following reasons:

1) There is no improvement in the accuracy of the satellite directions from the larger plate areas.

2) Fewer stars are used in more than one reduction per plate, thereby

decreasing the correlation between consecutive satellite directions.

3) The number of stars appearing twice in the same reduction is small.

During this part of the investigation, an additional fact became evident. With proper choice of satellite images, each plate could have been divided into three entirely independent plates. They would be independent in the sense that three astrometric reductions could have been performed without using any star image in more than one reduction. This particular choice of satellite images was not compatible with other parts of the study so it was not attempted here.

The standard deviations in right ascension and declination listed in Table 3, when combined, result in a total standard deviation of about one arc second. It is important to realize that this figure represents only a comparison of the astrometric and ESSA's photogrammetric coordinates. An estimate of the absolute error is unattainable.

A graphical comparison is made in Figs. 12 and 13. Plotted are photogrammetric minus astrometric coordinates; the astrometric coordinates are from the $3^{\circ}.8$ areas Also plotted on the figures are the SAO results from their astrometric reduction when they reduced the data from the same three plates.

From these investigations we may conclude that if one is willing to settle for slightly less than the maximum attainable accuracy, then satisfactory results can be obtained at a great saving by measuring only a few star images in the neighborhood of a desired satellite image and performing an astrometric reduction of each area separately. Furthermore, if the overlap between plate areas is minimized, the satellite directions so obtained should be relatively independent.

4. Polynomial Curve Fits to Satellite Images

Several investigations were made into the methods by which a polynomial curve could be fit to the measured satellite images. We first investigated the possibility of taking several fictitious satellite images from a single curve, fit to all the measured images on the plate. Fig. 14 shows the uncertainty of a

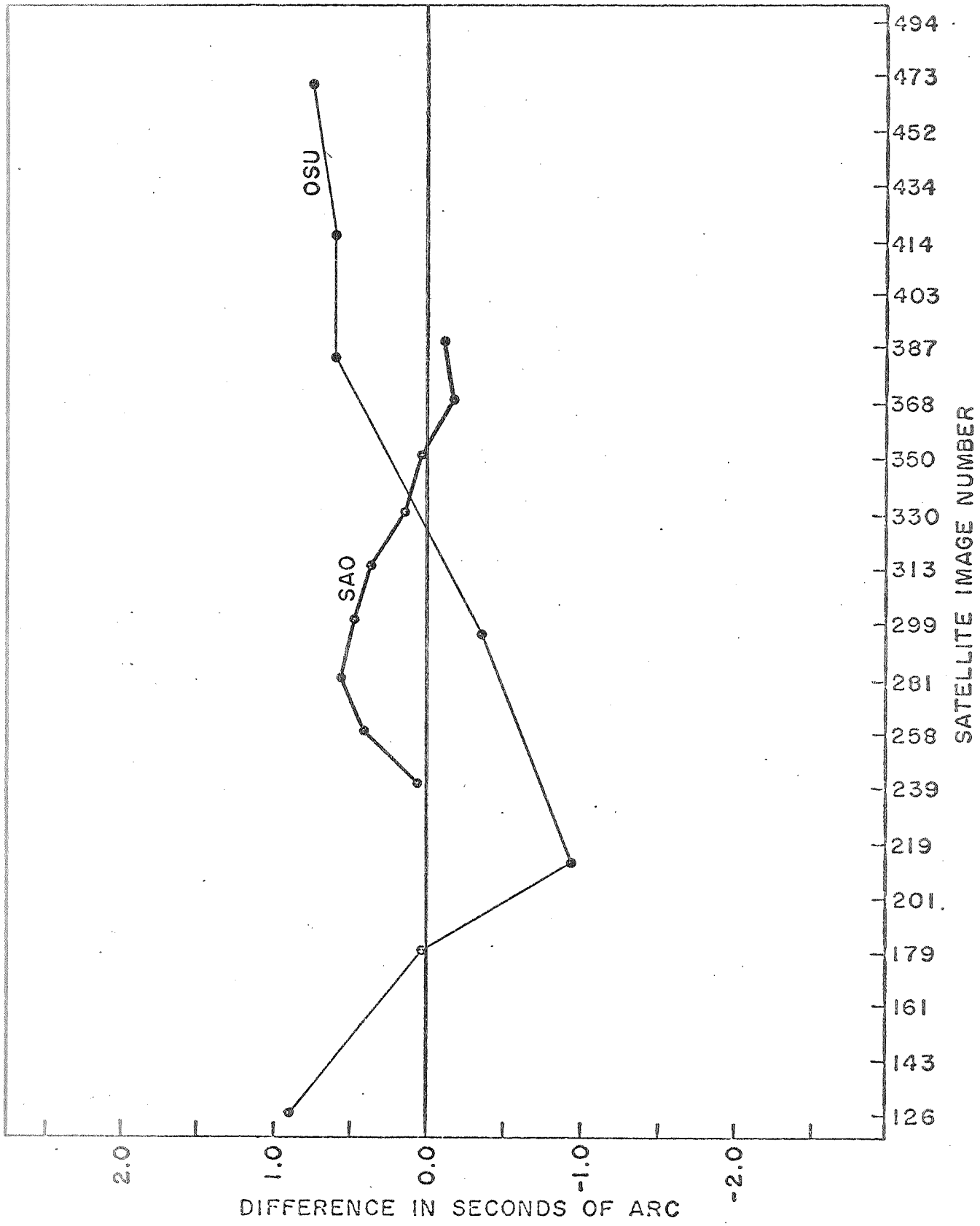

Fig. 12 Plate 6132: Right Ascensions (Photogrammetric - Astrometric)

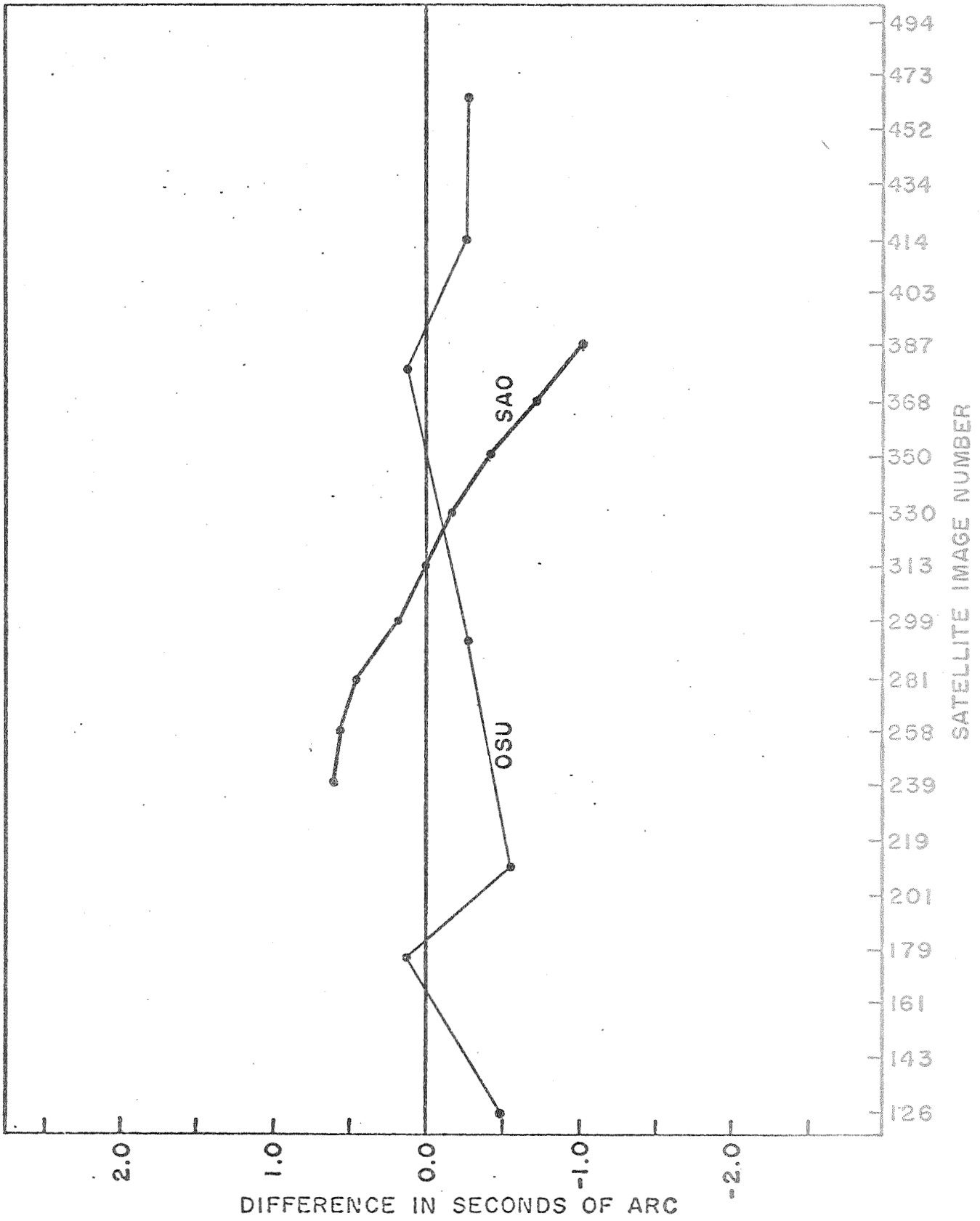

Fig. 13 Plate 6132: Declinations (Photogrammetric - Astrometric)

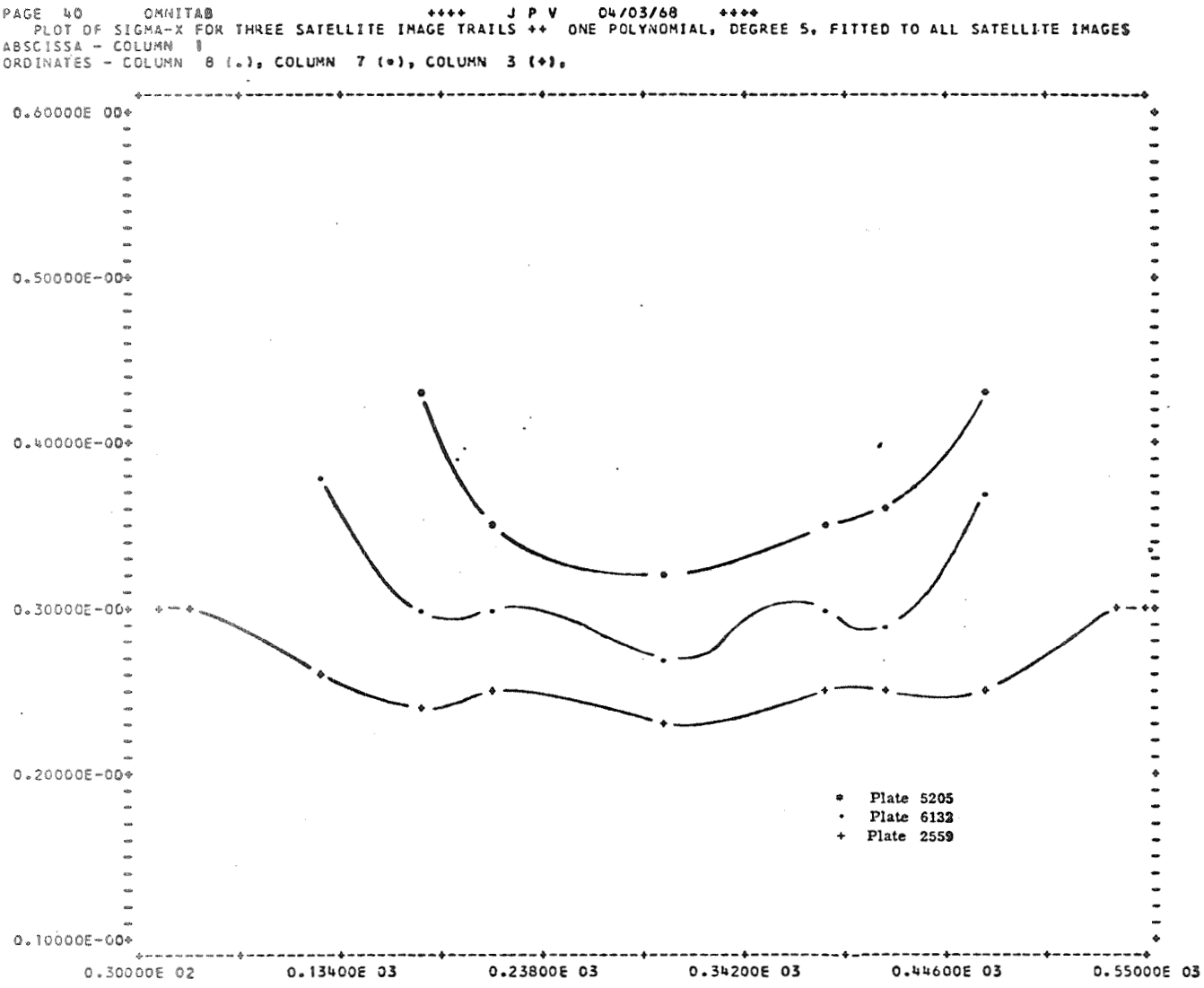

Fig. 14 Plot of Standard Deviations (σ_x) Along ESSA X Polynomials—Degree 5

Plate 2559 — 450 Images
Plate 5205 — 297 Images
Plate 6132 — 360 Images

fictitious image as a function of its position on the curve. There are several inflections in these curves, but the uncertainty of a fictitious image does not really vary too drastically away from the plate center. Fig. 15 and 16 show the uncertainties of a fictitious image for various degree curve fits. For the even degree curve fits, the uncertainty rises in the middle of the plate, while for odd degree curve fits the uncertainty is least at the middle. Also note that in this particular example the lower third degree curve has smaller uncertainties across the plate than the higher fourth degree.

One of our main goals was to investigate the possibility of obtaining several fictitious images from a satellite trail, since it appeared to us that a certain amount of geometrical information is lost by compressing all the information on the plate into a single fictitious image (the previous ESSA practice). We expected that we could break the trail into several shorter trails, fit lower degree polynomials to each of the shorter trails, and obtain fictitious images from each of the shorter curve fits that would each be almost as precise as the single fictitious image from the curve fit to the entire plate. The satellite trail was broken into segments containing 90 images (18 seconds of time). A third degree polynomial curve was found to be appropriate for most of these shorter segments A fictitious image was computed near the center of each of these segments, and a corresponding fictitious image was computed from the fifth degree curve fit to the entire plate. Table 5 shows the coordinate computed from the long polynomial and the difference between it and the coordinate computed from the 90 image short polynomial.

The maximum difference between a fictitious image coordinate computed from the long polynomial versus the ninety image polynomial was 0.51μ. The mean difference was 0.27μ or $0''.17$. When considering both x and y coordinates together, the largest total difference was approximately 0.6μ or less than $0''.5$. This indicates that the shorter polynomials gave nearly the same interpolated values as the longer polynomial.

Another comparison between the various polynomials was made through the precision estimates (σ_x, σ_y) for the coordinates of the fictitious points. The

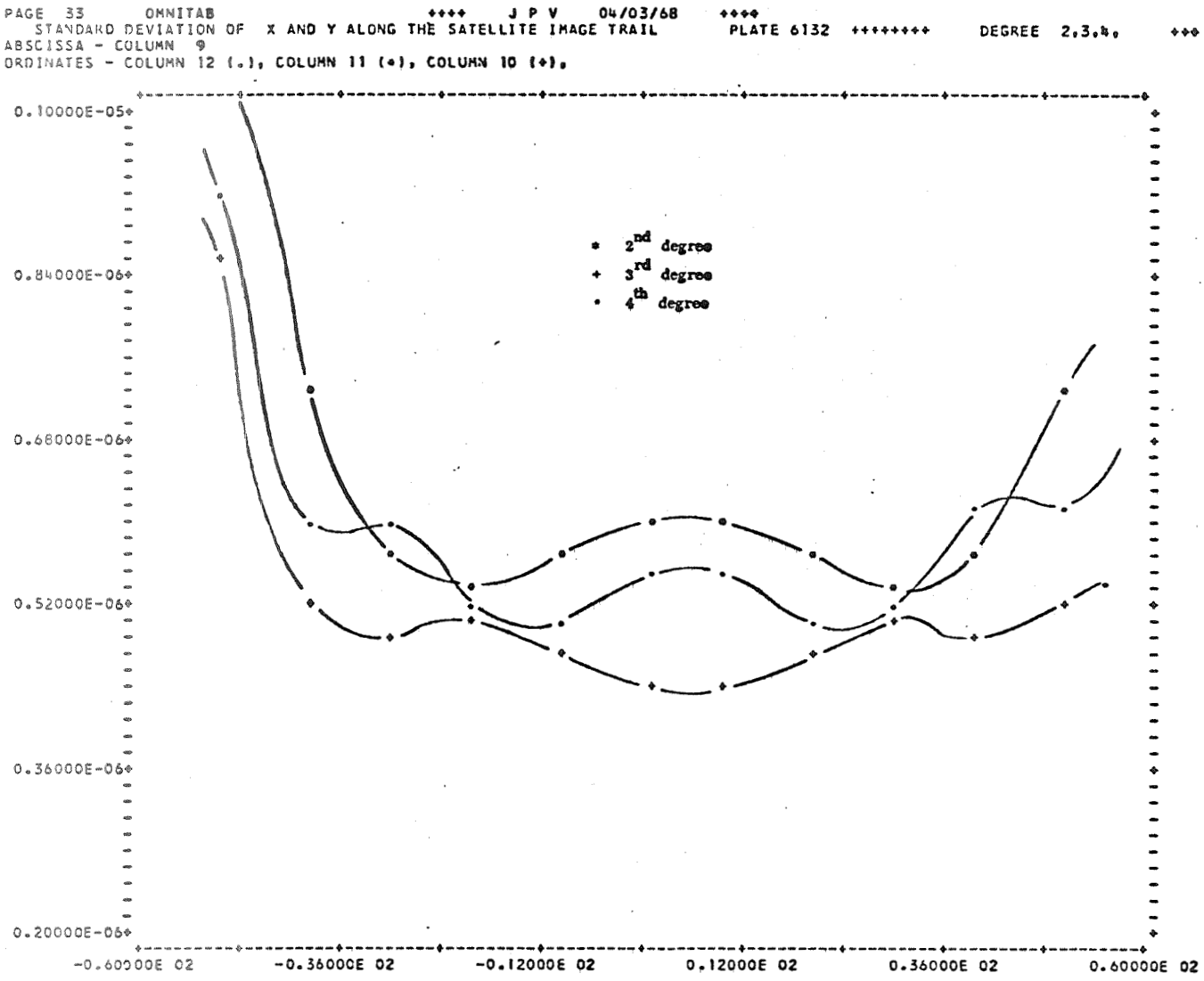

Fig. 15 Plot of Standard Deviations (σ_x) Along X Polynomials of Various Degrees Fitted to 90 Satellite Images — Plate 6132

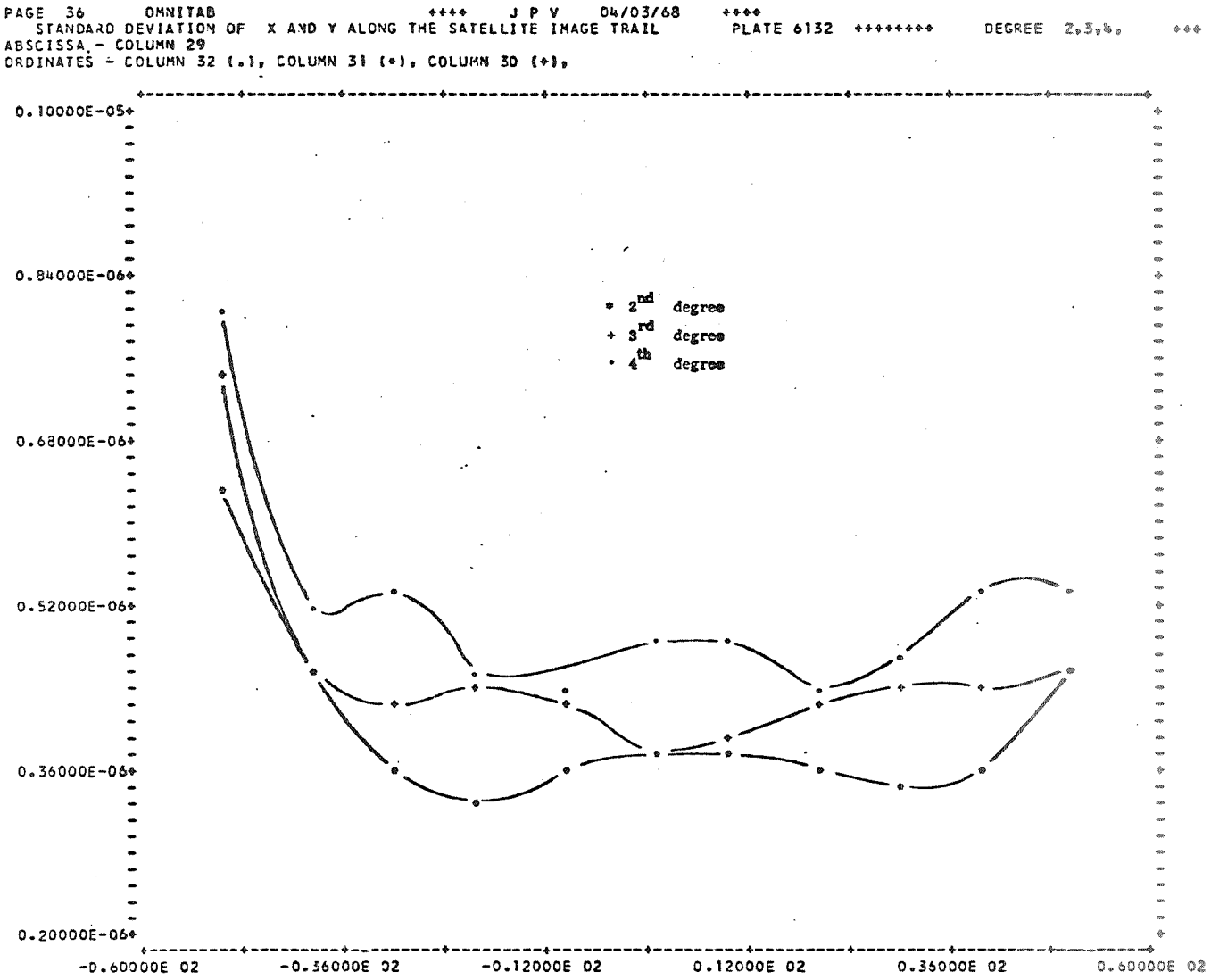

Fig. 16 Plot of Standard Deviations (σ_y) Along Y Polynomials of Various Degrees Fitted to 90 Satellite Images — Plate 6132

Table 5

Computed Coordinates and Standard Deviations

(μ)

Plate 2559	ESSA POLYNOMIAL				SHORT POLYNOMIAL			
Point Number	degree 5 X	σ_x	450 images Y	σ_y	degree 3 X	σ_x	90 images Y	σ_y
57.98700	45 719.26	.30	11 866.65	.30	+.47	.47	-.18	.39
178.98635	25 447.39	.24	5 585.44	.24	+.03	.41	-.37	.42
295.98510	4 873.95	.23	- 1 108.30	.22	+.51	.38	+.30	.39
414.98400	-17 220.80	.24	- 8 611.80	.24	-.08	.37	+.41	.39
533.98330	-40 717.16	.29	-16 928.25	.29	-.09	.41	+.25	.38

Plate 5205	ESSA POLYNOMIAL				SHORT POLYNOMIAL			
Point Number	degree 5 X	σ_x	297 images Y	σ_y	degree 3 X	σ_x	90 images Y	σ_y
178.97325	11 496.48	.43	35 307.67	.33	+.13	.48	+.12	.38
295.97380	3 447.03	.32	1 853.93	.25	+.29	.46	+.45	.34
414.97460	-4 139.90	.36	-30 505.26	.28	-.01	.47	-.13	.39

Plate 6132					degree 3		90 images	
178.98005	-2 762.79	.30	-30 250.24	.29	+.15	.39	-.50	.39
295.97875	267.05	.27	- 4 973.64	.26	-.50	.45	+.21	.48
414.97765	4 004.26	.29	22 670.91	.28	+.49	.43	+.38	.38

precision figures are listed in Table 5. The x and y coordinates of a fictitious satellite image computed from the shorter image trails did suffer a significant decrease in precision. It averaged about 60% for an image near the plate center for the ninety image third degree polynomials and less away from the center.

In summary, the interpolated fictitious image coordinates are very nearly the same from either the long or short image trails. The short image trails yield larger precision estimates, but at least three reliable directions per plate are now available, containing more geometric information than the single fictitious image. Therefore we recommended that shorter satellite image trails and lower degree polynomials be considered for use with BC-4 data, resulting in additional observations per plate.

5. Conclusions

The investigations described in this paper provided some answers to the first two questions raised in the introduction.

1) The astrometric method can be used if one is willing to settle for slightly less than the maximum obtainable accuracy. If a valid set of calibration constants for the camera are available, distortions may be removed and the whole plate reduced with the projective equations. Otherwise, the projective equations may be satisfactorily used to reduce a small area of the plate around the satellite image.

2) The satellite trail can be satisfactorily broken in three shorter trails, and a lower degree polynomial fit to each. Investigations described in another paper [Schwarz, 1969] indicate that information is indeed lost if only a single fictitious image from each plate is used. Better results were obtained both by using three fictitious images obtained from three separate curve fits and by using ten individual images per plate.

REFERENCES

Hornbarger, Daniel H. (1968). "Comparison of Astrometric Plate Reduction Techniques for a Wild BC-4 Camera." Reports of the Department of Geodetic Science No. 106. The Ohio State University, Columbus.

Mueller, Ivan I., and Daniel H. Hornbarger (1968). "Comparison of Photogrammetric and Astrometric Data Reduction Results for the Wild BC-4 Camera." Presented at the Conference on Photographic Astrometric Technique, University of South Florida, Tampa, March 18-20.

Mueller, Ivan I., James P. Veach, and Charles R. Schwarz (1968). "Geodetic Utilization of Satellite Photography." Presented at the Seventh National Fall Meeting of the American Geophysical Union, San Francisco, Dec. 2-5. Abstract in Transactions, American Geophysical Union, Vol. 49, No. 4.

Mueller, Ivan I. (1969). "Analyzing Passive-satellite Photography for Geodetic Applications." Presented at the Fourth Meeting of the Western European Sub-Commission of the International Commission for Artificial Satellites, International Association of Geodesy, Paris, February.

Schwarz, Charles R. (1969). "The Use of Short Arc Orbital Constraints in the Adjustment of Geodetic Satellite Data." Reports of the Department of Geodetic Science No. 118. The Ohio State University, Columbus.

Veach, James P. (1968). "Investigations into the Utilization of Passive Satellite Observational Data." Reports of the Department of Geodetic Science No. 110. The Ohio State University, Columbus.

The work described in this paper was supported by NASA under contract NGR 36-008-093.

EXPERIMENTS WITH THE USE OF ORBITAL CONSTRAINTS IN THE CASE OF SATELLITE TRAILS ON WILD BC-4 PHOTOGRAPHIC PLATES

by
Charles R. Schwarz

Department of Geodetic Science
The Ohio State University
Columbus

Presented at the GEOS-2 Review Conference
NASA Goddard Space Flight Center
June 22-24, 1970

1. Introduction

The purpose of the experiments described in this paper was to determine the feasibility of adjusting satellite directions determined from BC-4 photographic plates in the short arc orbital mode, and to compare the solution obtained in the orbital mode with the corresponding geometric mode solution. These experiments were part of a continuing series of investigations conducted at OSU into the various methods of utilizing passive satellite observational data, especially the data deposited in the National Space Science Data Center. Results of previous investigations are reported in [Hotter, 1967; Hornbarger, 1968; and Veach, 1968].

2. The Form of the Data

The BC-4 camera is providing the data for the establishment of the U.S. World Geometric Satellite Net. This program is directed by the U.S. Coast and Geodetic Survey of the Environmental Science Service Administration, which schedules observations and reduces and analyzes the data. Observations are scheduled only in the simultaneous mode. Successful simultaneous photography by two or more stations is termed an event. Since the passage of the satellite through the field of view takes two to five minutes, "simultaneous" in this context means that the time spans of the two plates overlap. In practice, observations are scheduled and the cameras are aimed so that the overlap is large and the satellite passes near the center of each plate at nearly the same time. The opening of the shutter is controlled by the station clocks. Since each clock defines its own time system, and because of the finite time required for the light from the satellite to reach the stations, the images are not exactly simultaneous. The star images are measured by the USCGS and are used to perform a sophisticated stellar camera calibration, which is summarized in [Hotter, 1967]. The accuracy of the computed direction of the optical axis is thought to be about $0''.5$.

Each satellite image is also measured. For the data presently in the National Space Science Data Center, each satellite image is converted to a right ascension and declination by use of the plate constants. The satellite

images are treated as unknown stars in this conversion. The right ascensions and declinations of the satellite images include atmospheric refraction and stellar aberration, so that the coordinates deposited in the NSSDC are "apparent" in the sense of the apparent place of a star. The time associated with each image is the UT1 of the instant the image was received (mid-opening of the shutter) modified by the addition of 44ms to refer to the old adopted longitude of the U.S. Naval Observatory. In order to obtain the geometrical direction of the center of the satellite, it is necessary to correct the listed coordinates for phase angle, parallactic refraction, and parallactic aberration (light-time correction) [Veach, 1968, p. 91]. The investigations described in this paper apply to the data in the form of satellite right ascensions and declinations, although it is expected that the measured plate coordinates (x,y) will be deposited in the Data Center in the future.

3. Satellite Images and Curve Fitting

The sheer abundance of data available from even a single BC-4 plate creates several interesting problems, since each user must decide how best to use such a huge amount of data. The method employed by the USCGS involves the fitting of polynomials to the satellite trail, but not all investigators agree that this is the best approach. In particular, it may be possible to use only a selected set of images and obtain the same information by processing the data in the orbital mode.

3.1 The Use of Every Single Image

The most obvious approach is to treat each image as a separate observation. However, there are several good reasons why this is unsatisfactory. The main problem is that there is just too much data to be processed for the amount of geometrical information that may be obtained. Although they may provide statistical information, adjacent images are so close together in direction that they provide essentially the same geometrical information. Thus it would appear that the same amount of geometrical information could be obtained from only a selected set of images. Although using the several hundred images on

each plate will not necessarily harm an adjustment, it is usually not advisable to generate superfluous observation equations, since the processing of a greater number of equations on the computer will usually result in a greater accummulation of round-off error. Furthermore, the generation of several hundred observation equations that give little useful information would be a needless waste of computer time. A second consideration is that certain components of error, such as emulsion creep or anomalous refraction, may be nearly the same in adjacent images. This could mean that the errors in adjacent images are significantly correlated, and that an adjustment that fails to take account of this time-wise (or serial) correlation may be biased. A third consideration is that the images on the two or more plates that constitute an event are not simultaneous. Therefore some sort of curve fitting procedure, if only as an interpolation tool, will have to be employed anyway.

3.2 The Use of a Few Selected Images

If only a few, such as ten or twenty images, are selected from the plate, and if these are spaced fairly well apart, then the correlation between adjacent images arising from such effects as emulsion creep and image motion may by neglected. However, if a single plate reduction is done for the whole plate, the directions computed for different images will still be correlated. The plate constants are determined from measurements of the star images, and thus have statistical uncertainties. Since the computed right ascensions and declinations of the different satellite images all involve the same set of plate constants, these will all be correlated; i.e., although the plate coordinates (x,y) of the different images are not correlated, the right ascensions and declinations are. This consideration also applies to photographs of sequences of flashing lights, such as the ANNA or GEOS optical beacons. Since this consideration applies to other photographic systems, such as the MOTS and PC-1000, it will be examined in some detail.

Let the error in the right ascension of a single image be written

$$\delta\alpha_1 = \delta\alpha_{1_m} + \delta\alpha_{1_s} + \delta\alpha_{1_p} \qquad (1)$$

where $\delta\alpha_{1_m}$ is the component of the error arising from accidental measurement error on the comparator, $\delta\alpha_{1_s}$ is the error from shimmer, image motion, and emulsion creep, and $\delta\alpha_{1_p}$ is the error arising from any errors in the plate constants; i.e.,

$$\delta\alpha_{1_m} = \frac{\partial\alpha_1}{\partial x_1}\,\delta x_1 + \frac{\partial\alpha_1}{\partial y_1}\,\delta y_1,$$

etc. There are, of course, several other small sources of error, but consideration of them is not necessary for this analysis. Since the dominating source of error in the plate constants is the errors in the catalogued positions of the stars, it may reasonably be assumed that these components of error are independent. Then the variance of this right ascension may be written

$$\sigma^2\{\alpha_1\} = \epsilon[\delta\alpha_1^2] = \epsilon[\delta\alpha_{1_m}^2] + \epsilon[\delta\alpha_{1_s}^2] + \epsilon[\delta\alpha_{1_p}^2].$$

Similarly, the variance of the right ascension of another image from the same plate is

$$\sigma^2\{\alpha_2\} = \epsilon[\delta\alpha_{2_m}^2] + \epsilon[\delta\alpha_{2_s}^2] + \epsilon[\delta\alpha_{2_p}^2].$$

The covariance between α_1 and α_2 is then given by

$$\text{cov}\{\alpha_1\alpha_2\} = \epsilon[\delta\alpha_1\,\delta\alpha_2]. \qquad (2)$$

This expression will contain the expectancies of six cross products. The measurement errors may reasonably be assumed to be independent, and, if the images are sufficiently well spaced, the errors arising from shimmer and image motion may also be assumed to be independent. However, the errors in the two images arising from the plate constants will be very nearly the same, and will both be very nearly the error in the right ascension of the estimated direction of the optical axis. Thus the only cross product which does not vanish in (2) will be

$$\epsilon[\delta\alpha_{1_p}\,\delta\alpha_{2_p}] \approx \epsilon[\delta\alpha_p^2].$$

The problem presented by covariances between different images is that they lead to large, nondiagonal, weight matrices. Covariance between the right ascension and declination components of one image presents little problem, since it leads only to a weight matrix with 2 x 2 blocks on the main diagonal. However, covariance between different images produces blocks whose dimension is twice the number of images taken from each plate. For example, let n be the number of images used from a plate and let the observation equations be arranged in the order $\{\alpha_1, \delta_1, \alpha_2 \ldots \delta_n\}$. For simplicity, assume that right ascensions and declinations have the same variance σ^2 and that right ascensions are uncorrelated with declinations. Also let

$$r = \frac{\epsilon[\delta\alpha_p^2]}{\sigma^2}$$

be the correlation between any pair of right ascensions or declinations. Then the covariance matrix for the observations on a single plate is

$$\sigma^2 \begin{array}{c} \begin{array}{cccccccc} \alpha_1 & \delta_1 & \alpha_2 & \delta_2 & & \alpha_n & \delta_n \end{array} \\ \left(\begin{array}{cccccccc} \underline{1} & 0 & r & 0 & \ldots & r & 0 \\ & \underline{1} & 0 & r & \ldots & 0 & r \\ & & \underline{1} & 0 & \ldots & r & 0 \\ & & & & & \vdots & \vdots \\ & & & & & \underline{1} & 0 \\ & & & & & & 1 \end{array} \right) \end{array} . \qquad (3)$$

The total weight matrix for the adjustment of all observations on all plates is made up of blocks such as this along the main diagonal. Since this matrix is highly patterned, its inverse may be formed analytically with little trouble. However, most computer programs for the adjustment of satellite directions are not set up to deal with correlations of this type, since a rigorous treatment of these correlations would necessitate storing the observation equations arising from all the images on a plate in the machine at the same time,

and this would result in a somewhat cumbersome program. The orbital constraint program used in these experiments will take account only of correlation between the right ascension and declination of a single image, and this is also true of the geometric mode program used for the comparisons described in section 4. Therefore, it is reasonable to consider what will happen if these correlations between different images are neglected and a diagonal weight matrix is used.

First, the solution will still be unbiased even if the wrong weight matrix is used [Hamilton, 1964, p. 146]. However, the solution will not have the property of minimum variance, since this requires that the weight matrix be inversely proportional to the covariance matrix of the observations. Let the weight coefficient matrix of the solution obtained using a diagonal weighting matrix be denoted Q_D, and let that of the minimum variance solution be denoted Q_{MV}. Then

$$Q_{MV} \leq Q_D$$

since Q_{MV} is minimum by definition. However, it is also possible to find an upper bound for Q_D in terms of Q_{MV} [Magnus and McGuire, 1962, p. 469]. This is given by

$$Q_D \leq \frac{1}{4}(\lambda_{max} + \lambda_{min})\left(\frac{1}{\lambda_{max}} + \frac{1}{\lambda_{min}}\right) Q_{MV}$$

where λ_{max} and λ_{min} are the maximum and minimum eigenvalues of the true correlation matrix of the observations. The correlation matrix in (3) is highly patterned, and its eigenvalues turn out to be a function only of the correlation coefficient r and the number n of images used from the plate. The applicable values are

$$\lambda_{max} = 1 + (n-1)r ,$$

$$\lambda_{min} = 1 - r .$$

The factor $\frac{1}{4}(\lambda_{max} + \lambda_{min})\left(\frac{1}{\lambda_{max}} + \frac{1}{\lambda_{min}}\right)$ is tabulated in Table 1 for r = 0.06

and r = 0.1. These correlation coefficients were used because they represent the correlation between individual images on BC-4 plates for the 300 mm and 450 mm lenses, respectively. The interpretation of this table is that the solution obtained by neglecting correlations between different images is no worse than this factor times the covariance matrix of the minimum variance solution. Thus it is possible to make a quantitive judgment as to whether or not the worsening of the solution caused by neglect of these correlations is tolerable.

Table 1
Worsening Factors for the Effect of the Neglect of Correlations Between Observations

Number of Images per Plate	Worsening Factor	
	r = 0.06	r = 0.1
1	1.0	1.0
2	1.0036	1.010
3	1.007	1.021
4	1.013	1.034
5	1.019	1.049
10	1.062	1.146
15	1.117	1.260
20	1.179	1.383
25	1.245	1.511

3.3 Curve Fitting and the Orbital Constraint

In the method used by ESSA to process the BC-4 plates, there is no problem of correlation between images, since only one image is considered and one pair of observation equations per plate is generated. This method entails the use of two polynomials to describe the trail of the satellite across the plate, and a single "fictitious image" is computed from these polynomials. Since the polynomial curve fitting smoothes out measurement error, shimmer,

and other errors, this fictitious image is of higher quality than any of the single images. The two polynomials describe the plate coordinates x and y as functions of time, where the x and y axes lie in the photographic plate and are oriented in the direction of, and perpendicular to, the approximate direction of the satellite trail. (The ESSA computations never involve the right ascension and declination of each image.) The satellite trail on the plate appears to be a straight line to the unaided eye; however, careful analysis shows that higher degree polynomials fit significantly better [Veach, 1968, p. 73]. Normally fifth degree polynomials are used, but seventh degree polynomials have also been used, especially for the ECHO plates which generally have a greater number of images than PAGEOS plates. The coefficients of the polynomials are determined by least-squares curve fitting to the corrected x and y plate coordinates. The fictitious image is computed by selecting an epoch, usually specififed as the UT1 of the time the light left the satellite, correcting this epoch for light travel time, transforming it into the time system in which the curve fitting was done (e.g., the station clock system), and evaluating the x and y polynomials for the epoch. The light-time correction and the transformation between time systems is discussed in detail and an example of the computations is given in [Veach, 1963, p. 100].

The USCGS procedure of using two polynomials has the effect of collapsing all of the images into a single image, and thus may be viewed as an information compression technique. Thus an important question is whether any significant information is lost in the compression process. A companion question is whether the information contained in the single fictitious image could be obtained by using some subset of the images on the plate. Another question, discussed by [Veach, 1968] and by [Hornbarger, 1968], is whether the same information could be obtained by dividing the plate into small areas and doing an astrometric plate reduction (which is much cheaper than the photogrammetric reduction), fitting polynomials, and obtaining a fictitious image for each area.

The technique of fitting a curve to the satellite trail has a certain intuitive

justification; since the path of the satellite in space is a smooth curve, its trail on the photographic plate should be constrained to be a smooth curve also. The problem is that the curve fit uses too many parameters to describe the constraint. If fifth degree polynomails are used, a total of twelve parameters are used to describe the trail on each plate. It two plates are involved in the event, a total of 24 independent parameters are used to describe the motion of the satellite, and if three plates are involved, 36 independent parameters are estimated. However, the path of the satellite should be equally well described by the six parameters of a Keperian or other simple orbit model for the two to five minutes spanned by the plate. It follows that the excess over six of curve fitting parameters are superfluous, and the problem is said to be "overparameterized."

The danger of overparameterization is that the observations may fit the constraint too well. Brown claims that there are several possible sources of error that are periodic across the plate with periods of the order of one or a few minutes [Brown, 1967, p. 91]. The curve fit will conform to these low frequency components of error, rather than constrain the images to the true projection of the satellite path onto the plate. Brown concludes that a low frequency error whose amplitude is one micron could easily be accommodated by the curve fit, and that this error could occur in and dominate the fictitious image. It appears then that the images on the satellite trail should be constrained, but the constraint should be expressed by short arc methods rather than by polynomial curve fitting.

4. Experiments Performed with BC-4 Plates

In order to answer some of the questions raised in the previous section, a selection of BC-4 data obtained from the NSSDC was processed by a short arc orbital constraint program . In order to afford a comparison with the geometrical approach, much of the same data was also processed by a geometric mode adjustment program. Several series of experiments were performed. These experiments used data from the following four BC-4 stations:

6001 Thule, Greenland

6002 Beltsville, Maryland

6003 Moses Lake, Washington

6038 Revilla Gigedo Island, Mexico

The first series of experiments used 12 plates and the second series used 45 plates. Five adjustments were performed in each series: 20 individual images from each plate were adjusted in both the short-arc and geometric modes; 10 individual images per plate were adjusted in both the short-arc and geometric modes; and a single fictitious image per plate, analogous to the ESSA fictitious image, was adjusted in the geometric mode. From these experiments it appeared that the most information could be obtained by processing 20 individual images per plate in either the short-arc or geometric mode, although some allowance must be made for the worsening of the solution if the correlation between different images on the same plate is neglected. The way in which the data was selected appeared to have at least as great an effect on the solution as the mode in which the data was processed.

The third series of experiments concerned a minimal data set consisting of nine plates and five events; the fourth series involved 74 plates, which constituted all the data available from the four stations. Nine adjustments were performed in the 74 plate series. Their characteristics were

(1) orbital mode, 20 individual images per plate (obtained by second-order interpolation using three points)

(2) orbital mode, 10 individual images per plate

(3) geometric mode, 20 individual images per plate

(4) geometric mode, 10 individual images per plate

(5) geometric mode, 1 fictitious image per plate

(6) geometric mode, 3 fictitious images from 3 separate curve fits per plate

(7) geometric mode, 3 fictitious images from 3 separate curve fits per plate

The input to the curve fitting procedure was the fully corrected observations obtained by applying corrections for parallactic refraction, light travel time, and phase angle effect to the data furnished by the Data Center (magnetic

tape Astro 221). The curve fits were performed in terms of orthogonal polynomials, with the degree of the polynomial depending on the declination of the satellite. Fifth-degree polynomials were used for low declinations, seventh-degree for moderate declinations, and ninth-degree for very high declinations.

The last two experiments utilized the orthogonal polynomial curve fits prepared by the Hawaii Institute of Geophysics ["Orthogonal Polynomial Representation of BC-4 Traces," Progress Report on IGGS, Vol. 1, by A. Mancini and L. Gambino. Prepared for NASA under Contract NAS 12-001-005 by the Hawaii Institute of Geophysics, University of Hawaii]. These polynomials were fit directly to the data furnished by the Data Center without application of the corrections mentioned above. The coefficients of the polynomials were furnished OSU directly by the Hawaii Institute of Geophysics. Fully corrected fictitious images were produced from these polynomials by the following process:

(a) The polynomials for two coobserving stations were evaluated for some selected time epoch. Since the independent argument of the polynomials is the UT1 at which the image is received this produced two images which were received simultaneously, but did not necessarily refer to the same satellite position.

(b) These two images, together with the approximate coordinates of the cameras, were used to compute an approximate satellite position.

(c) The satellite position was used to compute the light travel time for each photograph.

(d) The time of observation was corrected by the light travel time, and the polynomials were evaluated again with the new values. This produced two images which referred to the same satellite position.

(e) A new satellite position was computed from the new images, and the range to each of the two cameras was computed.

(f) The images were then corrected for phase angle and parallactic refraction. A standard temperature of 10°C and a standard pressure of 760 mm Hg was used in this step.

Two experiments were performed with data obtained by the above process. There were

(8) geometric mode, 3 fictitious images per plate

(9) geometric mode, 7 fictitious images per plate

For all the adjustments, the coordinates of Beltsville (6002) on the SAO C-5 datum were held fixed, and the scale was introduced by constraining the chord distance from Beltsville to Moses Lake (6003) to 1 part in 1,000,000. The results of the 74-plate series of experiments are shown in Table 2.

Surprisingly, the uncertainties obtained from the orbital mode solutions are only slightly smaller than those from the geometric mode adjustments. On the other hand the orbital mode solution is more difficult to handle operationally, since an extra step is required to obtain approximate orbital elements. Furthermore, the trails on the BC-4 plates are all quite short, seldom exceeding five minutes of time. This means that some of the orbits tend to be poorly determined, and the adjustment tends to be prone to numerical problems. The slight improvement in the uncertainties of the adjusted coordinates obtained in the orbital mode solution does not seem to justify coping with these added difficulties.

Experiments 6 and 7 indicate that the use of three fictitious images, obtained either from a single curve fit or from 3 separate curve fits, produces results that are equivalent to the results obtained by using 10 individual images. The large differences between the results obtained with the Hawaii polynomials and the results of the other adjustments has not been explained. The process of fitting curves to the uncorrected images and then correcting the fictitious images taken from the curves should produce a corrected fictitious image equivalent to that obtained by first correcting all the images and then performing the curve fit.

The data used in experiment 9 was intended to represent the planned procedures of the U.S. Coast and Geodetic Survey, since it appears that USCGS intends to use seven directions from a single curve fit per plate. The main difference between the USCGS procedure and that used to prepare

Table 2

74 Plate Data Set

Experiment	Moses Lake			Revilla Gigedo			Thule			Degrees of freedom	A posteriori stand. dev. of single obs.
	X	Y	Z	X	Y	Z	X	Y	Z		
	-2127800 m +	-3785800 m +	4656000 m +	-2160900 m +	-5642700 m +	2035300 m +	546500 m +	-1390000 m +	6180200 m +		
1. Orbital Mode 20 ind. images	-24.4 (2.1)	-81.2 (6.9)	27.0 (6.0)	-62.0 (5.4)	- 0.5 (8.1)	81.4 (9.3)	57.3 (6.1)	-16.9 (9.0)	- 8.4 (10.9)	2278	1".6
2. Orbital Mode 10 ind. images	-24.7 (2.7)	-81.5 (9.1)	25.2 (8.0)	-56.2 (7.2)	- 4.6 (11.0)	86.5 (12.9)	65.4 (8.2)	- 7.5 (11.4)	-10.1 (14.9)	1106	1.6
3. Geometric Mode 20 ind. images	-24.6 (3.6)	-77.9 (7.5)	20.2 (6.5)	-64.5 (6.8)	+3.7 (9.1)	66.0 (10.4)	45.0 (6.8)	-23.1 (10.0)	-34.0 (12.1)	601	1.7
4. Geometric Mode 10 ind. images	-24.3 (4.0)	-77.3 (10.4)	20.7 (9.1)	-55.6 (8.7)	- 1.7 (12.7)	69.5 (14.7)	59.9 (9.3)	- 7.6 (13.3)	-17.1 (16.9)	306	1.7
5. Geometric Mode 1 fictitious image	-27.8 (5.6)	-90.5 (17.8)	23.9 (13.9)	-64.6 (12.3)	-35.9 (18.5)	85.9 (22.1)	65.3 (15.0)	-28.5 (19.8)	+29.8 (26.0)	23	0.8

Table 2 (continued)

6. Geometric Mode 3 fictitious images	-24.2 (4.7)	-79.8 (10.6)	24.8 (8.3)	-66.8 (8.1)	- 9.7 (11.5)	85.4 (13.3)	50.4 (8.6)	-32.8 (17.6)	-14.8 (15.8)	84	0.8
7. Geometric Mode 3 curve fits	-23.7 (4.6)	-77.2 (10.3)	23.6 (8.9)	-70.0 (8.8)	-20.4 (12.0)	83.9 (14.6)	52.9 (9.0)	-38.3 (13.6)	-17.4 (16.3)	89	0.9
8. 3 fictitious images from Hawaii curves	-15.5 (6.5)	-42.6 (15.2)	9.0 (12.4)	-47.0 (11.5)	-25.5 (16.1)	54.9 (19.7)	58.6 (11.7)	12.8 (17.5)	3.6 (20.4)	78	1.1
9. 7 fictitious images from Hawaii curves	-15.7 (5.6)	-42.7 (9.7)	7.6 (7.9)	-43.0 (8.2)	-25.3 (10.2)	56.6 (12.6)	59.9 (7.5)	9.9 (11.7)	7.6 (13.2)	192	1.1

Beltsville is held fixed on the SAO C-5 datum. The first row of each entry gives the adjusted coordinate, and the second row gives the standard deviation.

the data for experiment 9 is that USCGS performs the curve fit in terms of x, y plate coordinates instead of right ascension and declination, thus it can account for the existing correlations between the seven directions. In order to test the significance of this difference, the multiple fictitious images as computed by the USCGS were also requested directly from that agency. However, this data could not be provided, since almost all of the plates involved were being remeasured. The results of experiment 9 are inconclusive, since the a posteriori standard deviation is much higher than expected, indicating some problem in the data.

In summary, it appears that when using right ascensions and declinations as the basic data the best results can be obtained either by using three to five fictitious images, preferably obtained from three to five separate curve fits, or by using 10 individual images in the geometric mode. The use of 20 images from each plate does not appear to be justified in view of the worsening of the solution caused by correlation between observations. Due to the shortness of the trails, the orbital mode adjustment does not offer sufficient improvement to justify its use.

ACKNOWLEDGEMENT

The work described in this paper was partially supported by NASA under Contract No. 36-008-093.

REFERENCES

Brown, Duane C. (1967). Review of Current Geodetic Satellite Programs and Recommendations for Future Programs. D. Brown Associates, Inc., Eau Gallie, Florida.

Hamilton, Walter C. (1964). Statistics in Physical Science. Ronald Press, New York.

Hornbarger, Daniel H. (1968). "Comparison of Astrometric and Photogrammetric Plate Reduction Techniques for a Wild BC-4 Camera." Reports of the Department of Geodetic Science No. 106. The Ohio State University, Columbus.

Hotter, Frank D. (1967). "Preprocessing Optical Satellite Observations." Reports of the Department of Geodetic Science No. 82. The Ohio State University, Columbus.

Magnuss, T.A., and J.B. McGuire (1962). "Comparison of Least Squares and Minimum Variance Estimates of Regression Parameters." Annals of Mathematical Statistics, 33, 2.

Mueller, Ivan I., James P. Veach, and Charles R. Schwarz (1968). "Geodetic Utilization of Satellite Photography." Presented at the Seventh National Fall Meeting of the American Geophysical Union, San Francisco, Dec. 2-5. Abstract in Transactions, American Geophysical Union, Vol. 49, No. 4.

Mueller, Ivan I. (1969). "Ananlyzing Passive-satellite Photography for Geodetic Applications." Presented at the Fourth Meeting of the Western European Sub-Commission of the International Commission for Artificial Satellites, International Association of Geodesy, Paris, February.

Schwarz, Charles R. (1969). "The Use of Short Arc Orbital Constraints in the Adjustment of Geodetic Satellite Data." Reports of the Department of Geodetic Science No. 118. The Ohio State University, Columbus.

Veach, James P. (1968). "Investigations into the Utilization of Passive Satellite Observational Data." Reports of the Department of Geodetic Science No. 110. The Ohio State University, Columbus.

EXPERIMENTS WITH SECOR OBSERVATIONS ON GEOS - I

by
Ivan I. Mueller
James P. Reilly
Charles R. Schwarz
Georges Blaha

Department of Geodetic Science
The Ohio State University
Columbus

Presented at the GEOS-2 Review Conference
NASA Goddard Space Flight Center
June 22-24, 1970

I. Introduction

These experiments concerned the use of the SECOR observations on GEOS-I taken from the Pacific Tracking Network. There are approximately 60,000 of these range observations in the Data Center. This set of data presents some interesting and unique problems, since it constitutes a geodetic network that is completely unattached to any other network. The SECOR Pacific Network was begun in Japan, with three stations on the Japanese Datum, and extended through the Pacific Ocean to the West Coast of the United States. Thus it was connected to major datums on both ends. However, observations on GEOS-I were only taken in the middle of the network, from Truk Island to Maui so that the network determined by the GEOS-I observations alone cannot be attached to any major geodetic datum. Furthermore, the primary satellites for this network were the EGRS series of the U. S. Army Corps of Engineers, so that GEOS-I was not always fully observed when the primary satellites were available. This means that the network determined by the GEOS-I observations has some weak ties caused by an insufficient number of observations.

As a further complication, the quality of a large amount of the data is questionable, since in its early days the SECOR system was plagued by ambiguities, calibration errors, and possibly unreliable determinations of ionospheric refraction. Theoretically, it is possible to determine station positions, orbit unknowns, and coefficients of observational error models all in one simultaneous short-arc adjustment. However, all of our attempts to do this failed to converge, mainly because there were just too many unknowns and not enough a priori constraints to afford a reasonably well determined solution.

Thus we were essentially faced with a bootstrap operation: if one has fairly good station positions one can find and remove bad data; conversely, if one has all good data a rigid geodetic network can be easily constructed. Having neither reliable data nor station positions we had to proceed in stages.

II. Internal Adjustment

As a first step it was necessary to find a set of data that was at least internally consistent. We performed many adjustments, often deleting, and sometimes adding, data, until we got a set of residuals that were reasonably small and fairly randomly distributed. In all of these adjustments it was necessary to impose only the minimum set of constraints necessary to define the coordinate system. Since we did not know the relative positions of any of the stations, any larger set of constraints would increase the residuals and mask the internal consistency of the data set. Also, since we did not know the geodetic position of any of the stations on any major datum, we were free to define the adjustment coordinate system arbitrarily.

In the case of range observations, the minimum number of constraints necessary to define the coordinate system is six: three to define the origin and three to define the orientation; the scale of the system is determined by the observations themselves.

At first these constraints were realized by constraining the three coordinates of one station, two coordinates at a second station and one coordinate at a third station. We found that if the stations and the coordinates to be constrained were not selected with care, the coordinate system would be poorly defined, and this would result in poor error propagation characteristics, a weak network, and numerical difficulties. Later we found that the best way to define the coordinate system was to use the set of constraint equations called "inner adjustment constraints" [Rinner et. al, 1969]. These equations essentially define the adjustment coordinate system by holding fixed the mean position and orientation of the network as obtained from the approximate coordinates of all the stations. When the problem is to arbitrarily define a coordinate system for the adjustment, and to do so in a way that will result in the strongest network, the inner adjustment equations will give better results than any other minimal set of constraints.

After a great deal of trial and error, we obtained a set of coordinates for nine of the ten stations, from Truk Island to Midway Island, that was internally

consistent, yielding an estimated standard deviation of a single range observation of slightly more than 5 meters. We were not able to extend the network to Maui with the GEOS-I data, since all of the GEOS-I data from Maui gave quite large residuals. Therefore, we requested and received EGRS-7 data from the U.S. Army Topographic Command to connect Maui to Kusaie, Johnston and Midway Islands. This data brought the estimated standard deviation up to about 8 meters. However, we felt that this was about the best set of data we could hope to get, since removing any of the data with the larger residuals would have ruined the geometrical integrity of the network.

III. Connections to the North American Datum

We were now ready to connect the network to the North American Datum. Although we did not have NAD coordinates for any of the SECOR stations, we were able to find several indirect ties by which such connections could be effected (Tables 5 and 6).

First, there was a BC-4 station on Maui. Since this station was part of the Worldwide Geometric Satellite Network, its NAD coordinates had been computed by and were available from ESSA. Both this BC-4 station and the SECOR station had been tied into the local survey system, so that their relative coordinates were known and the NAD coordinates of the SECOR station could be inferred.

Secondly, there was a PC-1000 camera on Johnston Island, at the same site that had been occupied by the SECOR station. This PC-1000 camera had observed PAGEOS, ECHO I, and ECHO II simultaneously with BC-4 cameras on Maui, Wake, and Christmas Islands [Huber, 1969]. Since the three BC-4 stations were tied to the World Net, coordinates of the Johnston PC-1000 could be determined on the North American Datum, as carried into the Pacific through the BC-4 World Net. The observational data was obtained from ACIC and used to determine NAD coordinates of the PC-1000 camera, and the coordinates of the SECOR station were inferred from those of the camera (Table 5).

Thirdly, a TRANET Doppler station was located on Midway Island, and both it and the Midway SECOR had been tied to the local survey system. The coordinates of the Doppler station on the Mercury Ellipsoid had been published

as part of the NWL-8D solution. Performing a datum transformation and using the relative position of the two stations, we were able to infer NAD coordinates for the Midway Doppler.

This gave us three stations (Maui, Johnston, and Midway) at which the GEOS-I SECOR network could be tied to the North American Datum. Unfortunately, all three stations were at the eastern end of the network. Due to the cantilever effect of the error propagation, the station position determinations at the western end of the net were quite weak, especially in the vertical direction. Therefore, more external information was brought into the adjustment in the form of geodetic heights for seven stations in the western part of the net. These geodetic heights were determined as follows: 1) A geoid map based on the latest SAO gravity field was obtained from SAO. 2) Geoid heights at each of the SECOR stations were read from the map. 3) The reference ellipsoid for the geoid heights was transformed from a = 6378155m, 1/f = 298.255, to the parameters of the North American Datum, using the transformation parameters $\Delta x = -27m$, $\Delta y = 155m$, $\Delta z = 167m$. 4) The leveled height of each station was added to the height of the geoid above the NAD to produce a geodetic height. Having been derived from a geoid map, these height determinations were quite uncertain. We estimated that 25 meters was a reasonable figure for the standard deviation of a single height determination and derived weights for the height constraint equations from this figure. Even though they had relatively low weight, these constraint equations effectively nullified the cantilever effect and greatly improved the determination of station positions at the western end of the network.

IV. Results

Two solutions are presented in Table 1. Both use a large amount of SECOR GEOS-I data and some SECOR EGRS-7 data. Both use the height constraints on the western stations. In solution SP-5 the NAD coordinates of Johnston and the directions inferred from the ACIC camera observations from Johnston to both Maui and Midway are constrained by weighted constraint equations, so that the scale of the solution comes from the SECOR observations

alone. In solution SP-6, the NAD coordinates of Johnston, Maui, and Midway are all constrained, so that these coordinates also contribute to the scale determination. Significantly, distances determined by the SECOR observations alone differ only slightly from distances on the North American Datum, as extrapolated into the Pacific through the BC-4 World Net and TRANET system.

V. Future Plans

Now that we have a set of station coordinates that appear to be reasonably consistent, some of the data that was deleted should be re-examined. We suspect that by performing short-arc orbital mode adjustments in which the station coordinates are all constrained, we should be able to solve for calibration and other error model unknowns for at least some passes. Once these calibration and other unknowns are determined, it should be possible to use that data to strengthen the network.

ACKNOWLEDGEMENT

The work described in this paper was supported by NASA under Contract No. 36-008-093.

REFERENCES

Anderle, Richard J. and Steve J. Smith (1967). "NWL-8 Geodetic Parameters Based on Doppler Satellite Observations." NWL Technical Report No. 2106. Dahlgren, Virginia.

Huber, Donovan N. (1969). "Johnston Island Preliminary Satellite Network Coordinates." ACIC Technical Report No. 113. St. Louis.

Rinner, Karl, Karl Killian, and Peter Meissl (1969). "Beitrage zur Theorie der geodetische Netze im Raum." Deutsche Geodetische Kommission, Reihe A, Heft 61, Munchen. (In English as: Rinner, Karl (1966). "Systematic Investigations of Geodetic Networks in Space," Annex F. European Research Office. AD 482852).

Table 1: SECOR PACIFIC SOLUTIONS

	SP-5	SP-6
Number of Range Observations	976	976
Number of External Constraint Equations	23	25
Degrees of Freedom	228	230
Estimated Standard Deviation of a Single Range	8.6m	8.6m

Table 2: Solution Coordinates (meters)

GOCC #	Name		SP-5	σ	SP-6	σ
5401	Truk	x	-5576035	20	-5576033	20
		y	2984497	22	2984494	24
		z	822208	35	822221	41
5402	Swallo	x	-6097428	14	-6097428	14
		y	1486310	27	1486315	33
		z	-1133415	23	-1133408	27
5403	Kusaie	x	-6074515	13	-6074515	14
		y	1854183	17	1854183	20
		z	583632	23	583641	28
5404	Gizo	x	-5805376	16	-5805373	16
		y	2485135	27	2485138	32
		z	-893090	29	-893079	35
5405	Tarawa	x	-6327906	11	-6327907	13
		y	784398	18	784401	22
		z	150640	17	150645	20
5406	Nandis	x	-6070177	19	-6070178	19
		y	270469	35	270479	41
		z	-1933025	21	-1933021	23
5407	Canton	x	-6304289	16	-6304288	16
		y	-917822	22	-917814	26
		z	-307267	15	-307267	15
5408	Johnston	x	-6007958	8	-6007957	6
		y	-1111399	9	-1111395	8
		z	1823991	8	1823990	7
5410	Midway	x	-5618697	15	-5618698	13
		y	-258347	20	-258350	13
		z	2997059	21	2997058	13
5411	Maui	x	-5467994	11	-5467988	9
		y	-2381574	12	-2381566	9
		z	2253010	8	2253002	10

Table 3: North American Datum Coordinates of the SECOR Pacific Stations

(Solution SP-5)

GOCC	Name	Lat	σ	Long (+E)	σ	h	σ
5401	Truk	7° 27′ 25.″3	1.″1	151° 50′ 33.″7	0.″7	-117 m	21
5402	Swallo	-10 18 19.2	0.7	166 18 2.6	0.9	-30	14
5403	Kusaie	5 17 9.3	0.7	163 01 32.6	0.6	-66	12
5404	Gizo	-8 06 13.7	0.9	156 49 31.6	0.8	-15	18
5405	Tarawa	1 21 45.2	0.5	172 56 1.5	0.6	-78	11
5406	Nandis	-17 45 36.7	0.7	177 26 55.5	1.2	57	20
5407	Canton	-2 46 48.3	0.5	188 16 59.9	0.7	-1	17
5408	Johnston	16 43 44.2	0.3	190 28 49.9	0.3	-89	8
5410	Midway	28 12 45.0	0.6	182 37 57.4	0.7	-113	18
5411	Maui	20 49 24.7	0.3	203 32 7.6	0.4	-2	12

Table 4: North American Datum Coordinates of the SECOR Pacific Stations

(Solution SP-6)

GOCC	Name	Lat	σ	Long (+E)	σ	h	σ
5401	Truk	7° 27′ 25.″7	1.″3	151° 50′ 33.″7	0.″8	-119m	21
5402	Swallo	-10 18 18.9	0.9	166 18 2.5	1.1	-30	14
5403	Kusaie	5 17 9.6	0.9	163 01 32.6	0.7	-65	13
5404	Gizo	-8 06 13.4	1.1	156 49 31.5	1.0	-17	18
5405	Tarawa	1 21 45.4	0.6	172 56 1.4	0.7	-77	12
5406	Nàndis	-17 45 36.6	0.7	177 26 55.2	1.4	58	20
5407	Canton	-2 46 48.3	0.5	188 16 59.7	0.8	-3	17
5408	Johnston	16 43 44.2	0.2	190 28 49.8	0.3	-91	6
5410	Midway	28 12 45.0	0.4	182 37 57.4	0.5	-113	14
5411	Maui	20 49 24.6	0.3	203 32 7.4	0.3	-13	10

Table 5. Adopted Coordinates of Stations Used to Orient the Network

GOCC	Name	Type	Datum	Lat	σ	Long (+E)	σ	h	σ	Note
6011	Maui	BC-4	NAD	20° 42′ 26″.139	0″.351	203° 44′ 42″.886	0″.396	3001.4m	12.2m	1
6012	Wake	BC-4	NAD	19 17 28.247	0.470	166 36 43.564	0.515	-159.2	17.2	1
6059	Christmas	BC-4	NAD	2 0 13.185	0.487	202 35 20.508	0.380	-22.4	13.3	1
3475	Johnston	PC-1000	NAD	16 43 44.209	0.254	190 28 49.931	0.313	-90.2	7.9	2
2724	Midway	Doppler	Mercury	28 11 48.79		182 36 40.13		-14		3
2724	Midway	Doppler	NAD	28 11 50.47		182 36 46.16		-117		4

Notes:

1. ESSA World Net preliminary coordinate
2. Obtained at OSU by adjusting the ACIC optical data, weighting the coordinates of Maui, Wake, and Christmas according to their uncertainties.
3. NWL-8D Solution [Anderle and Smith, 1967, p. A16]. Uncertainty is 25m in each coordinate.
4. Obtained from NWL-8D Mercury Datum Coordinate, using datum transformation parameters of $\Delta x = -40$m, $\Delta y = 163$m, $\Delta z = 186$m. [Anderle and Smith, 1967, p. B1]

Table 6. Relative Positions from Local Surveys

From To			Δx	Δy	Δz	Estimated σ in each coordinate
5408	Johnston	SECOR	3.8m	0.8m	-1.2m	1.0m
3475	Johnston	PC-1000				
5411	Maui	SECOR	2002.5	-22991.8	-10965.6	0.1
6011	Maui	BC-4				
5410	Midway	SECOR	-882.6	1911.2	-1481.4	0.2
2724	Midway	Doppler				

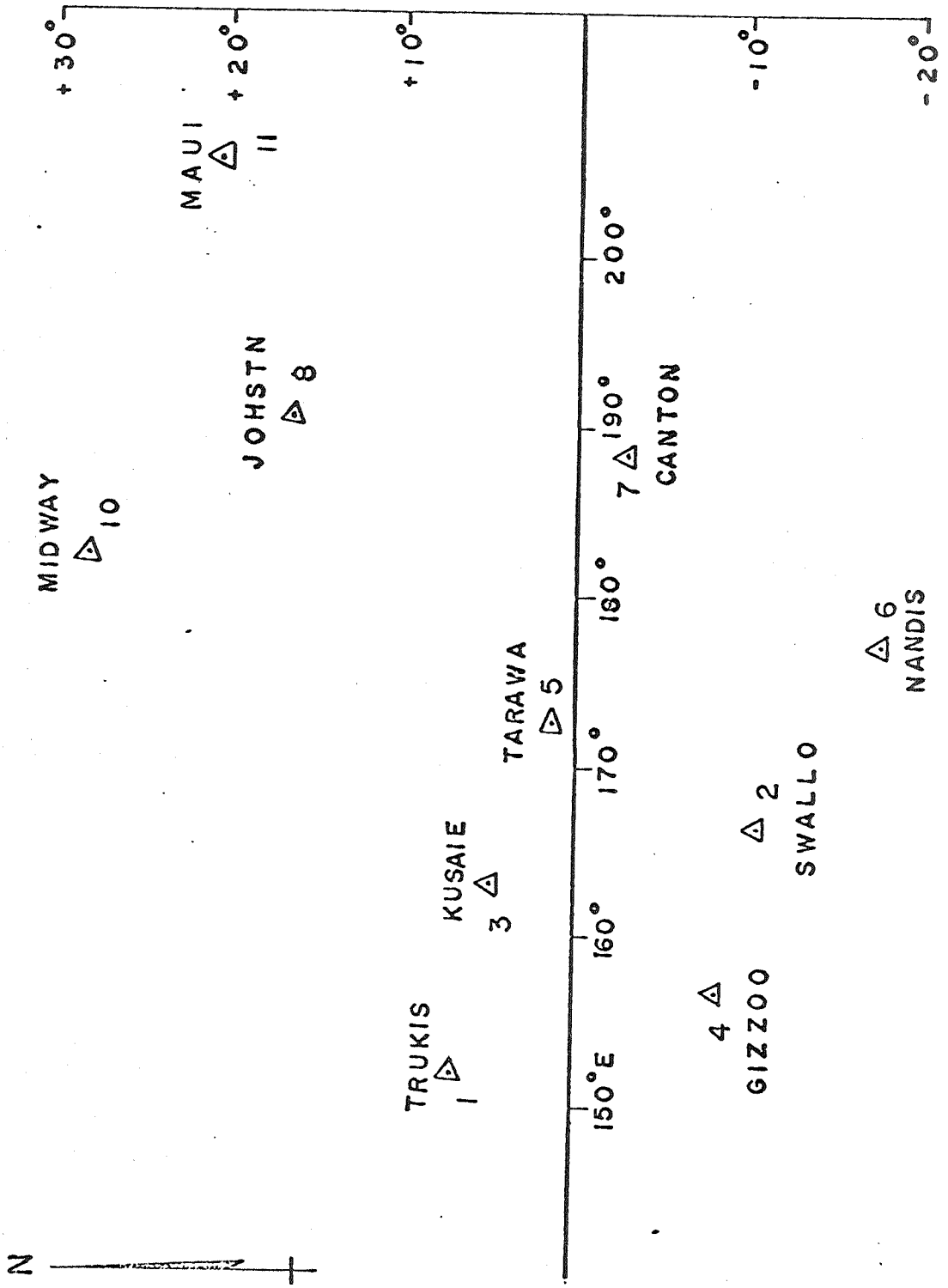

Fig. 1 Locations of the ten SECOR stations that were used in the network adjustment

COMPARISONS OF INDEPENDENT INVESTIGATOR'S SURVEY ADJUSTMENTS ON THE NAD USING GEOS DATA

Prepared for the GEOS-2
REVIEW CONFERENCE
June 22 - 24, 1970

By

J. Berbert
F. Loveless

COMPARISONS OF INDEPENDENT INVESTIGATOR'S SURVEY ADJUSTMENTS ON THE NAD USING GEOS DATA

J. Berbert
F. Loveless

INTRODUCTION

Four independent investigations of GEOS station survey adjustments on the North American Datum (NAD) were reported at or shortly after the National Spring Meeting of the AGU in April, 1969. The investigations (see References 1, 2, 3, 4) were done at Goddard Space Flight Center (GSFC), Air Force Cambridge Research Laboratory (AFCRL), Ohio State University (OSU), and the Smithsonian Astrophysical Observatory (SAO).

Since the different investigators reported their results in different coordinate systems and relative to different initial surveys, it was not evident to what extent their adjustments agreed. To determine the extent of agreement, this paper compares the survey adjustments relative to a standard set of initial positions for 9 stations common to the above investigations. The results of this comparison were reported to the Annual Fall Meeting of the DIA Mapping, Charting, and Geodesy Conference, October, 1969 (Reference 5), and to the Fall Meeting of the AGU, December, 1969. Since these presentations, it was discovered that about 10% of the MOTS data used in the above survey adjustments were subject to a small systematic computer programming error (Reference 6). The corrected MOTS data were obtained from the NSSDC and used to repeat the GSFC survey adjustment to determine the effect of the error on the solutions (Reference 7).

COMPARISONS

The different data and techniques employed in the various survey adjustments are summarized in Table 1. Short arc techniques were employed by GSFC, AFCRL, and OSU. In these solutions GSFC and OSU used optical data only. AFCRL used optical and ranging data. In other solutions OSU also tried geometric techniques, once with optical data only, and again with optical and ranging data. SAO reported results from a geometric solution and from a combination of geometric and long arc solutions.

It is not known to what extent the data used in the different solutions are independent. However, as indicated in Table 1, different numbers and types of cameras and ranging systems were employed over different numbers of orbital arcs. Some of the data in different solutions must therefore be independent, although some overlap is likely.

Other factors which differ in the solutions compared, and which are known to influence the results, are the survey origin, the datum, the value of GM, the type of observational data, and the various baseline constraints (Reference 8).

The SAO reported results on a GLOBAL datum and defined the transformation between this datum and the NAD27. This transformation was used to convert the SAO results to the NAD for comparison with the other solutions on the NAD.

OSU, in their short arc ORB solution, used the SAO GLOBAL geocentric coordinates for Columbia, the survey origin, but reported results on the NAD27 by removing the constant translation between the GLOBAL and NAD geocenters.

The different solutions are compared by differencing the final positions on the NAD with a standard set of initial NAD positions. The standard initial positions were identical to the OSU initial positions given in Reference 3.

In each solution, the components of the station position shift vectors were expressed in an E, N, V local coordinate system. For each solution, mean E, N, V shifts for the network of 9 comparison stations were calculated and removed from the E, N, V shifts for each of the 9 stations, including the origin station, to allow for error in the fixed origin station position. The E, N, V shifts with means removed are given in Table 2 for the 9 comparison stations.

The revised GSFC results due to using the corrected MOTS data are given in Reference 7, where most of the changes to the ENV components are shown to be within the noise level of about 3 to 5 meters.

RESULTS

The last three columns of Table 2 give the composite or mean horizontal and vertical displacements from the initial NAD positions for each station averaged over all solutions. The overall average horizontal and vertical displacements are also given, along with the RMS of the compositie displacements. The RMS of the composite horizontal displacements for the 7 continental U.S. stations is 5.1 meters, which is better than the uncertainty in the NAD horizontal positions as previously predicted from Simmon's Rule (1σ= 1:20, 000$M^{1/3}$, M in miles), which yields a one sigma error of about 8 meters per 1000 miles, but not as good as predicted from the Revised Simmon's Rule (replaces 1σ by 2σ), which yields a one sigma error of about 4 meters per 1000 miles. Also the RMS of the composite vertical displacements for the 7 continental U.S. stations is 5.6 meters, which is larger by a factor of 2 or 3 than the uncertainty in the NAD geodetic heights of about $\pm$2 meters (Reference 9). This indicates that the first order relative position accuracies of stations on the continental U.S. are probably somewhat but not much better than the composite or average of the various satellite survey adjustments reported here.

The shift of 24 ±7 meters to the East in the composite satellite solution for Bermuda seems to be the only significant shift from the initial NAD positions detected by these satellite solutions. The initial NAD position for Bermuda is given in the Goddard Directory of Tracking Station Locations (GDTSL), as taken from the Coast and Geodetic Survey BC-4 camera results from the 1964/65 satellite triangulation program. In this satellite triangulation and distance derived for the baseline between cameras in Aberdeen, Maryland, and Jupiter, Florida, was 16.5 meters less than the same distance determined from the Cape Canaveral (CC) traverse. In the longer CC baseline between these two cameras were used in the satellite triangulation solution for Bermuda, the result would be an approximate 18 meter shift to the East, in closer agreement with the present results.

Also, the -6.4 meter adjustment in the composite solution for Bermuda height would have been +3.6 meters if the initial NAD height chosen for Bermuda had been the +21 meter station geodetic height given in the GDTSL rather than the +31 meter station height above MSL given in the GDTSL.

CONCLUSIONS

1. The composite satellite survey adjustments to the 7 continental U.S. station positions compared in this paper exhibit an RMS horizontal and vertical scatter of 5.1 meters and 5.6 meters about the NAD station positions compared with the expected average horizontal and vertical errors in these positions of about 4 meters and 2 meters (as determined by Simmon's Modified Rule).

2. These satellite solutions seem to have detected a significant error in the GDTSL position of Bermuda. An adjustment of 25 ±7 meters to the East is indicated.

TABLE I

COMPARISON OF METHODS

	GSFC	AFCRL	OSUORB	OSUNA2	OSUNA4	SAO GEOM	SAO COMB
Mode	Short Arc	Short Arc	Short Arc	Geometric	Geometric	Geometric	NOTE 1
Data Type	13 MOTS	8 MOTS 7 PC-1000 4 SECOR 1 LASER	15 MOTS 15 PC-1000	15 MOTS 15 PC-1000	15 MOTS 15 PC-1000 4 SECOR	12 MOTS 23 SAO 1 EUROPEAN	7 MOTS 5 SAO
No. of Orbital Arcs	38	27	86				
No. of Stations	13	20	30	30	34	36	12
Survey Origin	Columbia (7037)	Hunter (5649)	Columbia (7037)	Columbia (7037)	Columbia (7037)	Jupiter (9010)	Jupiter (9010)
Datum:	NAD27	NAD27	GLOBAL-NAD	NAD27	NAD27	GLOBAL-NAD	GLOBAL-NAD
Constraints:							
Origin	held fixed	held fixed	held fixed	weighted (.11)	weighted (.11)	held fixed	held fixed
GM	Note 2a	Note 2b	Note 2c				Note 2a
Range Data		SECOR/LASER			SECOR		
Baseline		Note 3	Note 4	Note 4	Note 4	Note 5	Note 5

NOTE: 1 - Geometric solution using results from a dynamic or orbital solution as input.
2a - GM = 3.986013×10^{14} m^3/sec^2 used in GSFC and SAO-COMB solutions.
2b - GM = 3.986032×10^{14} m^3/sec^2 used in AFCRL solution.
2c - GM = 3.986031×10^{14} m^3/sec^2 used in OSUORB solution.
3 - Chord and Angle constrained between Herndon Secor (5001) and Aberdeen Camera (3657), and between Homestead Secor (5861) and Camera (3861).
4 - Chord constrained between Homestead, Fla. (3861) and Greenbelt, Md. (7043) using USC&GS Traverse (1:750,000
5 - Chord constrained between Jupiter, Fla. (9010) and Organ Pass, N.M. (9001), using SAO 1966 Standard Earth. Chord constrained between stations less than 200 km apart, using ground survey information.

REFERENCES

1. J. J. Lynn, D. C. Brown, J. H. Berbert, "Short Arc Optical Survey of the GEOS North American Optical Tracking Network", April, 1969. Presented at the Annual meeting of the AGU in Washington, April, 1969.

2. G. Hadgigeorge, J. E. Trotter; "Numerical Results from Short Arc Geodetic Adjustments Using Combinations of Directional and/or Ranging Observations from GEOS-1 Satellite", April, 1969. Presented at the Annual Meeting of the AGU in Washington, April, 1969.

3. I. Mueller, E. R. Schwarz, J. P. Reilly, "The North American Datum in View of GEOS-I Observations", Ohio State University Department of Geodetic Science Report No. 125, June, 1969. Preprint.

4. Kurt Lambeck, "A Spatial Triangulation Solution for a Global Network and the Position of the North American Datum Within It", April, 1969. Presented at the Annual Meeting of the AGU in Washington, April, 1969.

5. J. Berbert, "GEOS Station Position Solution Comparisons", Presented at the DIA MC&G Fall Meeting, October, 1969, and the AGU Fall Meeting, December, 1969.

6. D. Harris, "NASA - GSFC GEOS-I MOTS Optical Validation Report". NASA X-514-69-83. January, 1969.

7. F. Loveless, J. Lynn, J. Berbert "NAD Survey Adjustments From Short Arcs Using GEOS-I Observations". GEOS-2 Review Conference, June, 1970.

8. J. Lynn, "Short Arc Optical Survey of The GEOS North American Network". Presented at COSPAR, Prague, May, 1969.

9. "Goddard Directory of Tracking Station Locations", 1970 Edition, in preparation.

Table 2

CORRECTIONS IN LOCAL CARTESIAN COORDINATES
(E, N, V) MEAN CORRECTION REMOVED (METERS)

Station	GSFC	AFCRL	OSUORB	OSUNA2	OSUNA4	SAO GEOM	SAO COMB	Average Correction	Avg. Horiz.	Avg. Vert.
BPOIN E	1.0		-10.5	-7.3	-9.3	-13.2	-9.6	-8.2 ± 4.9		
1021 N	-10.6	NA	2.9	8.7	7.0	7.5	11.2	4.5 ± 7.9		
V	9.0		-1.9	-9.2	-8.0	-7.5	-4.4	-3.7 ± 6.8		
ACVM								10.0 ± 11.5	9.3	-3.7
FTMYR E	1.2	-6.7	9.5	-1.4	-1.8			0.2 ± 6.0		
N	2.3	1.1	-2.9	0.6	3.5	NA	NA	0.9 ± 2.4		
V	0.4	-0.8	5.8	-0.7	0.3			1.0 ± 2.7		
ACVM								1.4 ± 7.0	0.9	1.0
BERMD E	27.5	13.5	33.1	25.8	19.2	24.6		24.0 ± 6.8		
N	3.8	5.9	-1.8	-1.1	0.2	12.5	NA	3.3 ± 5.4		
V	-6.9	-0.1	-15.7	-14.1	-14.0	12.2		-6.4 ± 10.9		
ACVM								25.0 ± 13.9	24.2	-6.4
DENVR E	-7.3		-1.0	6.5	11.8	-0.9	0.2	1.6 ± 6.7		
N	1.4	NA	1.3	3.3	0.3	2.6	4.5	2.2 ± 1.5		
V	5.0		2.0	9.1	9.7	2.1	4.2	5.4 ± 3.4		
ACVM								6.0 ± 7.6	2.8	5.4
EDINB E	-7.9	9.5	-0.4	-1.8	1.8	-3.0	0.0	-0.3 ± 5.3		
N	-1.3	1.0	-10.8	-2.2	0.6	-7.1	-6.4	-3.7 ± 4.4		
V	11.3	13.6	17.5	12.6	11.9	-0.8	0.0	9.4 ± 7.0		
ACVM								10.2 ± 9.8	3.7	9.4
COLBA E	-4.9	-8.2	4.3	-4.9	-2.6	-1.4	1.4	-2.3 ± 4.2		
N	-6.3	-6.6	-10.4	-5.0	-7.9	-8.0	-5.1	-7.0 ± 1.9		
V	2.3	-1.8	4.2	8.0	6.0	0.0	0.9	2.8 ± 3.5		
ACVM								7.9 ± 5.8	7.4	2.8
GFORK E	-9.7	-7.0	0.0	-2.8	0.9	3.4	5.0	-1.5 ± 5.4		
N	9.1	-3.4	2.8	-3.1	-8.7	-4.8	-0.6	-1.2 ± 5.8		
V	2.9	9.9	2.2	8.0	7.8	3.3	4.4	5.5 ± 3.0		
ACVM								5.8 ± 8.4	1.9	5.5
PURIO E	-0.4	1.7	-39.7	-1.0	-7.0	-6.9		-8.9 ± 15.5		
N	2.6	-3.2	26.8	-4.1	3.2	0.2	NA	4.3 ± 11.4		
V	-17.9	-24.3	7.0	-7.7	-9.2	-0.4		-8.8 ± 11.4		
ACVM								13.2 ± 22.4	9.8	-8.8
ROSMA E	0.4	-2.7	4.9	-12.8	-13.2	-2.4	2.8	$-3.3 \quad 7.2$		
N	-1.1	5.2	-8.0	2.8	2.2	-3.0	-3.4	$-0.8 \quad 4.5$		
V	-6.2	3.6	-20.7	-5.8	-4.4	-8.8	-5.0	$-6.8 \quad 7.3$		
ACVM								7.6 ± 11.1	3.4	-6.8
Overall Average								± 9.7	$+7.0$ -7.2	-0.2 ± 6.5
σ of Overall Average								± 6.6		
RMS (All 9 stations)									9.8	6.1
RMS (7 continental stations)									5.1	5.6

ESTIMATES OF C-BAND RADAR STATION POSITIONS AND INTERSITE DISTANCES

by
CLIFFORD D. LEITAO
National Aeronautics and Space Administration
Wallops Station
Wallops Island, Virginia

RONALD L. BROOKS
Wolf Research and Development Corporation
Range Engineering Department
Pocomoke, Maryland

Prepared for Presentation at
GEOS-II Review Conference
Goddard Space Flight Center
Greenbelt, Maryland
June 1970

ESTIMATES OF C-BAND RADAR STATION POSITIONS AND INTERSITE DISTANCES

by

Clifford D. Leitao

National Aeronautics and Space Administration

Ronald L. Brooks

Wolf Research and Development Corporation

ABSTRACT

Estimates of the geodetic positions of selected C-Band radars that tracked the GEOS-II satellite during the period 28 January 1969 to 18 February 1969 are presented. The geodetic positions were estimated dynamically on the SAO C-6 datum using the SAO 1969 gravity model. Intersite distances between some of the sites are also presented.

1. INTRODUCTION

The GEOS-II C-Band Project has been highly successful in achieving one of its primary goals, i.e., the calibration of the radars in the C-Band radar network. Many of the radars which participated in the intensive tracking experiment during the period 28 January to 18 February 1969 are believed calibrated to the point that the project is achieving its second primary goal of utilizing radar observations to estimate geodetic parameters. The C-Band radar net is shown in Figure 1.

2. DATA

The observations being used to estimate the geodetic parameters (ϕ, λ, h) come from two instrumentation sources, 11 C-Band radars in the C-Band radar network and two Goddard Space Flight Center lasers. The raw radar data was preprocessed correcting it for tropospheric refraction, transit time, and a calibration derived

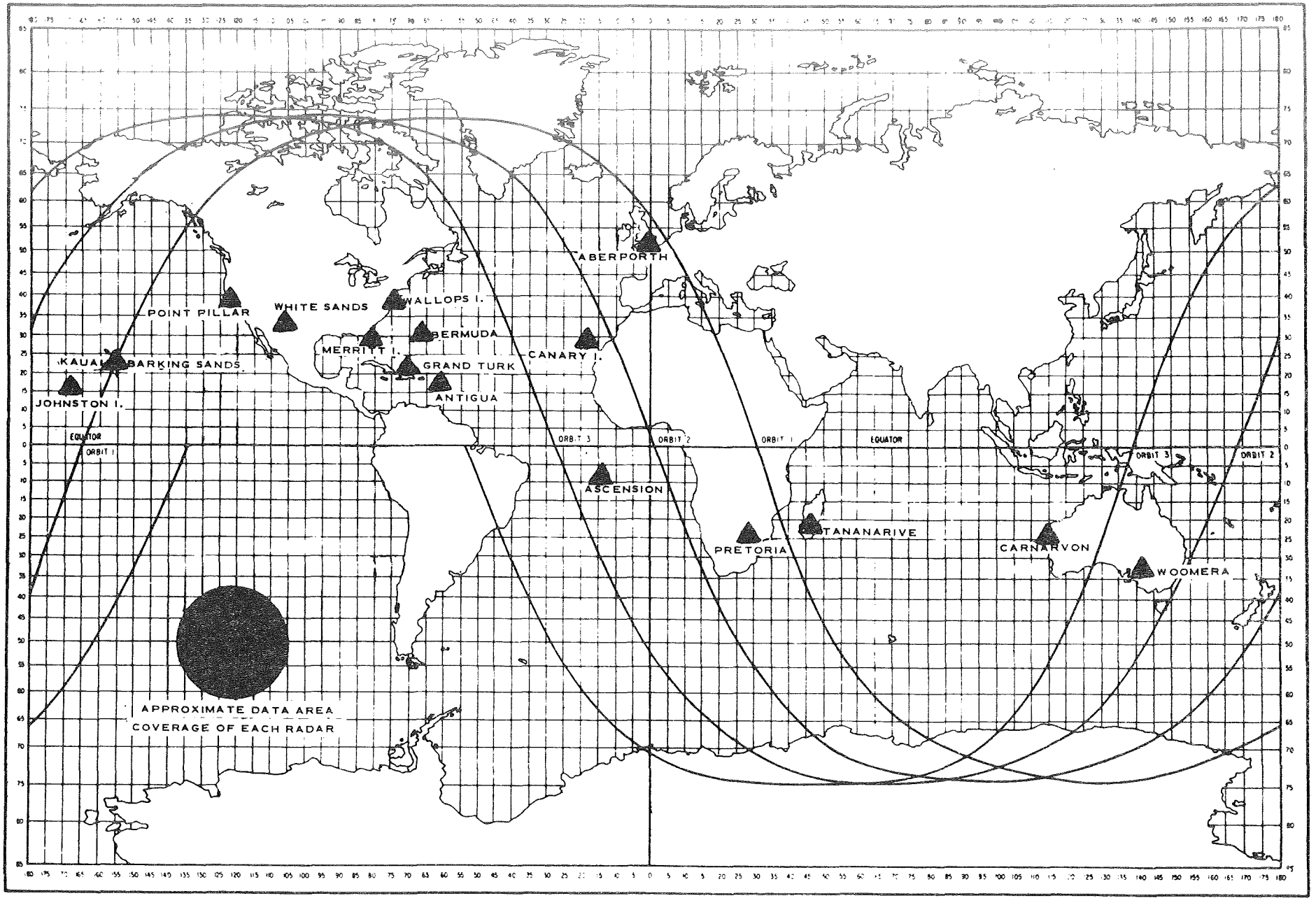

Figure 1 C-BAND RADAR NETWORK

zero-set correction[1]. The radar data was then validated in single-station short-arc orbital solutions using the A/OMEGA data reduction program[2]. The range precision was estimated to lie between one and two meters[3,4]. The radar range data was further validated in long arc orbital solutions where both timing errors and range biases were recovered from some radar data. See Table 1. The laser data was obtained from the NGSP Data Center.

3. SYSTEMS AND MODELS

The instrumentation that supplied range data used in this report are shown in Table 2 and the geodetic datum information for these stations is found in Table 3.

The data was reduced using the following models and data restrictions:

1) Station coordinates SAO C-6 datum

$$A_e = 6378155 \text{ meters}$$
$$f = 1/298.25$$
$$GM = 3.986013 \times 10^{20} \text{ cm}^3/\text{sec}^2$$

2) Gravity model - SAO gravity model presented at 1969 Fall AGU meeting.

3) Data rate - one observation every 20 seconds

4) Data type - range data where elevation was greater than ten degrees

5) Timing - UTC time was corrected to UT1 time in A/OMEGA orbit determination program

4. STATION POSITION ESTIMATES

The Wallops Island AN/FPQ-6 radar, NWALI3, was chosen as the origin for the C-Band radar datum. It was decided to fix the NWALI3 station position for several reasons.

TABLE 1

RADAR RANGE AND TIMING RECOVERIES

STATION	ESTIMATE ERROR	ACTUAL VALUE	VERIFICATION	CAUSE
WOOR38	+ 24.9 m seconds	+ 25. m	WRE Australia	Software record skip at 40 PPS
WTRKAU	- 52 meters	Unknown	WTRKAU Radar site	radar transmitted & calibrated in 1 μsec pulse width
NBER05	+ 15 meters	Approx 15 m	NBER05 Radar personnel	pulse width mis-match
WTRVAN	-19 mseconds	Unknown	Partial verification from Vandenberg Timing personnel	radar pre-knock time

TABLE 2

INSTRUMENTATION

STATION NAME	STATION NUMBER	LOCATION	INSTRUMENTATION
ETRPRE	4050	Pretoria, South Africa	FPS-16
ETRANT	4061	Antigua, BWI	FPQ-6
ETRAS8	4080	Ascension Island	TPQ-18
ETRGRT	4081	Grand Turk, BWI	TPQ-18
ETRMRT	4082	Merritt Island, Florida	TPQ-18
NELHAR	4690	Ely, Nevada	HAIR
NBER34	4740	Bermuda	FPS-16
NTANAN	4741	Tananarive, Malagasy Rep.	FPS-16
WTRKAU	4742	Kauai, Hawaii	FPS-16
NWALI3	4860	Wallops Island, Virginia	FPQ-6
WOOR38	4946	Woomera, Australia	FPS-16
GODLAS	7052	Greenbelt, Maryland	LASER
CRMLAS	7054	Carnarvon, Australia	LASER

TABLE 3

GEODETIC DATUMS

STATION NAME	STATION NUMBER	LOCAL DATUM	NOMINAL COORDINATES SAO C-6 DATUM ϕ	λ	h
ETRPRE	4050	CAPE (ARC)	-25° 56' 38".257	28° 21' 28".238	1598.15
ETRANT	4061	NAD 1927	17° 08' 37".552	298° 12' 25".760	-7.25
ETRAS8	4080	ASCENSION ASTRO	-7° 58' 22".779	345° 35' 53".898	105.38
ETRGRT	4081	NAD 1927	21° 27' 45".632	288° 52' 04".114	-32.79
ETRMRT	4082	NAD 1927	28° 25' 28".976	279° 20' 07".480	-44.16
NELHAR	4690	NAD 1927	39° 18' 30".788	244° 54' 46".315	2787.97

TABLE 3 (Contd.)

GEODETIC DATUMS

STATION		LOCAL DATUM	NOMINAL COORDINATES SAO C-6 DATUM		
NAME	NUMBER		ϕ	λ	h
NBER34	4740	NAD 1927	32° 30' 53".333	295° 20' 47".430	-39.13
NTANAN	4741	TANANARIVE	-19° 00' 06".479	47° 18' 53".021	1320.15
WTRKAU	4742	OLD HAWAIIAN	22° 07' 23".948	200° 20' 03".599	1131.70
NWALI3	4860	NAD 1927	37° 51' 36".969	284° 29' 25".946	-58.70
WOOR38	4946	AUSTRALIAN	-30° 49' 07".202	136° 50' 17".291	121.20
GODLAS	7052	NAD 1927	39° 01' 13".649	283° 10' 18".461	-6.91
CRMLAS	7054	AUSTRALIAN	-24° 54' 16".666	113° 42' 58".223	2.46

1) We are most familiar with its data

2) We are confident of its accuracy

3) Its timing system is well documented

4) It is located on the North American Datum

5) It is easily transformed to the SAO C-6 Datum

Therefore NWALI3 was used as reference and all the range measurements were weighted one meter. Assuming the uncertainty in (ϕ, λ, h) of all station except NWALI3 to be 10 seconds in latitude and longitude, and 10 meters in geodetic height, the data was reduced using the multi-station multi-arc mode of A/OMEGA to estimate the geodetic location parameters. A sample geometry plot of station NBER34 is shown in Figure 2. This is an indication of the geometrical strength of the experiment. Table 4 shows the results obtained thus far in estimating the station position of selected instrumentation referenced to a C-Band oriented datum.

5. INTERSITE DISTANCE ESTIMATES

To further evaluate the radar ranging capabilities, intersite distances were estimated using range data from only two sites per solution. In each solution, one site's geodetic coordinates are held fixed while the other station is allowed to adjust. These radar solutions for intersite distances are then compared with existing transcontinential "Classical Geodesy" Surveys.[5]

To date, solutions have been made for the stations shown in Table 5.

6. SUMMARY

The recoveries of C-Band station coordinates and intersite distances to date are very encouraging, considering the geometrical

FIGURE 2 NBER34 PASS GEOMETRY

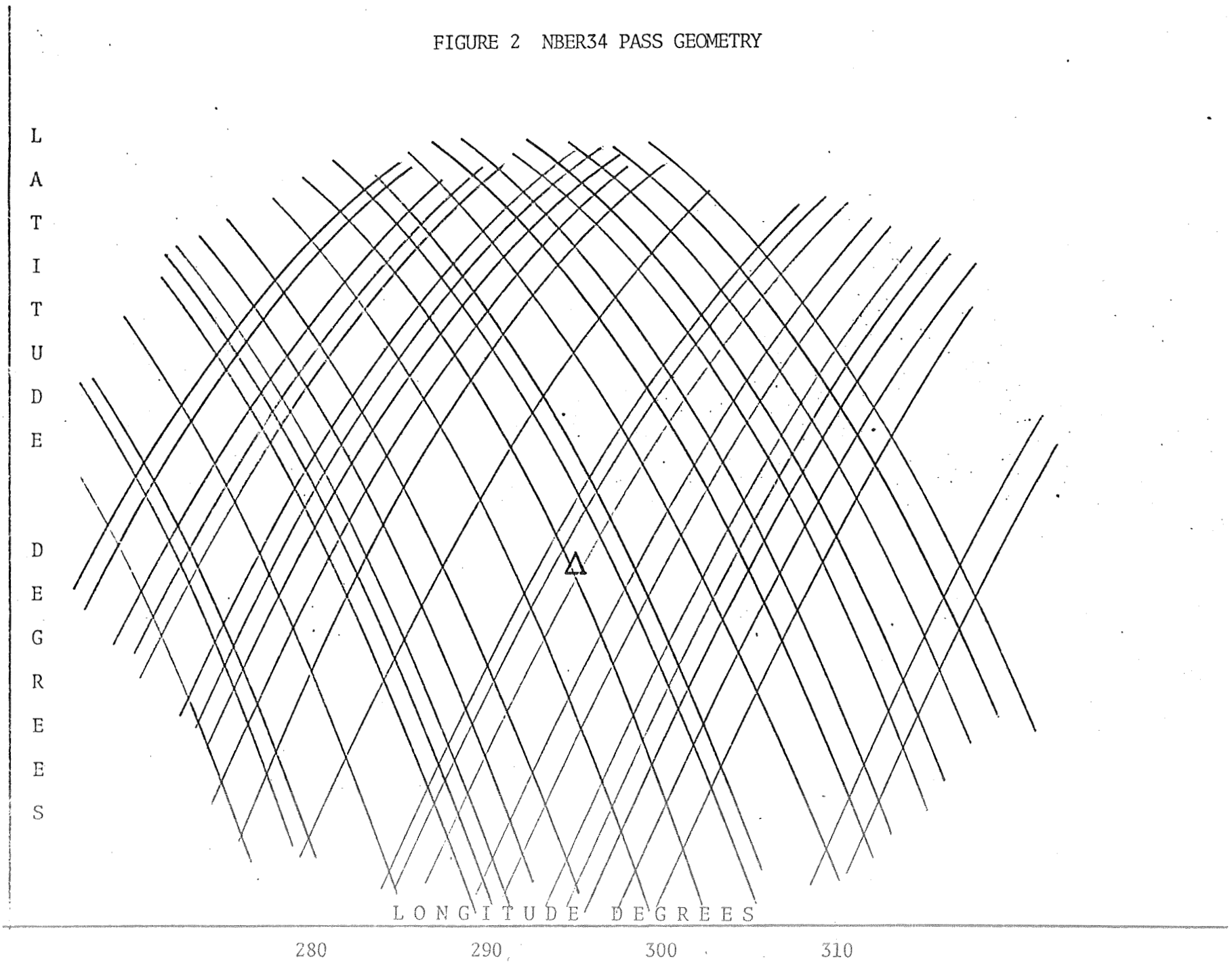

TABLE 4

IMPROVED STATION COORDINATES
ON SAO C-6 DATUM

STATION NAME	STATION NUMBER	ϕ	λ	h
ETRPRE	4050	-25° 56' 38".629	28° 21' 28".656	1559.00
ETRANT	4061	17° 08' 36".611	298° 12' 25".814	-27.98
ETRAS8	4080	-7° 58' 21".711	345° 35' 54".567	136.58
ETRGRT	4081	21° 27' 45".660	288° 52' 03".894	-16.10
ETRMRT	4082	28° 25' 29".160	279° 20' 07".320	-43.83
NBER34	4740	32° 20' 52".766	295° 20' 46".592	-42.56
NTANAN	4741	-19° 00' -6.809	47° 18' 52".287	1290.25
WTRKAU	4742	22° 07' 23.652	200° 20' 02".710	1126.09
NWALI3	4860	37° 51' 36".969	284° 29' 25".946	-58.70
WOOR38	4946	-3 ° 49' 6.781	136° 50' 17".360	136.55
CRMLAS	7054	-24" 54' 16".870	113° 42' 58".595	-0.15

TABLE 5

INTERSITE DISTANCES (METERS)

	NAD	CCD	RECOVERED
ETRMRT TO NELHAR	3,342,603		3,342,590
ETRMRT TO GODLAS	1,225,626	1,225,636	1,225,623
ETRMRT TO ETRANT	2,288,007		2,288,029
NWALI3 TO NBER34	1,160,594		1,160,592

strength and the consistency of the orbital solutions. Studies at Wallops Station are progressing rapidly toward the calibration and station estimations of additional participating C-Band radars.

REFERENCES

1 Brooks, R.L., Vetter, J.R., Pre-Processing of Wallops Station AN/FPQ-6 GEOS-II Data. Prepared for NASA/Wallops Island by Wolf Research and Development Corporation, 1970.

2 Martin, T.V., The Operations Manual for the A/OMEGA Program. Prepared for NASA/Wallops Island by Wolf Research and Development Corporation, 1969.

3 Leitao, C.D., and Brooks, R.L., C-Band Radar Measurements: An Assessment of Accuracy. Presented at International Association of Geodesy Symposium on Electronic Distance Measuring; Boulder, Colorado, June 1969.

4 Dempsey, D.J., An Evaluation of the Wallops Island C-Band Radar Experiment (WICE) Radar Range Errors. Prepared for Wolf Research and Development Corporation by Radio Corporation of America, Moorestown, N.J., September 1969.

5 Brooks, R.L., Leitao, C.D., C-Band Radar Network Intersite Distances. Presented at American Geophysical Union National Fall Meeting; San Francisco, California, 1969.